



**Investigation into the cellular function of the  
Opitz Syndrome gene, *MID1* and its homologue,  
*MID2***

**By**

**Yi Zou**

**(Bachelor of Medicine, Master of Science)**

A thesis submitted in fulfillment  
for the requirements of the degree of  
Doctor of philosophy

**Discipline of Genetics  
School of Molecular and Biomedical Science  
The University of Adelaide**

**July, 2004**

The work contained in this thesis contains no material that has been accepted for the award of any other degree or diploma in any university or other tertiary institution and, to the best of my knowledge and belief, contains no material previously published except where due reference has been made.

I give consent to this copy of my thesis, when deposited in the University Library, being available for loan and copying.

7. 10. 2004

Yi Zou (Bachelor of Medicine, Master of Science)

## **Acknowledgement**

First and foremost, I would like to thank my supervisor Tim for giving me the opportunity to do a PhD in his lab. His ongoing support, encouragement, patience and most importantly, friendship has enabled me to get through the past 4 years with confidence and enjoyment. I would also like to thank Kieran and Blair for their valuable words of scientific wisdom, and cooperation, which greatly aided me in succeeding in what I set out to do. A special thanks also goes out to Belinda-for spending her precious hours supporting me during writing of this thesis and her valuable friendship over the last 4 years. A big thanks to the rest of the Cox Lab: Liza, Saidi and Quenten for making me feel so at home and making my time in the lab fun.

A special thank-you to the Centre for the Molecular Genetics of Development for giving me financial support, which without I may have found myself in a difficult situation in continuing my PhD.

## Table of Contents.

<b>Acknowledgements</b> .....	2
<b>Chapter One: General Introduction</b> .....	<b>9</b>
1.1 Opitz syndrome or BBBG syndrome.....	9
1.2 Genetics of Opitz syndrome.....	10
1.2.1 Opitz syndrome is heterogenous .....	10
1.2.2 OS cases with different genetic defects are clinically indistinguishable....	11
1.2.3 The OS phenotype represents a defect in tissue fusion and/or remodeling during early development.....	12
1.3 Comparison of OS with other 22q11.2 deletion syndromes.....	13
1.3.1 The clinical features of the 22q11.2 deletion syndrome .....	13
1.3.2 Potential causative genes for the 22q11.2 deletion syndrome.....	13
1.4 Identification of <i>MID1</i> as the causative gene in X-linked OS.....	15
1.4.1 Identification of <i>MID1</i> mutations in OS.....	15
1.4.2 The expression pattern of <i>MID1</i> also supports a OS candidate gene.....	16
1.5 Characterization of <i>MID1</i> .....	17
1.5.1 The RBCC protein family.....	17
1.5.2 The B30.2 domain.....	19
1.5.3 The cellular localization of <i>MID1</i> .....	20
1.5.4 Protein interactors of <i>MID1</i> .....	21
1.5.5 A potential ubiquitin E3-ligase activity for <i>MID1</i> .....	23
1.5.5.1 E3 ubiquitin-ligases and protein ubiquitylation.....	24
1.5.5.2 Ubiquitylation in the regulation of protein degradation.....	25
1.5.5.3 Ubiquitin and membrane trafficking.....	25
1.5.5.4 Potential target/targets for ubiquitylation.....	26
1.6 <i>MID2</i> , a homologue of <i>MID1</i> , has correlated functions.....	26
1.6.1 <i>MID1</i> and <i>MID2</i> are likely to have originated from a common ancestral gene .....	26
1.6.2 Functional similarities of <i>MID1</i> and <i>MID2</i> .....	27
1.6.3 A role for <i>MID2</i> in the pathogenesis of OS?.....	27
1.6.4 The CI subfamily: sharing a common cellular function?.....	28
1.7 <i>MID1</i> / <i>MID2</i> and microtubule-dependent cellular processes.....	29



1.7.1 Microtubule dynamics.....	29
1.7.2 Microtubules and other cytoskeletal networks.....	30
1.7.3 Connection between microtubules and membrane.....	31
1.7.3.1 Microtubule-membrane cross-linking proteins.....	31
1.7.3.2 Microtubule motors .....	32
1.7.3.3 Phosphoinositides and the microtubule-membrane connection.....	33
1.7.3.4 The PH-domain and PI-binding.....	34
1.7.4 Microtubule-dependent cellular processes.....	35
1.7.4.1 Microtubules and cell motility .....	35
1.7.4.2 Microtubules and positioning of intracellular membrane compartment .....	35
1.7.4.3 Microtubule-dependent vesicle trafficking.....	36
1.7.4.4 Coupling of trafficking and signalling during development.....	37
1.8 Outlines of this project.....	39
<b>Chapter Two: Materials and Methods.....</b>	<b>41</b>
2.1 Abbreviations .....	41
2.2 Materials .....	42
2.2.1 Chemical and Reagents.....	42
2.2.2 Stains and Dyes .....	43
2.2.3 Enzymes .....	43
2.2.4 Antibiotics and Indicators .....	44
2.2.5 Fluorescent Probes .....	44
2.2.6 Kits and Miscellaneous Materials .....	45
2.2.7 Solutions and Buffers .....	45
2.2.8 Nucleic acid and protein molecular weight standards.....	51
2.2.9 Cloning and expression vectors.....	51
2.2.10 Bacterial strains .....	51
2.2.11 Bacterial media .....	51
2.2.12 Yeast strains .....	52
2.2.13 Yeast media .....	53
2.2.13.1 Amino acids and Carbon source.....	53
2.2.13.2 Liquid media .....	53
2.2.13.3 Solid media .....	53

2.2.14 Libraries .....	54
2.2.15 Tissue Culture Cell Lines and Media.....	54
2.2.15.1 Cell Lines .....	54
2.2.15.2 Media .....	54
2.2.16 Antibodies .....	54
2.2.17 Oligonucleotides .....	55
2.2.18 MID1 and MID2 domain deletions.....	55
2.3 Methods .....	56
2.3.1 Ethanol precipitation of nucleic acids.....	56
2.3.2 Restriction endonuclease digestions.....	56
2.3.3 Agarose gel electrophoresis of DNA.....	56
2.3.4 Extraction of DNA fragments from agarose gels.....	57
2.3.5 Preparation of electroporation competent bacterial cells.....	57
2.3.6 Sub-cloning restriction fragments into plasmid DNA vectors.....	57
2.3.6.1 Preparation of vectors and restriction fragments.....	57
2.3.6.2 Ligation of restriction fragments in to vector DNA.....	58
2.3.6.3 Transformation of competent bacterial cell by electroporation.....	58
2.3.6.4 Plating of transformed cells.....	58
2.3.7 Determination of DNA concentration.....	59
2.3.8 Plasmid DNA preparation.....	59
2.3.8.1 Small scale preparations .....	59
2.3.8.2 Large scale preparations .....	59
2.3.9 End-filling restriction endonuclease digested DNA .....	59
2.3.10 Automated sequencing of PCR products.....	60
2.3.11 Polymerase Chain Reaction (PCR) .....	60
2.3.12 Preparation of PCR products for cloning .....	60
2.3.13 Yeast two-hybrid screening of cDNA library .....	61
2.3.13.1 Preparation of the PROQUEST™ Two-Hybrid Mouse Embryo 10.5 day cDNA library.....	61
2.3.13.2 Screening the library .....	61
2.3.14 Plasmid transformation into yeast .....	61
2.3.15 Yeast DNA preparation .....	61
2.3.16 Maintaining cultured cell lines .....	62
2.3.17 Transfection of cultured cells with Fugene .....	62

2.3.18 Immunofluorescent analysis of cultured cells .....	63
2.3.19 Cryo-Immunogold Electron Microscopy .....	63
2.3.20 Wortmannin treatment .....	63
2.3.21 Golgi staining with WGA-Alexa Fluor 350 .....	64
2.3.22 Estimation of Fluid-phase endocytosis .....	64
2.3.23 Receptor-mediated endocytosis analysis .....	64
2.3.24 FRAP analysis for membrane microviscosity .....	65
2.3.25 Non-denaturing protein extraction from cultured cells .....	65
2.3.26 Protein concentration: Bradford assay .....	65
2.3.27 Co-Immunoprecipitation .....	66
2.3.28 Protein gel electrophoresis and western blotting .....	66
2.3.29 Protein sample preparation from cultured cells for gel filtration .....	66
2.3.30 Gel filtration .....	67
2.3.31 Protein sample concentration .....	67
2.3.32 Two-dimensional protein electrophoresis .....	67
2.3.32.1 Sample rehydration .....	67
2.3.32.2 Isoelectric focusing (first dimension) .....	68
2.3.32.3 Protein separation on SDS-PAGE (second dimension) .....	68
2.3.33 Coomassie blue staining and silver staining .....	68
2.3.34 Protein recognition .....	69
2.3.35 GST fusion protein expression and purification .....	69
<b>Chapter Three: Functional redundancy between MID1 and MID2? .....</b>	<b>71</b>
3.1 Introduction .....	71
3.2 Results .....	72
3.2.1 MID1 and MID2 heterodimerize .....	72
3.2.2 The normal microtubule-association of MID2 is disrupted in an OS derived cell line .....	73
3.2.3 MID2A358D – a polymorphism or a OS-causative mutation .....	74
3.3 Discussion .....	75
<b>Chapter Four: PEPP2 was identified as a MID2 interactor.....</b>	<b>81</b>
4.1 Introduction .....	81
4.2 Results .....	82
4.2.1 Yeast two-hybrid screen for MID2 interactors .....	82
4.2.2 Identifying the potential interactors .....	84

4.2.3 Validation of the interaction between MID2 and the “positives” identified in the Y2H .....	85
4.2.3.1 NY-CO-3 is unlikely to be a interactor of MID2 .....	85
4.2.3.2 PEPP2 was identified as a potential interactor of MID2 .....	86
4.2.4 The interaction between PEPP2 and MID2 was verified in mammalian cells .....	87
4.2.4.1 Co-localization of MID2 and PEPP2 .....	87
4.2.4.2 Regulation of MID2 and PEPP2 interaction by MID1/MID2 heterodimerization .....	88
4.3 Discussion .....	89
<b>Chapter Five: The cellular function of MID2 and PEPP2 .....</b>	<b>95</b>
5.1 Introduction .....	95
5.2 Results .....	96
5.2.1 The non-uniform distribution of membrane-associated PEPP2 .....	96
5.2.1.1 The membrane-associated PEPP2 is enriched sites of at cell-cell contact .....	96
5.2.1.2 The membrane-association of PEPP2 is directed by phosphoinositide-binding .....	97
5.2.1.3 Membrane-associated PEPP2 is enriched at the actin polymerisation site .....	98
5.2.2 PEPP2 mediates redistribution of MID2 $\Delta$ BB to the Golgi .....	99
5.2.3 MID2/PEPP2 affect membrane microviscosity .....	99
5.2.4 The potential role of PEPP2 and MID2 in regulating endocytosis .....	100
5.2.4.1 The influence of MID2 and PEPP2 on fluid-phase endocytosis .....	101
5.2.4.2 Receptor-mediated endocytosis is affected by an overexpressed MID2 truncating mutation .....	102
5.3 Discussion .....	103
<b>Chapter six: Unpacking MID1/MID2 protein complexes .....</b>	<b>115</b>
6.1 Introduction .....	115
6.2 Results .....	117
6.2.1 Immuno-precipitation of the MID1 protein complexes .....	117
6.2.1.1 1-D electrophoresis of MID1 complexes purified by immunoprecipitation .....	117

6.2.1.2 2-D electrophoresis of MID1 complexes purified by immunoprecipitation .....	117
6.2.2 MID1 and MID2 exist in high molecular weight complexes .....	118
6.2.2.1 Determination of protein complexes using FPLC .....	118
6.2.2.2 MID1/MID2 protein complexes determined by FPLC .....	119
6.2.3 Decoding the MID protein complexes .....	120
6.2.3.1 The presence of Dynein heavy chain in MID1 complexes .....	120
6.2.3.2 Identification of eukaryotic translation elongation factor 1 beta in MID1 complexes .....	121
6.3 Discussion .....	123
<b>Chapter Seven: Final Summary .....</b>	<b>127</b>
<b>Bibliography .....</b>	<b>137</b>

## Amendment

P29, line21: The expression “Microtubules are microfilaments” should be “Microtubules are filaments”

P33, line17: In the sentence “In addition, it is a precursor to generate the most important intracellular secondary messenger, inositol(1,4,5)P<sub>3</sub>, through hydrolysis by phospholipase D (PLD)”, “phospholipase D (PLD)” should be “phospholipase C (PLC)”

P74, line8: “localization of the assessed” should read “localization of the fusion protein assessed”

P74, line19: “missence” should be “missense”

Fig 3.1 B: “Colocalization of GFP-MID1 and MYC-MID2 on microtubules was shown by indirect immuno-fluorescence using monoclonal anti-MYC and a Texas-red conjugated secondary antibody” should be “Colocalization of GFP-MID1 and MYC-MID2 on microtubules was shown by GFP fluorescence and indirect immunofluorescence using monoclonal anti-MYC and a Texas-red conjugated secondary antibody”

Figure 3.3: “Both microtubule-association (A and C) and cytoplasmic clumping (B and D) were observed with GFP-MID2 and GFP-MID1 in OS cells” should be “Both microtubule-association (A and C) and cytoplasmic clumping (B and D) were observed with GFP fluorescence of GFP-MID2 and GFP-MID1 in OS cells”

Figure 3.3: “The heterodimerization between MID2 and MID1 C-terminal truncation mutation was also demonstrated by colocalization (yellow) of a GFP-MID1 $\Delta$ CTD fusion protein and MYC-tagged MID2 in COS1 cells” should read “The heterodimerization between MID2 and MID1 C-terminal truncation mutation was also demonstrated by colocalization (yellow) of a GFP-MID1 $\Delta$ CTD fusion protein (green GFP fluorescence) and MYC-tagged MID2 (red, indirect immunofluorescence using anti-MYC and Texas-red conjugated secondary antibody) in COS1 cells”

Figure 3.4: “Aspartical” should be “Aspartic”

P75, line13: “where heterodimerizations has been observed” should be “where heterodimerizations have been observed”

P75, bottom line: “And consistent with previous data” should read “Consistent with previous data”

P76, line19: “a reflection of the relative recent duplication” should be “a reflection of the relatively recent duplication”

P77, line4: “The OS derived fibroblast cells used carry a 1483C>T nonsense mutation” should read “The OS derived fibroblast cells carry a 1483C>T nonsense mutation”

P77, line 21: “aggaregates” should be “aggregates”

P79, line6: “dimerization of MID2A358D and MID1/MID2 in yeast two-hybrid system” should read “dimerization of MID2A358D and MID1/MID2 in a yeast two-hybrid system”

P82, line20: “were screened by the expression of *HIS3* gene” should read “were screened for the expression of the *HIS3* gene”

P83, line11: “comparison” should be “comparisons”

Figure 4.2: “Repeated attempts gave the same results and the positive phenotype of the yeast colonies were assumed to be false positives” should read “Repeated attempts gave the same results and the yeast colonies were assumed to be false positives”

Figure 4.5 B: “full-length mNYCO3 does not interact with MID2 when is expressed” should read “full-length mNYCO3 does not interact with MID2 when it is expressed”

Figure 4.7: “The sequences alignments” should be “The sequence alignments”; “covered the ~75% of the C-terminal end of the of mPEPP2” should read “covered ~75% of the C-terminal end of mPEPP2”

Figure 4.8: “to monitor the expression of URA3 reporter” should read “to monitor the expression of the URA3 reporter”

P89, line10: “can not exclude weak interaction” should read “can not exclude a weak interaction”

P89, line12: “was recognized as” should be “were recognized as”

P89, line13: “may due to” should be “may be due to”

P89, line18: “mediam” should be “medium”

P89, line19: “medium” should be “media”

P90, line22: “results from both in yeast two-hybrid and indirect immunofluorescence” should read “results from both yeast two-hybrid and indirect immunofluorescence”

P90, line24: “suggesting” should be “suggest”

P91, Figure 4.13: “has been shown interaction with MID2” should read “has been shown to interact with MID2”

P93, line7: “the cellular localization of PEPP2, which may be critical for its function” should read “the cellular localization of PEPP2 may be critical for its function”

P93, line10: “These data also support a modifying role for potential MID2 in the presentation of OS” should read “These data also support a modifying role for MID2 in the presentation of OS”

P99, line10: “However, this Golgi localization of GFP-MID2 $\Delta$ BB” should read “This Golgi localization of GFP-MID2 $\Delta$ BB”

P100, line5: “The same analysis were performed” should be “The same analysis was performed”

Figure 5.6: “Nuclei was shown by DAPI staining” should be “Nuclei were shown by DAPI staining”

Table 5.1 and Table 5.2 “A small area (~ um range)” should read “A small area (~um in diameter)”

P101, line5: “interation” should be “interaction”

P101, line22: “post-nuclear cell lysate has been verified” should read “post-nuclear cell lysate was verified”

Table 5.3 “Fluid-phase endocytosis were increased” should be “Fluid-phase endocytosis was increased”

P103, line5: “slowing growing ends” should be “slow growing ends”

P103, line9: “which are comprise of two chains of global monomers” should read “which comprise two chains of global monomers”

P104, line24: “Given the interaction between” should read “Given that the interaction between”

P105, line11: “transmission electron microscope” should be “transmission electron microscopy”

P105, line14: “given overexpressed PEPP2 enhances the Golgi localization” should read “given that overexpressed PEPP2 enhances the Golgi localization”

P118, line1: “poly-acrilamide” should be “polyacrylamide”

Figure 6.1: “A protein of the similar molecular weight” should be “A protein of similar molecular weight”

Figure 6.2 should be in color (see attached)

Figure 6.5: “GFP fusion protein in these fractions were detected” should be “GFP fusion protein in these fractions was detected”

Figure 6.8 and Figure 6.9: “The overexpressed GFP-MID1 (~110kDa, PI6.3) and GFP-MID1 $\Delta$ CTD (~86kDa, PI6.0) were not definitive” should read “The overexpressed GFP-MID1 (~110kDa, PI6.3) and GFP-MID1 $\Delta$ CTD (~86kDa, PI6.0) were not clearly evident as defined spots”



P124, line6: “than does MYC-tagged form” should be “than does the MYC-tagged form”

P132, line1: “Interstingly,” should be “Interestingly,”

P132, line15: “the latter of which regulates actin” should read “the last of which regulate actin”

## Chapter One: General introduction

Human congenital disorders impose a large impact not only on the affected individuals and their immediate families but also on communities, often inflicting great healthcare burdens. This thesis concentrates on one congenital disorder, Opitz Syndrome, which is a genetic disorder caused by mutations in *MIDI*. Opitz Syndrome (OS) patients present an array of clinical features including some of the more commonly found congenital structural anomalies, such as cleft lip and palate and hypospadias. The information gained from an enhanced understanding of the important cellular and molecular processes and pathways involved in Opitz Syndrome will subsequently aid in the elucidation of the basis of the individual clinical features. Only through an increased understanding of the underlying mechanisms of these congenital malformations can advances be made in prevention, diagnosis and ultimately treatment of them.

### 1.1 Opitz syndrome or BBBG syndrome

Opitz *et al.*, 1965 first reported a syndrome of hypospadias and hypertelorism in 1965. He later called it BBB syndrome and also described the G syndrome with apparent hypertelorism, epicanthal folds, hypospadias, and laryngotracheo-esophageal defects (Opitz *et al.*, 1969ab). Dysphagia was considered specific to the G syndrome, while the characteristic anomalies of the nose and more commonly mentioned mental retardation were reported in the BBB syndrome. In 1989, Opitz *et al.* 1989 described a nephew of the propositus in one of the original BBB families who was affected with G syndrome. Around the same time, Verloes *et al.*, 1989 reported on a family where the propositus had G syndrome, including laryngeal cleft, and another relative had facial anomalies typical of the BBB syndrome. Since these observations suggested that these two

different syndromes were in fact the same condition, they were subsequently grouped and named Opitz syndrome or BBBG syndrome.

The clinical features of Opitz syndrome include a variable array of abnormalities but generally with a characteristic facial gestalt (Figure 1.1), that often consists of hypertelorism/telecanthus, prominent nasal bridge or depressed nasal root, mild micrognathia and posteriorly angulated ears with abnormal helices. Structural anomalies of the lip, palate, larynx, trachea and esophagus are also frequently present. Other defects in OS patients include congenital heart defects, inguinal and umbilical hernias, cryptorchidism and imperforate/anteriorly displaced anus (McDonald-McGinn *et al.*, 1995). CNS anomalies, e.g. psychomotor delay and mental retardation, have also been reported (Guion-Almeida *et al.*, 1992; MacDonald *et al.*, 1993). In considering the developmental processes that form the various structures affected in OS patients, including the midface, external genitalia and heart, a defect in tissue fusion and/or remodeling seems the most plausible explanation (Schweiger and Schneider, 2003ab; Cox, 2004;)

## **1.2 Genetics of Opitz syndrome**

### ***1.2.1 Opitz syndrome is heterogenous***

Opitz syndrome is genetically heterogeneous with both X-linked and autosomal loci confirmed by linkage analysis and cytogenetic anomalies. The linkage and breakpoint data suggested that the gene responsible for the X-linked form of OS resided at Xp22.3. The study of a large french family, in which the OS phenotype co-segregated with a pericentric inversion of the X chromosome,  $inv(X)(p22.3q26)$ , provided the first definitive evidence for an X-linked form of OS (Verloes *et al.*, 1995). Confirmation of an Xp22.3 locus came from linkage studies in OS families, with linkage to *DXS987*

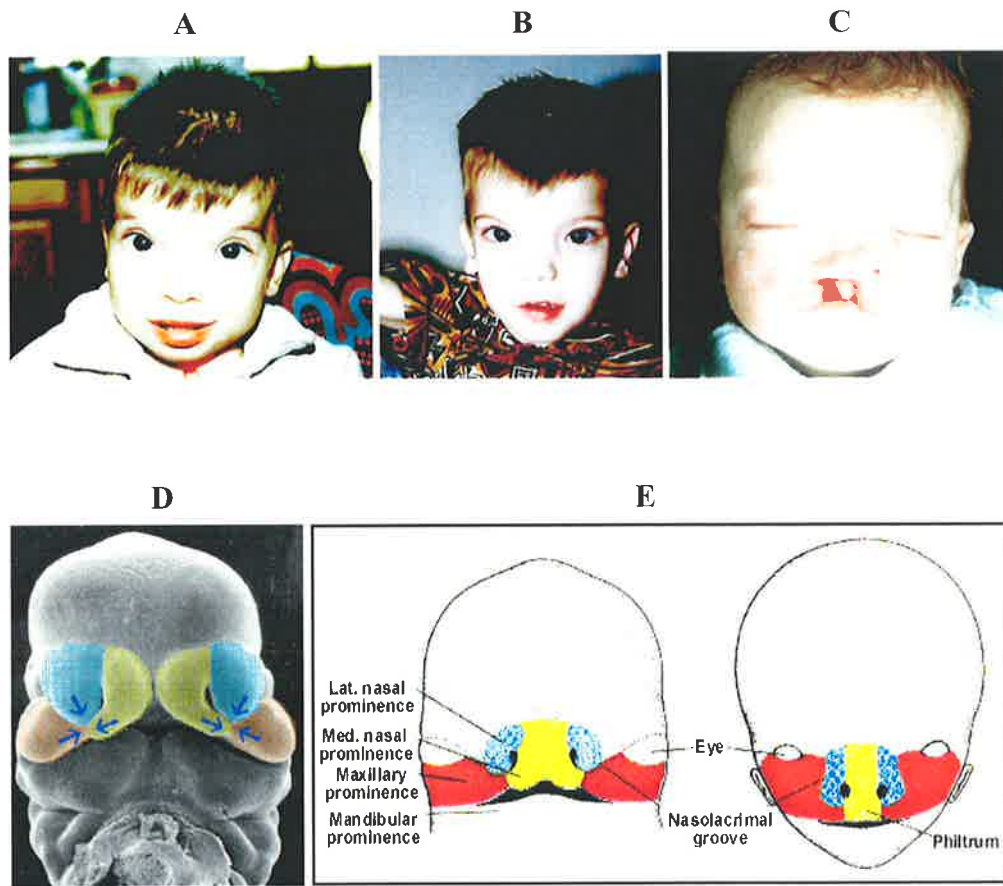


**Figure 1.1 Craniofacial presentation in Opitz Syndrome.**

The craniofacial abnormalities seen in OS include hypertelorism, a prominent nasal bridge or depressed nasal root, and posteriorly angulated ears (A and B). Structural anomalies of the lip are common in more severe cases (C).

Normal development of the midface (D) depends on the proper union of the **medial nasal prominences** with the **lateral nasal prominence** and **maxillary prominence** at ~ 5 weeks gestation. Different growth rates of each of these prominences are critical determinants of midfacial morphology. The contributions of each of these prominences to the final facial forms is indicated in colours in (E). Defects in this morphogenetic process result in facial anomalies, such as those seen in OS. Picture obtained from the web site of the School of Medicine, University of North Carolina ([http://www.med.unc.edu/embryo\\_images/](http://www.med.unc.edu/embryo_images/)).

demonstrated in three families (Robin *et al.*, 1995) and to *DXS7104* in Xp22 in a separate family (May *et al.*, 1997).

Male-to-male transmission in a few reported OS families also suggested the existence of an autosomal dominant form (Farndon *et al.*, 1983; Stoll *et al.*, 1985). Thereafter, linkage studies in OS families revealed an autosomal locus on 22q11.2 (Robin *et al.*, 1995). In one case (McDonald-McGinn *et al.*, 1995), a deletion of approximately 2 Mb was found to start between D22S427 and D22S36 and which extended to the HCF2 locus (see Figure 1.3). Deletion of the overlapping region on 22q11.2 has also been found in other syndromes with shared clinical features, such as DiGeorge syndrome (DGS), velo-cardio-facial syndrome (VCFS), and conotruncal anomaly face syndrome (CAFS) (Scambler, 2000). Their phenotypes will be discussed further in the following section. Other autosomal loci have also been implicated by cytogenetic anomalies in individual OS cases, including del (13q32.3-13qter) (Urioste *et al.*, 1995), dup (5p12 – 13) (Leichtman *et al.*, 1991) and the unbalanced der (3) t (3; 14)(q29; q11.2), -14 (Kurczynski *et al.*, 1998), although none have been confirmed by linkage studies.

### ***1.2.2 OS cases with different genetic defects are clinically indistinguishable***

There is insufficient clinical evidence to differentiate between X-linked and autosomal dominant forms of OS. Confounding this has been the significant inter-individual phenotypic variability with even male relatives that inherit an identical X-linked mutation presenting differently (Cox *et al.*, 2000; So *et al.*, 2004). It is believed that this variability in presentation is influenced largely by other genetic and/or environmental factors.

From the latest review by So *et al.*, 2004 the more common features in *MIDI* mutation positive OS patients include: a characteristic facial gestalt (widely-spaced eyes [98%],

low-set ears [45%]), cleft lip and palate [50%], laryngotracheo-oesophageal (LTE) defects including LTE clefting [50%], significant structural heart defects [22%], genital anomalies (hypospadias [72%]), and developmental delay [42%]. Although studies have been unable to phenotypically distinguish the X-linked and autosomal forms (Robin *et al.*, 1996), a recent study indicates that MID1 mutation positive cases show a significantly higher incidence of cleft lip and/or palate (CLP), LTE anomalies and hypospadias than mutation negative cases, which in contrast have a slightly higher incidence of cardiac structural defects (So *et al.*, 2004). However, it should be noted that the overall incidence of cardiac defects in both forms of OS is likely to be underestimated, since dysphagia (difficulty in swallowing due to constriction of the oesophagus by aberrant remodelling of cardiac tissue during embryogenesis) is a common, and yet likely under-diagnosed, feature. Nevertheless, the slightly higher incidence of congenital heart defects in mutation negative cases may reflect the contribution of the principal autosomal OS locus (22q11.2), which is likely to be encompassed by the region commonly deleted in the “22q11 deletion syndrome” that accounts for approximately 5% of all congenital heart defects (Glover, 1995; McDonald-McGinn *et al.*, 2001).

### ***1.2.3 The OS phenotype represents a defect in tissue fusion and/or remodelling during early development***

As mentioned earlier, Opitz syndrome is characterized by craniofacial anomalies such as cleft lip/palate, urogenital (hypospadias) and congenital heart defects (primarily defects in cardiac septation and vascular remodeling). Each of these malformations also occur with high incidence as isolated birth defects and therefore may reflect a commonly used developmental mechanism. Indeed, developmental studies support a

common cellular basis for these abnormalities that likely involves cell programming and/or tissue fusion (Figure 1.2).

### **1.3 Comparison of OS with other 22q11.2 deletion syndromes**

#### ***1.3.1 The clinical features of the 22q11.2 deletion syndrome***

The overlapping clinical features of the 22q11.2 deletion syndrome, which includes OS, DGS, VCFS and CAFS, are well described by the CATCH22 acronym (Cardiac defects, Abnormal facies, Thymic hypoplasia, Cleft palate, Hypocalcemia and 22q11.2 anomalies). Conotruncal heart defects are common in DGS/VCFS. However, patent ductus arteriosus (a type of heart lesion), which is rarely found in these two groups, is commonly seen in OS. In addition, some prominent manifestations of OS, such as hypertelorism, cleft lip, laryngotracheal abnormalities, dysphagia, and hypospadias are not commonly observed in DGS/VCF (Robin *et al.*, 1996). The differences in these phenotypes (which can share a common genetic lesion) may well be explained by factors other than the size of the deletion, such as genetic background, environment and other modifying genes during development.

#### ***1.3.2 Potential causative genes for the 22q11.2 deletion syndrome***

The majority of patients with 22q11.2 deletion syndrome have a similar 3-Mb deletion (Figure 1.3), the typical deleted region (TDR) (Edelmann *et al.*, 1999). Further studies of patients with atypical deletions of 22q11.2 was done in order to establish the shortest region of deletion overlap. Comparison of terminal deletions and translocations confirmed a ~750kb overlap—DiGeorge syndrome chromosomal region (DGCR), and a ~150kb minimal DGCR (MDGCR) in the proximal region of the DGCR (Scambler, 2000).

To date, over 30 genes have been identified in the TDR. However, despite extensive investigations, none of these genes by themselves are likely to be responsible for all of the features of the clinical phenotype of patients hemizygous for 22q11.2. Studies in patients with atypical deletions, which have no overlap with the MDGCR or even with the TDR, indicate that the haplo-insufficiency in 22q11.2 could be influenced by long-range effects of genes outside the region. Therefore, it is noteworthy that *UbcH7* (described in section 1.5.5), which is located immediately distal to the DGCR, has been implicated in the molecular pathways underlying the pathogenesis of OS.

A number of genes in the DGCR, such as *Tbx1* and *UFDIL*, have received considerable attention because of their appropriate expression as well as functional data that support their involvement. The *Tbx1* gene is located at the centre of the TDR. It encodes a member of the T-box family of transcription factors. Whole-mount *in situ* hybridisation in mouse embryos has shown that *Tbx1* is expressed in the mesodermal core of pharyngeal arches and in mesenchyme surrounding the neural tube at E9.5 and is expressed along the third aortic arch artery and in the mesodermal core of the third pharyngeal arch at E10.5 (Garg *et al.*, 2001). Subsequent studies have revealed that the expression of *Tbx1* is under the regulation of Sonic hedgehog (*Shh*), which is necessary for normal craniofacial development (Garg *et al.*, 2001).

*UFDIL*, which is located at the region adjacent to the MDGCR, has also been considered as a contributory gene for the 22q11.2 deletion syndrome due to its expression in the branchial arches, frontonasal mass and outflow tract of the heart (Pizzuti *et al.*, 1997) and since functional knockdown of *UFDIL* in chicken embryos also demonstrated an increased incidence of conotruncal septation defects (Yamagishi *et al.*, 2003). Although mutation screens in 39 non-deletion DGS/VCFS patients did not reveal any mutations in the *UFDIL* coding region, a polymorphism located in the



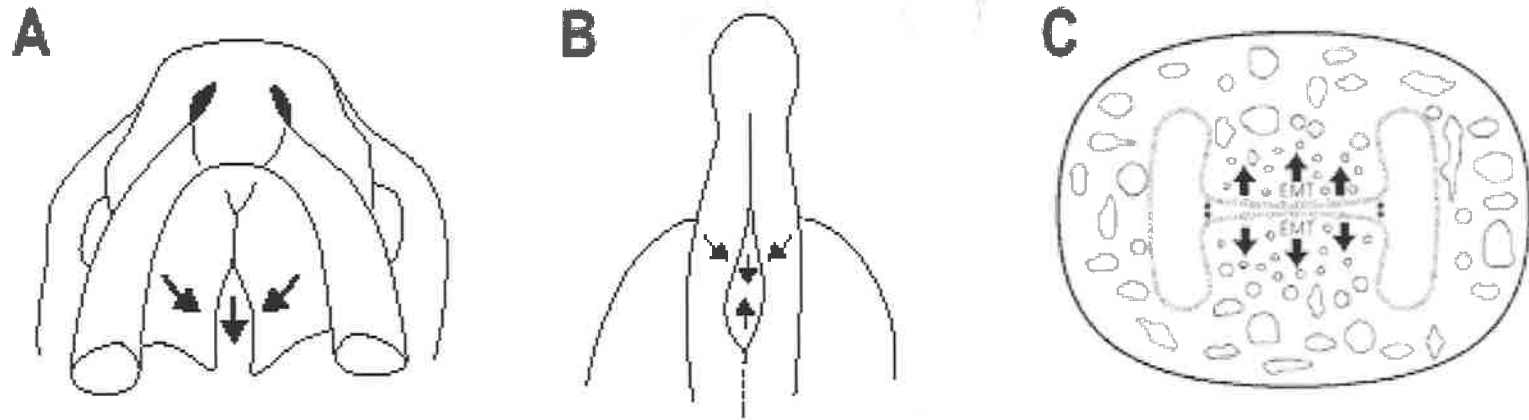


**Figure 1.2 Major morphogenetic events during human embryogenesis involve tissue fusion and/or remodelling.**

Formation of the lip/palate (A), male external genitalia (B), and cardiac septa (C) require fusion of epithelial-lined tissue and epithelial to mesenchymal transdifferentiation (EMT) to subsequently remove the bilayered epithelial seam. The process of EMT begins with activation of epithelia/endothelia (i.e. disruption of cell-cell adhesion) followed by their conversion to a mesenchymal fate (i.e. a migratory cellular phenotype)

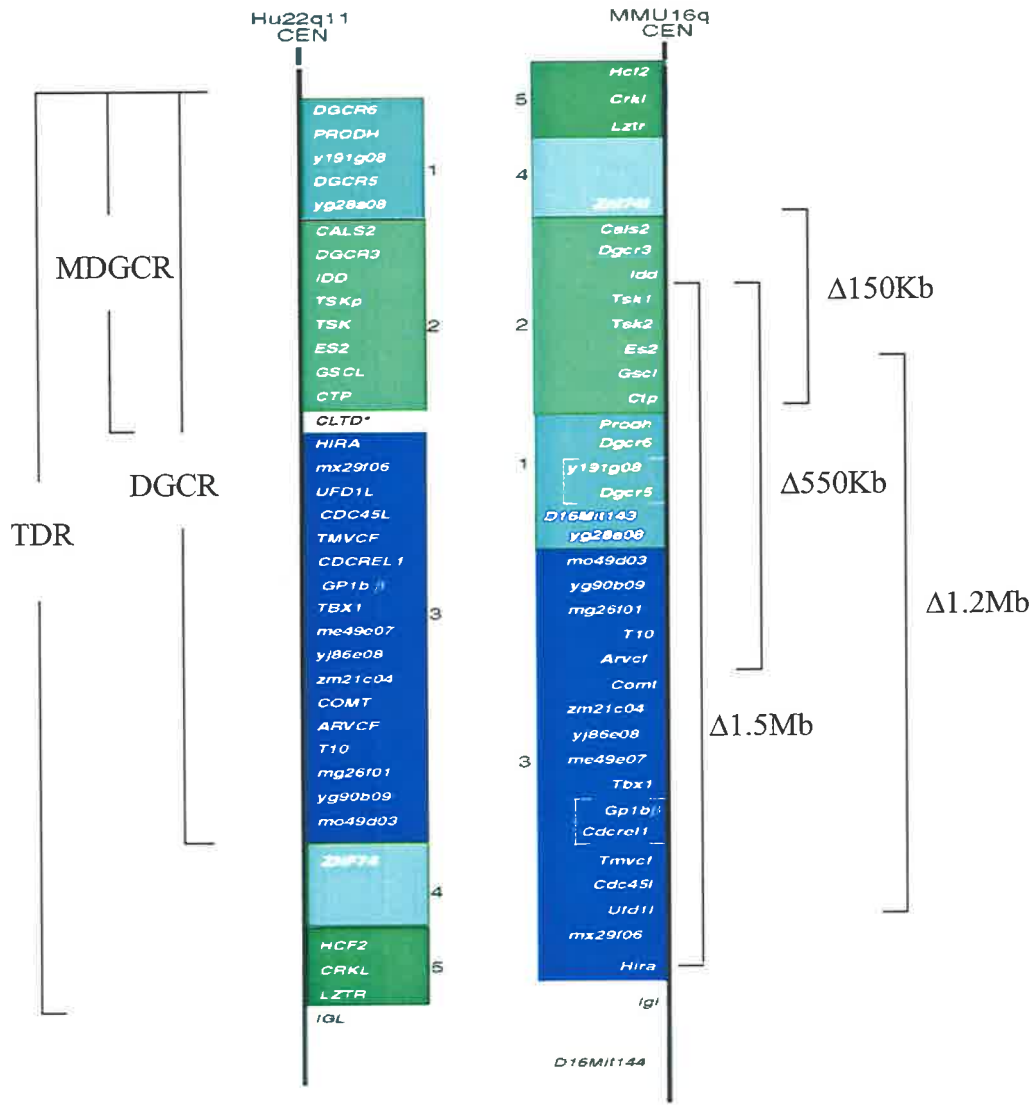


**Figure 1.3 Schematic representation of genes in the DGCR and the syntenic region of mouse chromosome 16 (MMU16).**

The typically deleted region (TDR), the minimal DiGeorge chromosomal region (MDGCR), and the genes deleted in the mentioned knockout mice are as indicated. The overlapping region deleted in autosomal OS is indicated by a thick black line. All protein-encoding genes, except *CLTD*, have a counterpart on MMU16, although a number of intrachromosomal rearrangements have been observed, as highlighted in different colors and numbers. Figure was edited from Scambler, 2000.

promoter region, -227A/G, has been found associated with the schizophrenia subtype of DGS/VCFS (Wadey *et al.*, 1999; De Luca *et al.*, 2001).

Mice hemizygous for different deletions in the TDR display a normal phenotype or cardiovascular abnormalities only. Mice hemizygous for either a conventional ~ 150 kb deletion of seven genes from *Znf741* to *Ctp* or a ~ 550 kb deletion spanning from *Idd* to *Arvcf* were apparently normal (Kimber *et al.*, 1999; Puech *et al.*, 2000). An even larger (~ 1.2 Mb) hemizyosity, however, resulted in fetal cardiovascular defects similar to those seen in DGS/VCFS patients (see Figure 1.3) (Lindsay *et al.*, 1999).

Of interest, the *Tbx1* null mice exhibited cardiac anomalies most similar to that seen in the human syndrome, e.g. cardiac outflow tract anomalies, hypoplasia of the thymus and parathyroid glands and abnormal facial structures (Jerome and Papaioannou, 2001). Further study of the mouse *Tbx1* gene knockout indicated disrupted signals derived from pharyngeal arch endoderm and/or mesoderm that ultimately affect neural crest cell differentiation and survival in the arches (Vitelli *et al.*, 2002). The exogenous *Tbx1* could also partially rescue the vascular anomalies seen in a 1.5 Mb DGCR knockout mice (Merscher *et al.*, 2001). However, deletions without interrupting *Tbx1* have been found in CATCH22 patients and no mutation of *Tbx1* has been found in non-deletion patients indicating the story is far from complete. All these investigations suggest that haplo-insufficiency of more than one gene, or genes adjacent to the deletion region, might control the presentation of the 22q11.2 deletion phenotype.

## **1.4 Identification of *MID1* as the causative gene in X-linked OS**

### ***1.4.1 Identification of *MID1* mutations in OS***

Using a positional cloning approach, a gene was identified that spanned the Xp22.3 breakpoint region from the original family where a pericentric inversion segregated with

the OS phenotype (Quaderi *et al.*, 1997; Van den Veyver *et al.*, 1998). This gene was named *MIDI* based on its predicted role in midline development. However, it is also known as *FXY*—ring finger on X and Y, since its mouse homologue spans the pseudoautosomal boundary and therefore in this species also has part of the gene duplicated on the Y chromosome.

*MIDI* mutations identified in unrelated affected individuals confirmed that *MIDI* is responsible for the X-linked form of OS. To date, 36 different mutations (Figure 1.4) have been found in sporadic and familial OS cases (Cox *et al.*, 2000; De Falco *et al.*, 2003; So *et al.*, 2004). Interestingly, in a case with no detectable ORF mutation, haplotype data supported the notion that mutations in non-coding regions that affect the expression of *MIDI* may also be present in some cases (Cox *et al.*, 2000). This hypothesis was further supported by the finding of a premature stop codon in one case that was due to a duplication of the first exon of the *MIDI* gene, a mutation that was not detected by routine exon amplification during screening of mutations in the open reading frame (Winter *et al.*, 2003). In summary, *MIDI* mutations are scattered throughout the gene, although more are represented in the 3' region (Figure 1.4). Missense and nonsense mutations, deletions, splice-acceptor and frame-shift mutations have all been found with most resulting in truncated protein products. These findings suggest that loss-of-function of *MIDI* is the mechanism underlying the pathogenesis of OS (Cox *et al.*, 2000).

#### **1.4.2 The expression pattern of *MIDI* also supports a OS candidate gene**

In chick, mouse, and human, *MIDI/Midl* is expressed ubiquitously throughout embryogenesis although at varying levels depending on the tissue and cell type. Notably, the highest levels of expression are found in the developing CNS, craniofacial

complex and in the region of the developing external genitalia. In the developing face of the above mentioned species, expression is strongest in the ectoderm but also detectable in the proliferating mesenchyme that underlies epithelia preparing for contact and fusion (Dal Zotto *et al.*, 1998; Richman *et al.*, 2002). Fetal kidney and lung were also found to highly express *MID1*, while the fetal liver showed a relative low level of *MID1* expression. The developing heart (E10.5), which was reported negative for *Mid1* expression in the original *in situ* hybridisation studies on mouse embryos (Dal Zotto *et al.*, 1998), has since been found to express *Mid1* at low levels as detected by the expression of beta-galactosidase following knock-in of the *LacZ* gene into the *MID1* locus and therefore under the control of the native promoter (Jaafar *et al.*, unpublished). This finding is consistent with the recent *in situ* studies of *MID1* expression in both chick and human embryos (Richman *et al.*, 2002; Pinson *et al.*, 2004) and in line with the defects in this organ seen in affected humans.

## 1.5 Characterization of MID1

*MID1* encodes an RBCC (RING-Finger, B-Box and Coiled-Coil) protein with Fibronectin type III and B30.2 domains at the C-terminus, as shown schematically in Figure 1.4.

### 1.5.1 The RBCC protein family

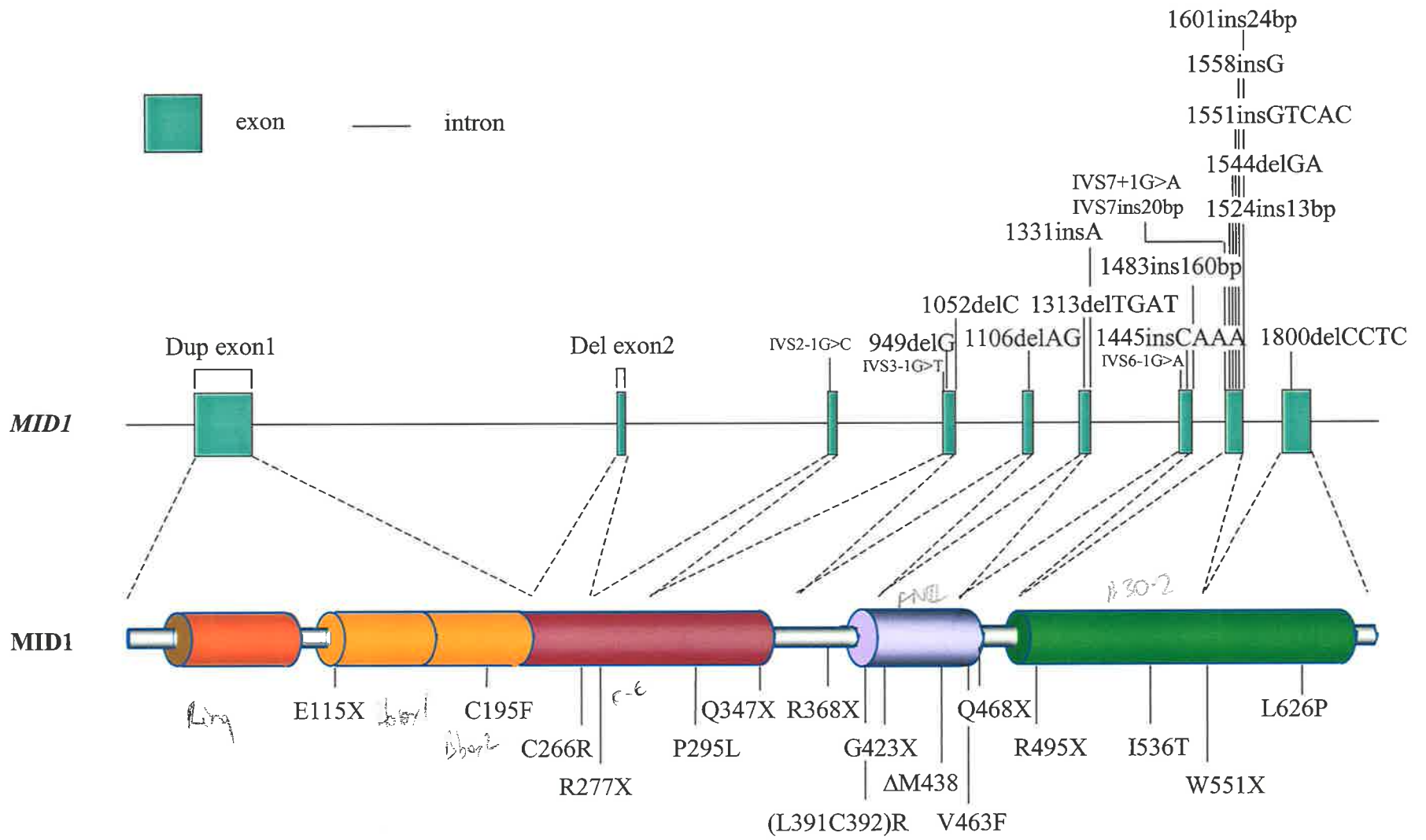
The RBCC family is a growing protein family that includes over 50 members such as, RFP, AFP, PML, KAP-1 and *MID1* (Reymond *et al.*, 2001). Some of the RBCC proteins have been implicated in disease processes, such as PML, RFP and TIF1 in tumourigenesis and *MID1* in X-linked OS, but only a few have been characterised in any detail.

The tripartite RBCC domain is exclusively found at the NH<sub>2</sub>-terminus of members of this protein family. The consensus of the RING-finger domain contains seven conserved cysteine residues and a single conserved histidine residue: CI-X<sub>2</sub>-C<sub>2</sub>-X<sub>(9-39)</sub>-C<sub>3</sub>-X<sub>(1-3)</sub>-H<sub>1</sub>-X<sub>(2-3)</sub>-C<sub>4</sub>-X<sub>2</sub>-C<sub>5</sub>-X<sub>(4-48)</sub>-C<sub>6</sub>-X<sub>2</sub>-C<sub>7</sub> (Henry *et al.*, 1998). These 8 conserved residues bind two zinc atoms in a cross-brace system (Borden, 2000). The B-box is also a cysteine-rich zinc-binding motif (C<sub>1</sub>-X<sub>2</sub>-H<sub>1</sub>-X<sub>7</sub>-C<sub>2</sub>-X<sub>7</sub>-C<sub>3</sub>-C<sub>4</sub>-X<sub>5</sub>-H<sub>2</sub>-X<sub>2</sub>-H<sub>3</sub>) found in the majority of RBCC proteins and is thought to independently fold into a globular domain (Borden, 1998). Several variations in this core zinc-binding motif were first described in PML and were referred to as B-box1 (C<sub>1</sub>-X<sub>2</sub>-C<sub>2</sub>-X<sub>7-10</sub>-C<sub>3</sub>-X<sub>2</sub>-C<sub>4</sub>-X<sub>4-5</sub>-C<sub>5</sub>-X<sub>2</sub>-C<sub>6</sub>/H<sub>1</sub>-X<sub>3-6</sub>-H<sub>2</sub>-X<sub>2-8</sub>-H<sub>3</sub>) and B-box2 (C<sub>1</sub>-X<sub>2-4</sub>-H<sub>1</sub>/C<sub>2</sub>-X<sub>4-9</sub>-C<sub>3</sub>-X<sub>2</sub>-C<sub>4</sub>/H<sub>2</sub>-X<sub>4</sub>-C<sub>5</sub>/H<sub>3</sub>-X<sub>2</sub>-C<sub>6</sub>/H<sub>4</sub>) (Torok and Etkin, 2001). RBCC proteins can possess one or both B-boxes that are adjacent to each other. The final motif, the leucine-rich coiled-coil domain, is comprised of spaced hydrophobic residues and is predicted to form an extended  $\alpha$ -helical region (Reymond *et al.*, 2001). The relative spacing between the RING, B-box and coiled-coil motifs is conserved, suggesting that the interaction between them is important for protein function.

Despite some distinct roles and varied subcellular localizations, all RBCC proteins are thought to act as scaffolds for the assembly of larger multiprotein complexes (Reymond *et al.*, 2001). Each of these domains has been implicated (either directly or indirectly) in mediating protein-protein interactions. Recent studies on Rfp demonstrate that although the B-box motif is not providing a protein-protein interaction interface, it is important for the correct orientation of the RING and Coiled-Coil domains (Torok and Etkin, 2001). However, in MID1, the B-box does provide the interface for protein-protein interaction (Short *et al.*, 2002). More consistently, the RING-finger motif has been found to function in protein-protein interactions and in many instances, such as PML

**Figure 1.4 Schematic representation of the MID1 gene and protein product with the relative positions of mutations found to date in OS patients.**

The MID1 domains—RING-Finger, B-Box1, B-Box2, Coiled-Coil, FNIII and B30.2, are presented with the colored columns from left to right. The regions encoded by each exon of the *MID1* gene are as indicated. Most of the mutations are nonsense mutations and frameshift mutations clustered in the C-terminal region of MID1 and result in truncated protein products. Mutations found in the non-coding sequences in *MID1*, such as splice variants and a duplication of exon1 that results in premature stop codon, are shown on the gene structure image; whereas missense and nonsense changes are indicated only at the protein level.





and Efp, affects subsequent protein stability, which is further discussed in 1.6.5 (Jackson *et al.*, 2000). The Coiled-Coil motif constitutes the interface for oligomerization, which has been found with almost all RBCC proteins (Reymond *et al.*, 2001). For example, the proteins of the TIF family—KAP-1, TIF1a and TIF1r, exist in a homo-oligomeric state (Peng *et al.*, 2002). MID1 also forms homodimers and the Coiled-Coil domain has been found both necessary and sufficient for this dimerization (Cainarca *et al.*, 1999). In most of the cases, oligomerization is a prerequisite for the subsequent formation of high order protein complexes. To highlight this, oligomerization of PML is important for the interaction with p53 and pRB and the oligomerization of KAP-1 is necessary for KAP-1/KRAB/DNA complex formation (Jensen *et al.*, 2001; Peng *et al.*, 2002).

### ***1.5.2 The B30.2 domain***

The B30.2 domains are found at the C-terminus of over half of the RBCC proteins. The B30.2 domain was named because of its homology to the coding potential of an identified exon (B30.2) from the MHC class I region on chromosome 6p21.3 (Vernet *et al.*, 1993). This domain is globular in nature and consists of about 170 amino acids. It comprises the C-terminal part of three different types of proteins: RBCC proteins, IgV and IgC1 containing proteins and two unclassified lethal proteins, stonustoxin  $\alpha$  and  $\beta$  (Henry *et al.*, 1998). In fact, the B30.2 domain is the only known domain found in transmembrane proteins, intracellular proteins and secreted proteins, although its exact function remains unclear (Henry *et al.*, 1998).

Proteins possessing B30.2 domains have been reported to be involved in autoimmune diseases and developmental disorders, such as systemic lupus erythematosus (SLE) (Itoh *et al.*, 1991) and OS. The SPRY domain which has been identified as a subdomain

within the B30.2-like domain, has been classified as an immunoglobulin-like fold (Seto *et al.*, 1999).

### ***1.5.3 The cellular localization of MID1***

Both endogenous MID1, detected by indirect immunofluorescence, and overexpressed GFP-MID1 fusion protein (or other tagged forms) co-localize with microtubules throughout cell cycle in all cell types tested (Cox *et al.*, 2000; Schweiger *et al.*, 1999). This microtubule-association of MID1 has also been confirmed by cell fractionation (Schweiger *et al.*, 1999). The physiological function of the microtubule-associated MID1 is unclear. Results from Schweiger *et al.*, 1999 suggested that overexpression of MID1 protects microtubules from colcemid-induced depolymerization (Schweiger *et al.*, 1999). However, similar protection was not seen by Cainarca *et al.*, 1999 in vinblastine-induced depolymerization (Cainarca *et al.*, 1999). The contradictory results might be due to differences in the mechanisms of action of the depolymerizing drugs. However, at physiological levels, MID1 is unlikely to significantly affect microtubule dynamics based on the following observations: no difference in microtubule stability was seen between OS embryonic fibroblast cells and control cells following treatment with colcemid/nocodazole; and overexpression of mutant MID1 did not affect the microtubule distribution in COS7 cells (Cainarca *et al.*, 1999; Schweiger *et al.*, 1999).

As mentioned previously and consistent with a number of other investigated RBCC proteins, MID1 likely functions in an oligomeric form and that the coiled-coil domain is necessary for both microtubule-association and oligomerization. However, intriguingly, altered cellular localisation has been seen upon overexpression of nearly all domain-specific deletions of MID1 (Short *et al.*, 2002). Unlike tagged MID1 $\Delta$ RF that only minimally affects microtubule coverage, MID1 $\Delta$ BB, MID1 $\Delta$ FNIII and MID1 $\Delta$ CTD

formed cytoplasmic clumps/aggregates with variable cellular distributions. In contrast, the Coiled-coil mutant, MID1 $\Delta$ CC, was distributed diffusively in the cytoplasm, consistent with the observation that this same mutant had lost its ability to dimerize in the yeast two-hybrid system, while the other mentioned domain-specific deletions still did. As expected, two OS-associated MID1 missense mutations, C266R and I536T, which didn't affect the Coiled-Coil domain, also maintained their ability to homo-interact (Schweiger *et al.*, 1999).

Of note, the aggregates of overexpressed GFP-MID1 $\Delta$ BB and GFP-MID1 $\Delta$ FNIII still appear to associate with microtubules, consistent with the altered microtubule-association observed for the overexpressed OS-associated mutation, MID1 $\Delta$ M438 (deletion of a single Met codon in the FNIII domain) (Schweiger *et al.*, 1999). So far, overexpression of all the tested OS causative MID1 mutants, including MID1C266R, MID1E115X, MID1delExon2, MID1R368X and MID1L626P, displayed altered cellular distribution (Cainarca *et al.*, 1999; Cox *et al.*, 2000), suggesting that complete microtubule coverage by MID1 is important for its proper cellular function. Since microtubules are involved in many cellular processes including the regulation of cell proliferation, cell migration, signal transduction and organelle trafficking (which will be further discussed in section 1.7), a role for MID1 in any of these processes could be envisaged.

#### ***1.5.4 Protein interactors of MID1***

As mentioned above, RBCC proteins are thought to act as scaffolds to facilitate formation of large protein complexes, a conclusion consistent with data obtained for MID1 (Schweiger *et al.*, 1999). In order to shed light on the subcellular function of

MID1, a number of groups, including our own, set out to identify the protein interactors in these MID1 complexes.

A mammalian homologue of yeast Tap42, called Alpha4, was identified independently by a few groups as a strong interactor of MID1 (Liu *et al.*, 2001; Trockenbacher *et al.*, 2001; Short *et al.*, 2002). Alpha 4 is recognized as a unique regulatory subunit of PP2-type phosphatases (e.g. PP2A) and in yeast, is a key component of the rapamycin-sensitive (TOR) signaling pathway. Mammalian TOR, like its yeast counterpart, is a protein kinase whose activity is increased in response to mitogenic and nutritional signals. In yeast, activation of TOR leads to enhanced phosphorylation of Tap42, which in turn increases its affinity for the catalytic subunit of PP2A (PP2Ac)/SIT4. The association of Tap42-PP2Ac/SIT4 lowers the catalytic activity of PP2Ac/SIT4 and in turn, affects many and diverse cellular functions, such as gene transcription, cell cycle progression and cellular morphology (Inui *et al.*, 1998; Harris *et al.*, 1999).

As one of the most abundant cellular serine/threonine phosphatases in mammalian cells, the activity of PP2Ac is also regulated by a regulatory A subunit (PR65). The interaction between the A subunit and a variety of regulatory B subunits directs the catalytic activity of PP2Ac towards different downstream targets, such as Cdc2/Cdc25 that governs the G2/M cell cycle transition,  $\beta$ -catenin in Wnt signalling, and a number of kinases, including MEK1 and ERK-family kinases (Janssens and Goris, 2001). The interaction between Alpha4 and PP2Ac interferes with PP2Ac binding to the A subunit/PR65, thus preventing its involvement in signalling pathways other than those regulated by the TOR pathway as mentioned above (Janssens and Goris, 2001). Recent studies also suggested that PP2Ac is involved in membrane trafficking by regulating the phosphorylation of a number of trafficking and cytoskeletal proteins (Friant *et al.*, 2000; Varlamov *et al.*, 2001; Guatimosim *et al.*, 2002; Smith, 2002).

Like PP2Ac, both endogenous and overexpressed Alpha4 is found throughout the cytoplasm, although in some cells overexpressing Alpha4, faint microtubule-association can be seen (Short and Cox, unpublished data). However, when the levels of MID1 are not limiting (i.e. when MID1 is overexpressed), Alpha4 is readily recruited onto microtubules (Liu *et al.*, 2001; Short *et al.*, 2002). It is therefore likely that MID1 at physiological levels tethers a proportion of Alpha4 to the microtubules. In doing so, MID1 could affect the local (microtubule-directed) activity of PP2-type phosphatases. Alternatively or additionally, the Alpha4-MID1 interaction may direct PP2A phosphatase activity to specific targets on microtubules. Evidence, however, supports the former (Troddenbacher *et al.*, 2001). An important *bona fide* role for the MID1-Alpha4 interaction is further supported by the finding of a putative mutation in the promoter region of *Alpha4* identified in a patient with a novel syndrome, with dysmorphic features not unlike those seen in OS patients (Graham *et al.*, 2003). Recently, a second MID1 interactor, MIG12, was reported (Berti *et al.*, 2004). MIG12 represents a novel transcript with unknown function. MIG12 is similarly recruited onto microtubules by MID1, leading to increased resistance to the microtubule depolymerizing agent, nocodazole. However, the functional significance of their interaction is still unclear.

#### ***1.5.5 A potential ubiquitin E3-ligase activity for MID1***

The hypothesis of a ubiquitin E3-ligase activity for MID1 was suggested, due to the commonly found E3-ligase activity with RING-Finger domains from different proteins (Schweiger *et al.*, 1999, Cox *et al.*, 2000). Recently, indirect evidence for a potential ubiquitin E3-ligase activity of MID1 came from the finding that ubiquitylation of PP2Ac was dramatically reduced in OS derived cells while the amount of ubiquitylated

proteins from a cellular microtubule fraction was found to be elevated in cells overexpressing MID1 (Schweiger *et al.*, 2003).

#### **1.5.5.1 E3 ubiquitin-ligases and protein ubiquitylation**

The protein ubiquitylation mediated by E3 ubiquitin-ligases can promote either protein degradation or changes to protein trafficking. These processes will be addressed separately in the following section.

Ubiquitylation is a process whereby free ubiquitin (Ub), a highly conserved 76-amino acid polypeptide, is attached to target proteins by an isopeptide bond between the COOH-terminal glycine of ubiquitin and the  $\epsilon$ -amino group of a lysine residue in the substrate. This process is mediated by a multienzyme cascade that involves a ubiquitin-activating enzyme (E1), a ubiquitin-conjugating enzyme (E2) and a ubiquitin-protein ligase (E3). A ubiquitin chain assembly factor (E4) that co-operates with E1, E2 and E3 has also been identified (Hatakeyama and Nakayama, 2003). E1 activates ubiquitin by catalysing the formation of a thioester bond between the E1 cysteine and the COOH-terminus of Ub, which is subsequently transferred to a cysteine residue within the ubiquitin-conjugating (UBC) domain of the E2 enzyme. An E3 enzyme then catalyzes the ubiquitylation of the target protein by bringing the E2 and the target protein together. Consequently, the E3 enzyme may itself not necessarily be modified with ubiquitin. To date, three protein families—the HECT, the RING-finger and the U-box families, have been shown to possess E3 enzyme activity. From our lab's unpublished data, the interaction of MID1 and an E2, UbcH7, has been observed using both a yeast two-hybrid system and indirect immunofluorescence (Hopwood *et al.*, unpublished).

### 1.5.5.2 Ubiquitylation in the regulation of protein degradation

Additional ubiquitin monomers can be added to substrate-bound ubiquitin in a sequential manner through the linkage between lysine-48 of the last ubiquitin and the COOH-terminus of the new ubiquitin molecule. Poly-ubiquitylated proteins are then degraded by the ubiquitin-proteasome system, which consists of a 2000-kDa ATP-dependent proteolytic complex. Along with lysosomes, proteasomes are considered to be the major protein degradation systems, ensuring protein quality control in eukaryotic cells.

Of interest with respect to a possible role for MID1, misfolded/unassembled/damaged proteins frequently aggregate and are delivered in a microtubule-dependent manner to aggresomes, which are morphologically detectable intracellular foci known as inclusion bodies that also contain proteasomes and ubiquitin, that localize to the juxtannuclear region in the vicinity of the centrosomes (Hatakeyama and Nakayama, 2003). The impairment of the ubiquitin-proteasome system has been indicated in many diseases, including protein metabolic diseases such as systemic amyloidosis, and neurodegenerative diseases such as Alzheimer's disease, Parkinson's disease and Huntington disease (Bence *et al.*, 2001).

### 1.5.5.3 Ubiquitin and membrane trafficking

The same ubiquitylation system is also used in controlling endocytosis and other membrane trafficking events (Dupre *et al.*, 2001; Katzmann *et al.*, 2001). Different from the protein degradation pathway, the endocytic proteins are only modified with one (at most two) ubiquitin molecules (monoubiquitination). Proteins that are monoubiquitinated include receptor proteins that are to be sorted into lysosomes and endocytic proteins, such as Eps15, Eps15R, Epsins and Hrs, that are involved in vesicle

internalisation as well as other steps in membrane trafficking (Gent *et al.*, 2002; Klapisz *et al.*, 2002; Longva *et al.*, 2002; Oldham *et al.*, 2002; Raiborg and Stenmark, 2002; Shih *et al.*, 2002). Most of these proteins contain a UIM (ubiquitin interacting motif) signature, that provides the signal for monoubiquitylation, and at the same time, permitting interaction with other monoubiquitylated membrane trafficking proteins. In this way, trafficking proteins could build up on membranes to regulate membrane transport (Clague, 2002; Riezman, 2002).

#### **1.5.5.4 Potential target/targets for ubiquitylation**

Although the turnover of PP2Ac is thought to be directed by MID1 through the interaction with Alpha4, the MID1 directed ubiquitin transferring activity has not been definitively proven. Since microtubules are involved in both the protein degradation pathway and membrane trafficking, whether the potential target/targets for MID1 are signalling proteins to be degraded or trafficking proteins to be modified with ubiquitin or both remains unclear.

### **1.6 MID2, a homologue of MID1, has correlated functions**

#### ***1.6.1 MID1 and MID2 are likely to have originated from a common ancestral gene***

Subsequent to the cloning of the MID1 gene, sequence similarity searches identified numerous highly related sequences represented in the EST databases (Buchner *et al.*, 1999; Perry *et al.*, 1999). Retrieval and assembly of full length cDNA revealed an ORF of 2055 bp, encoding a 685-amino-acid protein with 83% amino acid similarity (76% identity) with MID1. This protein was subsequently called MID2.

Consistent with the high degree of sequence similarity at both the nucleotide and the amino acid level, the *MID1* and *MID2* genes are also similarly structured, comprising of



nine coding exons (MID1 has an additional five non-coding exons at the 5' end of the first coding exon) with conserved exon sizes and splice junctions (Figure 1.5). Further support for these genes having evolved from a common ancestor comes from their chromosomal locations: MID1 at Xp22.3 and MID2 at Xq22. These regions share a number of other gene homologues, for e.g., *PRPS2* and *PPEF1* (Xp22), *PRPS1* and *PPP6C* (Xq22) (Figure 1.5), suggesting an ancient intrachromosomal duplication of the X chromosome (Perry *et al.*, 1999).

### ***1.6.2 Functional similarities of MID1 and MID2***

As expected, MID2 is also an RBCC protein with an essentially identical domain arrangement as that of MID1 (Figure 1.6). Like MID1, MID2 can form homo-dimers on microtubules and, consistent with the high level of primary sequence identity, can also interact with Alpha4 with a comparable strength as judged by the reporter systems in the yeast two-hybrid assay (Short *et al.*, 2002). However, in contrast to MID1, MID2 interacts a little more strongly with a different ubiquitin E2-conjugating enzyme, UbcH5b, which not only supports the notion of E3-ligase activity but also that the two may have at least evolved some separate functions (Hopwood *et al.*, unpublished). However, it is also possible that other than a simple representation of sequence similarity, the MID1 and MID2 dimerization represents a mechanism, by which their interaction with different substrates can be regulated or their functions co-ordinated during early development.

### ***1.6.3 A role for MID2 in the pathogenesis of OS?***

Besides the structural and functional similarity as mentioned above, the possibility of a redundant or compensatory role for *MID2*, is also supported by the expression patterns

of *MID2* in early development. Compared with *Mid1*, *Mid2* is expressed at relatively lower levels in most tissues during the early mouse development, although it shows noticeably higher expression in the developing heart (Buchner *et al.*, 1999; Perry *et al.*, 1999). It is therefore worth considering whether *MID2* might be a modifier of the OS phenotype, particularly in the penetrance of cardiac anomalies, although other tissues should also not be excluded. In this regard, we have recently shown (in collaboration with Prof. Ray Runyan, Arizona) that treatment of endocardial cushion explants with antisense oligos to either *cMID2* or *cMID1*, appear to increase endothelial cell activation and mesenchymal invasion, a process critical for early cardiac septation. Interestingly, the effects of these oligo treatments was found to be additive, supporting the notion of a potential role for *MID2* in the pathogenesis of OS. A similar epithelial cell activation and conversion to mesenchyme is also required to enable fusion of the facial prominences and the urethral folds of the male external genitalia. Defects in this process are thought to give rise to cleft lip/palate and hypospadias, respectively, which are also two of the most prominent OS features.

#### ***1.6.4 The CI subfamily: sharing a common cellular function?***

Determining the physiological roles of *MID1/MID2* is essential to understand the etiology of OS. To this end, our group has recently used a Hidden-Markov-Model-based algorithm, HMMER (Truong and Ikura, 2002), as a sensitive means to detect distant evolutionary relationships, to delineate the complete human RBCC complement and subclassify these on the basis of their C-terminal domain composition (Short and Cox, unpublished). With this approach we have found that *MID1* is part of a subfamily (CI subfamily) of six RBCC proteins that includes the highly related *MID2* (76% identity, 83% similarity), *SPRING* (*TRIM9*), *TNL*, *TRIFIC* and *HAPRIN* (*TRIM36*) (Figure

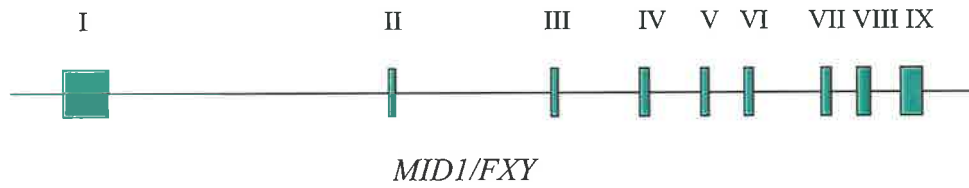
**Figure 1.5 (A) Genomic structure of *MID1* and *MID2*.**

Both *MID1* and *MID2* consist of 9 coding exons (indicated by blue boxes and Roman numerals), with the position of splice junctions and exon sizes similar in both genes.

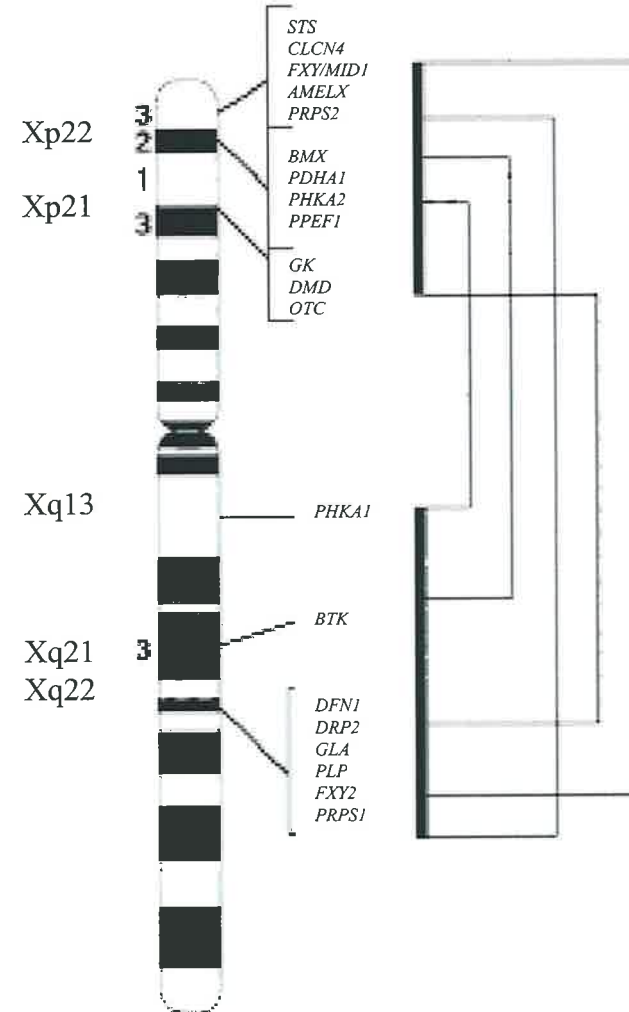
**(B) Mapping of *MID1*(Xp22) and *MID2* (Xq22) in humans suggests an intrachromosomal duplication.**

A potential duplication between Xp22 and Xq22 is indicated by a thick black line and the duplication of genes within these regions are linked by thin black lines (Picture edited from Perry *et al*, 1999). The gene homologues are: *MID1* and *MID2*; *PRPS2* and *PRPS1*; *DMD* and *DRP2*; *BMX* and *BTK*; *PHKA2* and *PHKA1*; *PPEF1* and *PPP6C*; *PRPS1* and *PRPS2*.

**A**



**B**



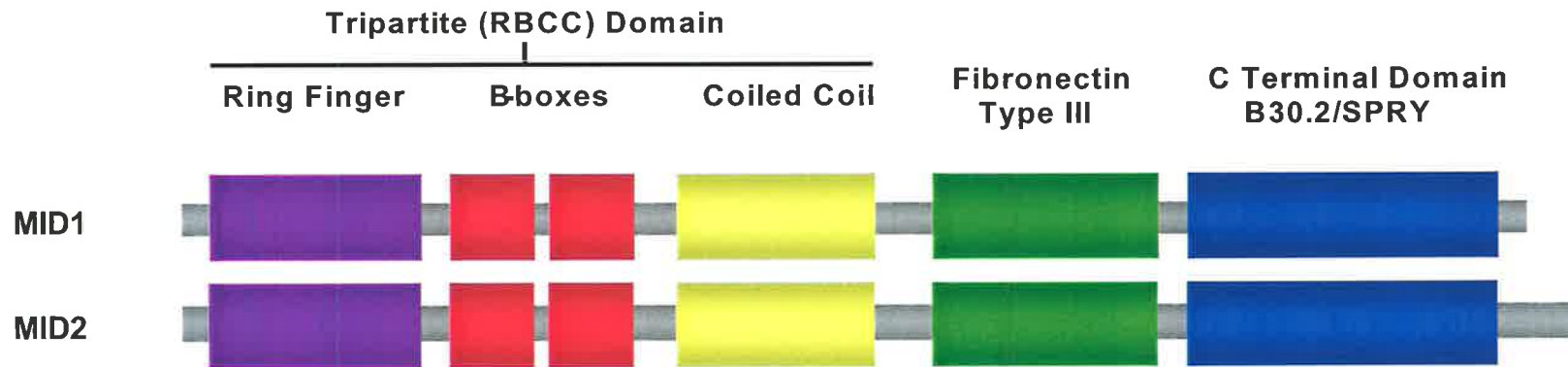


**Figure 1.6 Domain organization of the MID1 and MID2 RBCC proteins.**

The primary structure (amino acid sequence) and the domain organization of MID2 are highly conserved with those of MID1, with differences largely restricted to a C-terminal 19-amino-acid extension and an potential N-terminal 20-amino-acid extension (not experimentally proven).

For both MID1 and MID2, the N-terminal RBCC tripartite motif (RING-Finger: residue 10-60; B-box1: residue 114-164; B-Box2: residue 170-212; and Coiled-Coil: residue 219-345) is followed by a Fibronectin type III domain (residue 382-475) and a C-terminal B30.2 domain (residue 538-658).

1.7). This group is characterised by both a single Fibronectin type III (FNIII) motif and a C-terminal B30.2 domain (Cox *et al.*, 2000; Short and Cox, unpublished).

Interestingly, all 6 members of the subfamily have been found to associate with microtubules (Short and Cox, unpublished), raising the possibility of a common basic cellular function. Both Spring and Haprin, the only two members that have been partly characterised to date, have an emerging role in the regulation of membrane trafficking events: Haprin implicated in regulating the acrosome reaction (exocytosis of the sperm vesicle) (Kitamura *et al.*, 2003); Spring involved in regulating SNARE complex formation and exocytosis of synaptic vesicles (Li *et al.*, 2001). Results presented in this thesis suggest that this function may extend to the other CI subfamily members. Consequently, a concise review of the relevant trafficking literature is presented in the following sections.

## **1.7 MID1/MID2 and microtubule-dependent cellular processes**

The physical characteristics of microtubules and their interaction with other microfilaments, intracellular organelles and chromosomes through cross-linking proteins inextricably link this cytoskeletal network to a vast array of cellular processes including: the maintenance of cell shape, the control of cell growth/division and the directed delivery of intracellular cargo, such as signalling complexes, membrane vesicles and intracellular organelles.

### ***1.7.1 Microtubule dynamics***

Microtubules are microfilaments that are highly dynamic in nature, undergoing continuous polymerization and depolymerization. They are composed of both  $\alpha$ - and  $\beta$ -tubulin in a head-to-tail orientation, and therefore represent a polarized structure with

distinct ends—described as plus ends (fast growing ends) and minus ends (slowing growing ends). A GTP cap on  $\beta$ -tubulin at the growing ends stabilizes microtubules while its hydrolysis results in depolymerization. The minus ends of microtubules are anchored at two centrioles via a third form of tubulin,  $\gamma$ -tubulin, which with centriolar matrix, are known as the microtubule organizing center (MTOC). Nucleation of microtubules starts with the formation of the  $\gamma$ -tubulin ring complex primarily at the MTOC (Heald and Nogales, 2002).

Microtubule stability is promoted to a large degree by microtubule-associated proteins (MAPs). Classical MAPs either bind to the surface of microtubules (MAP2 and Tau) to neutralize the negative surface charge, or bind to the ends of microtubules (CLIP-170 and EBI) to anchor them on kinetochores/cellular membranes through interaction with other proteins. In contrast, microtubule-destabilizing factors, such as Op18/Stathmin and XKCM1, distort the microtubule lattice or promote GTP hydrolysis at microtubule ends (Anderson and Jacobson, 2002; Heald and Nogales, 2002). Not surprisingly, the actual regulation of microtubule dynamics *in vivo* is much more complicated since most of the stabilizing/destabilizing factors themselves are temporally and spatially regulated and are modified by phosphorylation/dephosphorylation.

### ***1.7.2 Microtubules and other cytoskeletal networks***

Microtubules, actin microfilaments and intermediate filaments are the three components of the cellular cytoskeleton. Their crosstalk underlies many of the cellular processes that require dynamic cellular asymmetries to be established or maintained, including cell morphology and motility, cell division, wound healing and intracellular trafficking (Mayer and Jurgens, 2002).

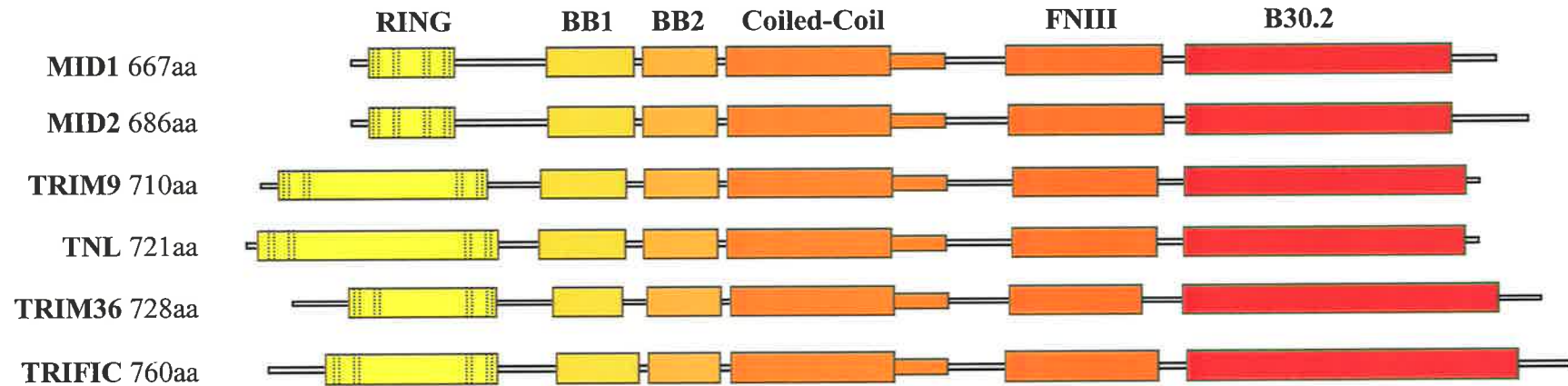


**Figure 1.7 The CI subfamily of RBCC proteins.**

Six RBCC proteins comprise the CI subfamily that has been subclassified on the basis of their C-terminal domain composition: a single Fibronectin type III (FNIII) motif and a C-terminal B30.2-like (or RFP-like) domain. In addition to MID1, CI subfamily includes the highly related MID2, TRIM9 (Spring), TNL, TRIFIC and TRIM36 (Haprin) proteins. The large RING-finger domains observed in both TRIM9 and TNL reflect insertion of additional residues between the conserved co-ordinating zinc-binding residues (indicated by vertical dashed lines).



The dynamics of microtubules and actin are co-regulated by small GTPases from the Rho family (Lee and Gotlieb, 2002). For example, RhoA mediates the formation of contractile actin structures and at the same time promotes microtubule stabilization. The activity of Rho proteins is also regulated by microtubules and actin. Microtubule growth and shortening are thought to activate Rac1 and RhoA signaling, respectively, which in turn regulates actin structure and function (Lee and Gotlieb, 2002).

The three components of the cytoskeleton are also physically linked by numerous cytolinkers containing both actin- and microtubule-binding activity, such as plectin and MACF (microtubule actin crosslinking factor), or linked by the interaction between microtubule-/actin-based motors and microtubule-/actin-associated proteins, such as the interaction between MAP2c, Myo5a and kinesin, and the interaction between dynein and dynectin (Rodriguez *et al.*, 2003).

### ***1.7.3 Connection between microtubules and membrane***

In addition to coordinating their growth and retraction with actin and other microfilaments, microtubules are also connected to both the plasma membrane and intracellular membranes. The dynamics of membrane vesicles and the integrity of endomembrane compartments, such as the Golgi complex, the endoplasmic reticulum and mitochondria, all rely on intact cytoskeletal filaments and the membrane-cytoskeleton interaction.

#### **1.7.3.1 Microtubule-membrane cross-linking proteins**

Cross-talk between membranes and the microtubule cytoskeleton is critical for signal transduction, intracellular trafficking and organelle positioning (Mayer and Jurgens, 2002). The establishment of membrane-cytoskeleton linkages relies on both protein-

protein and protein-lipid interactions. Crosslinking proteins, which establish the connection between microtubules and subcellular membranes, can serve as multiple docking sites for both organelle localization and vesicle trafficking (Schroer, 2000).

Among the best characterized crosslinking proteins are members of the CLIP family that are noted by the presence of a central coiled-coil domain flanked by one or more CLIP-170-like microtubule-binding motifs (Schroer, 2000). For example, CLIP-170, which binds to the growing ends of microtubules, was originally reported to associate with early endosomes (Le Bot *et al.*, 1998), while CLIP-115, CLIPR and p150<sup>glued</sup> bind different membrane vesicles (dendritic lamellar bodies, peroxisomes and endosomes, respectively) and been implicated in regulating membrane dynamics (Burkhardt *et al.*, 1997; De Zeeuw *et al.*, 1997; Thiemann *et al.*, 2000).

However, a large number of proteins aside from the CLIP family have also been implicated in membrane-microtubule cross-linking, although through less understood mechanisms. Among these are metabolic enzymes, dynamin and other MAPs (Orzech *et al.*, 2001; Walenta *et al.*, 2001).


### **1.7.3.2 Microtubule motors**

Microtubules are the tracks on which various intracellular cargo is delivered to its final destination. Correct delivery relies on motor-cargo interaction and the coordination with opposite-polarity motors. The plus-end directed and minus-end directed motors, kinesin and dynein, respectively, which are responsible for dynamic transport of membrane organelles, have also been found to possess anchoring activity. In addition to the well characterized kinesin and dynein membrane binding partners, kinectin and dynectin, respectively, kinesin and dynein can also bind their membrane cargo through many newly identified interactors (Karcher *et al.*, 2002). For example, KIF13A from the

kinesin superfamily interacts with the AP-1 complex associated with clathrin-coated pits on the trans-Golgi network while KIF3 has been suggested to use the non-erythroid spectrin, fodrin, to link itself to Fodrin-associated vesicles in neuron cells (Nakagawa *et al.*, 2000; Takeda *et al.*, 2000).

### 1.7.3.3 Phosphoinositides and the microtubule-membrane connection

Apart from binding to their membrane receptors or membrane partners, it is common that cross-linking proteins also utilize protein-lipid interactions to help them anchor to membranes. For example, the microtubule motor, dynein, also interacts with membrane lipids to assist its membrane docking (Schroer, 2000).

Phosphatidylinositols (PtdIns) are intrinsic components of lipids on the cytoplasmic surface of membranes. The different combination of phosphorylation on the inositol rings gives rise to different phosphoinositides, with their synthesis temporally and spatially controlled by various kinases and phosphatases (Figure 1.8). For example, PI(4,5)P<sub>2</sub>, generated from PtdIns by sequential activation of PI(4)-Kinases and PI(5)-Kinases, is abundant on the plasma and Golgi membranes and is recognized as an important membrane signaling molecule that regulates vesicle trafficking/cytoskeleton assembly. In addition, it is a precursor to generate the most important intracellular secondary messenger, inositol(1,4,5)P<sub>3</sub>, through hydrolysis by phospholipase  (PLD) (Simonsen *et al.*, 2001). Interestingly, a novel pathway for PI(4,5)P<sub>2</sub> synthesis from PI(5)P has also been recognized and occurs via the activity of PI(5)P-4-kinase, a type II PI(4)P-5-kinase, indicating regulation of the synthesis of this lipid is more complicated than previously assumed (Rameh *et al.*, 1997; Tronchere *et al.*, 2004).

Compared to PI(4,5)P<sub>2</sub>, PI3P, which is a product of PI3-Kinase, is primarily found in membranes of early endosomes and internal vesicles, and has been implicated in

regulating the early endocytic pathway (Gillooly *et al.*, 2001). In contrast, PI(3,4,5)P<sub>3</sub> and PI(3,4)P<sub>2</sub> are lipid second messengers whose cellular levels increase dramatically in response to stimulus-induced actin polymerization (Insall and Weiner, 2001; Lemmon, 2003). The functions of each phosphoinositide are described in more detail in the relevant sections below.

### 1.7.3.4 The PH-domain and PI-binding

Proteins that interact with phosphoinositides often contain specific PI-binding domains, such as the PH-domain, FYVE-domain, PX domain and ENTH domain. Different PI-binding domains or the same domain from different proteins display various affinities and specificities in PI-binding, and thus direct their involvement in different aspects of intracellular processes (Itoh and Takenawa, 2002). For instance, AP-180 and epsin bind PI(4,5)P<sub>2</sub> via their ENTH domains, while EEA1 (early endosome antigen-1) binds PI3P via its FYVE domain.

The first PI-binding domain described was the PH domain in pleckstrin, a major protein kinase C substrate of platelets (Tyers *et al.*, 1988). The PH domain is shared by various proteins, including signaling proteins, trafficking proteins and cytoskeletal proteins and consists of a conserved region of 100-120 amino acids (Lemmon *et al.*, 2002). PH domains have been found in proteins that have binding specificity for all different phosphoinositides and, as such, are involved in many different cellular processes. For example, the activity of the Bbl family of guanine nucleotide exchange factors (GEFs), which couple receptor signaling with actin organization, are regulated by their interaction with PI(4,5)P<sub>2</sub> through their PH domains (Russo *et al.*, 2001). Dynamin, which induces the conformation change at the membrane neck of invaginating vesicles and thus necessary for membrane fission, is also recruited onto the

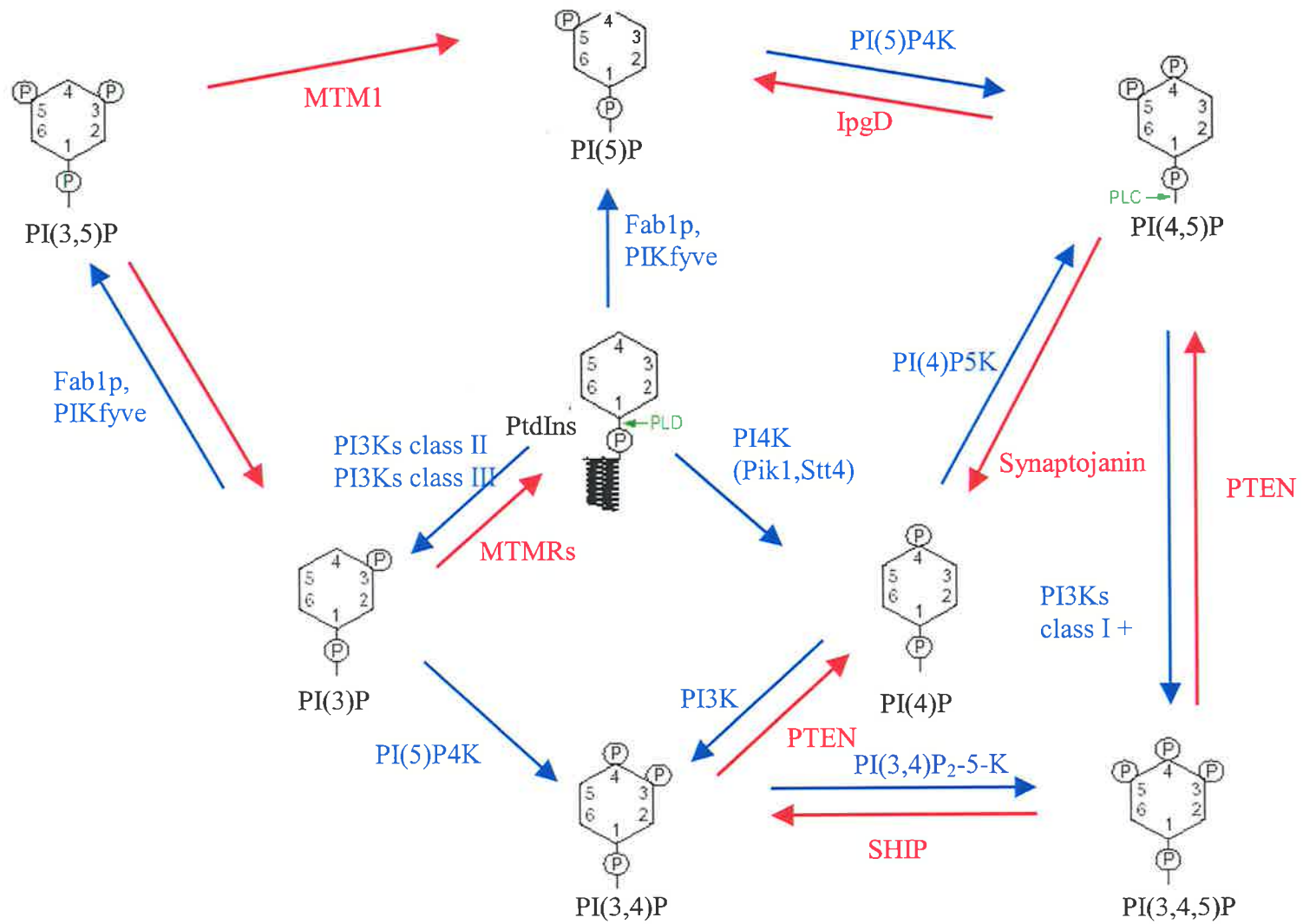
**Figure 1.8 The biosynthesis of phosphoinositides.**

Different combinations of phosphorylation on the inositol rings of PtdIns gives rise to different phosphoinositides. These phosphoinositides, which are located on the cytoplasmic surface of membranes, are involved in signaling and protein-lipid interaction. Their synthesis is strictly controlled by temporally and spatially activated kinases (indicated in blue) and phosphatases (indicated in red).

MTMRs: myotubularin-related proteins

PTEN: phosphatase and tensin homolog deleted on chromosome 10

SHIP: Src homology 2 domain-containing inositol phosphatase



membrane through the interaction of its PH domain and PI(4,5)P<sub>2</sub> (Itoh and Takenawa, 2002). Akt/PKB, a kinase involved in regulating actin polymerization, binds PI(3,4,5)P<sub>3</sub>/PI(3,4)P<sub>2</sub> through its PH domain (Thomas *et al.*, 2002).

### ***1.7.4 Microtubule-dependent cellular processes***

#### **1.7.4.1 Microtubules and cell motility**

Cell migration begins with a protrusion of the plasma membrane at the leading edge, which is driven by directed polymerization of actin and extension of microtubules, followed by the formation of adhesive complexes at the front and release of adhesion at the rear of the cell (Horwitz and Parsons, 1999). This turnover of focal adhesive complexes is microtubule dependent: disruption of the microtubule network leading to decreased turnover of focal complexes and a non-polarized distribution of focal adhesions, increased tension and reduced protrusion (Horwitz and Parsons, 1999).

#### **1.7.4.2 Microtubules and positioning of intracellular membrane compartment**

The importance of microtubules and their crosslinking proteins in keeping the integrity and positioning of subcellular organelles is most evident by the close relationship between microtubules and the Golgi apparatus. In eukaryotic cells, the Golgi which is critical for protein sorting via the secretory pathway, is formed by interconnected stacks of cisterna, tubules and small vesicles in the perinuclear region in close proximity to the MTOC (Lippincott-Schwartz and Zaal, 2000). In fact, microtubules are required for the structural integrity of the Golgi, as seen by the dispersal of the Golgi into small cytoplasmic vesicles upon addition of microtubule depolymerizing agents (reviewed by Thyberg and Moskalewski, 1999). CLIPs, such as p63, GMAP-210, CLIPR-59 and HOOK3 have also been implicated in positioning of the ER and the Golgi, and help

these organelles to remain tightly associated with microtubules (Schweizer *et al.*, 1993; Klopfenstein *et al.*, 1998; Walenta *et al.*, 2001; Infante *et al.*, 1999; Perez *et al.*, 2002). Similarly, the positioning of mitochondria and their delivery during mitosis is dependent on their interaction with the plus-end directed microtubule motor, kinesin (Pereira *et al.*, 1997). Other organelles, such as polyribosomes, are also associated with the cytoskeleton in eukaryotic cells and are transported along microtubules and actin filaments (Hamill *et al.*, 1994).

#### **1.7.4.3 Microtubule-dependent vesicle trafficking**

It has been well recognized that the transport of vesicles from early to late endosomes/lysosomes is dynein-directed, while the invagination of the forming endocytic vesicles is thought to be propelled by polymerizing actin (Apodaca, 2001; Conner and Schmid, 2003; Hamm-Alvarez and Sheetz, 1998). Microtubules have also been implicated in the secretory pathway since addition of microtubule depolymerizing agents inhibits exocytosis, and the movement of exocytic vesicles has been visualized on microtubules using GFP-labeling (Smith *et al.*, 2003). This microtubule-dependent exocytosis is most apparent in neuronal cells, where the kinesin-directed transport on microtubules is responsible for the long-range movement of vesicles containing neuronal transmitters while the short-range movement is directed by the actin based motor, myosin V (Brown *et al.*, 2004). Interestingly, the evidence for a direct interaction between kinesin and myosin-V suggests these cytoskeletal networks cooperate to co-ordinate vesicle trafficking (Brown *et al.*, 2004).

Other interactions, such as that between the vesicle coat protein, AP-1, and microtubule-associated proteins (MAPs), suggest that even early stages of vesicle trafficking, including vesicle budding, may also be microtubule-facilitated processes (Orzech *et al.*,



2001). Finally, studies on transferrin-receptor (TfR)-mediated endocytosis, again using microtubule depolymerizing drugs, found dramatically reduced TfR on the plasma membrane, thus indicating that vesicle recycling may also be microtubule-dependent (Runnegar *et al.*, 1997).

Yet, despite being implicated in many aspects of vesicle trafficking, the precise roles that microtubules play is far from understood. The picture is further complicated by the fact that although the actin and microtubule cytoskeletons are essential for endocytosis, disruption of neither microtubules nor actin filaments in mammalian cells completely inhibits this cellular process. It may therefore be that alternative mechanisms exist in higher organisms to maintain this important function (Conner and Schmid, 2003).

#### **1.7.4.4 Coupling of trafficking and signalling during development**

Many developmental signals are secreted proteins found in the extracellular matrix that recognize cell surface protein receptors. Receptor tyrosine kinases (RTKs) and G-protein-coupled receptors (GPCRs) comprise the two major groups of signaling receptors (reviewed by Sorkin and Zastrow, 2002). RTKs recruit protein effectors containing enzyme activity and lead to subsequent modification of proteins or production of lipid secondary messengers. By contrast, GPCRs function as ligand-regulated guanine-nucleotide exchange factors (GEFs) to activate G protein heterotrimers ( $\alpha\beta\gamma$ ). The signals generated by the activated receptors lead ultimately to altered gene transcription and altered cellular function.

Most receptors undergo endocytosis after ligand-binding. Evidence suggested that such ligand-bound receptors cluster in clathrin-coated pits and are subsequently endocytosed, although clathrin-independent pathways also exist. The phosphoinositide, PI(4,5)P<sub>2</sub>, plays a important role in regulating this clathrin-mediated endocytosis. Upon receiving

external signals, the activated ARF/Rho family of GTPases recruit PI(4)P-5-kinase onto the membrane, resulting in an increased local concentration of PI(4,5)P<sub>2</sub> (Hsuan *et al.*, 1998). The PI-binding domain-containing proteins, AP-2, AP-180 and epsin, are subsequently recruited onto the plasma membrane through the binding of PI(4,5)P<sub>2</sub>. These recruited factors are critical for the correct formation of clathrin-coated pits at the beginning of endocytosis. By recruiting different effectors at different stages, PI(4,5)P<sub>2</sub> has also been shown to be involved in vesicle fission, docking and fusion, as well as in the subsequent trafficking of vesicles by regulating actin/microtubule nucleation and membrane-cytoskeleton association (Martin, 2001; Russo *et al.*, 2001; Popova *et al.*, 2002).

Endocytosed ligand-receptor complexes can be dissociated in the acidic environment of the endosome. Whether they are removed or remain associated depends on the status of ligand-receptor binding and the local concentration of both (reviewed by Sorkin and Zastrow, 2002). The preservation of ligand-receptor complexes in endosomes can result in the persistence of receptor dimers, raising the possibility that the endocytosed receptors may still maintain signaling activity and therefore activate potential signal pathways. This has challenged the traditional hypothesis that receptor endocytosis ends the signaling activated on the cell surface. Identification of signaling proteins in endosomes, including the growth-factor-receptor-bound protein 2 (Grb2), Ras-GTPase and PAK/ERK, has provided further evidence for endocytic signaling (reviewed by Sorkin and Zastrow, 2002).

A role for such endocytic signaling is perhaps best highlighted by the Trk-family of receptor tyrosine kinases in neurons. Upon nerve growth factor (NGF)-binding, the NGF-TrkA complexes are internalized and transported from the axon to the neural cell body, where the signaling NGF-TrkA complexes activate cyclic AMP-responsive

element binding protein (CREB), leading to gene transcription in the cell body (reviewed by Sorkin and Zastrow, 2002). The signaling endosomes are eventually delivered to late endosomes/lysosomes for degradation and termination of signaling .

However, internalization of activated receptors does markedly reduce the amount of receptors on the cell surface and results in reduced signaling on the plasma membrane. Receptors can be recycled from early endosomes (rapid recycling) or after they been sorted into multivesicular bodies (slow recycling). In addition to regulating signaling by controlling the concentration of receptors on cell surface, endocytosis also regulates ligand accessibility by removing them from extracellular matrix, on which cell migration and tissue patterning are depended during early development (Vincent *et al.*, 2003).

## **1.8 Outlines of this project**

The overall aim of this project is to understand the pathogenetic mechanism underlying OS by characterizing the cellular function(s) of MID1 and MID2. Both MID1 and MID2 are of interest as the following observations suggest they may have a partially redundant or co-ordinated function: (1) their high level of amino acid sequence similarity; (2) the fact that both dimerize on microtubules; (3) that both *MID1/Mid1* and *MID2/Mid2* are ubiquitously expressed albeit at variable levels in numerous embryologic tissues; (4) they both interact with Alpha4; (5) and they both are likely to have E3 ubiquitin ligase activity.

Under the hypothesis of partially redundant or co-ordinated functions, the project started from the screening for MID2 mutations in OS patients and characterizing the cellular behavior of MID2 in the OS cells carrying a MID1 mutation. However, the main strategy employed to characterize their function has been to identify the potential

protein partners for MID1 and MID2. The work in this thesis largely describes the results extending from these studies and begin to shed some light on the roles of these novel RBCC proteins and how their disruption may lead to the presentation of the malformations seen in Opitz syndrome.

## Chapter Two: Materials and Methods

### 2.1 Abbreviations.

APS: ammonium persulfate

bisacrylamide: N,N'-methylene-bisacrylamide

bp: base pairs

BSA: bovine serum albumin

CIP: alkaline calf intestinal phosphatase

DMEM: Dulbecco's minimal essential medium

DNA: deoxyribonucleic acid

dNTP: deoxyribonucleoside triphosphate

DTT: dithiothreitol

EDTA: ethylene-diamine-tetra-acetic acid

EtOH: ethanol

FBS: fetal bovine serum

FRAP: Fluorescence recovery after photo-bleaching

GST: glutathione-S-transferase

HEPES: 4-(2-hydroxyethyl)piperazine-1-ethanesulfonic acid

Hours: hrs

HRP: Horseradish peroxidase

IPTG: isopropyl  $\beta$ -D-thiogalactopyranoside

kb: kilobase pairs

Mins: minutes

PBX: phosphate buffered saline with 0.1% Triton X

PBS: phosphate buffered saline

PBST: phosphate buffered saline with 0.1% Tween 20

PCR: polymerase chain reaction

PEG: polyethyleneglycol

PGK-1: Phosphoglucokinase-1

PIPES: 1,4-piperazinediethanesulfonic acid

PM: Plasma membrane

PMSF: phenylmethanesulfonyl fluoride

RNase: ribonuclease

rpm: revolutions per min

SDS: sodium dodecyl sulphate

Sec: Seconds

UV: ultraviolet light

WGA: wheat germ agglutinin

X-gal: 5-Bromo-4-Chloro-3-indoyl  $\beta$ -D-galactopyranoside

## **2.2 Materials.**

### ***2.2.1 Chemicals and Reagents.***

General laboratory chemicals were of analytical research grade and were purchased from a range of manufacturers. Specialist reagents and their sources are listed below:

DMSO

BDH

IPTG

Boehringer Mannheim

PEG 4000

Sigma

Spermidine

Sigma

---

TEMED	BDH
LiOAc	BDH
Mineral oil	Sigma
Yeast Extract	Oxoid
DMEM	GibcoBRL
FBS	GibcoBRL
Thiourea	Sigma
Ampholytes (3-10)	Biorad
CHAPS	Sigma.
Iodoacetamide	Sigma
Gelatin	Merck
8% Glutaraldehyde	Sigma
Wortmannin	Sigma
Salmon sperm DNA	Sigma
O-Dianisidine	Sigma

### ***2.2.2 Stains and Dyes.***

Bromophenol blue	Sigma
Ethidium bromide	Sigma.
Coomassie blue	Sigma
Trypan blue	Sigma

### ***2.2.3 Enzymes.***

All restriction endonucleases and buffers were purchased from New England Biolabs.

Modifying enzymes were bought from the following manufacturers:

RNaseA	Sigma
T4 DNA ligase	Geneworks
T4 (PNK)	Geneworks
<i>Taq</i> DNA polymerase	Geneworks
Calf Intestinal Phosphatase	Boehringer Mannheim
Aprotinin	Sigma
Leupeptin	Sigma
Benzamidine	Sigma
PMSF	Sigma
Sodium Orthovanadate	Sigma
Pfx Polymerase	Invitrogen
HRP	Sigma

Appropriate reaction buffers (either 5 X or 10 X) and additional supplements were supplied with all enzymes.

#### ***2.2.4 Antibiotics and Indicators.***

Ampicillin	Sigma
X-gal	Sigma
Kanamycin	Sigma
IPTG	Sigma
Penicillin/Streptomycin	Invitrogen

#### ***2.2.5 Fluorescent Probes.***

WGA-Alexa Fluor 350 conjugate	Molecular Probes
EGF-Texas red	Molecular Probes



DiIC<sub>16</sub>(3)

Molecular Probes

**2.2.6 Kits and Miscellaneous Materials.**

Kits and other materials used in this project were obtained from the following manufacturers:

Glass beads, 150-212 $\mu\text{m}$	Sigma
Hybond <sup>TM</sup> -N+nylon membrane	Amersham
Hybond <sup>TM</sup> -C nylon membrane	Amersham
Sequencing Kit	USB
Hyperfilm <sup>TM</sup>	Amersham
Qiaex <sup>TM</sup> gel purification kit	Qiagen
Qiagen DNA mini kit	Qiagen
Qiagen DNA midi kit	Qiagen
Superose 6 PC 3.2/30	Amersham
ReadyStrip <sup>TM</sup> IPG strip (pH3-10, 7 cm)	Bio-Rad
Slide-A-Lyzer 10K Dialysis Cassette	Pierce
PlusOne Silver Staining Kit, Protein	Amersham

**2.2.7 Solutions and Buffers.**

Phenol/chloroform

50% (w/v) Phenol

48% (v/v) Chloroform

2% (v/v) Isoamyl alcohol, buffered with an equal volume of

Tris-HCl, pH 8.0

0.2% (v/v)  $\beta$ -mercaptoethanol.

1 X TE

10mM Tris-HCl, pH 8.0

1mM EDTA, pH 8.0.

1 X TAE

40mM Tris HCl

20mM Sodium acetate

2mM EDTA

adjusted to pH 7.8 with glacial acetic acid.

1 X GTS

0.2 M Glycine

25 mM Tris HCl

0.1% SDS

Adjust pH to 8.3 with NaOH

PHEM buffer, 0.4 M

100 ml 240 mM PIPES

100 mM HEPES

8 mM MgCl<sub>2</sub>

40 mM EGTA

Adjust pH to 6.9 with NaOH

2 X Glutaraldehyde (GA) fixative

0.2 M PHEM buffer

4% glutaraldehyde

Freshly prepared before use

10% Gelatin

10% Gelatin

0.1 M PBS pH 7.4

0.02% azide

DMEM

28 mM NaHCO<sub>3</sub>

19 mM Glucose

20 mM HEPES, pH 7.3

Yeast lysis buffer

300 mM NaCl

100 mM TrisCl, pH8.0

1 mM EDTA

0.1% SDS

PEG/LiAc/TE

40% PEG 4000

0.1 M Lithium Acetate

10 mM Tris·Cl, pH 7.5

1 mM EDTA

Non-denaturing lysis buffer

1% (v/v) Triton X-100

50mM Tris-HCl, pH7.4

300mM NaCl

5mM EDTA

0.02% (w/v) Sodium Azide

Added just prior to use:

10mM Iodoacetamide

1mM PMSF

2 $\mu$ g/ml Leupeptin.

Wash buffer

0.1% (w/v) Triton X-100

50mM Tris·Cl, pH 7.4

300mM NaCl

5mM EDTA

0.02% (w/v) sodium azide

5% Blotto

1 X PBS

5% Milk powder

Non-denaturing lysis buffer (gel filtration)

phosphate buffered saline with 0.1% NP-40

100 X protease inhibitor

200 ug/ml Aprotinin

400 ug/ml Bestatin

500 ug/ml Leupeptin

100 ug/ml Pepstatin

150 mM EDTA

2-D sample buffer (Lewis et al., 2000)

7M urea

2M thiourea

4% CHAPS

2% DTT

2% IPG buffer (pH 3-10)

1mM benzamidine

2ug/ml pepstatin-A

20ug/ml leupeptin

10ug/ml aprotinin

1.5mM EDTA

1.5mM EGTA

2-D rehydration buffer

2-D sample buffer with 0.001% bromophenol blue

SDS-PAGE equilibration buffer I (with DTT)

6M Urea

0.375M Tris pH8.8

2% SDS

20% glycerol

2% (w/v) DTT

SDS-PAGE equilibration buffer II (with iodoacetamide)

6M Urea

0.375M Tris pH8.8

2% SDS

20% glycerol

2.5% (w/v) iodoacetamide

Coomassie blue staining

0.25% Coomassie blue R-250

40% Methanol

10% acetic acid

Destain solution

40% Mehtanol

10% acetic acid

Glutathione Elution Buffer

50 mM Tris-HCl, pH 8.0

10 mM reduced glutathione

### 2.2.8 Nucleic acid and protein molecular weight standards.

1kb ladder	GibcoBRL
HyperLadder I	Bioline
BENCHMARK™ Prestained Protein Ladder	GibcoBRL

### 2.2.9 Cloning and expression vectors.

All pCMV and pPGK mammalian expression vector were obtained from Dr. T. Cox (University of Adelaide, South Australia).

### 2.2.10 Bacterial strains.

Strains	genotype
DH5 $\alpha$	<i>supE44</i> $\Delta$ <i>lacU169</i> ( $\phi$ 80 <i>lacZ</i> $\Delta$ M15) <i>hsdR17recA1</i> <i>endA1gyrA96thi-1relA1</i>
BL21	F <sup>-</sup> , <i>ompT</i> , <i>hsdS</i> ( $r_B^-$ , $m_B^-$ ), <i>gal</i> (38,39)

### 2.2.11 Bacterial media.

Luria broth (L-Broth)

1% (w/v) Tryptone

1% (w/v) Sodium chloride

0.5% (w/v) Yeast extract

adjusted to pH 7.2 with sodium hydroxide.

#### Luria Agar (L-Agar)

Luria broth with the addition of 1% (w/v) bacteriological agar  
No<sub>1</sub>.

#### SOC

2% Tryptone

0.5% Yeast extract

10 mM NaCl

2.5 mM KCl

10 mM MgCl<sub>2</sub>

10 mM MgSO<sub>4</sub>

#### **2.2.12 Yeast strains.**

Mav203: *MAT $\alpha$* , *leu2-3,112*, *trp1-901*, *his3 $\Delta$ 200*, *ade2-102*, *gal4 $\Delta$* , *gal80 $\Delta$* ,  
*SPAL10::URA3*, *GAL1::lacZ*, *HIS3<sub>UAS GAL1</sub>::HIS3@LYS2*, *can1<sup>R</sup>*, *cyh2<sup>R</sup>*

Mav201: *MAT $\alpha$* , *leu2-3,112*, *trp1-901*, *his3 $\Delta$ 200*, *ade2-102*, *gal4 $\Delta$* , *gal80 $\Delta$* ,  
*SPAL10::URA3*, *GAL1::lacZ*, *HIS3<sub>UAS GAL1</sub>::HIS3@LYS2*, *can1<sup>R</sup>*, *cyh2<sup>R</sup>*



### **2.2.13 Yeast media.**

#### **2.2.13.1 Amino acids and Carbon source.**

Tryptophan, Histidine, Leucine and Uracil were obtained from Sigma. Glucose was obtained from the central services unit (CSU) and Lactic acid (DL) was obtained from BDH.

#### **2.2.13.2 Liquid media.**

The composition of the media is given per litre. The appropriate amino acids and carbon source, obtained from sterile solutions, were added after autoclaving. Minimal media: yeast nitrogen base (1.7g), ammonium sulphate (5g) made up to 900mls with water, and autoclaved.

Complete Media (YPD): yeast extract (10g), bactopectone (20g),  $K_2HPO_4$  (0.5g) and  $KH_2PO_4$  (0.5g). Water was added to 900mls and autoclaved.

Yeast Broth: yeast nitrogen base (6.7g) in 900 ml  $H_2O$  and autoclaved. The appropriate carbon source and amino acids were added prior to use.

#### **2.2.13.3 Solid media.**

Yeast minimal media plates and complete media plates were made with either yeast minimal media or yeast complete media (respectively) with 2% bactoagar. The appropriate carbon source and amino acids were added prior to plate pouring.

**2.2.14 Libraries.**

The PROQUEST Two-Hybrid Mouse Embryo, 10.5 day cDNA Library was purchased from GibcoBRL.

**2.2.15 Tissue Culture Cell Lines and Media.**

**2.2.15.1 Cell Lines.**

Cos-1, Monkey Kidney cells (ATCC CRL-1650)

HEK-293T, Human Embryonal Kidney cells (ATCC CRL-1573)

Primary skin fibroblasts, from OS patient OSP#9 (Cox et al., 2000) and from an unrelated unaffected individual (gift from Dr. M.Fietz, Womens and Childrens Hospital, Adelaide)

**2.2.15.2 Media.**

All cells were grown in DMEM (Gibco) supplemented with 5-10% (v/v) FBS.

**2.2.16 Antibodies.**

Anti- $\alpha$ tubulin	monoclonal	Sigma
Anti-GFP	monoclonal	Rockland
Anti-MYC	monoclonal	gift from Dr. Stephen Dalton
Anti-EEA1	monoclonal	BDH
Anti-Dynein heavy chain	monoclonal	Sigma
Anti-Ubiquitin	monoclonal	Sigma

Anti-goat 10nm-gold conjugate monoclonal Aurion

### 2.2.17 Oligonucleotides.

PRIMER	SEQUENCE (5' → 3')	Ann Temp °C	SOURCE
<b>Vector primers</b>			
T3	CGAATTAACCCTCACTAAAGGG	55	Geneworks.
T7	GTAATACGACTCACTATAGGGC	55	Geneworks.
EGFP-60r	GTTTACGTCGCCGTCCAGCTC	55	Sigma Genosys.
EGFP-660	GATCACATGGTCCTGCTGGAG	55	Sigma Genosys.
PCMV-40MCS	GGGAGGTCTATATAAGCAGAGC	55	Sigma Genosys.
Gal4-AD	TATAACGCGTTTGGAACTACT	55	Sigma Genosys.
Gal4-DB	GAATAAGTGCACATCATCATC	55	Sigma Genosys.
Gal4-AD45-term	GTAATTTCTGGCAAGGTAGAC	55	Sigma Genosys.
Gal4-ADH-term-Sal1	ACGCGTCGACGTAAATTTCTGGCAAGGTAGAC	55	Sigma Genosys.
pGEX 5'	GGGCTGGCAAGCCACGTTTGGTG	55	Sigma Genosys.
<b>Gene-specific primers</b>			
PEPP2F-KpnI	GGGGTACCCATGGCGGCGGATCTAAAC	56	Sigma Genosys.
PEPP2B-KpnI	GGGGTACCCTACACACACACATGAAATGTGATCC		Sigma Genosys.
PEPP2PHF	GCGGTACCCGTGACTTCAGATTATGCAGTG	56	Sigma Genosys.
PEPP2PHF	GCGGTACCGTTTCTTTAGTTGGTGCAATTTTC		Sigma Genosys.
NYCO3F	CGGTCGACCATGTCGGGCTACGCGCGGC	60	Sigma Genosys.
NYCO3B	GCGTCGACTCAAGAGTCTTCCTCCTCGTC		Sigma Genosys.

### 2.2.18 MID1 and MID2 domain deletions.

Regions deleted in the MID1 and MID2 domain-specific deletions are indicated as following:

	MID1	MID2	Regions deleted
$\Delta$ RF	residue 1-71	residue 1-71	RING-finger domain
$\Delta$ BB	residue 72-211	residue 72-211	Two B-Boxes
$\Delta$ CC	residue 212-349	residue 212-349	Coiled-Coiled domain
$\Delta$ FNIII	residue 350-489	residue 350-489	Fibronectin type III domain
$\Delta$ CTD	residue 490-667	residue 490-685	B30.2 domain

## **2.3 Methods.**

### ***2.3.1 Ethanol precipitation of nucleic acids.***

Samples were adjusted to 0.3M NaAc pH 5.2 using a 3M stock solution. Three volumes of redistilled EtOH was then added, mixed thoroughly by vortexing, and chilled at -20°C for at least 30 min. The precipitated nucleic acid was then pelleted by centrifugation at 15,000 X g for 15 min. The supernatant was carefully removed and the pellet then washed in 70% (v/v) EtOH. The samples were dried *in vacuo* then resuspended in water.

### ***2.3.2 Restriction endonuclease digestions.***

All restriction endonuclease digestions of DNA dissolved in water (or TE) were carried out in the supplied 10 X restriction buffer with addition of BSA. Analytical digests of DNA (up to 2µg) were carried out using 2 units of enzyme in a reaction volume of 15µl for 1-2 hrs at 37°C. Preparative digests of DNA (> 2µg) were carried out using 2-3 units of enzyme for each µg of DNA, in a reaction volume of 50-100µl, and allowed to proceed for at least 2-3 hrs at 37°C.

### ***2.3.3 Agarose gel electrophoresis of DNA.***

Electrophoresis of DNA was carried out in agarose gels of appropriate percentage and size. Molten agarose in 1 X TAE was poured into plastic trays provided with the electrophoresis tanks with plastic combs to provide the wells. The gels were submerged in TAE in an electrophoresis tank and the DNA samples containing an appropriate amount of loading buffer (final concentration 1 X) were loaded into the wells. 60-80V was applied until the dye had moved to the required distance. The DNA was visualised

under long or medium wave UV light after staining with ethidium bromide (10mg/ml) for approximately 10 min.

### ***2.3.4 Extraction of DNA fragments from agarose gels.***

Following electrophoresis on an appropriate percentage agarose gel, DNA was isolated by staining the gel with ethidium bromide and excising the band of DNA with a scalpel under long wave UV light. DNA was then isolated from the gel slice using the Qiaex II™ gel extraction kit following the suppliers protocol.

### ***2.3.5 Preparation of electroporation competent bacterial cells.***

Single bacterial cells were inoculated in 10ml of luria broth and grown in a shaking incubator overnight at 37°C. 5 ml of each culture was used to seed 500ml of luria broth. Large cultures were grown with shaking at 37°C until an OD600 of approximately 0.6-0.8 was obtained. The cultures were placed on ice for 15 min, then centrifuged in a JA14 rotor at 7,000rpm. Cell pellets were resuspended in 500 ml of ice cold Milli-Q water and re-pelleted by centrifugation at 7,000rpm in a JA14 rotor at 4°C for 15 min. Cell re-suspension and pelleting was repeated a further two times before final resuspension in 2ml of ice cold 10% glycerol per 50ml of original culture. Cells were stored in 80µl aliquots at -80°C.

### ***2.3.6 Sub-cloning restriction fragments into plasmid DNA vectors.***

#### **2.3.6.1 Preparation of vectors and restriction fragments.**

Linearised vector DNA and restriction fragments were prepared by digestion with the appropriate restriction enzymes. The 5'-terminal phosphate group from the linearised

vector was removed using calf intestinal phosphatase (CIP) essentially as described by Maniatis *et al* (1989). The vector DNA and the restriction fragments were purified from agarose gels (as described above).

#### **2.3.6.2 Ligation of restriction fragments into vector DNA.**

DNA fragments to be ligated were placed in excess (approximately 3 volumes) within a mix containing 0.1 volumes of 10 X ligation buffer and 1 unit of T4 ligase in a total volume of 10 $\mu$ l. The reaction was incubated at room temperature for 1 hour.

#### **2.3.6.3 Transformation of competent bacterial cell by electroporation.**

Ligation reactions were ethanol precipitated and resuspended in 20 $\mu$ l Milli-Q water. To this, 40 $\mu$ l of electroporation competent cells were added and the mixture stored on ice for 5 min. The ligation mixture was then transferred into sterile cuvettes and subjected to a 2.5kV pulse (25 $\mu$ FD) in the Gene Pulser before 200 $\mu$ l SOC medium was used to wash the cells out into another 800  $\mu$ l of the medium. The transformed cells were incubated at 37°C for approximately 30 min and spun at 350 X *g* in a centrifuge for 5 min. The pellet was resuspended in 100 $\mu$ l Milli-Q water.

#### **2.3.6.4 Plating of transformed cells.**

Using a sterile glass spreader, transformed cells were plated onto L-agar containing 100 $\mu$ g/ml ampicillin or 50 $\mu$ g/ml kanamycin and left overnight at 37°C. For vectors facilitating blue/white colour selection 4 $\mu$ l IPTG (200mg/ml) and 20 $\mu$ l X-gal (20mg/ml) were added to cells immediately prior to plating.

### ***2.3.7 Determination of DNA concentration.***

The concentration of DNA samples was estimated by comparing their intensity to bands of known concentration on an agarose gel. For more accurate estimation of DNA concentration, UV absorbance at 260nm was determined using a UV-visible spectrophotometer (50µg/ml of DNA per absorbance unit).

### ***2.3.8 Plasmid DNA preparation.***

#### **2.3.8.1 Small scale preparations.**

Plasmid DNA was routinely isolated from 2ml overnight cultures using the QIAprep Spin Miniprep Kit protocol (QIAGEN).

#### **2.3.8.2 Large scale preparations.**

Large scale plasmid preps were completed with the QIAGEN plasmid midi kit from 50ml overnight cultures of single colonies.

### ***2.3.9 End-filling restriction endonuclease digested DNA.***

Both 5' and 3' overhangs were end-filled with T4 DNA polymerase. 1µg of restricted DNA was incubated with 0.2mM dNTP's, 1 X T4 DNA polymerase buffer and 2.5 units of the polymerase at 37°C for 1 hour. The enzyme was heat inactivated at 68°C for 10 min and the end product purified by phenol/chloroform extraction and ethanol precipitation.

### ***2.3.10 Automated sequencing of PCR products.***

All automated sequencing runs were completed at the IMVS Molecular Pathology Sequencing Unit, South Australia. Automated sequencing reactions were carried out using 7-8 $\mu$ l of terminator ready reaction mix, 5 $\mu$ l of Template (30mg/ $\mu$ l), 3.2 pmole primer and approximately 4-5  $\mu$ l of water. The cycles completed on the DNA engine were: 96°C - 15 secs, 50°C - 5 secs, 60°C - 4 min, and completed 25 times.

### ***2.3.11 Polymerase Chain Reaction (PCR).***

PCR's were performed in 50 $\mu$ l volumes containing 0.5mM dNTP's, 1 X PCR reaction buffer, 5mM MgCl<sub>2</sub>, 0.7-1.0 $\mu$ M each primer, 1.5U of *Taq* DNA polymerase and template DNA. Amplification was performed in a Peltier Thermal Cycler 200 programmed with an initial template denaturation at 94°C for 3 min followed by 30-35 cycles of denaturation at 94°C for 1 min, a primer annealing step and extension at 72°C. Annealing temperature and time varied depending on the primer pairs.

### ***2.3.12 Preparation of PCR products for cloning.***

PCR products were ethanol precipitated as detailed in Section 2.3.1, resuspended in water and then digested with the appropriate enzyme. The digest was gel purified as detailed in Section 2.3.4, again resuspended in water and an appropriate amount of the purified fragments used in ligation reaction as detailed in Section 2.3.6.



### ***2.3.13 Yeast two-hybrid screening of cDNA library.***

#### **2.3.13.1 Preparation of the PROQUEST™ Two-Hybrid Mouse Embryo 10.5 day cDNA library**

Amplification and preparation of plasmid DNA from the cDNA library was following the instructions provided with the kit.

#### **2.3.13.2 Screening the library**

The ORF of hMID2 was cloned into the pDBLeu vector. Sequential transformation with pDBLeu-MID2 and the pPC86-Library was then performed following the instructions provided by the manufacturer.

### ***2.3.14 Plasmid transformation into yeast***

Transformation of plasmids into yeast was performed essentially as described by Elble R., 1992. Briefly, a single fresh yeast colony ( $\sim 10^7$ - $10^8$  cells) was suspended in 500ul PEG/LiAc/TE and mixed by gentle vortexing. 100ug of carrier DNA (in 10ul) was then added plus 1ug transforming DNA and again mixed by vortexing. The mixture was then incubated overnight at room temperature. Fifty ul of settled cells were removed and spread onto selective plates for incubation.

### ***2.3.15 Yeast DNA preparation***

Three ml cultures of yeast in appropriate selective media were grown overnight at 30°C, span down the pellet and resuspended by vortexing in 300ul yeast lysis buffer. Glass beads ( $\sim 450$  microns diameter) were then added and the sample vortexed (bead beat) for 3 min. 0.5ml phenol/CHCl<sub>3</sub>/isoamyl alcohol (25:24:1) was then used to extract the

upper layer, with the DNA subsequently precipitated with 2X volumes of absolute EtOH at -20° for 30min. The DNA was routinely resuspended in 40ul 1X TE or H<sub>2</sub>O.

### ***2.3.16 Maintaining cultured cell lines.***

All cultured cell lines were routinely grown in 75-150cm<sup>3</sup> flasks (Falcon) at 37°C in an atmosphere of 5% CO<sub>2</sub>. Cell lines were maintained by subculturing approximately 1:10-1:20 dilutions every 3-4 days. Harvesting and subculturing adherent cells was completed by first removing the culture media, washing twice with PBS before the addition of 1-2ml of trypsin/EDTA solution. The cells were left at room temperature until they began to detach from the surface of the flask, after which time 7ml of culture media was added and the flask washed to remove any remaining cells. Harvested cells were washed twice in PBS and pelleted by centrifugation at 1,200 X g for 5 min before being resuspended in the appropriate buffer.

### ***2.3.17 Transfection of cultured cells with Fugene.***

Cells were seeded into appropriately sized dishes to approximately 60-80% confluence in growth media. The cells were allowed to attach to the surface of the flasks or inserted coverslips for at least 4 hrs and transfected with a mixture of Fugene (Roche) diluted with DMEM and the appropriate DNA construct (as per manufacturers recommendations). Following at least 24 hrs of expression, cells were utilised for either protein extraction or immunofluorescence.

### ***2.3.18 Immunofluorescent analysis of cultured cells.***

24 hrs (unless is otherwise indicated) post transfection cells plated on coverslips were rinsed twice PBS and fixed with 3.5% PFA in PBS. Following permeabilisation with 0.2% Nonidet-P40 in PBS, mitochondria were stained with the appropriate dilution of primary antibody for 1 hr. Excess primary antibodies were washed off with PBS and attached antibodies were then detected with appropriate dilutions of conjugated secondary antibodies. The coverslips were inverted and mounted onto glass slides for visualisation under appropriate wavelength light on an Olympus AX70 microscope and images captured using a Photometrics CE200A cooled CCD camera.

### ***2.3.19 Cryo-Immunogold Electron Microscopy.***

Cultured HEK-293T cells (on 10 cm dishes) that were transformed with the indicated constructs were harvested and washed once with 1 X PBS. The cells were then fixed in 2X glutaraldehyde fixative for 1hr, washed in 1 X PBS with 4% sucrose, and then resuspended in 100 ul 10% gelatin. Cryosectioning of the samples was completed by Lyn Waterhouse (CEMMSA, Adelaide University, SA). Immunogold labelling of the cryo-sections was performed according to the procedure in Current Protocols in Cell Biology (1999). Sections were visualized on a Philips CM100 transmission electron microscope and images captured using a Soft Imaging System MegaView II digital camera.

### ***2.3.20 Wortmannin treatment***

Wortmannin was added to cell culture media (DMEM+10%FCS) at a final concentration of 100 nM (Simonsen et al., 1998). Following addition, cells were cultured for a further 30 minutes before immunofluorescence analysis.

### ***2.3.21 Golgi staining with WGA-Alexa Fluor 350***

WGA was applied together with the secondary antibody at a final concentration of 10ug/ml onto coverslips and incubated for 1.5 hours for immunofluorescence analysis.

### ***2.3.22 Estimation of Fluid-phase endocytosis***

Duplicate cultures of HEK-293T cells (transfected with the indicated constructs) were grown in 6-well 35 mm diameter trays and used for fluid-phase endocytosis analysis as previously described (Bucci et al., 1992). Briefly, cells were incubated with 5 mg/ml HRP in a serum free buffer at 37° for 10 min then collected after an intensive wash. The cells were then lysed with 10 mM HEPES (pH 7.4) plus 0.2% Triton X-100. Protein concentration in the post-nuclear supernatant (supernatant from the collected cell lysate after spinning at 4000 rpm, 4° for 10 min) was determined by the Bradford assay (section 2.3.25). The HRP activity/50ug total protein in the post-nuclear supernatant was estimated using *O*-Dianisidine, as described (Marsh et al., 1987). The reaction was stopped after 3 min and HRP activity was determined by the absorbance at 460 nm.

### ***2.3.23 Receptor-mediated endocytosis analysis***

Cells transfected with the indicated constructs were grown on coverslips in 6-well 35 mm trays. The culture media were substituted with the labelling media containing DMEM plus 25 mM HEPES, 1% BSA and 1 ug/ml EGF-Texas red (Itoh *et al*, 2001). Cells were labelled for 10 min at 37° and then washed twice with 1X PBS. Fixation and imaging were done as described in 2.3.18

**2.3.24 FRAP analysis for membrane microviscosity.**

Cells were grown on 90 mm dishes, which were modified with 1.5 cm diameter holes drilled at the centre of the base and sealed with coverslips. Plasma membrane was labelled with 8.3 ug/ml DiIC<sub>16</sub> at 4° for 15 min and medium replaced with serum-free DMEM plus 25 mM HEPES before labelling (Ghosh *et al*, 2002). Photobleaching of approximately a micron diameter region on the plasma membrane were made with short pulses from a 543nm HeNe laser beam at 100% power and the fluorescence recovery was monitored by scanning the bleached area with an attenuated beam of 20% power using a BioRad Radiance 2100 confocal microscope.

**2.3.25 Non-denaturing protein extraction from cultured cells.**

10cm plates containing either transfected or untransfected cells that were 80-90% confluent were rinsed twice with ice-cold PBS. Cells were collected by physical removal with a cell scraper in 1ml of ice-cold non-denaturing lysis buffer and transferred to a microcentrifuge tube. Following a brief vortex for 10 sec the cells were incubated on ice for 30 min and stored at -20°C.

**2.3.26 Protein concentration: Bradford assay.**

Bradford reagent (Biorad) was diluted 1:5 with Milli-Q water. Between 1-5µl of protein was made up to 200µl with dilute Bradford reagent and mixed by pipetting. The assay solution was placed into a 96 well plate and the absorbance at 590nm was measured on a UV spectrophotometer. BSA protein standard assays were obtained between the range 0-40mg/ml. Approximate concentration of the test sample was determined against a

linear plot produced by the BSA standard. All assays were completed in duplicate and the mean result determined.

### ***2.3.27 Co-Immunoprecipitation.***

Standard co-immunoprecipitation has been done according to the Current Protocols in Cell Biology (1999).

### ***2.3.28 Protein gel electrophoresis and western blotting.***

All SDS-PAGE of protein samples and subsequent western transfer to nitrocellulose or nylon membranes, Coomassie blue staining of gels were performed as described in Current Protocols in Cell Biology (1999). Nitrocellulose and Nylon blots were washed thoroughly with PBST and then blocked for 1 hr in PBST 5% Blotto. Primary and Secondary antibody incubations were carried out overnight at 4°C or for 45 min at room temperature with the appropriate dilutions of antibody in the aforementioned blocking solution. All secondary antibodies were conjugated to horseradish peroxidase (Amersham) and detected by Enhanced Chemiluminescence (Amersham).

### ***2.3.29 Protein sample preparation from cultured cells for gel filtration***

HEK-293T cells were grown to confluence on 90mm diameter dishes and were transfected with GFP-MID1 fusion protein expressing construct or other constructs as described in Chapter six. The cells were then lysed (lysis buffer plus 1 X protease inhibitors), sonicated and centrifuged at 10 000g at 4° for 10 min (Cainarca *et al*, 1999). The supernatant was ultracentrifuged at 150 000g at 4° for 30 min before being loaded

onto a lysis buffer-equilibrated Superose 6 gel filtration column on a Pharmacia FPLC system.

### ***2.3.30 Gel filtration***

Protein samples were eluted at 0.4 ml/min with the lysis buffer and were monitored by a UV spectrophotometer at OD<sub>280</sub>. 0.5 ml fractions were collected and 10 ul aliquots of each was separated by 10% SDS polyacrylamide gel electrophoresis and then subjected to western blotting with appropriate antibodies.

### ***2.3.31 Protein sample concentration.***

Fractions containing the peak elution of GFP-MID1 fusion protein and the corresponding fractions of controls were each pooled. Samples were then dried down under vacuum to ~1 ml and then dialysed twice against 1L H<sub>2</sub>O at 4° overnight by using Slide-A-Lyzer 10K Dialysis Cassettes. The dialysed sample (~3 ml) was again dried under vacuum and then resuspended in 300 ul 2-D sample buffer.

### ***2.3.32 Two-dimensional protein electrophoresis***

#### ***2.3.32.1 Sample rehydration***

7 cm (pH3-10) IPG strips were passively rehydrated in a tray with 125 ul rehydration sample buffer containing the indicated amount of protein sample. The sample was then overlain with 2 ml mineral oil to prevent evaporation. The strips were finally rehydrated overnight (~16 hrs) at room temperature.

### **2.3.32.2 Isoelectric focusing (first dimension)**

Protein samples were focused in the PROTEAN IEF cell (Bio-Rad) under the following standard program. The actual focusing conditions were slightly modified according to the loaded sample with the total voltage X hours no less than 20 000V-hr and the current not exceeding 50 uA/Strip

Start Voltage	End Voltage	Time	Temp
0 V	250 V	2 hrs	20°
250 V	4000 V	2 hrs	20°
4000 V	4000 V	5 hrs	20°

### **2.3.32.3 Protein separation on SDS-PAGE (second dimension)**

The IPG strips from the first focusing step were equilibrated in 2.5 ml SDS-PAGE equilibration buffer I and II for 10 min each. The strips were then mounted onto 10% SDS polyacrylamide gels and overlaid with 0.5% agarose solution. Gels were then run under standard conditions.

### **2.3.33 Coomassie blue staining and silver staining**

SDS polyacrilamide gels were stained in coomassie blue for 1-2 hours and then in destain solution on a platform shaker until the background colour was clear.

Silver staining was performed following the instructions provided with the PlusOne silver staining kit (Amersham).



### ***2.3.34 Protein recognition***

The in-gel trypsin digestion, reverse phase HPLC of the resultant peptides and mass spectrometry were done by Dr. Chris Bagley at the Hanson Institute's Protein Core Facility, Division of Human Immunology, I. M. V. S.

### ***2.3.35 GST fusion protein expression and purification***

An overnight culture of BL21 cells carrying the GST fusion protein expressing construct was diluted 100 fold into fresh L-broth +ampicillin and incubated at 37° with vigorous shaking until the A<sub>600</sub> reached 1.0. Cells were then induced with 0.2mM IPTG at 37° for additional 3 hours, after which they were pelleted by centrifugation at 7,700 X g for 10 min and resuspended in 1/100 volume of STE plus 5mM DTT and 1.5% Sarkosyl. Collected cells were subsequently lysed on ice by sonication in short bursts. The insoluble fraction was separated by centrifugation at 12,000 X g for 5 min. 1/50 volume 50% slurry of Glutathione Sepharose 4B was then added to the remaining supernatant and incubated with gentle agitation at room temperature for 30 min. The Glutathione Sepharose 4B matrix was then washed three times with 1 X PBS. The bounded GST or GST fusion protein was finally eluted with an equal volume of Glutathione Elution Buffer.



---

## Chapter Three: Functional redundancy between MID1 and MID2?

### 3.1 Introduction

The *MID1*-related *MID2* gene was initially identified after sequence similarity searches of the EST databases using the *hMID1* cDNA sequence. Like *MID1*, *MID2* maps to the X chromosome but to the long arm at band Xq22 (Xp22 for *MID1*). Analysis of gene composition and order on the X-chromosome indicated that Xp22 and Xq22, the loci for *MID1* and *MID2*, respectively, may have resulted from an ancient intrachromosomal duplication (Perry *et al.*, 1999; Buchner *et al.*, 1999). Consistent with this notion, the genomic structures of *MID1* and *MID2* are highly conserved, consisting of 9 coding exons that encode proteins sharing 76% identity (see Figure 1.5).

Although mutations in *MID1* had originally been found in a significant proportion (nearly 50%) of OS cases (Cox *et al.*, 2000), more recent mutation screening programs that have included many mildly presenting patients (i.e. showing only some of the characteristic features of OS) have revealed *MID1* mutations in only 17% of patients (De Falco *et al.*, 2003; So *et al.*, 2004). The low proportion of cases with *MID1* coding region mutations may reflect a genetically heterogeneous patient cohort (i.e. related but genetically distinct syndromes). However, the variability in clinical phenotype may also suggest the existence of mutations with less severe consequences in non-coding regions of the *MID1* gene, for example the promoter elements or, alternatively, the existence of other modifying genes.

It has been hypothesised that MID2 is one of the modifying factors given its similar cellular distribution and primary structural similarity. The results presented and discussed in this chapter provide some of the first evidence in support of the hypothesis.

## 3.2 Results

### 3.2.1 *MID1 and MID2 heterodimerize*

MID1 and MID2 encode highly related RBCC proteins that associate with the microtubule network following homodimerization. The high level of sequence identity, including the Coiled-Coil motif that is responsible for dimerization, raised the possibility of the two proteins also binding as heterodimers to microtubules.

To determine whether this was indeed the case, a directed yeast-based two-hybrid assay was employed. In this system, the protein of interest is expressed as a GAL4-DNA-Binding domain (DB) fusion protein and the bait expressed as a GAL4-Activation domain (AD) fusion protein. A positive protein-protein interaction drives the expression of three reporter genes (*HIS3*, *URA3* and *lacZ*), which confers to the host strains a selective phenotype (i.e. selection media or X-gal assay). Importantly, the yeast expressing vectors of DB-(pDBLue-X) and AD-(pPC86-Y) fusion proteins are low-copy-number vectors, such that the expression levels remain close to physiological conditions albeit in a heterologous system.

MID1 and MID2 were cloned into both pDBLue and pPC86 vectors and expressed as GAL4-DB or GAL4-AD fusion proteins in different combinations (Dr. Blair Hopwood, Cox lab, The University of Adelaide). Besides the homodimerization as expected for MID1 and MID2, heterodimerization was also observed. Comparable growth of the transformed yeast on selective media suggested that the heterodimerization was of similar strength to that of their homo-interaction (Figure 3.1A).

Due to the well characterized role of the Coiled-Coil domain in mediating the dimerization of RBCC proteins, the Coiled-Coil domain deletion constructs of MID1 and MID2 in the pDBleu and pPC86 vectors were subsequently generated and their interactions with wild type MID1 and MID2 tested. As expected, both MID1 $\Delta$ CC and MID2 $\Delta$ CC lost their ability to mediate homo- and hetero-dimerization with wild type MID1 and MID2 while deletion of the adjacent B-boxes (MID1 $\Delta$ BB and MID2 $\Delta$ BB) did not significantly affect their dimerization capacity. These results are consistent with the complete co-localization of both wild type GFP and MYC tagged proteins on the microtubule network in COS1 cells (Figure 3.1B) that was also Coiled-Coil dependent (Kieran Short, data not shown).

### ***3.2.2 The normal microtubular distribution of MID2 is disrupted in an OS derived cell line***

As the majority of OS-related *MID1* mutations are C-terminal truncating mutations that form aggregates, it was expected that these mutants would retain the ability to dimerize since their Coiled-Coil domain was unaffected. Consequently, it was hypothesized that wild type MID2, or indeed wild type MID1, may also be present in these aggregates—with their removal from the microtubules contributing to the phenotypic severity. Therefore, the localization of wild type MID1 and MID2 was monitored in an OS primary skin fibroblast cell line carrying a typical C-terminal truncation mutation of MID1, MID1R495X.

Using anti-MID1 antisera, it was first shown that, as expected, endogenous wild type MID1 was associated with the microtubule cytoskeleton in skin fibroblasts derived from an unaffected control while the endogenous MID1R495X displayed cytoplasmic clumping in the patient cells (Figure 3.2A and B). This cellular distribution was similar

to that observed with GFP-MID1 $\Delta$ CTD in COS1 cells. The disrupted distribution was unlikely due to structural change of the microtubules since the microtubule network appeared normal in the OS fibroblast cells (figure 3.2C). Of interest was the observation of some fluorescence on the leading edge membranes for endogenous wild type MID1 (see Figure 3.2A), a localization not seen for overexpressed wild type MID1.

To determine whether the patient's MID1R495X C-terminal truncation mutation still retained the ability to interact with wild type MID2, a construct to express GFP-MID2 was transfected into the OS patient cells and the localization of the <sup>fusion protein</sup> assessed. In some cells, the normal microtubule-associated distribution of MID2 was observed (Figure 3.3A). However, in other cells, instead of the normal microtubule-associated distribution, wild type MID2 was tethered into the MID1R495X cytoplasmic clumps inferring dimerization of the MID2 and MID1R495X protein (Figure 3.3B). A similar experiment using GFP-tagged MID1 gave essentially identical results (Figure 3.3C and D). These observations suggested that the function of wild type MID2 could be perturbed in these OS cells.

### ***3.2.3 MID2A358D – a polymorphism or a OS-causative mutation***

Given the possibility of *MID2* being a contributory factor in the pathogenesis of OS, seven OS patients were screened for sequence changes in the 9 coding exons of *MID2* (Lillian R. Allen, MSc thesis, University of Adelaide). Notably, a missense change (resulting in an amino acid change A358D) was found in one patient (Figure 3.4). Screening of a further nine patients for this change showed it to be present in two additional patients, but surprisingly not in 100 unaffected individuals, indicating a possible role for this rare polymorphism in OS.

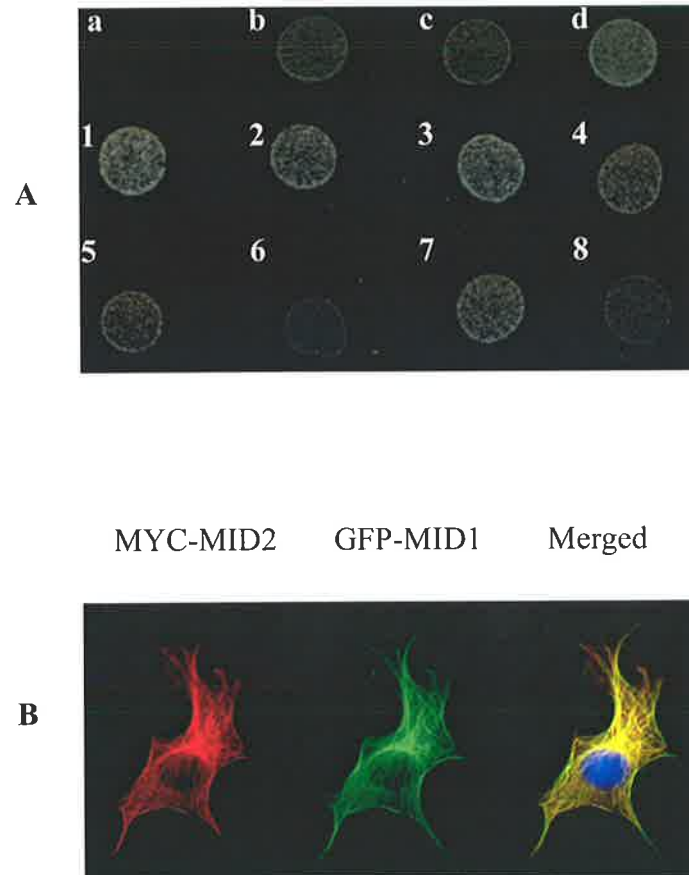


**Figure 3.1 The heterodimerization of MID1 and MID2.**

A. MID1 and MID2 homo-/hetero-dimerize through their Coiled-Coil domains in yeast two-hybrid.

a, b, c and d: represent the control yeast strains provided by the manufacturer, indicating increasing protein-protein interaction strength.

- |                              |  |
|------------------------------|--|
| 1: pDBleu-MID1 + pPC86-MID1; | 5: pDBleu-MID1 + pPC86-MID1 $\Delta$ BB; |
| 2: pDBleu-MID1 + pPC86-MID2; | 6: pDBleu-MID1 + pPC86-MID1 $\Delta$ CC; |
| 3: pDBleu-MID2 + pPC86-MID1; | 7: pDBleu-MID2 + pPC86-MID1 $\Delta$ BB; |
| 4: pDBleu-MID2 + pPC86-MID2; | 8: pDBleu-MID2 + pPC86-MID1 $\Delta$ CC. |

B. MID1 and MID2 colocalize on microtubules.

COS1 cells were cotransfected with the constructs expressing fusion proteins of GFP-MID1 and MYC-MID2. Colocalization of GFP-MID1 and MYC-MID2 on microtubules was shown by indirect immuno-fluorescence using monoclonal anti-MYC and a Texas-red conjugated secondary antibody.

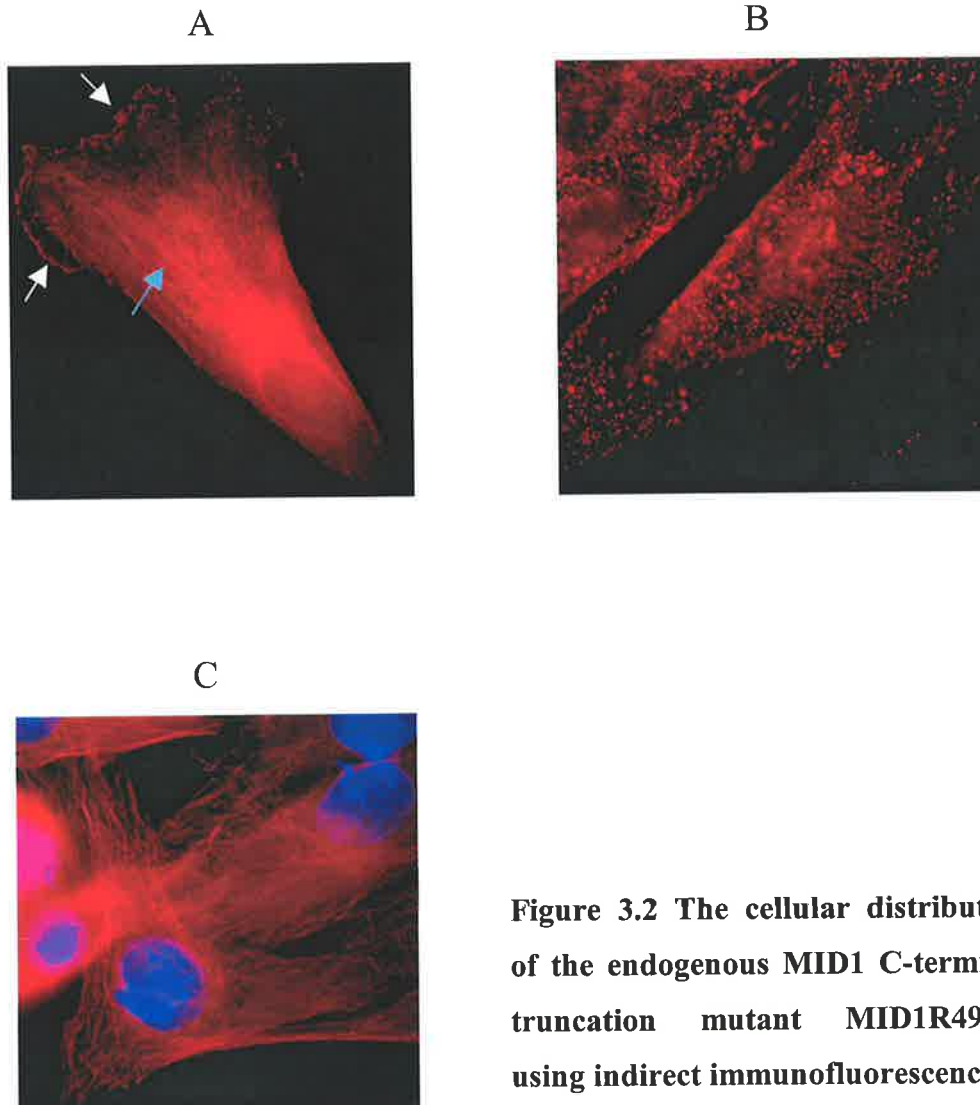


**Figure 3.2 The cellular distribution of the endogenous MID1 C-terminal truncation mutant MID1R495X, using indirect immunofluorescence.**

The endogenous MID1 was detected using rabbit anti-human MID1 antisera and a Texas-red conjugated secondary antibody: (A). The endogenous wild type MID1 is microtubule-associated (indicated by blue arrow) in primary skin fibroblasts derived from a unaffected control, although some fluorescence is apparent on the membrane ruffles at the leading edge (indicated by white arrows). (B). Endogenous MID1R495X was found in cytoplasmic clumps in primary skin fibroblast cells derived from an OS patient. (C). The microtubule network in OS fibroblast cells is unaffected as evidenced using a monoclonal anti-tubulin antibody and a Texas-red conjugated secondary antibody. Nuclei shown by blue DAPI staining.



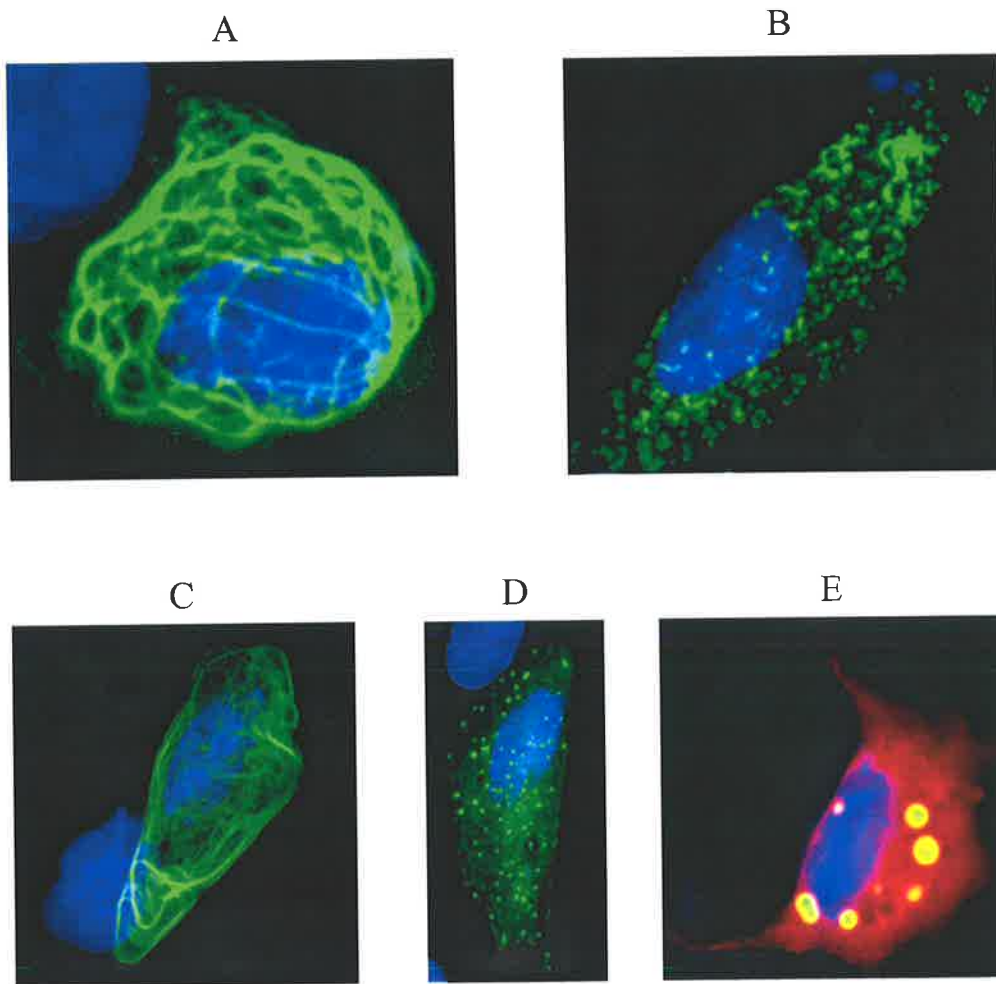


**Figure 3.3 The endogenous MID1R495X C-terminal truncation acts dominantly to disrupt the microtubular distribution of wild type MID2 and MID1.**

Wild type MID2 (A and B) or MID1 (C and D) were expressed as GFP fusion proteins in OS primary skin fibroblasts. Both microtubule-association (A and C) and cytoplasmic clumping (B and D) were observed with GFP-MID2 and GFP-MID1 in OS cells, indicative of homodimerization/heterodimerization between endogenous MID1R495X and GFP-MID1/GFP-MID2.

E. The heterodimerization between MID2 and MID1 C-terminal truncation mutation was also demonstrated by colocalization (yellow) of a GFP-MID1 $\Delta$ CTD fusion protein and MYC-tagged MID2 in COS1 cells. Nuclei were shown by DAPI staining (blue).



**Figure 3.4 The MID2A358D variation identified in OS patients.**

A missense mutation (1073C>A), resulted in an Alanine358 to Aspartic acid change at a position C-terminal to the MID2 Coiled-Coil domain, was identified in three unrelated OS patients.

However, overexpression of the MID2A358D in both COS1 cells and OS cells revealed a similar pattern of fluorescence as seen with wild type MID2 (Figure 3.5B), inferring this amino acid change does not dramatically alter the ability to dimerize or to bind microtubules. This conclusion was also supported by showing that MID1A358D could still form homo-/hetero-dimers (Figure 3.5A) in a yeast two-hybrid assay (Dr. Blair Hopwood, Cox lab, The University of Adelaide).

### 3.3 Discussion

An ability to homodimerize is a common but not obligatory property of RBCC proteins (reviewed by Reymond *et al.*, 2001). However, through dimerization, RBCC proteins can be further organized into higher oligomeric states, which is necessary for their interaction with other protein factors in even larger protein complexes. However, cross-talk is rarely found between family members, indicating a high specificity for the dimerization interface. The rare examples where heterodimerizations has been observed are between PML and Rfp; and between TIF $\alpha$  and TIF $\beta$ , the two closely related TIF family members (Cao *et al.*, 1998; Peng *et al.*, 2002).

Early investigations, using immunoprecipitation, failed to demonstrate heterodimerization between MID1 and MID2 (Cainarca *et al.*, 1999). This however, may have reflected a limitation in the sensitivity of the pull-down assay employed since the same investigations subsequently confirmed the results described in this chapter and the immunoprecipitation of the heterodimers by Dr. Blair Hopwood in our lab (Short *et al.*, 2002). The data in this chapter suggest that MID1 and MID2 heterodimerize with a strength comparable to the strong self activation of the full-length GAL4 in the control strain (Figure 3.1A). And consistent with previous data on RBCC proteins, the Coiled-

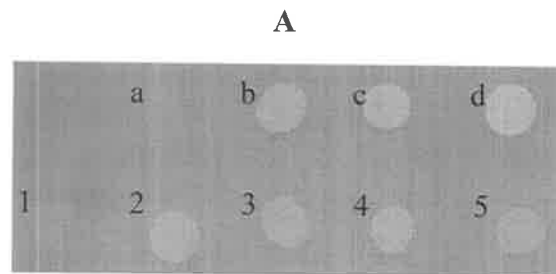
Coil domain of MID1 and MID2 was necessary for both homo- and heterodimerization.

Perhaps indicative of this strong interaction is the high level of sequence identity over the RBCC domains of MID1 and MID2 (RING-finger 85%, B-boxes 79.5% and Coiled-Coil 70%), much higher than that between TIF $\alpha$  and TIF $\beta$  (RING-finger 36%, B-boxes 59% and Coiled-Coil 32%). Interestingly, given the high similarity shared by members of the CI subfamily, heterodimerization only occurs between MID1 and MID2 but not between other gene pairs: Spring-MID1/MID2 (over 30% similarity over the entire RBCC domains) and TRIFIC-Haprin (over 50% similarity over the entire RBCC domains), further supporting that the heterodimerization of MID1/MID2 is specific.

The functional significance of MID1/MID2 dimerization is not clear, although dimerization is a prerequisite for their microtubule-binding (Short *et al.*, 2002). In a similar situation, the trimerization of the RBCC protein, KAP-1, is a prerequisite for its binding to the Krüppel associated box (KRAB) domain of zinc-finger proteins and the oligomerization of PML is also required for its binding to other factors in the PML nuclear body (Jensen *et al.*, 2001; Peng *et al.*, 2002). The dimerization of MID1/MID2 may also result in an increased affinity for their protein interactors and/or direct their interactions to different protein targets, with homo- to hetero-dimers having different 'activities'. The heterodimerization may also simply be a reflection of the relative recent duplication that has given rise to these genes—a fact also supporting the notion of shared or partially redundant functions.

Previous investigations revealed the lost or decreased microtubule-association of all tested OS-related MID1 mutations when overexpressed in COS cells. However, information on the cellular distribution of endogenous MID1 was limited due to: 1. the low level of expression; and 2. the sensitivity of MID1 antisera to detect MID1 along

**Figure 3.5 MID2A358D showed apparently normal microtubule-association and dimerization capability.**



A. The homo-/hetero dimerization of MID2A358D was unaffected.

a, b, c and d: The control yeast strains provided by the manufacturer, indicating increasing protein-protein interaction strength.

1: pDBleu + pPC86-MID2A358D;            2: pDBleu-MID1 + pPC86-MID2A358D;

3: pDBleu-MID2 + pPC86-MID2A358D; 4: pDBleu-MID1 + pPC86-MID2;

5: pDBleu-MID2 + pPC86-MID2

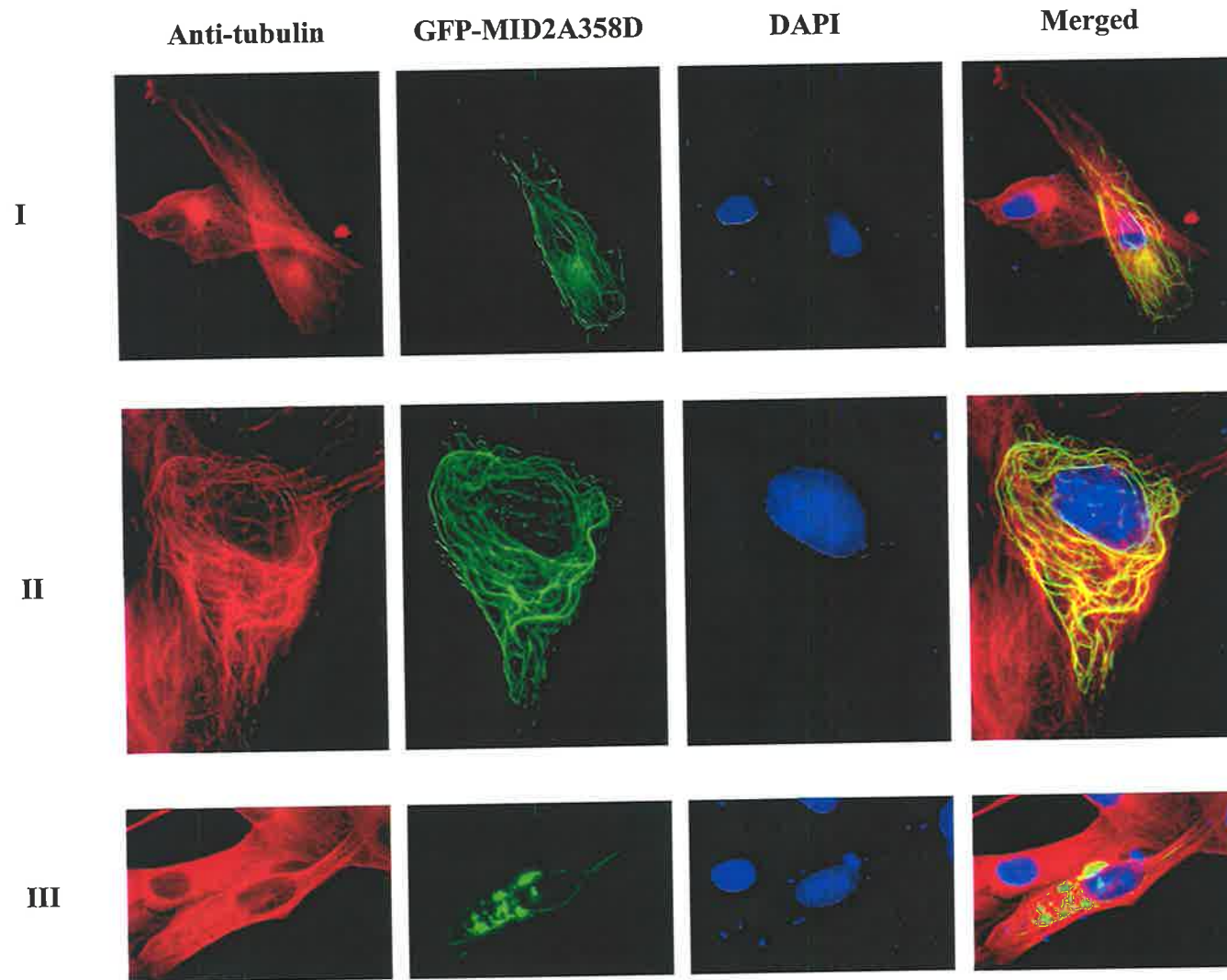
B. The cellular distribution of MID2A358D in control and OS cells.

MID2A358D, the MID2 variant identified in OS patients, was expressed as a GFP fusion protein in fibroblast cells derived from either an unaffected individual (I) or an OS patient bearing the MID1R495X truncating mutation (II and III). The overexpressed GFP-MID2A358D was viewed by direct fluorescence and the microtubules were shown by indirect immuno-fluorescence using a monoclonal anti-tubulin antibody.

Panel I: GFP-MID2A358D was microtubule-associated in normal fibroblast cells.

Panel II and III: Both microtubule-association (II) and cytoplasmic clumping (III) were observed with the overexpressed GFP-MID2A358D in OS fibroblast cells, indicating hetero-dimerization between GFP-MID2A358D and MID1R495X.

**B.**



the length of microtubule network. However, in this chapter, a distinct cellular distribution of endogenous MID1 has been demonstrated in normal versus OS derived primary fibroblast cells by indirect immunofluorescence using MID1 antisera generated in our lab. The OS derived fibroblast cells used carry a 1483C>T nonsense mutation, which results in a truncated protein product missing most of the C-terminal B30.2 region (from residue 495 to 667). The strong signal of the cytoplasmic clumps seen with the MID1R495X mutant were due to enhanced fluorescence as a result of the abnormally aggregated MID1R495X, similar to the distribution of the overexpressed MID1 $\Delta$ CTD in COS1 cells. Notably, in addition to the filamentous distribution of endogenous wild type MID1, some fluorescent signal was also observed on the plasma membrane at the leading edge of cells, which had not been found for overexpressed tagged MID1. The dominant microtubule-association of overexpressed MID1 may make it difficult to pick up the lesser amount of membrane-associated MID1—a problem inherent to many camera detection systems. However, the localization of MID1 in these two distinct cellular compartments may reflect its role in connecting the membrane and microtubule cytoskeleton, a conclusion further supported by the results in the following chapters. Low level fluorescence observed throughout the cytoplasm in both control and OS derived fibroblast cells was assumed to be due to background resulting from the crude nature of the MID1 anti-sera.

Of particular note was the observation that the overexpressed MID1 and MID2 (as GFP fusion proteins) was also recruited to the cytoplasmic aggregates formed by endogenous mutant MID1 in some OS cells. This finding suggested that a disruption of the cellular function of endogenous MID2 could be expected in OS cells, and therefore may also contribute to the pathogenesis of OS.

In those OS cells where an apparently normal microtubule distribution of overexpressed GFP-MID1/GFP-MID2 was observed, this may indicate that the event is stochastically determined, such that the composition of MID1, MID2 and mutant MID1 in the oligomers varies according to their cellular level; i.e. the ratio of MID2(MID1):MID1R495X in their oligomer may be critical for the cellular localization of these protein complexes. Excess unbound wild type MID1/MID2 would remain distributed along the microtubules and the MID1R495X protein complexes that have excess MID1/MID2 could also be reloaded onto microtubules. Consistent with this is the demonstration that wild type MID1 and MID2 were only present in the cytoplasmic clumps formed by overexpression of the MID1 $\Delta$ CTD mutant in COS1 cells (Figure 3.3E). Given its overlapping but variable level of expression during early embryogenesis, variation of the composition in the oligomer under physiological conditions may therefore explain the variable severity of the clinical features of different, or even related, OS patients. This also raises the question of whether mutations in *MID2* would also result in a similar phenotype to that of OS or whether only tissues expressing high levels of MID2 and low of MID1 would be affected.

Finally, the role of a single amino acid change, A358D, previously found in three unrelated OS patients was briefly investigated. Interestingly, Alanine358 is conserved in human, mouse and chick MID2, although an Aspartic acid residue is at this position in one of the non-interacting CI subfamily members of the RBCC family. Although only a relatively small number of unaffected individuals (100) were screened, the increased incidence of this variant in OS patients suggested that it may have a functional role. Curiously, the OS fibroblast cell line is from the only patient that harbors both a *MID1* truncating mutation and the A358D MID2 variant. The change from Alanine358 to Aspartic acid is at a position C-terminal to the MID2 Coiled-Coil region, the domain



critical for dimerization and microtubule-binding. However, this single amino acid change did not appear to affect the microtubule-binding of MID2 in control fibroblast cells, although quantitative assessments have not been done. That cytoplasmic clumping of GFP-MID2A358D still occurred in some of the OS fibroblast cells supported the reasonably strong heterodimerization capability. The result is also consistent with the dimerization of MID2A358D and MID1/MID2 in<sup>a</sup> yeast two-hybrid system. Compared with *MID1*, the lack of mutations in *MID2* gene and the lack of phenotype of the identified *MID2* variant at the cellular level may indicate a more conserved role for *MID2*. However, further investigations into the role of this variant are nevertheless still warranted and should be re-addressed as appropriate quantitative assays become available.



---

## Chapter Four: PEPP2 was identified as a MID2 interactor

### 4.1 Introduction

Protein-protein interactions are required for essentially all cellular processes and their regulation. Upon interaction, a protein's binding affinity for other factors or its enzyme activity may be modified, or the protein may be translocated to its destination. Identifying interactors of a given protein is critical in understanding its cellular function. This is particularly relevant for RBCC proteins since they provide an interface for numerous protein-protein interactions.

As addressed in the last chapter, the demonstrated ability of MID1 and MID2 to heterodimerize raised the possibility that the two proteins may perform at least partially redundant functions (i.e. based on their high level of sequence identity) or even coordinated functions during development. To investigate these possibilities, the ProQuest<sup>TM</sup> yeast two-hybrid system (Gibco) was used to identify potential interactors of MID2. This system was chosen because of its successful use in the previous MID1/MID2 dimerization studies (chapter 3). A screen for MID1 interactors was earlier conducted by Kieran Short in the lab (Molecular Biosciences, The University of Adelaide, SA), and is referred to, where relevant, to the results presented in this chapter. In this approach, MID1/MID2 were expressed as GAL4-DB fusion proteins and used as baits to screen a mouse 10.5 dpc whole embryo cDNA library. This library was chosen as *Mid1* and *Mid2* are ubiquitously expressed in the 10.5dpc mouse embryo, albeit at various levels in different tissues (Dal Zotto *et al.*, 1998; Buchner *et al.*, 1999).

Given the presence of incomplete ORFs in any cDNA library and the false positives that are commonly found in yeast two-hybrid systems due to self-activation (details in the next section), all potential interactors identified were further investigated by testing the

interaction between the full length interactors and MID1/MID2 in both directions (i.e. the ORFs of MID2 and the potential interactors were swapped into the constructs expressing GAL4-AD or GAL4-DB fusion proteins). Candidate interactors were then subjected to immunofluorescence and immunoprecipitation in mammalian cells to determine whether the interactions were likely to be physiologically relevant. Due to the sequence similarity of MID1 and MID2, putative MID2 interactors were also analyzed for their ability to interact with MID1 and vice versa.

## 4.2 Results

### 4.2.1 Yeast two-hybrid screen for MID2 interactors

Given the high level of amino acid identity (99%) between human MID2 and mouse Mid2, it was reasoned that human MID2 would function in an identical manner to the mouse protein with respect to interactions with other murine protein partners (i.e. conserved function). For this reason, as well as the immediate availability of only the full-length human MID2 cDNA, a construct (pDBLeu-hMID2) containing the hMID2 fused in frame and downstream of the yeast GAL4-DB was generated and used to screen the ProQUEST Two-Hybrid 10.5dpc mouse whole embryo cDNA library constructed in the pPC86 vector (Gibco). Inserts in this vector are placed downstream and potentially in frame with the yeast GAL4 activation domain.

Positive interactions between MID2 and potential protein interactors encoded by the cDNA library were screened <sup>for</sup> by the expression of *HIS3* gene. About  $10^6$  yeast colonies co-transfected with pDBleu-hMID2 and pPC86-Y (Y is any mouse cDNA from the library) were screened on 25 x 15cm plates containing synthetic complete medium lacking histidine ( SC-Leu-Trp-His+50mM3AT). *HIS3* encodes imidazole glycerol phosphate dehydratase, an enzyme involved in histidine biosynthesis. This enzyme can

be specifically inhibited in a dose-dependent manner by 3-aminotriazole (3AT). Since a basal level of HIS3 is expressed by MaV203 due to self-activation (transcription of HIS3 activated by DB-X only in the presence of AD), additional 3AT had to be included in the -His medium to inhibit this background expression and hence maximize the sensitivity of the HIS3 reporter gene for detecting weak protein-protein interactions. Inclusion of 50mM 3AT in the -His medium was shown to be sufficient to also inhibit the background *HIS3* expression induced by pDBleu-MID2 (results not shown). Twenty-two yeast colonies that grew strongly under these conditions were selected and restreaked onto a master plate (SC-Leu-Trp) along with the five control yeast stains provided by the manufacturer that represent varying interaction strengths that allow comparison<sup>s</sup> to be drawn with the test proteins (Figure 4.1A). To monitor the expression of three reporter genes, these yeast colonies were replica plated onto each of the following media:

1. SC-Leu-Trp-His+50mM3AT
2. SC-Leu-Trp-Ura
3. YPAD + nylon membrane

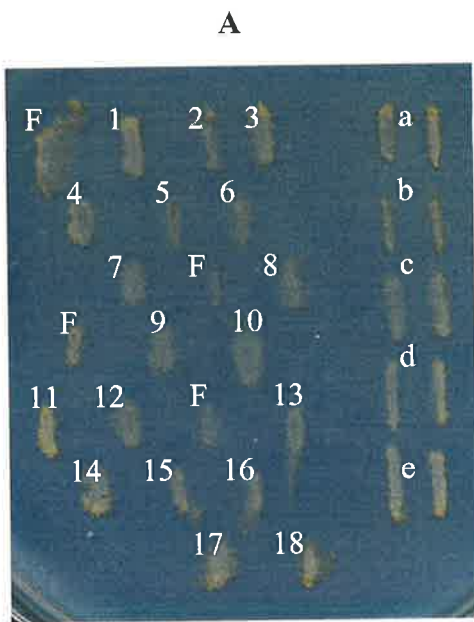
As the number of cells transferred onto the selection plates can affect the quantitation of this assay (i.e. background growth), replica cleaning was done to ensure that only a minimal number of yeast cells were plated onto the selection plates. After the replica cleaning, the yeast cells were incubated up to 48 hours on the selection media whereas they were incubated for only 18 hours on YPAD media before initiation of the X-gal assay (for details see section 2.3.13). Following this procedure, 18 of the 22 first round positives displayed consistent growth on -His+50mM3AT medium and -Ura medium, and were positive in the X-gal assay (Figure 4.1B, C and D).

#### ***4.2.2 Identifying the potential interactors***

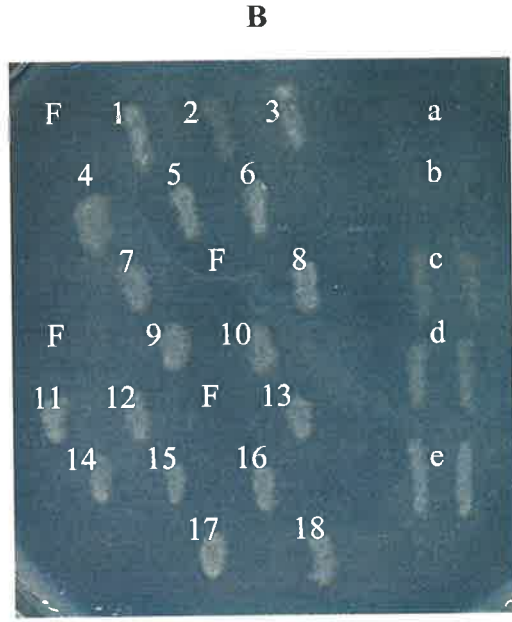
The plasmids from these 18 yeast colonies (Y2HP1-18 (Figure 4.2A)) were subsequently recovered using the standard protocol (see section 2.3.15). With the exception of Y2HP2 and Y2HP4 that did not yield plasmids of expected size (pPC86-Y, 7kb plus), the remaining 16 yeast plasmids were used as templates for PCR with pPC86 specific 5' (GAL4AD) and 3' (ADH-term) primers (Figure 4.2B). Inserts of different sizes were successfully amplified and the plasmids from these 16 yeast clones were subsequently sequenced using the primer designed to the GAL4-AD. These sequences were then used to search against the NCBI non-redundant nucleotide data base. Thirteen of the 16 (Y2HP1, Y2HP3, Y2HP5-9, Y2HP11-14, Y2HP16 and Y2HP17) were shown to encode mouse Alpha4. Y2HP10 contains 3' UTR sequence of mouse *plasma glutathione peroxidase (GPX)*, which when in pPC86, resulted in synthesis of a fusion protein of the GAL4 activation domain and an additional 50 amino acids (NH<sub>2</sub>-EGGSTHASAHASAKETQVLGPMVLLKPEHHSWGQHLPHAHTTHHQPPSSF-COOH) encoded by the 3'UTR (Figure 4.3). Blast searches with this peptide against known protein sequences and motifs failed to reveal any significant match. Y2HP15 represents an in-frame fusion with the C-terminal end of the mouse homologue of the human NY-CO-3 antigen. Y2HP18 contains an in-frame partial cDNA sequence encoding the C-terminal end of the mouse homologue of the human phosphoinositol three-phosphate-binding protein-2 (PEPP2).

**Figure 4.1 Yeast two-hybrid screen for potential MID2 interactors.**

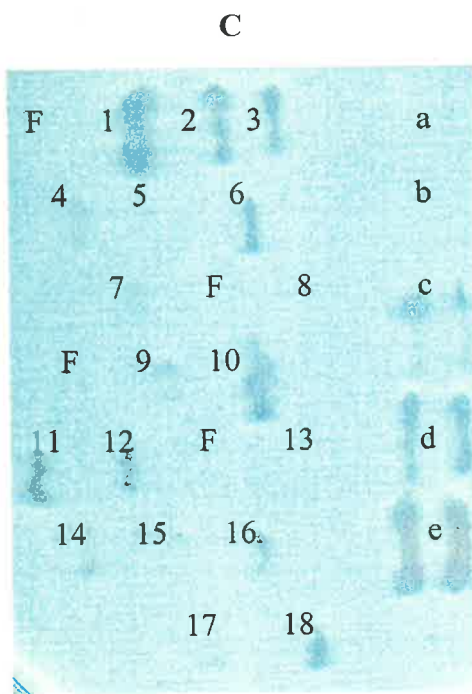
The 22 positive yeast colonies containing putative interactors of MID2 were plated on a SC-Trp-Leu master plate, along with five control strains (a—e) containing known interactors of increasing strengths of interaction (A). These yeast colonies were replica plated onto three selective plates for monitoring the induction of the three reporter genes: SC-Trp-Leu-His+50mM3AT for monitoring *HIS3* expression (B), SC-Trp-Leu-Ura for monitoring *URA3* expression (C) and X-gal assay for monitoring *LacZ* expression (D). 18 (Y2H1-Y2H18) out of 22 yeast strains were subsequently considered as *bona fide* positives, although Y2H5, Y2H8, Y2H13 and Y2H15 showed minimal growth on –URA medium, the most stringent selection, while displaying consistent growth on –His+50mM3AT and blue color in the X-gal assay. The four false positives (labeled with F) failed to grow on either SC-Trp-Leu-His+50mM3AT or SC-Trp-Leu-Ura, and displayed white or only pale blue color in the X-gal assay.



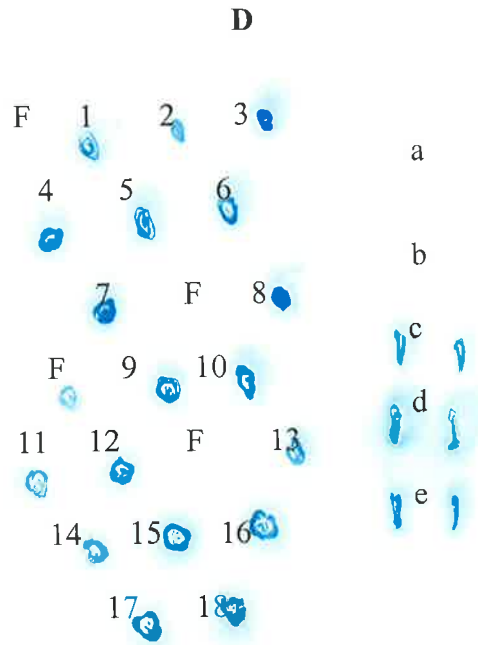
Master plate (SC-Leu-Trp)



Selective plate  
(SC-Leu-Trp-His+50mM3AT)



Selective plate  
(SC-Leu-Trp-Ura)



X-Gal

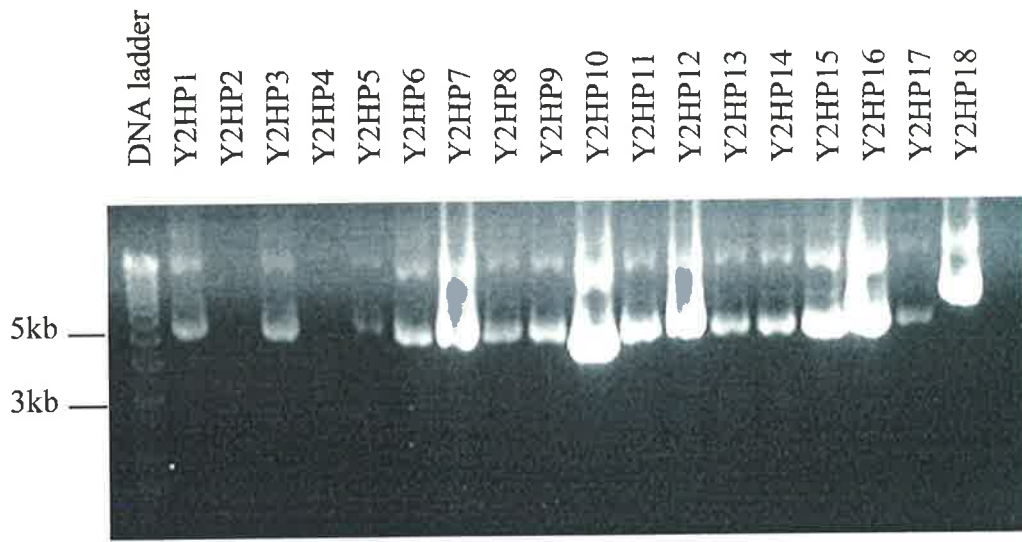


**Figure 4.2 The isolation and assessment of the putative MID2 interactors.**

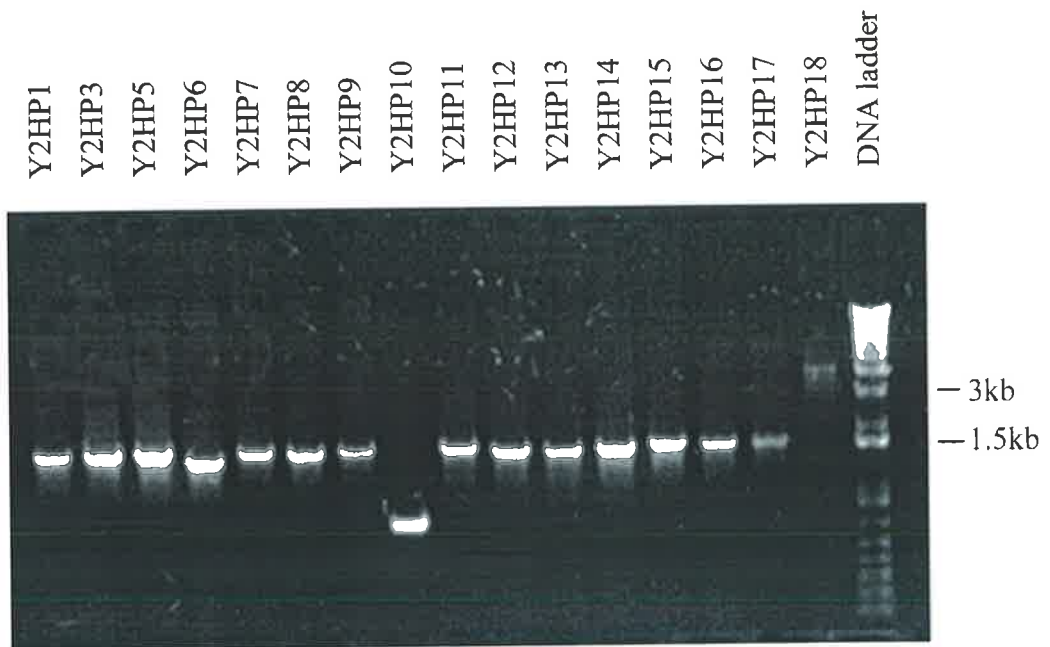
The pPC86-Y plasmids were extracted from the 18 positive yeast colonies from the Y2H screen and were electrophoresed on a 1% agarose-TAE gel (A). The Y2HP2 and Y2HP4 did not yield the expected pPC86-Y fusion constructs. Repeated attempts gave the same results and the ~~positive phenotype of the~~ yeast colonies were assumed to be false positives.

Insert sizes from 16 cured pPC86-Y plasmids were verified by PCR with pPC86 specific 5' and 3' primers (for sequences see section 2.2.18), and viewed following 1% agarose-TAE gel electrophoresis (B). These 16 plasmid clones were subsequently sequenced and BLAST searches performed with each.

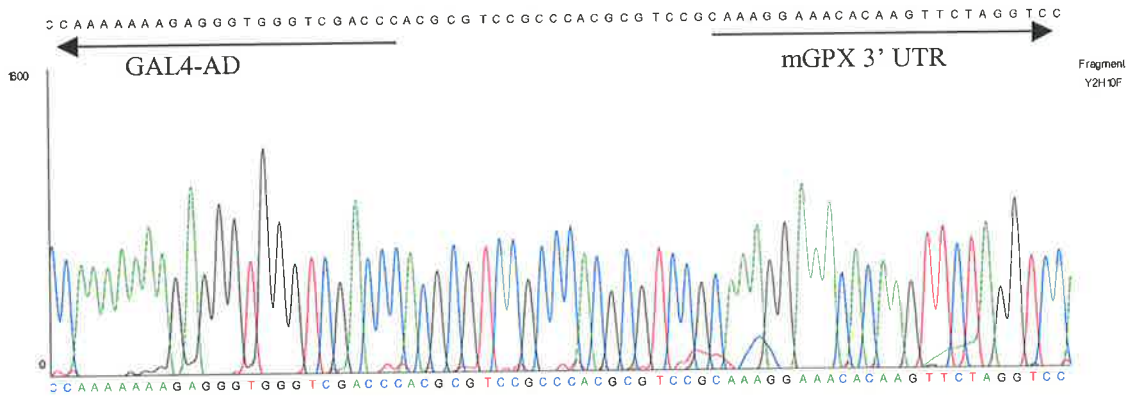
A.



B.



A.



B.

```

1  cgcgccccag ccgcccattgg ccgggatccc cggggcattcc tgaattctgt ccatgctcat
61  ggccggggttt gttccgcccgg gcgggggaba agagaagtct aagacagaact gccatggcgg
121  tatgagtggt adcatctacg agtatggagc cctcaccata gatggggagg aatacatcc
181  ttttaagcag tatgcaggca aatatatccc ctttgtcaac gttagccagct actgaggtct
241  gacagaccaa taccttgaac tgaatgcact acaagaagaa cttgggccc attggttgg
301  cactctgggc ttccttccca accaattagg caaacaggag ccaggcgaga actcggagat
361  aaccccccagt ctcaagtatg ttccgaccagg tgggggcttt gtgctaatt tccagctct
421  tgagaaagga gatgtgaaag ggyagaaga gcagaaatc tacacttcc tgaagaactc
481  ctgcccctcc actgcagaac tcttggctcc acctggccgc ctcttttggg aacccatgaa
541  gatccatgac atccgctgga actttgagaa gttectggtg gggccagatg gcatacgggt
601  tatgcgctgg taccaccgga ccacagtccg caacgtcaag atggacatcc tgbctbacat
661  gaggccgcaj gcagccctga gcgcacagggg gaagtaactg atgccccac cctacccta
721  cccctgccc atcatgcaag ggcgaggag gggctcttca ggaaggaagc cacattccca
781  gtcattctac cccaccccag attctcttcc ttattacata aaagacaagc ctggcacaac
841  tgtgtgtctg aaccactgtg gacacgtgac aattgtcca gtgtgtgcat ggctacacag
901  ccacgtatct gctgtcttga aaccaggga tggccatct gtgttacg cttggcaca
961  caccctcata ttttttccag ctttctgttc caaatgagcc caaaggaac acaagttcta
1021  ggtccaatgg ttctgctcaa acctgaacat cattcttggg gccagcatct cccacatgcc
1081  cactacac accaccagcc tcttcttcc ttctgaaag acctctga gcccccaagc
1141  ccatcccaca gtgctcctga gaccagccaa gacaactgtg agcgcgatgg ccgtgtacc
1201  caggtcaggg gtggtgtctc tatgaaggag gggcccgaag cccttgtggg cgggctccc
1261  ctgagcccgt ctgtgtgccc agcccttagt gcattcaggc ttaggctccc aggcagggac
1321  actaccccg cgcctctgga ggacatgcta tctctcact ctgtccactg gtatctcaac
1381  acccccatct gcccagtaa ggtcttctg cagca

```

**Figure 4.3 Y2HP10 contains an insert of mouse glutathione peroxidase 3' UTR.**

(A). Chromatogram showing the fusion of the sequence of mouse glutathione peroxidase 3'UTR with GAL4-AD. The start position of the glutathione peroxidase 3'UTR is indicated by the rightward arrow.

(B). The complete mRNA sequence of mGPX. The sequence contained in Y2HP10 is highlighted in yellow and the ORF of mGPX is highlighted in blue. The insertion of this 3'UTR resulted in the expression of a fusion protein containing the GAL4-activation domain and an additional 50 amino acids encoded by the underlined 3' UTR sequence.

### 4.2.3 Validation of the interaction between MID2 and the “positives” identified in the Y2H.

Verification of the interaction of MID2 with the full length Alpha4, NY-CO-3 and PEPP2, was necessary to determine whether they represented *bona fide* or physiologically relevant interactions. Since Alpha4 was also identified in the parallel yeast two-hybrid screen for putative MID1 interactors, indicating a common interactor for both MID1 and MID2, verification/characterization of the interaction between Alpha4 and MID2 was performed together with MID1 by Kieran Short (Short *et al.*, 2002). The interaction between MID2 and the other two putative interactors, NY-CO-3 and PEPP2, were investigated in this study. Their potential interactions with MID1 and with the domain-specific deletions of MID1/MID2 were also tested if their interaction with MID2 was confirmed.

#### 4.2.3.1 NY-CO-3 is unlikely to be an interactor of MID2

The full-length mouse NY-CO-3 cDNA was obtained from a purchased mouse EST (Genbank accession # AW320712). The ORF of the mNY-CO-3 sequence encodes a protein of 382 amino acids with a Coiled-Coil domain from aa209 to aa321, as predicted by the Coils2 program (Figure 4.4). The partial mNY-CO-3 selected from the Y2H screen includes the C-terminal 197 amino acids (from aa187 to aa382), as highlighted in the sequence (Figure 4.4B).

The complete ORF of mNY-CO-3 was cloned in-frame into both pDBLeu and pPC86 to produce GAL4-DB and GAL4-AD fusion proteins, respectively. The ORFs of hMID1 and hMID2 had been previously cloned into both pDBLeu and pPC86. The putative interactions between mNY-CO-3 and hMID1/ hMID2 were monitored from two

directions in the yeast two-hybrid system (AD-mNY-CO-3 + DB-hMID1/ DB-hMID2; DB-mNY-CO-3 + AD-hMID1/ AD-hMID2).

Unfortunately, full-length mNY-CO-3 induced the three reporter genes through self-activation when expressed as a DNA-binding domain fusion protein, while the AD-mNY-CO-3 fusion which displayed no detectable self-activation, failed to interact with either GAL4DB-hMID1 or GAL4DB-hMID2 (Figure 4.5). The C-terminal partial mNY-CO-3 sequence obtained in the initial yeast two-hybrid screen served as the 'positive' controls.

Consistent with the Y2H results with full length mNY-CO-3, the overexpressed mNY-CO-3 (as a MYC-tagged fusion protein) did not colocalize with microtubule-associated MID2 (GFP fusion) in COS1 cells, but displayed a cytoplasmic distribution (Figure 4.6).

#### **4.2.3.2 PEPP2 was identified as a potential interactor of MID2**

The full-length human PEPP2 cDNA was a gift from Dario R. Alessi (University of Dundee, UK). The hPEPP2 shares >85% amino acid identity with mPEPP2 (Figure 4.7A) and consists of 1116 amino acids, with two WW domains (WW1: residues aa11 to aa43; WW2: residue aa55 to aa89) at the N-terminal end followed by a PH domain (residues aa172 to aa271) (Figure 4.7B). The partial mPEPP2 selected from the yeast two-hybrid screen includes the C-terminal 861 amino acids (underlined sequence).

The ORF of hPEPP2 was cloned in-frame into pDBleu and pPC86. Significantly, a strong interaction between full-length hPEPP2 (DB-PEPP2) and hMID2 (AD-MID2) was observed, although in the swapped fusions (AD-PEPP2 and DB-MID2), an interaction could not be demonstrated (Figure 4.8). Such interactions in one 'direction' only are not uncommon and thought to reflect the possible interference of the fused



### A: Nucleotide sequence of mouse antigen NY-CO-3 ORF

```
1 atgtcgggct acgcgcggcg gcagggcgcg cccctctat cgcgagcgcg gagccttgtg
61 gttccccgacg gttttggcta tggaaagggg aaatgtacta accaaggtcc ttcggggagcc
121 cctgagacgc gctttggagg tgacaaactt gaagaccttg aagaagccaa tccattctcc
181 ttcaaagagt ttttgaaaac caagaacctc agcctgtcaa aagaagacac gaccaccagc
241 cgaatttacc caaaggaagc ctcaaggcac ccaactgggac tagagcacag ctcccctgcc
301 tcccagctca tgggatatgg cctggaatct cagcagccat tttttgaaga cccaacaaga
361 gccagcaacc tagaggagga tgaagatgat ggatggtata taacctactt gccatctgcc
421 gtggatcaga ctcatcctc tagagacaca caggactcac cgccctgtga cacctacctt
481 tcctttttct ccaactcgtc agagctggca tgtcccagat ctttgccccc atggacgctg
541 agtgacaccg actccaggat ctccccagcg tctccagctg ggagtcctaa tgcagaacttt
601 gcagctcatg aagaatccct aggggacaga cacctgcgga cgctgcagat aagttatgaa
661 gcaactgaaag atgaaaactc taagctcaga agaaagctaa atgaggttca gagcttctct
721 gaaactcaaa cagaaatggt gaggacactc gaacggaagt tggaggcgaa gatgatcaag
781 gaggagagtg acttccatga cctcgagtca gtagtccagc aagtogaaca gaaccttgaa
841 ctgatgacca aacgggctgt aaaagcagaa aatcatgtct tgaagctgaa acaggaata
901 aatttgcttc aggccagct ctcaaacttg aggcgagaaa atgaagccct gcggtcaggc
961 cagggtgcca gcctttctgt agtgaagcag aacaccgacg tggccttgca gaacctccac
1021 cttgtcatga acagtgcaca cgcattcaca aagcagctgg tgtctggggc agacacactg
1081 aaccttggtg ctgaaatcct caagtctatc gacagaatta gtgaagttaa agatgaggtg
1141 gactcttga
```

### B: Protein sequence of mouse antigen NY-CO-3 (382aa)

```
1 MSGYARRQGA PPLSRTRSLV VPDGFGYGKG KCTNQGPSGA PETRFGGDKL EDLEEANPFS
61 FKEFLKTKNL SLSKEDTTTS RIYPKEASRH PLGLEHSSPA SQLMGYGLES QQPFFEDPTR
121 ASNLEEDDD GWYITYLPSA VDQTHSSRDT QDSPPCDTYL SFFSNSSELA CPESLPPWTL
181 SDTDSRISPA SPAGSPNADF AAHEESLGDR HLRTLQISYE ALKDENSCLR RKLNEVQSFS
241 ETQTEMVRTL ERKLEAKMIK EESDFHDLES VVQQVEQNLE LMTKRAVKAE NHVLKCLKQEI
301 NLLQAQLSNL RRENEALRSG QGASLSVVKQ NTDVALQNLH LVMNSAHASI KQLVSGADTL
361 NLVAEILKSI DRISEVKDEV DS*
```

**Figure 4.4** The nucleotide (A) and protein sequences (B) of mouse NY-CO-3.

mNY-CO-3 consists of 382 amino acids and contains a Coiled-Coil motif from aa209 to aa321. The C-terminal mNY-CO-3 sequence encoded by the fusion construct, which has been shown to interact with hMID2 in Y2H, is highlighted in both sequences. This C-terminal mNY-CO-3 fragment included the entire Coiled-Coil motif.

**Figure 4.5 Monitoring the interaction between full length mNY-CO-3 and MID2/MID1 in Y2H.**

a—e: Five control yeast strains provided by the manufacturer, indicating increasing protein-protein interaction strength.

(A). mNYCO3 displays strong self-activation when expressed as a GAL4-DNA-binding domain fusion protein:

C1: pDBleu + pPC86-MID2

C2: pDBleu + pPC86-MID1

C3: pDBleu-NYCO3 + pPC86

(B). Although the C-terminal mNYCO3 interacts with MID2, full-length mNYCO3 does not interact with MID2 when it is expressed as a GAL4-activation domain fusion protein.

1: pPC86-NYCO3 + pDBleu;

1': pPC86-NYCO3 (C-terminal) + pDBleu

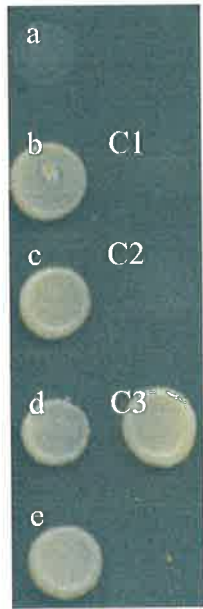
2: pPC86-NYCO3 + pDBleu-MID1; 2': pPC86-NYCO3 (C-terminal) + pDBleu-MID1

3: pPC86-NYCO3 + pDBleu-MID2; 3': pPC86-NYCO3 (C-terminal) + pDBleu-MID2

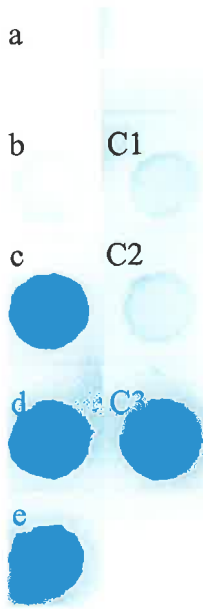
C1: pPC86 + pDBleu-MID1

C2: pPC86 + pDBleu-MID2

**A**

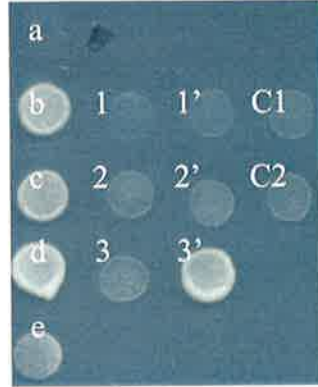


75mM3AT

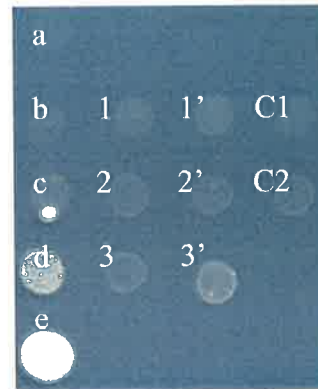


X-Gal

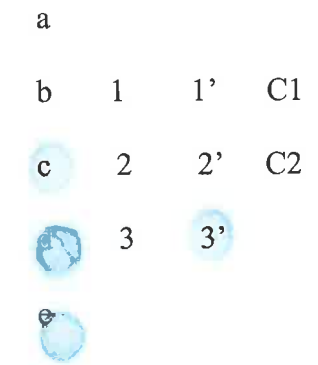
**B**



75mM3AT



-URA



X-Gal



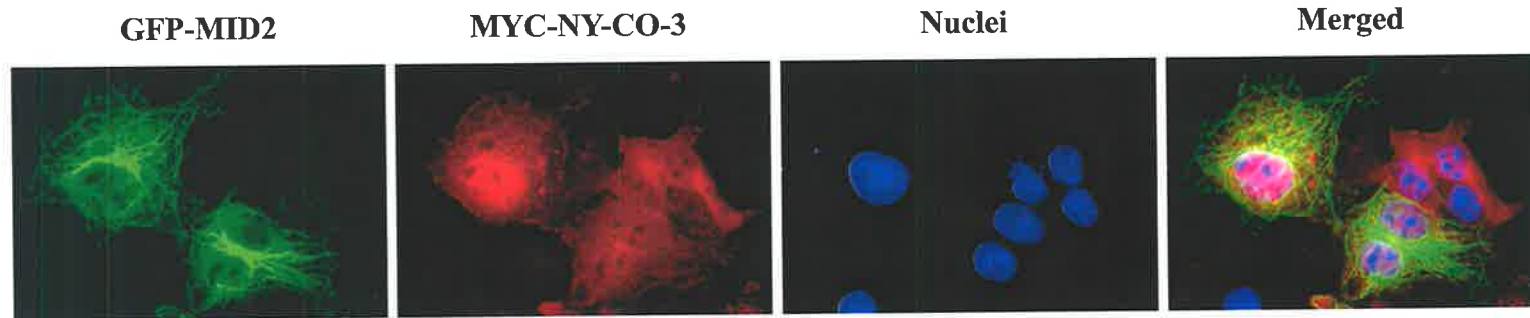


**Figure 4.6 Co-transfection of GFP-MID2 and MYC-NY-CO-3 in COS1 cells.**

The cellular distribution of mouse NY-CO-3 and human MID2 was viewed in COS1 cells expressing both fusion proteins. The overexpressed MYC-tagged wild-type mouse NY-CO-3 was detected by an anti-MYC monoclonal antibody and Texas-red conjugated secondary antibody (red). Poor co-localization was observed with the cytoplasmic NY-CO-3 and microtubular GFP-MID2 (green). Nuclei were stained with DAPI (blue).

### A: Alignment of hPEPP2 and mPEPP2 protein

hPEPP2 (1) MAADLNLEWI - SLPRSWTYGITRGGRVFFINEEAKSTTWLHPVTGEAVVTGHRRQSTDLP  
mPEPP2 (1) MAADLNLEWICSLPRSWTYGITRGGRVFFINEEAKSTTWLHPVTGEAVVTGHRRQSTDLP

hPEPP2 (60) TGWEEAYTFEGARYYINHNERKVTCKHPVTGQPSQDNCIFVVNEQTVATMTSEKKERPI  
mPEPP2 (61) TGWEEAYTFEGARYYINHNERKVTCKHPVTGQPSQDNCIFVVNDQTVATMTSEDKKERPI

hPEPP2 (120) SMINEASNYNVTSDYAVHPMSVPGRTSRASKKVHNFVKRSNSIKRNP NAPVVRGWLYKQ  
mPEPP2 (121) SMINEASNYNMASDYAVHPMSVPGRTSRASKKVHNFVKRSNSIKRNP NAPVVRGWLYKQ

hPEPP2 (180) DSTGMKWLKKRWFVLSLCLFYRDEKEEGILGSILLPSFQIALLTSEDHINRKYAFKAA  
mPEPP2 (181) DSTGMKWLKKRWFVLSLCLFYRDEKEEGILGSILLPSFQIAMLAEDHINRKYAFKAA

hPEPP2 (240) HPNMRTYYFCTDTGKEMELWMMKAMLDAAALVQTEPVKRVDKITSENAPTKETNNIPNHRVL  
mPEPP2 (241) HPXMRTYYFCTDTGKEMELWMMKAMLDAAALVQTEPVKRVDKITTDNASTKETNNIPNHRVL

hPEPP2 (300) TKPEIQNNQKNKEMSKIIEKKALEAEKYGFQKDGQDRPLTKINSVKLNSLPSEYESGSAC  
mPEPP2 (301) IRPEVQNHQKNKEISKIEEKRALEAERYGFQKDGQDRPLTKINSVKLNSLPSEYESGPDC

hPEPP2 (360) PAQTVHYRPIINLSSSENKIVNVSLADLRGGNRPNTGPLYTEADRVIQRTNSMQQLEQWIK  
mPEPP2 (361) PPQNVHYRPIINVNSSDGKAVNVSLADVRRGGSHPNAGPLATEADRVIQRTNSMQQLEQWIK

hPEPP2 (420) IQKGRGHEEETRGVISYQTLPRNMPSHRAQIMARYPEGYRTLPRNSKTRPESICSVTPST  
mPEPP2 (421) VQKGRGLEEEPRGVISYQTLPRNMPSHRAQILARCPEGYRTLPRNSKTRPESICSVTPSG

hPEPP2 (480) HDKTLGPGAEEKRRSMRDDTMWQLYEWQQRQFYHNKQSTLPRHSTLSSPKTMVNI SDQTMH  
mPEPP2 (481) HEKT - GPGAEEKRRSMRDDTMWQLYEWQQRQFYHNKQSTLPRHGCLSSPKAMVQVSDQTMH

hPEPP2 (540) SIPTSPSHGSI AAYQGYSPQRTYRSEVSSPIQRGDVTIDRRHRHHPKHVYV PDRRSVPA  
mPEPP2 (540) SIPTSPSHGSA AAYQGFSPQRTYRSEVTSPIQRGDVTIDRRHRPHHPKHVYVADRRSMPA

hPEPP2 (600) GLTLQSVSPQSLQGKTLQDEGRGTLKYRPEEVDIDAKLSRLCEQDKVVRHALEEKLQQL  
mPEPP2 (600) GLTLQAVSPQSLQGRTLQDECRGTLKYRPEEAGIDAKLSRLCEQDKVVRHALEEKLQQL

hPEPP2 (660) HKEKYTLEQALLSASQEIEMHADNPAAIQTVVLQRDDLQNGLLSTCRELSRATAELERAW  
mPEPP2 (660) HKEKYTLEQALLSASQEIEMNADNPAAIQTVVLQRDDLQNGLLSTCRELSRATAELERAW

hPEPP2 (720) REYDKLEYDVTVTRNMQEQLDHLGEVQTESAGIQRAQIQKELWRIQDVMEGLSKHKQQR  
mPEPP2 (720) REYDKLEYDVTVTRDQMGGQLDRLGEVQSESAGIQRAQIQKELWRIQDVMEGLSKHKQQR

hPEPP2 (780) GTTE - IGMIGSKPFS TVKYKNEGPDYRLYKSEPELTTVAEVDENGEKSEPVSEIETSV  
mPEPP2 (780) GSS ETVGLAGSKPFS SVKYKSEGPDYRLYKSEPELTTVAEVDENGEKSEPVSETEAPV

hPEPP2 (839) VKGSHFPVGVPPRAKSPTPESSITASYVTLRKTCKMMDLRTERPRSAVEQLCLAESTRP  
mPEPP2 (840) VKGSHFPVG - VPLRTKSPTPESSITASYVTLRKTCKMVELRTERPRSAVEQLCLAESARP

hPEPP2 (899) RMTVEEQMERIRRHQQA CLREKKKGLNVI GASDQSPLQSPSNLRDNPFRTTQTRRRDD - -  
mPEPP2 (899) RMTVEEQLERIRRHQQA CLREKKKGLSVLGASD - - - - - PSDVDRDSPRLRLTQTLRRDDNV

hPEPP2 (957) KELDTAIRENDVKPDHETPA TEIVQLKETEPQNVDFSKELKKTENISYEMLFEPENGVN  
mPEPP2 (953) KELDTVHRENDVKPDYETPAAQYAHLEDAEPQNA DIGRKLKRSESISFYEMLYTPEPNGMA

hPEPP2 (1017) SVEEMDKERNKDKMPE DVTFSPODETQTANHKPEEHPEENTKNSVDEQEETVISYESTPE  
mPEPP2 (1013) SEEVTEKERQKEQVHADGSCSPOEETAMTEHQMEGPEEEAE - - SLHEEEETLASCEPAPE

hPEPP2 (1077) VSRGNQTM AVKSLSPSESSASPVSTQPQITEGSHFMCV  
mPEPP2 (1071) IPRENQT - TVRSLSPSPDSS TAADPTTPQLREGSHFMCV

**B:**

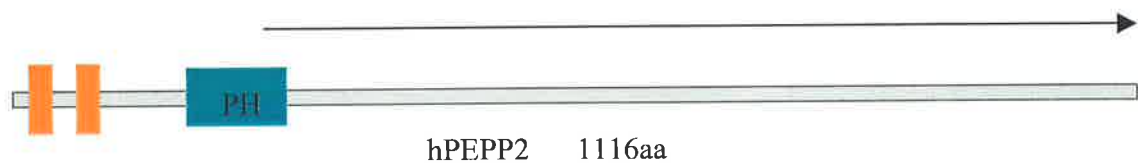


**Figure 4.7** The sequences/ alignments (A) of human/mouse PEPP2 protein and the schematic representation (B) of hPEPP2 primary structure.

hPEPP2 and mPEPP2 display about 85% overall amino acid identity, with much higher identity cross the N-terminal region which includes the two WW domains and the PH domain (A). The sequence encoded by the fusion construct, which has been shown to interact with hMID2 in the yeast two-hybrid screen covered the ~ 75% of the C-terminal end of the of mPEPP2. The equivalent position to this C-terminal mPEPP2 is indicated by the arrow on the hPEPP2 structural diagram (B).

domain with the presentation of the interaction surface (i.e. conformational changes). Subsequent co-expression of PEPP2 (DB-PEPP2) with the different MID2 domain-specific deletions (fused to the GAL4-AD) in the yeast two-hybrid system identified a requirement for both the RING-finger domain and the Coiled-Coil domain for the interaction between PEPP2 and MID2 (figure 4.8).

Of note, PEPP2 did not interact with either full length MID1 or any of its domain-specific deletions in the Y2H (figure 4.9). It is therefore, suggested that the interaction with PEPP2 is MID2 specific.

#### ***4.2.4 The interaction between PEPP2 and MID2 was verified in mammalian cells***

The detected interaction between PEPP2 and MID2 using the heterologous yeast two-hybrid system was further tested by co-transfection of differently tagged forms of each protein in mammalian cells.

##### **4.2.4.1 Colocalization of MID2 and PEPP2**

Using indirect immunofluorescence, overexpressed MYC-PEPP2 and GFP-MID2 were found to co-localize on microtubules in cultured COS1 cells (Figure 4.10A). PEPP2 was also tethered into the cytoplasmic clumps formed by MID2 domain-specific deletions (MID2 $\Delta$ BB, MID2 $\Delta$ FNIII and MID2 $\Delta$ CTD) (Figure 4.10B, C and D), consistent with the interactions of these domain-specific deletions in the yeast two-hybrid system.

As expected, MID1, which failed to interact with PEPP2 in the Y2H, did not co-localize with PEPP2 when they were co-overexpressed in COS1 cells (Figure 4.11). In fact, overexpressed PEPP2 displayed cytoplasmic diffused distribution with some membrane-association in cells overexpressing MID1 (discussed further in the next chapter).

#### **4.2.4.2 Regulation of MID2 and PEPP2 interaction by MID1/MID2 heterodimerization**

Association of PEPP2 and MID2 was also observed using co-immunoprecipitation. HEK-293T cells were co-transfected with constructs expressing fusion proteins of GFP- or MYC-tagged PEPP2 and MID2/MID1. The anti-GFP monoclonal antibody was used to immunoprecipitate the GFP-tagged protein from the cell lysate. Western blot analysis of the immunoprecipitated proteins using the monoclonal anti-MYC antibody revealed the association between PEPP2 and MID2, but again not with MID1 (Figure 4.12A).

The requirement of the MID2 Coiled-Coil domain (in addition to the RING-finger domain) for PEPP2 interaction suggested that dimerization of MID2 may be a prerequisite for PEPP2 binding. Given MID2 and MID1 can form heterodimers, the possibility that such heterodimers could also interact with PEPP2 was investigated by co-immunoprecipitation using extract from 293T cells transiently overexpressing GFP-PEPP2, MYC-MID2 and untagged MID1. The results show that in the presence of the excess cellular MID1, the interaction between MID2 and PEPP2 was reduced (Figure 4.12B). The presence of the overexpressed GFP-PEPP2, MYC-MID2 and MID1 in the cell lysates was verified by western blotting using the appropriate antibodies. These data indicate that heterodimerization of MID1/MID2 precludes or prevents the interaction between MID2 and PEPP2.

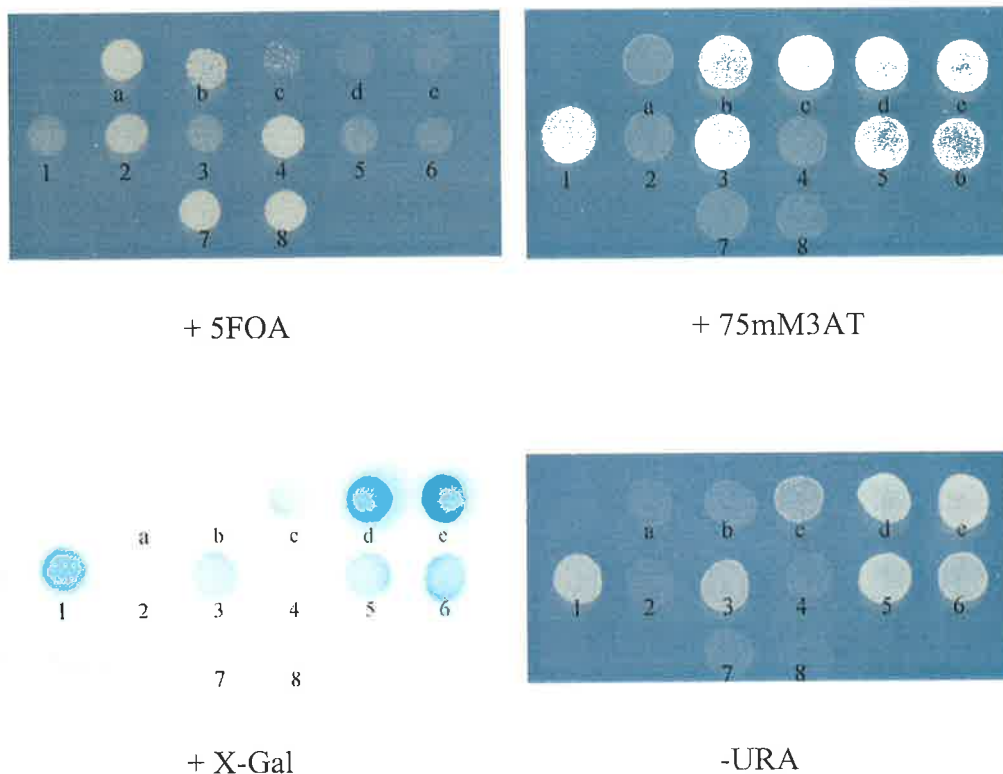


**Figure 4.8 Full length PEPP2 interacts with MID2 in a RING-finger and the Coiled-Coil domain-dependent fashion.**

Colonies on four selective plates (including 5-fluoro-orotic acid in SC-Leu-Trp is a complementary way to monitor the expression of <sup>the</sup>URA3 reporter, induction of which results in conversion of the 5FOA to 5-fluorouracil, which is toxic and inhibits the growth of yeast cells containing the positive interactions)

a—e: Five control strains provided by the manufacturer.

Mav203 yeast cells were co-transfected with pDBleu-PEPP2

+ pPC86-MID2 (1); + pPC86-MID2 $\Delta$ RF (2); + pPC86-MID2 $\Delta$ BB (3); + pPC86-MID2 $\Delta$ CC (4); + pPC86-MID2 $\Delta$ FNIII (5); + pPC86-MID2 $\Delta$ CTD (6).

Two external controls for monitoring self-activation:

7: pDBleu + pPC86-MID2

8: pDBleu-PEPP2 + pPC86

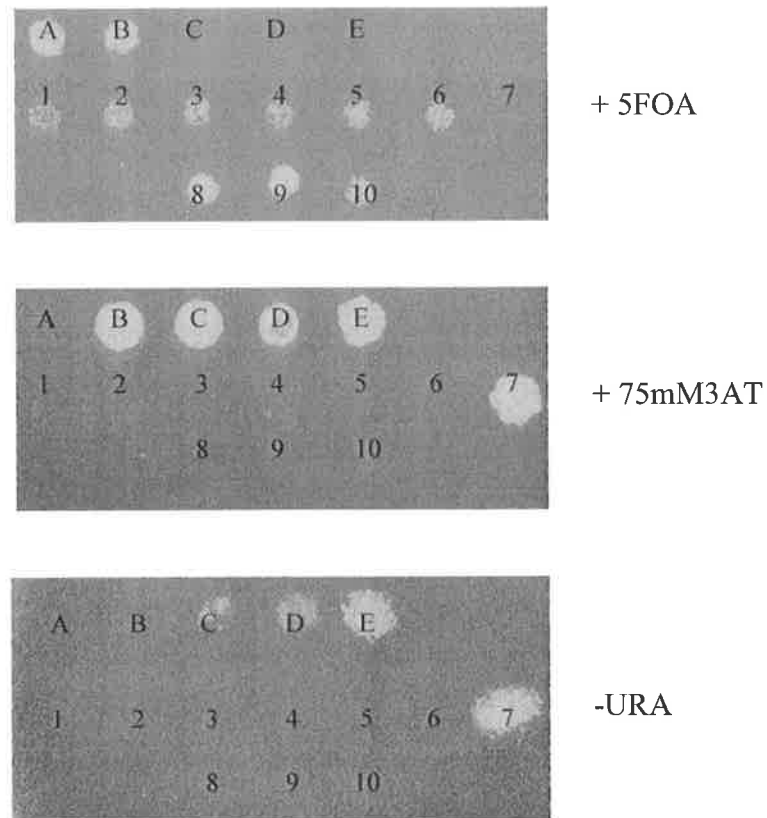


**Figure 4.9 PEPP2 does not interact with either wild type MID1 or any MID1 domain-specific deletions in yeast two-hybrid.**

A—E: Five control strains provided by the manufacturer.

Mav203 yeast cells were co-transfected with pDBleu-PEPP2

+ pPC86-MID1 (1); + pPC86-MID1 $\Delta$ RF (2); + pPC86-MID1 $\Delta$ BB (3); + pPC86-MID1 $\Delta$ CC (4); + pPC86-MID1 $\Delta$ FNIII (5); + pPC86-MID1 $\Delta$ CTD (6); + pPC86-MID2 (7, positive control).

Three external controls for monitoring self-activation.

8: pDBleu + pPC86-MID1

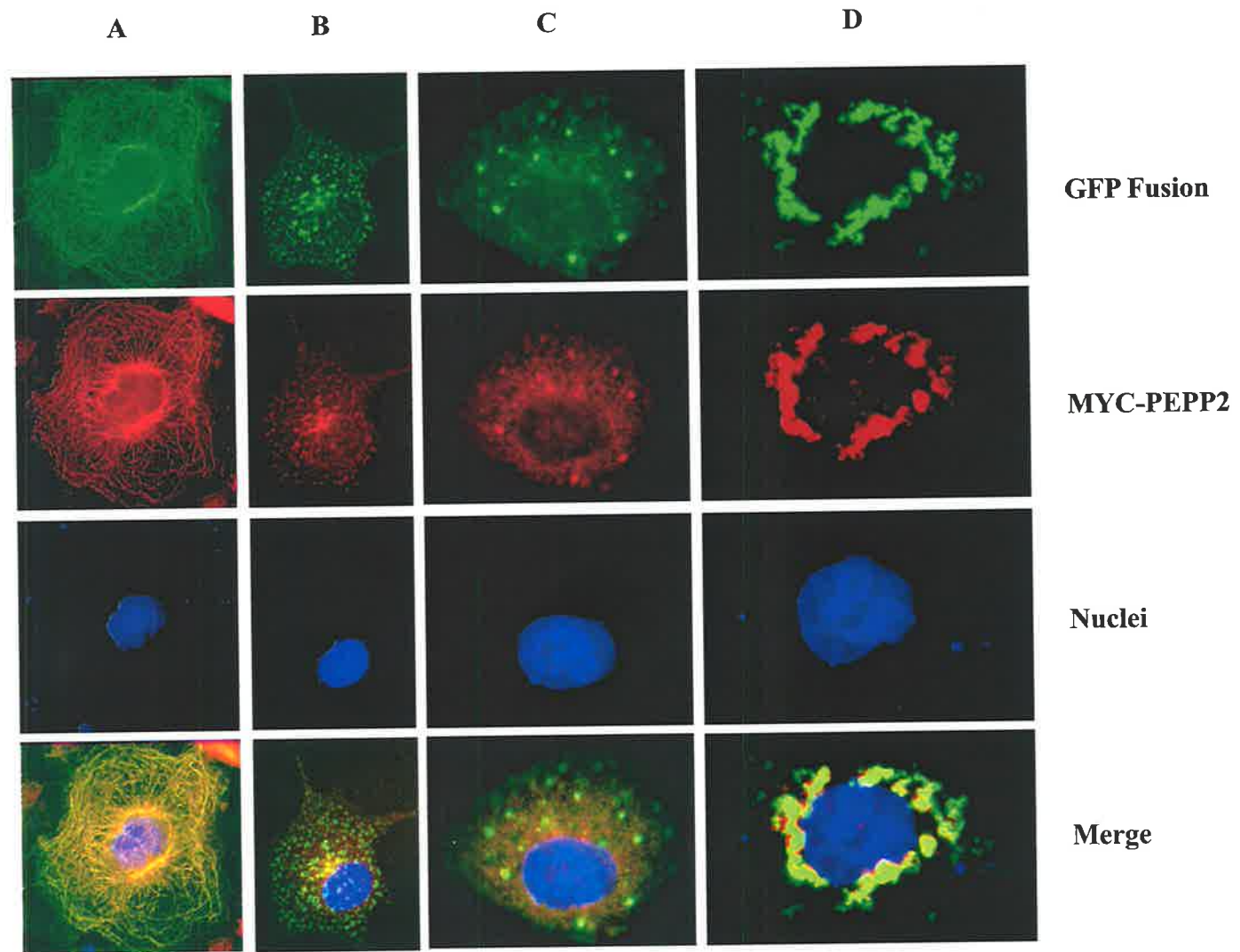
9: pDBleu + pPC86-MID2

10: pDBleu-PEPP2 + pPC86

**Figure 4.10 The colocalization of PEPP2 with MID2 and MID2 domain-specific deletions.**

COS1 cells were co-transfected with pCMV-MYC-PEPP2 and either pEGFP-MID2 (A), pEGFP-MID2 $\Delta$ BB (B), pEGFP-MID2 $\Delta$ FNIII (C) or pEGFP-MID2 $\Delta$ CTD (D). MYC-PEPP2 was detected with an anti-MYC monoclonal antibody and Texas-red conjugated secondary antibody (red). PEPP2 co-localization (yellow) was observed with GFP-MID2 on microtubules, as well as with GFP-MID2 $\Delta$ BB, GFP-MID2 $\Delta$ FNIII and GFP-MID2 $\Delta$ CTD cytoplasmic clumps. Nuclei were stained with DAPI (blue).





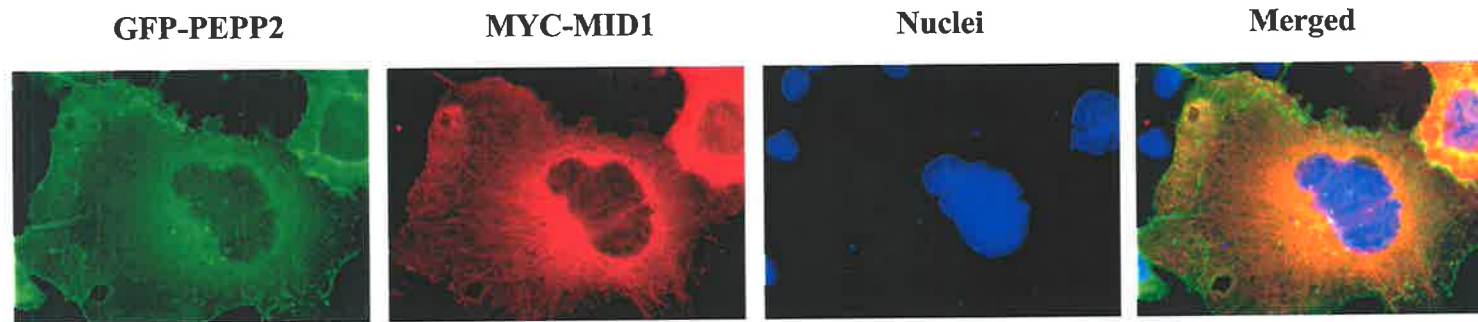


**Figure 4.11** The cellular distribution of co-expressed PEPP2 and MID1 in COS1 cells.

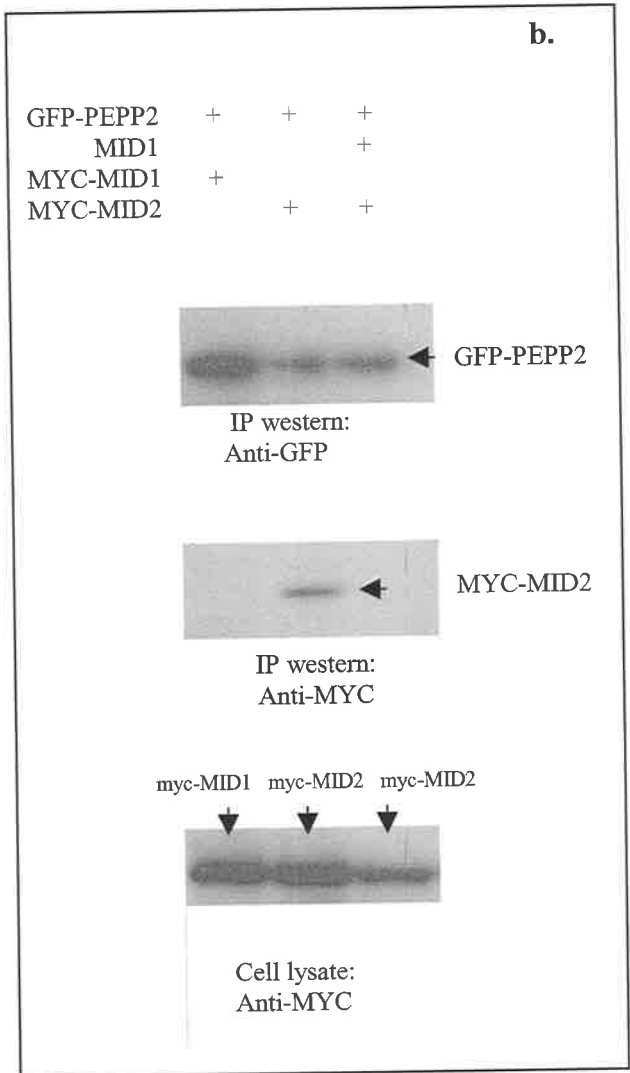
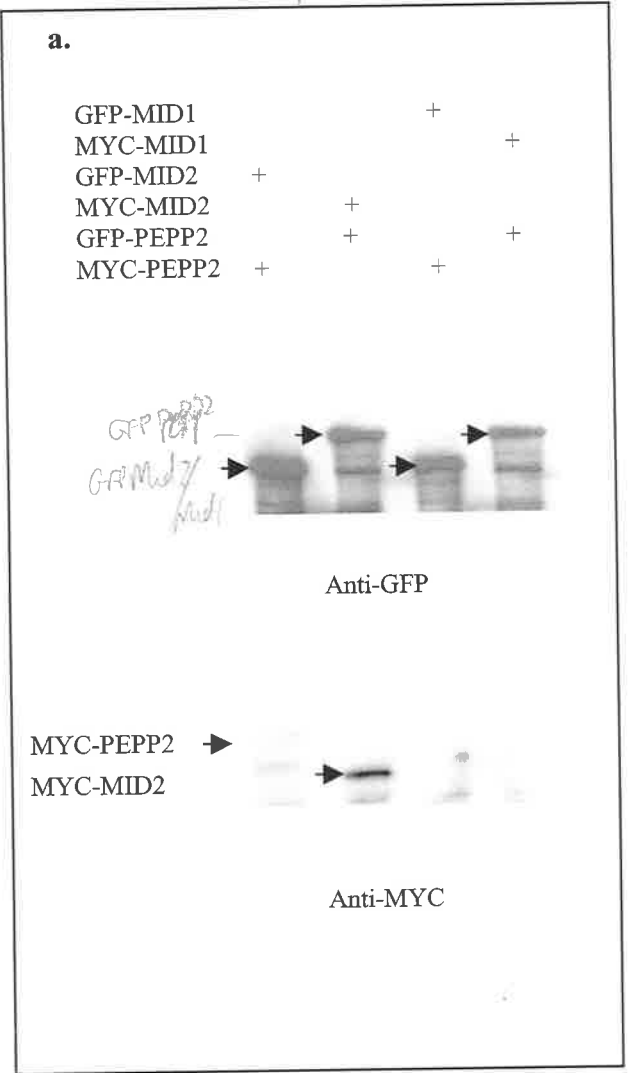
COS1 cells were co-transfected with constructs expressing the fusion protein of GFP tagged PEPP2 and MYC-tagged MID1, which was detected with anti-MYC monoclonal antibody and Texas-red conjugated secondary antibody using indirect immunofluorescence. No co-localization was observed for PEPP2 and microtubule-associated MID1.

**Figure 4.12 Co-immunoprecipitation of cell extracts overexpressing PEPP2 and MID1/MID2.**

a: Cell lysates were collected from HEK-293T cells transiently overexpressing GFP- or MYC-tagged PEPP2 and MID1/MID2 as indicated. Anti-GFP monoclonal antibody was used to immunoprecipitate over-expressed GFP fusion protein, and precipitates separated on a 10% SDS-poly-acrylamide gel. Western blot analysis was subsequently done with anti-GFP or anti-MYC antibody. MYC-PEPP2 co-precipitated with GFP-MID2 (lane 1), but not with GFP-MID1 (lane 3). Conversely, MYC-MID2 (lane 2), but not MYC-MID1 (lane 4), co-precipitated with GFP-PEPP2.

b: Cell lysates were collected from HEK-293T cells transiently overexpressing GFP-PEPP2 and MYC-MID1/MYC-MID2 or over-expressing GFP-PEPP2 and MYC-MID2 and untagged MID1 as indicated. The cell lysates were separated on a 10% poly-acrylamide gel and western blot analysis performed with an anti-MYC antibody revealed that the expression of MYC-MID1 and MYC-MID2 were at similar levels. Anti-GFP monoclonal antibody was used to immunoprecipitate over-expressed GFP fusion protein, with the resultant precipitant separated on a 10% SDS-ploy-acrylamide gel. Western blot analysis with anti-GFP or anti-MYC antibody revealed that MYC-MID2 (lane 2), but not MYC-MID1 (lane 1), associated with PEPP2. Notably, excess cellular MID1 prevented the association of MYC-MID2 and GFP-PEPP2 (lane3).

↳ GFP IP



### 4.3 Discussion

In this chapter, the results of a yeast two-hybrid screen for MID2 interactors are presented. 22 positive yeast colonies carrying potential interactors from about  $10^6$  yeast transformants were isolated. The expression of three reporter genes in these 22 positive strains was analyzed. The extent of growth of the same yeast strain on these three selective media may vary because of the properties of interactors (i.e. their ability to induce expression of the reporters based on the different genomic contexts of the regulatory sequences upstream of these genes), or because of the varied amount of yeast cells applied due to an uneven replica clean procedure. *URA3* is the least sensitive among these three reporter genes, and therefore lack of, or poor growth under  $-URA$  selection can not exclude<sup>a</sup> weak interaction. From these initial 22 yeast colonies, 18 showed consistent growth under both  $-HIS$  and  $-URA$  selection and were positive in the X-gal assay. The other four “negative” colonies that ~~was~~<sup>were</sup> recognized as “positives” in the initial screen may<sup>be</sup> due to the shortened time of incubation (48 hours after transfection), compared with up to 72 hours after transfection in the initial screen.

To identify the potential interactors, 16 pPC86-Y plasmids were successfully extracted from the 18 yeast strains, revealing inserts of different sizes. Since the self-activation of pDBleu-MID2 in the presence of pPC86 was inhibited by including 50mM 3AT in the  $-HIS$  media<sup>m</sup>, the growth of the other two false positive colonies on the two selective media<sup>a</sup> ( $-HIS$  and  $-URA$ ) may have been due to incomplete replica cleaning. However, mutations of these yeast strains or mutations in pDBleu-MID2 sequence may also have occurred thus resulting in the positive phenotype.

Sequencing of the remaining 16 pPC86 constructs followed by BLAST searches against the NCBI non-redundant nucleotide database revealed three putative interactors: Alpha4 (complete ORF cDNA sequence), mouse NY-CO-3 and mouse PEPP2 (incomplete

cDNA sequence). One pPC86 construct (Y2HP10) revealed a translation from the GAL4 activation domain through the 3'UTR of mGPX and resulted in expression of a fusion protein of activation domain and an additional 50 amino acids. Since BLAST searches of this 50 amino acid-peptide didn't reveal any sequence homology from the existing database, the positive phenotype of the yeast cells expressing this fusion protein may have been due to its self-activation activity or a biologically irrelevant interaction between this peptide and MID2 in yeast two-hybrid.

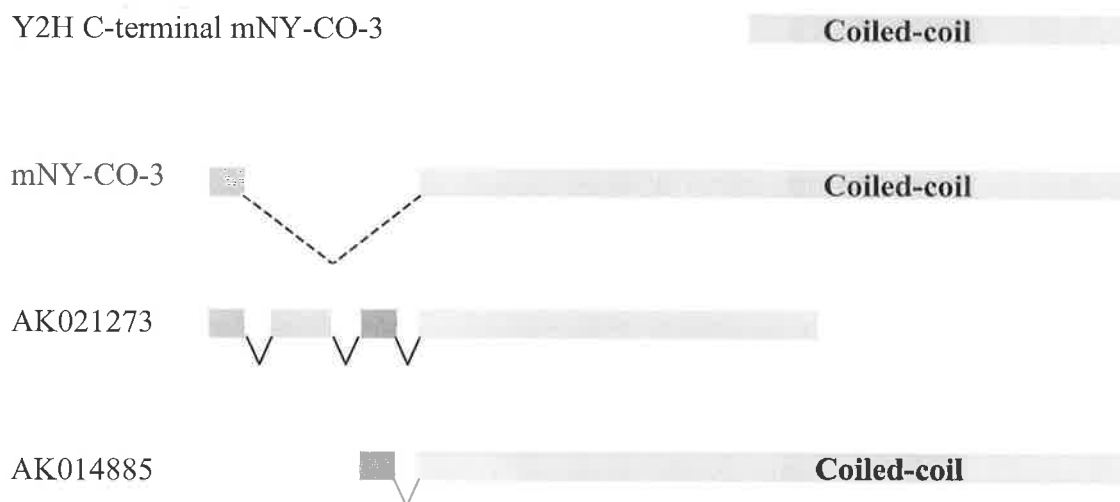
The presence of Alpha4 in 13 different positive yeast colonies reflects the high level of expression of this gene in the 10.5 dpc mouse embryo, consistent with the expression of MID2 and MID1 (Short *et al.*, 2002). The identification of Alpha4 as a common interactor for both MID1 and MID2 supports the hypothesis that the two proteins share at least some overlapping function. As a regulatory subunit of the PP2-type phosphatases (i.e. PP2Ac), recruitment of cytoplasmic Alpha4 onto microtubules by MID1 and MID2 (proven by indirect immunofluorescence, (Short *et al.*, 2002)) may affect the function of the microtubular portion of cellular PP2Ac (see section 1.5.4). Characterization of the cellular function of the Alpha4 and MID1/MID2 interaction is of particular interest to the lab, but not a component of this project.

Human NY-CO-3 is an auto-antigen that was originally found in a screen of a cDNA expression library derived from a human colon cancer (Scanlan *et al.*, 1998). No specific function has been assigned to hNY-CO-3 or its mouse homologue (share 76% identity). Although the interaction between the C-terminal 196 amino acids of mNY-CO-3 and MID2 has been confirmed in the yeast two-hybrid, results from both in yeast two-hybrid and indirect immunofluorescence using full-length mNY-CO-3 and MID2 do not support a *bona fide* interaction, and suggesting that in the absence of the N-terminal residues the peptide takes on a unique conformation or provides an interaction

surface that is normally not available. However, a recent BLAST search using the mNY-CO-3 ORF sequence identified another two splice variants, AK021273 and AK014885, which were derived from *Mus musculus* male testis cDNA libraries (Figure 4.13). Both of these splice variants encode proteins with different N-termini. Thus, it is possible that MID2 interacts with only one or both variants but not NY-CO-3. These variants have not been tested.

**Figure 4.13 The schematic representation of mNY-CO-3 and its splice variants.**

Blast search revealed two splice variants of mNY-CO-3. AK014885 possesses the identical C-terminal 358 amino acids, which covers the C-terminal mNY-CO-3 that has been shown <sup>to</sup> interact with MID2. Given that there is no polyA signal in the cDNA sequence it is predicted that AK021273 is a partial cDNA.



However, since the C-terminal 196 amino acids of mNY-CO-3 contains the intact Coiled-Coil motif, it is possible that the interaction with MID2 is due to non-specific interactions between their “sticky” Coiled-Coil domains.

In contrast to the other positives, the full-length hPEPP2, when expressed as a GAL4-DNA-binding domain fusion protein, interacted with AD-hMID2. Furthermore, their interaction was RING-finger and Coiled-Coil domain-dependent. This interaction was verified using both immunofluorescence and co-immunoprecipitation. Unlike Alpha4, the interaction between PEPP2 and MID2 seems to be MID2-specific, since MID1 failed to interact with PEPP2 in any assay system. This finding suggests that MID1 and MID2 may also have their unique cellular functions and that hetero-dimerization may act as a regulatory mechanism in some instances. This hypothesis was supported with the finding that the interaction between MID2 and PEPP2 was attenuated if excess cellular MID1 was present. Given that the Coiled-Coil domain of MID2 is required for both the PEPP2-MID2 interaction and MID1-MID2 dimerization, PEPP2 and MID1 may interact with MID2 in a competitive manner. However, given the requirement for the RING-finger and the Coiled-Coil domains for PEPP2 interaction, it is possible that the RING domain provides the interaction specificity following the homodimerization of MID2 through the Coiled-Coil domain. Such increased affinity towards protein partners upon dimerization is a mechanism commonly employed in regulating protein-protein interactions, best exemplified with the dramatically increased affinity to ligands upon the dimerization of receptors (Schlessinger, 2002). Instead of competing for the same binding site as PEPP2, excess MID1 might abolish MID2-PEPP2 interaction by preventing the formation of MID2 homodimers. Variation in the relative expression levels of MID1 and MID2 could therefore determine the formation of homo- or hetero-dimers which in turn may direct their interaction with different proteins.



Consistent with this are data from overexpression studies. As expected, overexpressed PEPP2 co-localized with MID2, but not with MID1, on microtubules in COS1 cells. In contrast, PEPP2 redistributed into cytoplasm/plasma membrane when MID1 was also overexpressed (MID1/MID2 heterodimerization was overwhelming the homodimerization of endogenous MID2), indicating that the microtubule-association of PEPP2 was MID2-dependent. These observations suggest that by regulating the PEPP2-MID2 interaction, the cellular localization of PEPP2, which may be critical for its function. It can therefore be envisaged that in OS cells, in which the regulation of MID1/MID2 homo-/hetero-dimerization is interrupted due to deficiency of MID1, the cellular function of PEPP2 may also be affected. These data also support a modifying role for potential MID2 in the presentation of OS. Further investigation of the potential cellular function of PEPP2 and the possible cellular processes that PEPP2 and MID2 may be involved in are discussed in the next chapter.

incomplete  
sentence



## Chapter Five: The cellular function of MID2 and PEPP2.

### 5.1 Introduction

In the previous chapter, initial attempts to elucidate the cellular function of MID1 and MID2 using a yeast two-hybrid system were described. Using this approach with the MID2 protein as bait, a newly identified PH-domain-containing protein, PEPP2, was found whose interaction with MID2 appeared to be regulated by MID1/MID2 heterodimerization. Apart from its ability to bind phosphoinositides, little is known about PEPP2. It was first necessary to carry out some preliminary studies on this protein in the hope of shedding light on both its role and the functions of MID1 and MID2.

The PH-domain was first identified in pleckstrin and subsequently in a wide range of signalling proteins as well as many constituents of the cytoskeleton (Lemmon *et al.*, 2002). The PH domain possesses multiple functions, foremost being the binding of phosphoinositides. Only a few PH domains bind phosphoinositides with high affinity and specificity, with most being PI(3,4,5)P<sub>3</sub>/PI(3,4)P<sub>2</sub> binding partners, such as protein kinase B (PKB/Akt). This high affinity and specificity of binding results in transient membrane recruitment of these proteins in line with the increase of these phosphoinositides upon agonist-stimulated cell surface receptor activation (Lemmon *et al.*, 2002).

Most PH-domain-containing proteins with low lipid-binding affinity and specificity remain uncharacterized. The PH domain of PEPP2 has been shown to bind PI(4,5)P<sub>2</sub> with medium specificity in an *in vitro* protein-lipid overlay assay (Alessi, personal communications). PI(4,5)P<sub>2</sub> is the most abundant phosphatidylinositol on the cytoplasmic surface of the plasma and Golgi membranes. The sequential synthesis from membrane phosphatidylinositol to PI(4)P and then PI(4,5)P<sub>2</sub> relies on the temporally

and spatially controlled recruitment and activation of PI-4-kinase and PI(4)P-5-kinase to the appropriate location on the membrane (Hsuan *et al.*, 1998).

In addition to being the precursor of the most important intracellular secondary messenger-inositol(1,4,5)P<sub>3</sub>, PI(4,5)P<sub>2</sub> is now recognized as an important membrane signalling molecule that regulates vesicle trafficking, membrane movement and cytoskeleton assembly (Hsuan *et al.*, 1998; Martin, 2001). It functions by recruiting cytoplasmic effector proteins that contain PI-binding domains. As mentioned previously, by recruiting different effectors at different stages, PI(4,5)P<sub>2</sub> is involved in vesicle fission, docking and fusion, as well as being involved in regulating actin/microtubule nucleation (Russo *et al.*, 2001; Martin, 2001; Popova *et al.*, 2002).

This chapter outlines the elucidation of PEPP2 function and the physiological significance of the PEPP2/MID2 interaction. The following functional studies, particularly in the phosphoinositide regulated cellular processes, such as cytoskeletal rearrangement and endocytosis, suggest a potential role for PEPP2/MID2 in regulating membrane trafficking.

## 5.2 Results

### 5.2.1 *The non-uniform distribution of membrane-associated PEPP2*

#### 5.2.1.1 **The membrane-associated PEPP2 is enriched sites of at cell-cell contact**

Overexpressed tagged forms of PEPP2 and MID2 co-localise on microtubules (see chapter 4). In cells overexpressing PEPP2 and MID1, PEPP2 was not microtubular in localization but redistributed into the cytoplasm and associated with the plasma membrane. In cells overexpressing PEPP2 alone, as a GFP fusion protein, two distinct subcellular localisations were noted – microtubule-associated and plasma membrane-associated (Figure 5.1).

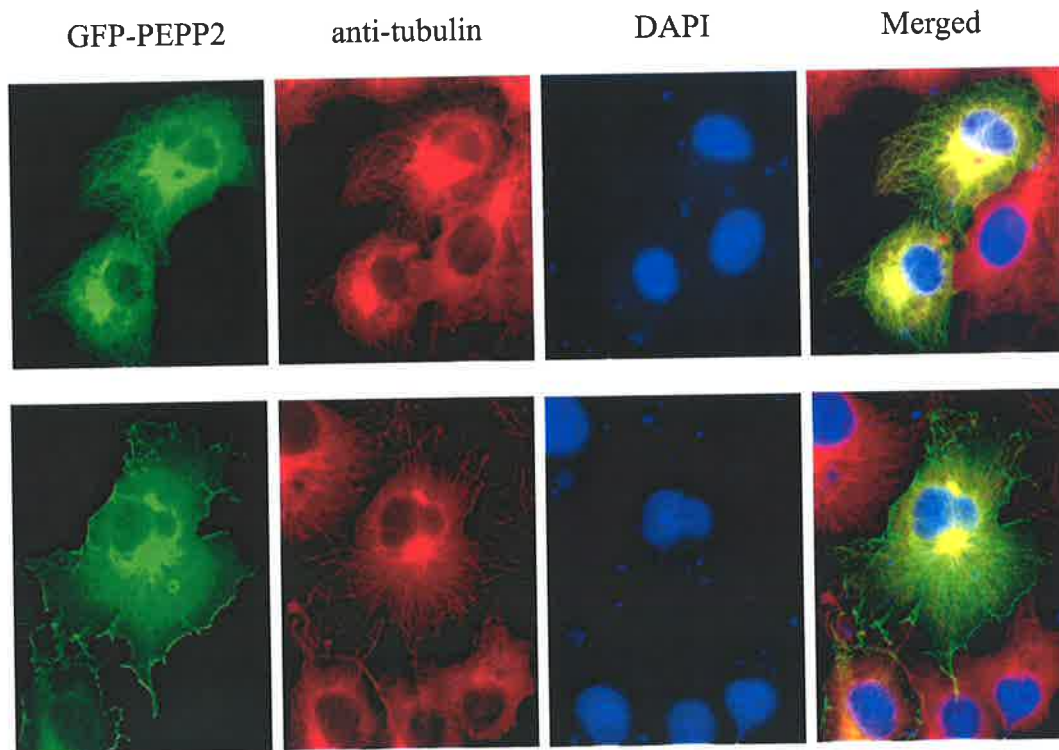


**Figure 5.1 The microtubule- and plasma membrane-associated PEPP2.**

Cellular localisation of overexpressed GFP-PEPP2 fusion protein in COS1 cells. Microtubule-association (top panel) and dual microtubule-/plasma membrane-association (bottom panel) of GFP-PEPP2 was observed. Microtubules were stained with monoclonal anti-alpha tubulin and a Texas-red-conjugated secondary antibody. Nuclei were stained with DAPI (blue). Enriched GFP-PEPP2 in the perinuclear region, in the proximity of the microtubule organisation center, was observed with both microtubule and membrane-associated distributions.

In some instances, both microtubule- and membrane-associated GFP-PEPP2 was found in the same cell, although PEPP2 was usually either microtubular or membrane-associated in most cells (Figure 5.2). A significantly increased amount of fluorescence of membrane associated GFP-PEPP2 was observed at cell-cell contacts in both mesenchymal COS1 cells and polarized MDCK cells (Figure 5.2A and B). Using a monoclonal anti-GFP primary antibody in conjunction with a gold-conjugated secondary antibody, GFP-PEPP2 could also clearly be observed at the plasma membrane by transmission electron microscopy (Figure 5.2C).

#### **5.2.1.2 The membrane-association of PEPP2 is directed by phosphoinositide-binding**

GFP-tagged PH domains have been used to localize the phosphoinositides that they recognize. For example, the cellular localization of PI(3,4,5)P<sub>3</sub> and PI(4,5)P<sub>2</sub> were visualized by the GFP-tagged PH domain of Akt and PLCδ1, respectively (Martin, 2001). The membrane-association of PEPP2 was consistent with the cellular distribution of PI(4,5)P<sub>2</sub> and some other phosphoinositides, the former having been suggested to be the lipid-binding partner of the PH-domain of PEPP2 based on *in vitro* studies (Alessi, personal communications). To verify that the PEPP2 PH domain is indeed responsible for localizing the protein *in vivo*, the coding sequence of the PH domain, amplified with PH-specific 5' and 3' primers (Figure 5.3), was cloned into pEGFP vector and expressed as a GFP-fusion protein in COS1 cells. As expected, the GFP-tagged PH-domain was also plasma membrane-associated (consistent with the cellular distribution of full-length PEPP2 and phosphoinositides such as PI(4,5)P<sub>2</sub>), with diffuse fluorescence in the cytoplasm and nucleus (Figure 5.4C and D). These observations

suggest that the protein-lipid binding also occurs *in vivo* and is likely to direct, or contribute to, the membrane-association of PEPP2.

Of note, this membrane association remained following treatment with wortmannin, which induces a dramatic reduction in the amount of PI3K products. In contrast, early endosome antigen 1 (EEA1), which normally associates with the membranes of early endosomes through binding to PI(3)P, redistributed to the cytoplasm under the same treatment (Figure 5.4A and B). This result suggests that PI3-K products, such as PI(3)P, PI(3,4)P<sub>2</sub> and PI(3,4,5)P<sub>3</sub>, are not likely to be the lipid partners for PEPP2 *in vivo*, consistent with the earlier *in vitro* binding studies.

### **5.2.1.3 Membrane-associated PEPP2 is enriched at the actin polymerisation site**

PI(4,5)P<sub>2</sub> has been suggested to be clustered in raft-like domains that are implicated in endo-/exo-cytosis and actin assembly. To further address whether PEPP2 is distributed in any of these discrete membrane domains, cell migration was induced in cultured HEK-293T cells by ‘scratching’ confluent HEK-293T cells that were transiently overexpressing GFP-PEPP2. When the cell migration was consequently promoted (i.e. for ‘wound’ healing), a non-uniform distribution of membrane-associated GFP-PEPP2 was found, with enrichment at the actin-polymerization site at the leading edge of the migrating cells (Figure 5.5). This finding is consistent with the conserved role of PI(4,5)P<sub>2</sub> in actin polymerization.

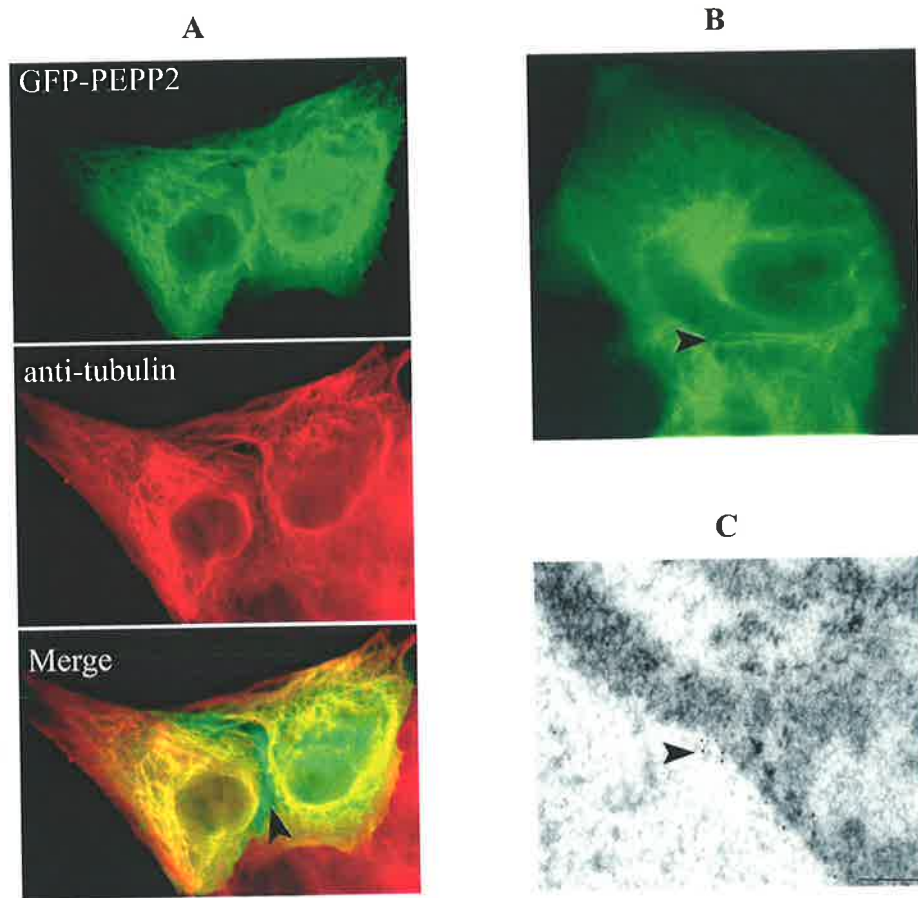


**Figure 5.2 Membrane-associated PEPP2 in different cell types.**

GFP-PEPP2 was overexpressed in the epithelial MDCK cells (A), and mesenchymal/fibroblastoid COS1 cells (B) and HEK-293T cells (C). Both membrane- and microtubule-association of PEPP2 was detected in some cells, although the majority of cells only displayed one type of distribution. A non-uniform distribution of GFP-PEPP2 on the plasma membrane was observed at cell-cell contacts of MDCK cells and COS1 cells.

A: Microtubule-associated PEPP2 and membrane-associated PEPP2 enriched at site of cell-cell contact (indicated by arrowhead) were observed in MDCK cells. Microtubules were stained with anti- $\alpha$ tubulin and Texas-red-conjugated secondary antibody.

B: GFP-PEPP2 in COS1 cells, enriched at site of cell-cell contact, indicated by arrowhead.

C: Transmission Electron microscope image showing the plasma membrane-associated GFP-PEPP2 in HEK-293T cells, detected by anti-GFP antibody and gold-conjugated secondary antibody (10nm gold particles, indicated by arrowhead). The scale bar is 500 nm.



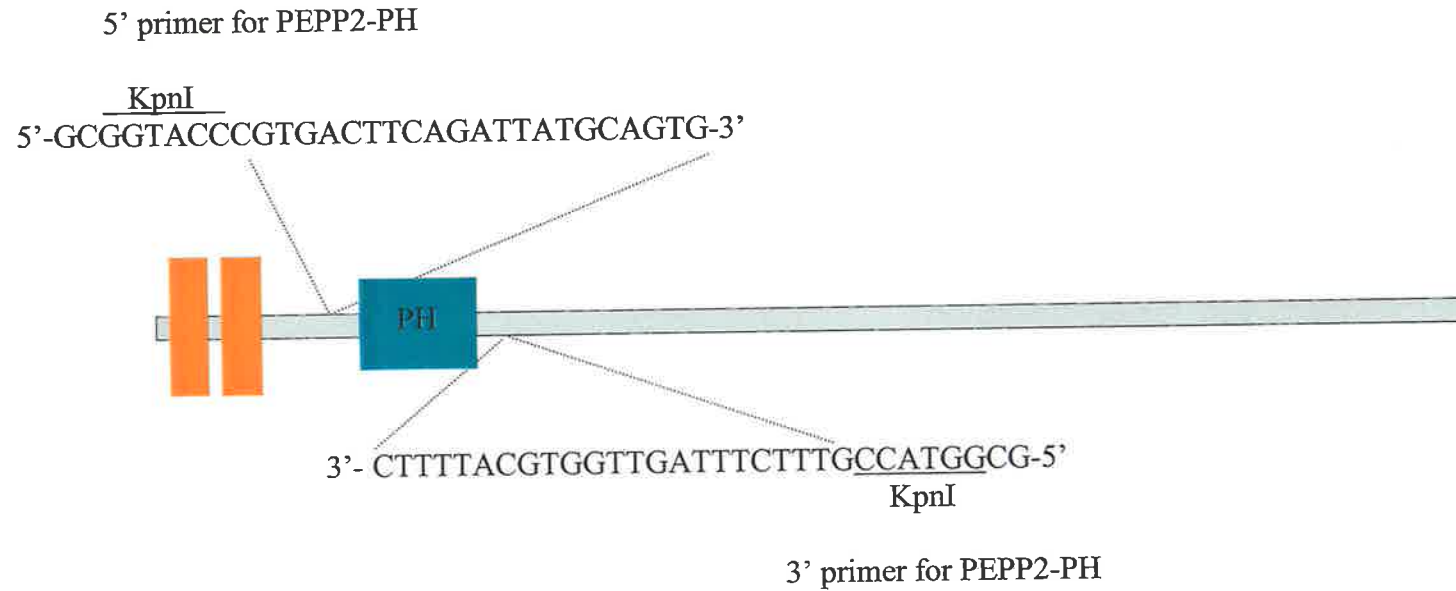


**Figure 5.3 Primers for amplification of the PH domain of PEPP2 for cloning into pEGFP-C2.**

Primer sequences and the KpnI linker on both primers are as indicated. These primers were used to amplify the PH domain of PEPP2 from pEGFP-PEPP2 using the polymerase chain reaction. The PCR product was digested with KpnI and cloned into the KpnI site of pEGFP-C2 vector.

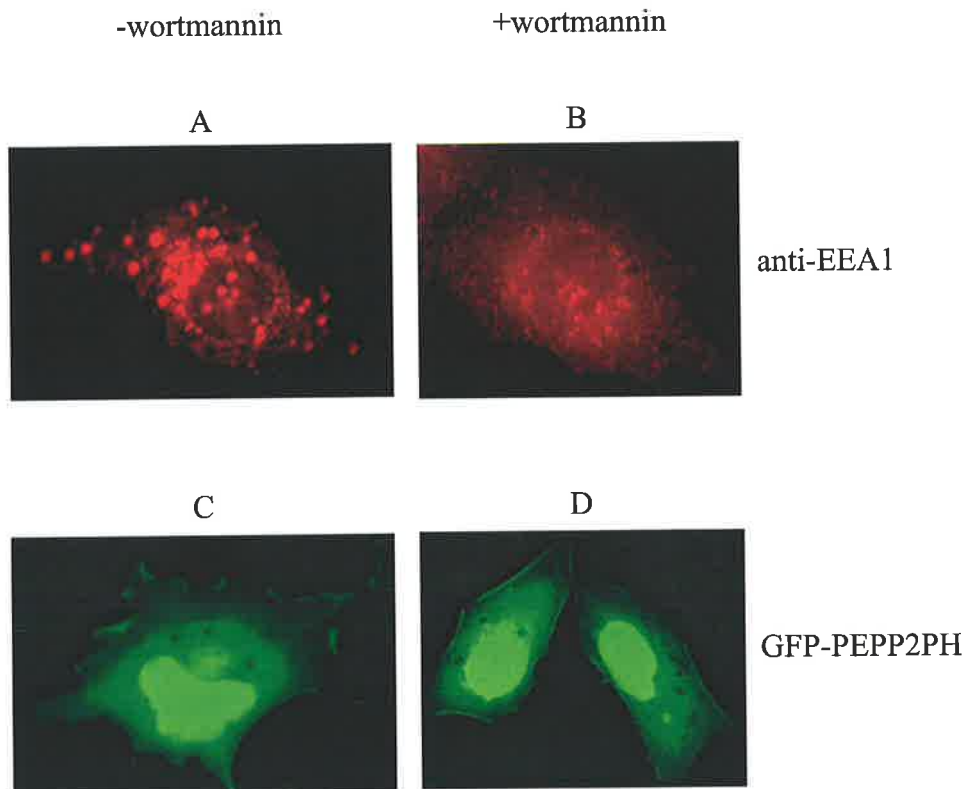


**Figure 5.4 The cellular distribution of PEPP2-PH suggests no association with PI3K products.**

The PH domain of PEPP2, expressed as a GFP fusion protein in COS1 cells (C and D), was observed on the plasma membrane as well as diffusely in both the cytoplasm and in the nucleus.

The plasma membrane-association of GFP-PEPP2PH remains unaffected after treatment with wortmannin (D), which inhibits PI3-kinase activity and reduces PI3K products, such as PI(3)P and PI(3,4,5)P<sub>3</sub>. Early endosome antigen 1 (EEA1), which associates with early endosomes (A) through interaction with PI(3)P on the early endosomal membrane, was redistributed into the cytoplasm (B) post wortmannin treatment.

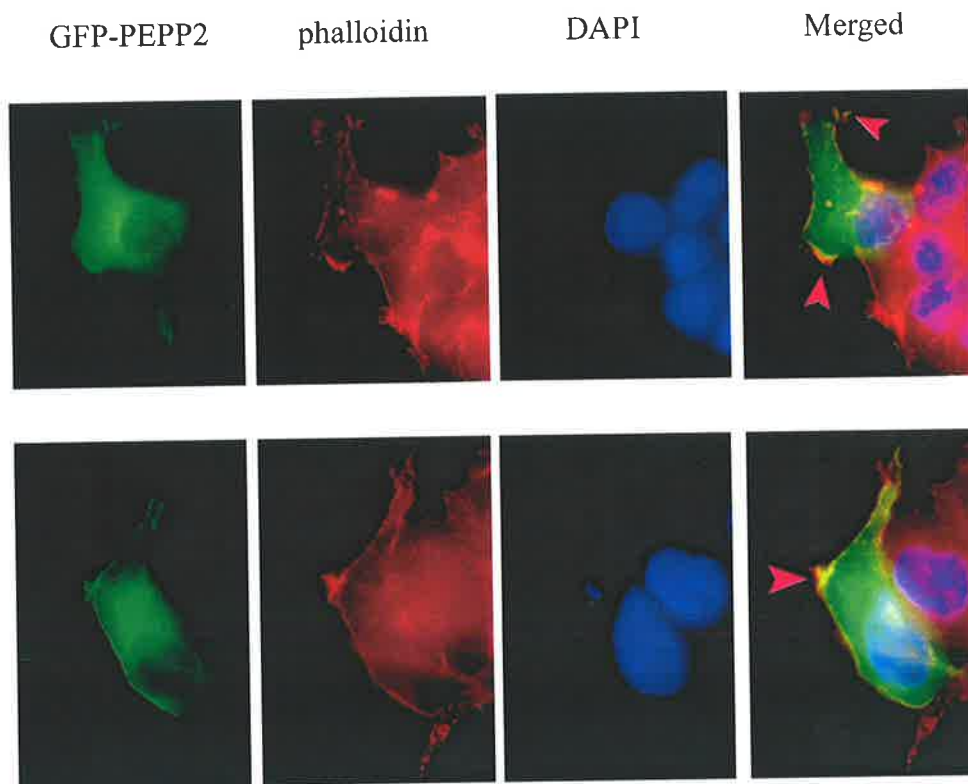


**Figure 5.5 The non-uniform distribution of GFP-PEPP2 on the plasma membrane colocalizes with the actin polymerization site.**

In confluent HEK-293T cells transiently expressing GFP-PEPP2, scratches were introduced to promote cell migration in wound healing. The actin filaments were stained with phalloidin (red). A non-uniform distribution of GFP-PEPP2 on the plasma membrane at the leading edge of migrating cells was observed using direct immuno-fluorescence. The membrane-associated GFP-PEPP2 colocalized with the actin polymerization site (yellow), indicated by arrowhead on merged images. Nuclei in these cells were stained with DAPI (blue).

### ***5.2.2 PEPP2 mediates redistribution of MID2 $\Delta$ BB to the Golgi***

As shown in the last chapter, when co-expressed, PEPP2 also co-localized with the various cytoplasmic clumps associated with some of the MID2 domain-specific deletions. Interestingly, the aggregates associated with MID2 $\Delta$ BB, which are normally found distributed throughout the cytoplasm when expressed alone as a GFP fusion protein (Figure 5.6), were found clustered in a juxtannuclear region when PEPP2 was also expressed in COS1 cells (Figure 5.7A). This juxtannuclear region co-stained with Alexa350-conjugated wheat germ agglutinin (WGA), indicated that it was likely localizing to the Golgi apparatus.

However, this Golgi localisation of GFP-MID2 $\Delta$ BB (overexpressed alone in 293T cells) was also observed by immunogold staining using an anti-GFP monoclonal antibody and a 10 nm gold-conjugated secondary antibody on cryo-sections 293T cells (Figure 5.7B) using electron microscopy. This indicated that the endogenous PEPP2 or even other membrane-associated proteins may link this microtubule-associated protein to intracellular membranes.

### ***5.2.3 MID2/PEPP2 affects membrane microviscosity***

Given that a significant proportion of PEPP2 is located on the plasma membrane, the effect of PEPP2 on a general plasma membrane property, membrane microviscosity, was investigated. Membrane viscosity is dependent on multiple conditions, such as the constitution of phospholipids and the cytoskeleton. Many cellular processes are in turn affected by membrane viscosity, such as endo-/exo-cytosis, cell mobility, cell shape and proliferation.

Fluorescence recovery after photo-bleaching (FRAP) has been shown to be easy and effective for measuring the lateral diffusion of membranes, which is inversely

proportional to membrane viscosity (Ghosh *et al.*, 2002; Vereb *et al.*, 2003). The plasma membrane of live COS1 cells was initially fluorescently labeled using DiIC<sub>16</sub>(3). A small defined area (um range) was then photo-bleached and the recovery of fluorescence in this spot subsequently monitored and imaged by scanning with a confocal microscope (Figure 5.8). The same analysis <sup>was</sup> ~~were~~ performed on COS1 cells overexpressing either GFP-PEPP2 or GFP-MID2ΔCTD, which was expected to recruit endogenous PEPP2 into its cytoplasmic clumps (i.e. acting as a dominant negative fusion). The fluorescence recovery was monitored in several cells expressing each fusion protein every second for 10 seconds post photo-bleaching (Table 5.1). The fluorescence recovery was enhanced in COS1 cells expressing PEPP2, compared with control COS1 cells, whereas COS1 cells expressing MID2ΔCTD displayed a decrease in recovery rate (Figure 5.9).

FRAP was also determined in a number of individual skin fibroblast cells derived from the OS patient bearing the truncating mutation, MID1R495X, and in fibroblast cells derived from an unaffected control (Table 5.2). No discernable change of membrane microviscosity was observed in the OS fibroblast cells when compared to controls (Figure 5.10).

#### ***5.2.4 The potential role of PEPP2 and MID2 in regulating endocytosis***

PI(4,5)P<sub>2</sub> and various other phosphoinositides have been implicated in vesicular function at several subcellular locations, including the plasma membrane, endoplasmic reticulum, Golgi, and nuclear membrane (Hsuan *et al.*, 1998). Endocytosis on the plasma membrane can be classified into two major groups: clathrin-dependent (receptor-mediated endocytosis) and clathrin-independent endocytosis, which includes the non-specific fluid-phase uptake of extracellular material through caveolae,

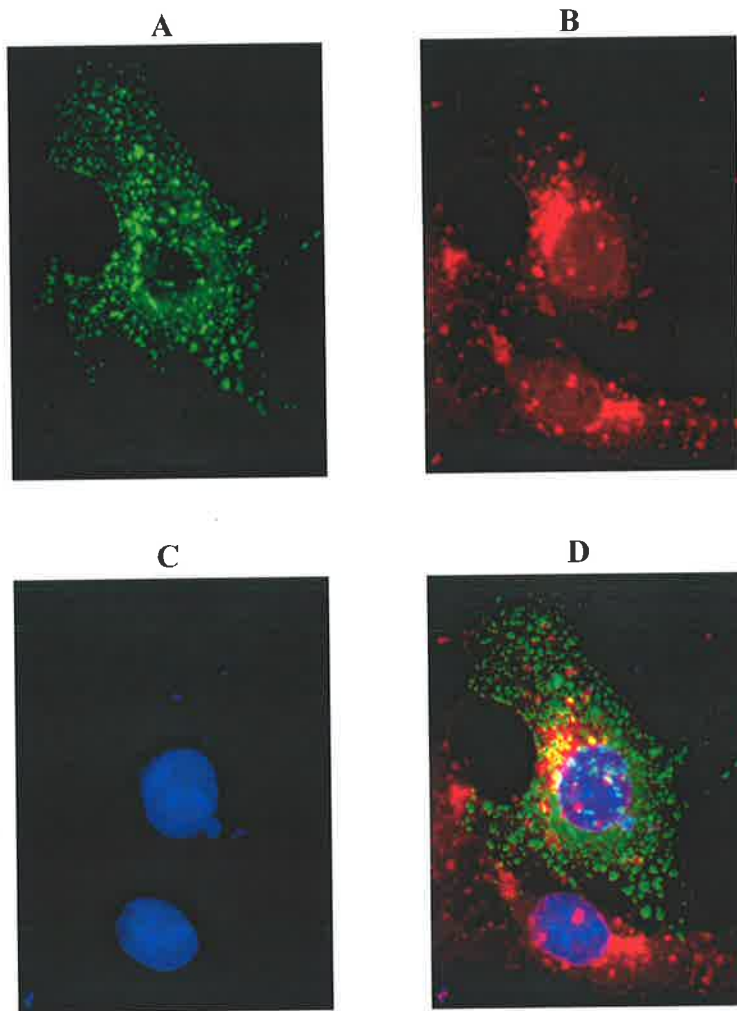


**Figure 5.6 Cytoplasmic aggregates formed by MID2 $\Delta$ BB.**

Overexpressed MID2 $\Delta$ BB (as a GFP fusion) protein displayed cytoplasmic clumping in COS1 cells (A), that did not display obvious co-localization with the Golgi apparatus (D), shown by Texas-red-conjugated WGA staining (B). Nuclei <sup>were</sup> shown by DAPI staining (C).

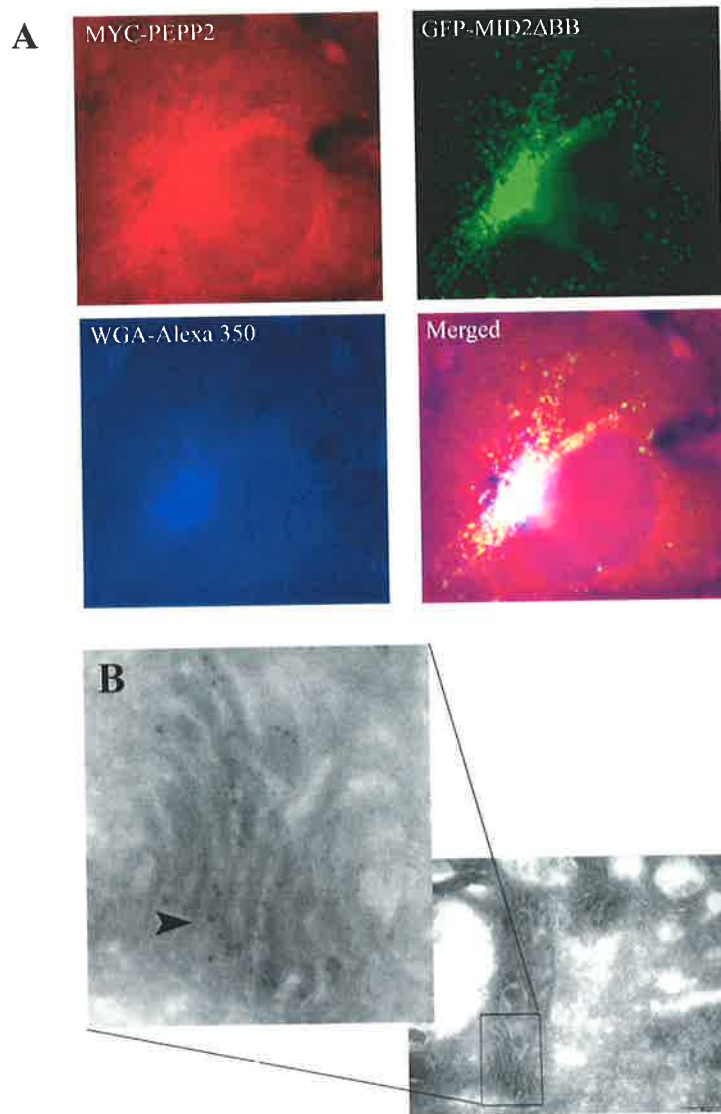


**Figure 5.7 Overexpressed PEPP2 and MID2 $\Delta$ BB colocalize in the Golgi.**

A: The GFP-MID2 $\Delta$ BB and MYC-PEPP2 were overexpressed in COS1 cells. The Golgi localization of GFP-MID2 $\Delta$ BB and MYC-PEPP2 is clearly seen using indirect immuno-fluorescence. The Golgi apparatus was stained with wheat germ agglutinin-Alexa 350 (blue) and MYC-PEPP2 was detected with anti-MYC and Texas-red conjugated secondary antibody (red). Co-localization in the Golgi is shown in white on the merged image.

B: Overexpression of GFP-MID2 $\Delta$ BB localizes in the Golgi apparatus in 293T cells, shown by anti-GFP and gold-conjugated secondary antibodies. The Golgi was shown as parallel stacks of membrane-enclosed flattened cisternae and GFP-MID2 $\Delta$ BB was represented by 10nm gold particles on the cryo-section of 293T cells using transmission electron microscopy. The scale bar represents 500nm.

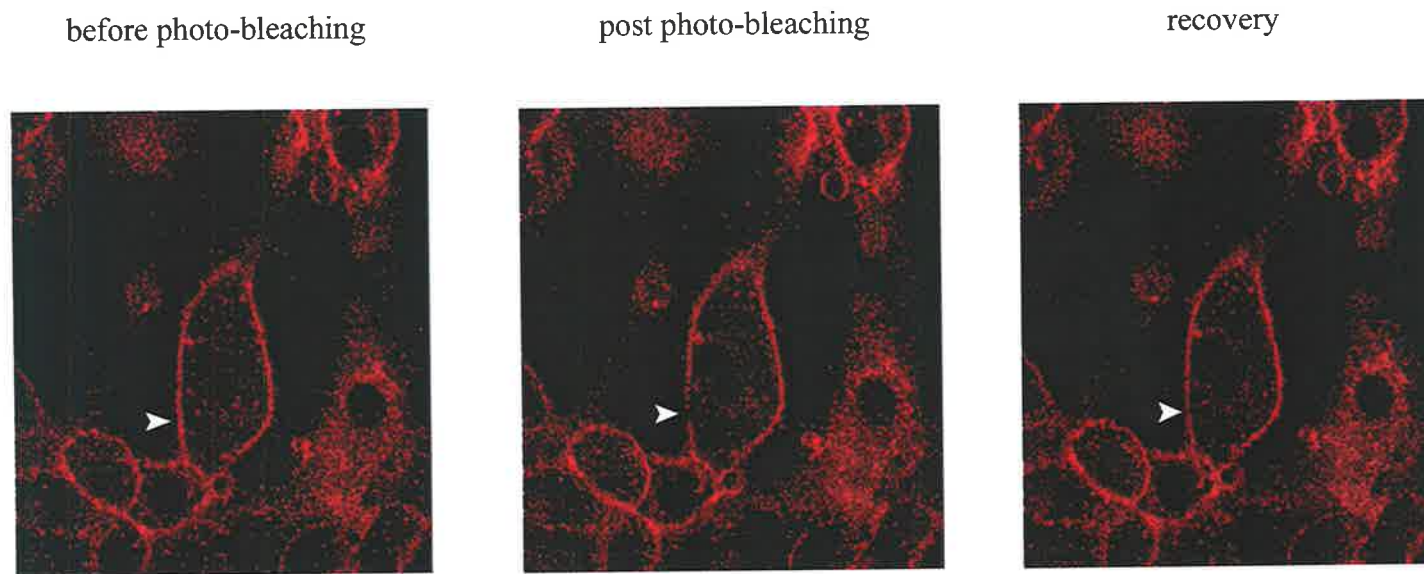


**Figure 5.8 Lateral diffusion of the plasma membrane as measured by FRAP (fluorescence recovery after photo-bleaching).**

The plasma membrane of live COS1 cells was labelled with fluorescent DiIC<sub>6</sub> (3) (red), which is an analogue of membrane lipids. A well defined region on the plasma membrane was bleached, as indicated by arrowheads on the consecutive images above. The intensity of fluorescence recovery in the bleached area, which represented the lateral diffusion of membrane, was monitored and imaged over the first 10 seconds post bleaching.



Time (sec) post photo- bleaching	Fluorescence recovery (%)		
	Control COS1 (n=6)	GFP-PEPP2 overexpressing (n=4)	GFP-MID2 $\Delta$ CTD overexpressing (n=7)
1	0.05	0.12	0.03
2	0.08	0.05	0.05
3	0.12	0.15	0.07
4	0.12	0.25	0.07
5	0.11	0.20	0.09
6	0.15	0.27	0.11
7	0.18	0.22	0.11
8	0.18	0.22	0.11
9	0.17	0.23	0.11
10	0.15	0.30	0.11

**Table 5.1 The influence of overexpressed PEPP2 or MID2 $\Delta$ CTD on the profiles of fluorescence recovery post photo-bleaching of the plasma membrane in COS1 cells.**

A small area (~  $\mu\text{m}$  range) on the DiI-C16 labelled plasma membrane from untransfected COS1 cells and COS1 cells overexpressing GFP-PEPP2 or GFP-MID2 $\Delta$ CTD was photo-bleached with the laser beam. The fluorescence recovery (%) in the bleached area was monitored with an attenuated laser beam over 10 seconds post bleaching. The profiles of recovery were collected from several individual cells of each group and the mean values of each group presented in the table above.

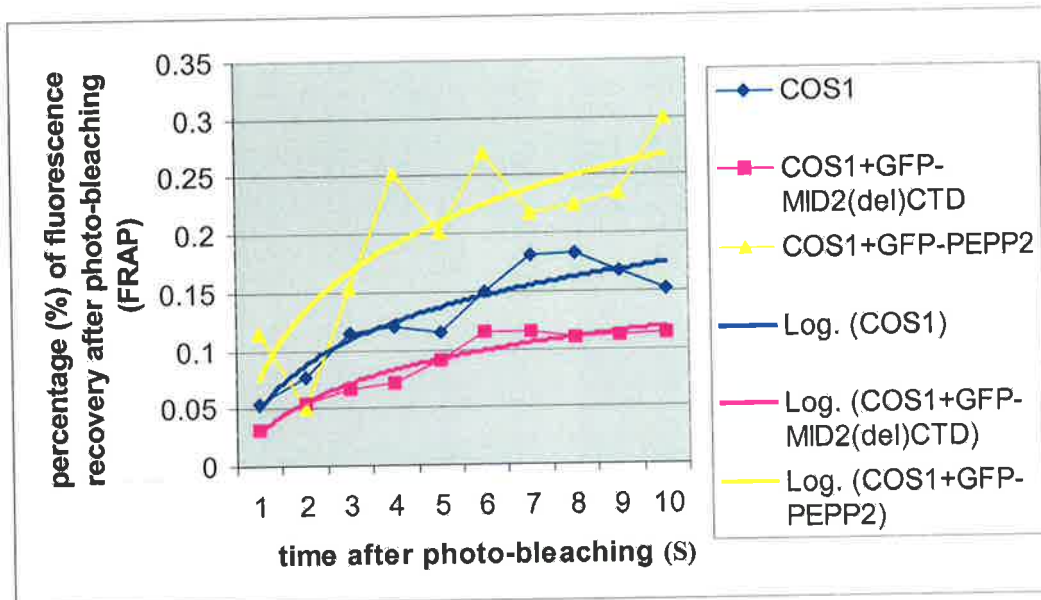


**Figure 5.9 Plasma membrane microviscosity of COS1 cells is affected by PEPP2 and MID2.**

The average recovery of fluorescence intensity (%) obtained from individual cells (see Appendix 2, 3 and 4) is presented in the chart above. Trend lines are also shown. Decreased membrane microviscosity has been seen with overexpressed PEPP2 while increased viscosity has been seen with overexpressed MID2 $\Delta$ CTD.

Time (sec) post photo- bleaching	Fluorescence recovery (%)	
	Control fibroblast cells (n=10)	OS derived fibroblast cells (n=8)
1	0.09	0.05
2	0.12	0.08
3	0.14	0.14
4	0.15	0.18
5	0.16	0.16
6	0.15	0.20
7	0.19	0.23
8	0.20	0.26
9	0.21	0.21
10	0.20	0.20

**Table 5.2 The profiles of fluorescence recovery post photo-bleaching of the plasma membrane in the fibroblast cells of the OS patient and the unaffected control.**

A small area (~  $\mu\text{m}$  range) on the DiI-C16 labelled plasma membrane of OS fibroblasts and control fibroblasts was photo-bleached with the laser beam. The fluorescence recovery (%) in the bleached area was monitored with an attenuated laser beam over 10 seconds post bleaching. The profiles of recovery were collected from several individual cells of each group and the mean values of each group presented in the table above.

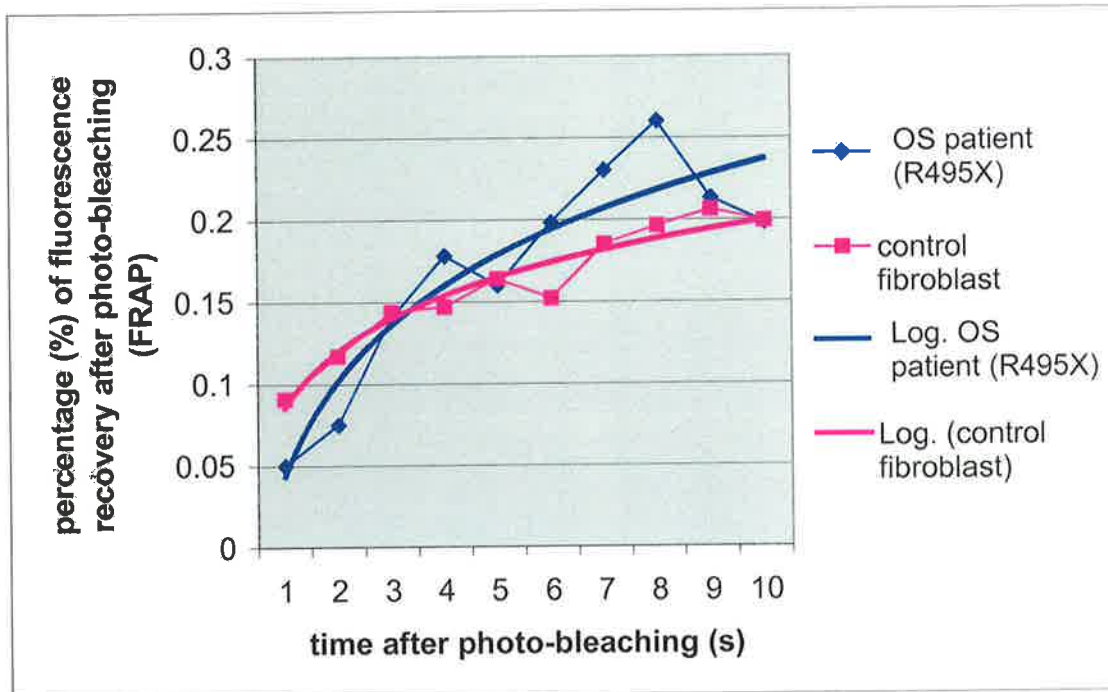


**Figure 5.10 The fluorescence recovery (%) on the plasma membrane of control and OS patient derived fibroblast cells.**

The average recovery of fluorescence intensity (%) on the plasma membrane obtained from individual OS derived fibroblast cells and control fibroblast cells derived from an unaffected control (see Appendix 5 and 6) is presented in the chart above. No significant difference in fluorescence recovery was observed at 10 seconds post photo-bleaching between the control and the OS fibroblast cells .

macropinocytosis and other uncharacterized pathways involving lipid raft domains (Conner and Schmid, 2003).

Given firstly that PI(4,5)P<sub>2</sub> is involved in the endocytotic pathway and secondly that it may mediate the plasma membrane association of PEPP2, the translocation of PEPP2 between membrane and microtubules and the interaction of PEPP2 with MID2, it was considered that this interaction could have a role in regulating endocytosis or other trafficking events. To investigate the potential influence PEPP2 and MID2 may have on these cellular processes, two well characterized molecular markers, horseradish peroxidase (HRP) and epidermal growth factor (EGF), were used to monitor the fluid-phase and receptor-mediated endocytosis, respectively.

#### 5.2.4.1 The influence of MID2 and PEPP2 on fluid-phase endocytosis

Extra-cellular HRP is internalized through fluid-phase endocytosis and intracellular HRP activity can be tested with the O-dianisidine assay after intensive washing (Marsh *et al.*, 1987; Cecilia Bucci *et al.*, 1992). In three independent experiments, HRP uptake increased up to 2.8 fold in 293T cells overexpressing both PEPP2 and MID2, compared with control 293T cells (Table 5.3). To further verify if the enhanced HRP uptake was due to the increased cellular level of PEPP2 and MID2, HRP internalization at different time points post transfection was monitored. It was found that the increasing expression of GFP-MID2 and MYC-PEPP2 facilitated HRP uptake after 8 hours following co-transfection. HRP uptake increased up to 3 fold in these GFP-MID2/MYC-PEPP2 co-expressing cells after 24 hours post-transfection (Figure 5.11B). The presence of overexpressed GFP-MID2 and MYC-PEPP2 in the post-nuclear cell lysate has been verified by western blot with anti-GFP and anti-MYC (Figure 5.11A). The poor

detection using anti-MYC on the western blots likely reflects the lack of effectiveness of this antibody in this procedure.

#### **5.2.4.2 Receptor-mediated endocytosis is affected by an overexpressed MID2 truncating mutation**

EGF endocytosis is a well characterized example of the receptor-mediated endocytic pathway. Upon binding to the EGF-receptor (EGFR) on the plasma membrane, EGF-EGFR is clustered in clathrin-coated pits, a process regulated at various stages by PI(4,5)P<sub>2</sub>. Fluorescent core (Texas-red) conjugated EGF was therefore used to evaluate the possible effects that PEPP2 and MID2 might have on this process. EGF-Texas-red was incubated with COS1 cells and internalized EGF-Texas-red was observed by direct fluorescence. No discernable difference was seen in cells overexpressing wild type MID2 or PEPP2 when compared with the control COS1 cells. However, a significant reduction in internalized EGF-Texas-red signal was observed in COS1 cells overexpressing the GFP fused MID2 $\Delta$ CTD (Figure 5.12). Interestingly, a similar reduction was observed in cells overexpressing GFP-fused MID1 $\Delta$ CTD (Figure 5.12).

	1		2		3	
	HRP activity/100ug total protein (OD at 460nm)	Transfection efficiency (% of GFP+ cells)	HRP activity/100ug total protein (OD at 460nm)	Transfection efficiency (% of GFP+ cells)	HRP activity/100ug total protein (OD at 460nm)	Transfection efficiency (% of GFP+ cells)
Control	0.44	80%	0.81	50%	0.25	80%
GFP-MID2/ MYC-PEPP2 co-transfected	0.89	80%	1.22	70%	0.70	80%
Folds increased	2		1.5		2.8	

**Table 5.3 Fluid-phase endocytosis were increased in 293T cells co-expressing MID2 and PEPP2.**

The transfection efficiency was determined by the percentage of GFP positive cells. The expression of each construct was confirmed by western blot analysis using anti-GFP and anti-MYC antibodies. The rate of fluid-phase endocytosis was determined by horse radish peroxidase uptake following incubation of cells with 5mg/ml HRP for 10min and monitoring internalised HRP amounts by the O-dianisidine assay, which gives maximum absorbance at 460nm after been oxidized. Duplicates were set up for each sample in all three experiments to minimize error. The HRP activity was increased in cells expressing MYC-PEPP2 and GFP-MID2 in all three independent experiments, compared with the HRP activity in control cells expressing GFP and MYC tag only.

**A.**



**B.**

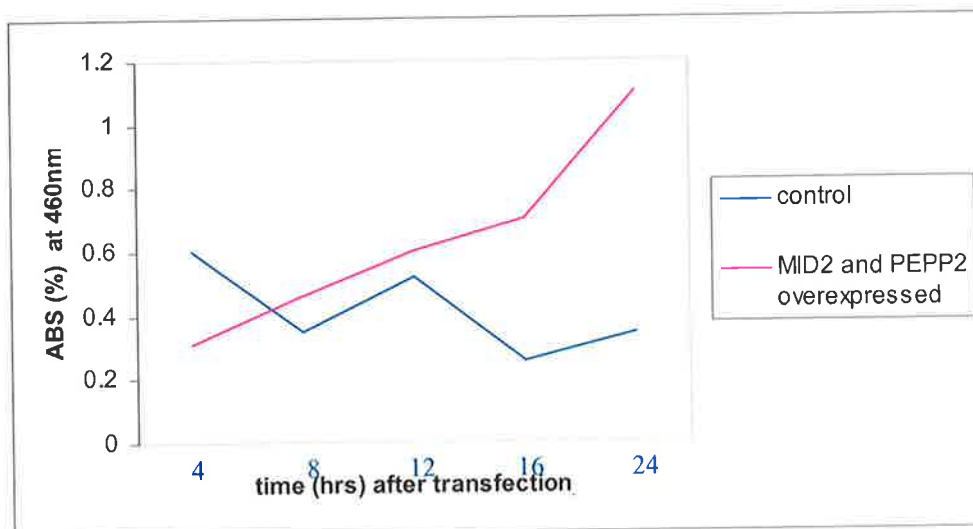


**Figure 5.11 The effect of MID2/PEPP2 on fluid-phase endocytosis.**

Fluid-phase endocytosis in HEK-293T cells was monitored using the HRP uptake assay. Increased HRP uptake was observed in cells co-expressing MID2/PEPP2 at each time point from 8 hours following transfection (pink line in B) and this effect is consistent with the increasing level of MID2/PEPP2 expression after transfection (shown by Western blot in A). Control cells were co-transfected with pEGFP/pCMV-MYC and expressed GFP- and MYC- tag only.



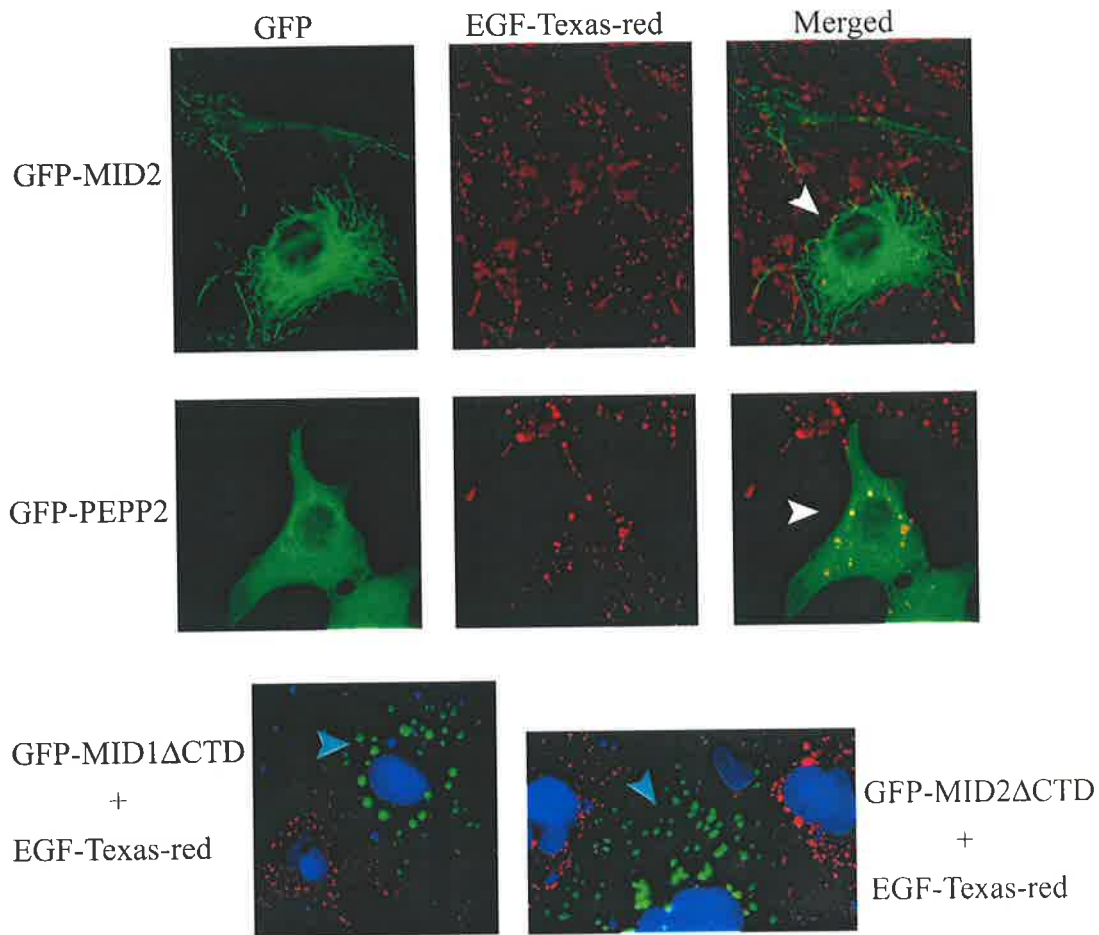


**Figure 5.12 Receptor-mediated endocytosis was inhibited by overexpression of mutant MID2 and MID1.**

EGF-Texas-red was used as a marker of receptor-mediated endocytosis in COS1 cells overexpressing GFP-PEPP2, GFP-MID2, GFP-MID2 $\Delta$ CTD or GFP-MID1 $\Delta$ CTD, as indicated. The expression of these fusion proteins and EGF internalisation were monitored using direct fluorescence. EGF uptake appeared normal in cells overexpressing wild-type MID2 or PEPP2 (indicated by white arrowheads), whereas uptake was noticeably impaired in cells overexpressing MID1 $\Delta$ CTD or MID2 $\Delta$ CTD (as indicated by blue arrowheads). The EGF uptake in the untransfected cells on the same images served as controls.

### 5.3 Discussion

Microtubules and actin are the two major components of the cytoskeleton. Microtubules are polarized but dynamically unstable microfilaments assembled from  $\alpha$ - and  $\beta$ -tubulin in a head-to-tail orientation. Microtubules continuously undergo polymerization and depolymerization mainly at their extremities (i.e. plus ends or fast growing ends), although their minus ends or ~~slowly~~ growing ends also show dynamic change. With the third form of tubulin,  $\gamma$ -tubulin, the minus ends of microtubules are anchored at two centrioles which, along with centriolar matrix, is known as the microtubule organizing centre (MTOC) (Andersen and Wittmann, 2002).

Actin filaments (F-actin), which ~~are~~ ~~comprise~~ ~~of~~ two chains of globular monomers (G-actin), are also under continuous cycles of polymerization and depolymerization. Its rearrangement underneath particular subdomains of plasma membrane is believed to be critical for cell shape maintenance, membrane invagination and cell adhesion (Lee and Gotlieb, 2002; Schafer, 2003).

Despite the distinct cellular roles, the interaction between microtubules and actin underlies most of the cellular processes that require dynamic cellular asymmetries to be established or maintained. They also link to the plasma membrane and intracellular membranes with the assistance of a large number of cross-linking proteins, including proteins of the CLIP family, metabolic enzymes and MAPs etc. (see section 1.7). These proteins play a central role in regulating dynamics of membrane vesicles and the integrity and positioning of endomembrane compartments such as the Golgi complex, ER and mitochondria.

As highlighted in chapter 4, PEPP2, a new PH-domain-containing protein, was identified as an interactor of MID2 in a yeast two-hybrid screen. Subsequent characterization of PEPP2 revealed that it could be detected on either microtubules or

on the plasma membrane, or both, in different cell types. The plasma membrane-association of PEPP2 was likely to be directed by the protein-lipid interaction between the PH domain and phosphoinositides since the overexpressed GFP fusion protein of the PH domain in COS1 cells also displayed association with the plasma membrane which is enriched with PI(4,5)P<sub>2</sub>. Although interactions have been noted between the PEPP2 PH domain and phosphoinositides other than PI(4,5)P<sub>2</sub> in the *in vitro* lipid interaction assay, the binding of PI-3-phosphate derivatives *in vivo* is unlikely since the membrane associated PH domain of PEPP2 remained unaffected following wortamannin (a PI3K inhibitor) treatment.

Under physiological conditions, however, the local concentration of each phosphoinositide and the interaction of PEPP2 with other proteins may be as, or more, important than the lipid-binding affinity in directing the protein-lipid interaction. For example, it is possible that the interaction between other proteins and the WW-domain or other uncharacterized regions of PEPP2 also helps to specify the membrane targeting and hence the cellular function of PEPP2. Such a mechanism is generally used by PH-domain-containing proteins with no clear ligand specificity and low binding affinity. For example, the PH domain of  $\beta$ -ARK ( $\beta$ -adrenergic receptor kinase) binds PI(4,5)P<sub>2</sub> and the C-terminal extension binds G <sub>$\beta\gamma$</sub> . However, only the simultaneous interaction with both ligands is sufficient to drive efficient membrane targeting (Lemmon *et al.*, 2002). In the case of MID2, homodimerization of MID2 and the interaction with PEPP2 could direct dimerization of PEPP2, with a resultant increased affinity for phosphoinositides. A precedent for such an effect has been reported for dynamin, where its monomeric form binds PI(4,5)P<sub>2</sub> with low affinity whereas oligomerization increases the affinity (Lemmon *et al.*, 2002). Given the interaction between PEPP2 and MID2 appears to be regulated by heterodimerization of MID1 and MID2, lipid binding by

PEPP2 and the plasma membrane-microtubule connection could be subsequently affected, representing a functional regulatory mechanism instead of a simple structural similarity between MID1 and MID2.

Another intracellular membrane structure that is enriched with PI(4,5)P<sub>2</sub> is the Golgi apparatus, which is close to the microtubule organizing centre. A potential PEPP2/MID2 directed microtubule-Golgi connection may also exist given that a coverage of the entire length of microtubules has been observed with overexpressed PEPP2 and MID2. Further support for this hypothesis comes with the observation of a Golgi-localized aggregation of overexpressed PEPP2 and MID2 $\Delta$ BB in COS1 cells. This Golgi-localized GFP-MID2 $\Delta$ BB was also found with the overexpressed GFP-MID2 $\Delta$ BB alone using transmission electron microscope, although the majority formed small aggregates that scattered throughout the cytoplasm. This observation suggests that this Golgi-microtubule connection also happens with endogenous levels of PEPP2, given overexpressed PEPP2 enhances the Golgi localization of MID2 $\Delta$ BB.

The Golgi membrane is abundant in the precursors of PI(4,5)P<sub>2</sub>, phosphatidylinositol and PI(4)P (Martin, 2001). The sequential activation of PI-4-kinases and PI-5-kinases and the subsequent local increase in synthesis of PI(4,5)P<sub>2</sub> is necessary for the maintenance of the Golgi architecture and the Golgi exocytic vesicle coat formation through recruiting the ARF class of small G proteins and coat proteins (Cockcroft and De Matteis, 2001). It is not clear whether PEPP2 and MID2 are involved in any of these processes, although they are unlikely to be necessary for maintaining the Golgi positioning since the Golgi morphology appeared normal in COS1 cells overexpressing the MID2 $\Delta$ CTD, which was assumed to recruit wild type PEPP2 into its cytoplasmic clumps (data not shown).

In migrating cells, a non-uniform distribution of PEPP2 was observed on plasma membrane ruffles, where actin polymerization occurs. Actin polymerization and microtubule protrusion at the leading edge of motile cells is required for directed cell migration (Nabi, 1999). Different phosphoinositides, including PI(3,4,5)P<sub>3</sub>, PI(3,4)P<sub>2</sub> and PI(4,5)P<sub>2</sub>, have been indicated in regulating actin dynamics (Insall and Weiner, 2001). The synthesis of PI(3,4,5)P<sub>3</sub> is consistent with the temporally and spatially restricted actin polymerization. The role PI(3,4,5)P<sub>3</sub> plays in serving as an instructive signal for stimulus-induced actin polymerization is thought to be mediated by activation of the guanine nucleotide exchange factors (GEFs) of the Rho family (Insall and Weiner, 2001).

The role of PI(4,5)P<sub>2</sub> in the control of actin polymerization is less clear. Clustering of PI(4,5)P<sub>2</sub> at the actin nucleation site on the plasma membrane has also been shown. (Tall *et al.*, 2000), with recent studies suggesting PI(4,5)P<sub>2</sub> may affect actin nucleation through activation of the WASP (Wiskott-Aldrich syndrome protein) protein family, since the actin polymerization induced by the increased PI(4,5)P<sub>2</sub> could be inhibited by the overexpression of a dominant negative WASP (Millard *et al.*, 2004). Instead of acting as an instructive signal to promote actin polymerization, PI(4,5)P<sub>2</sub> is more likely to direct the growing actin filaments to the plasma membrane due to its interaction with a number of different actin binding proteins, such as gelsolin and profilin (Hsuan *et al.*, 1998).

The observation that PEPP2 concentrated at the actin nucleation site raises the possibility of its influence on actin polymerization. BALB/c 3T3 fibroblasts injected with monoclonal antibodies against PI(4,5)P<sub>2</sub> to prevent the interaction between PI(4,5)P<sub>2</sub> and cytoskeletal proteins failed to form stress fibres or focal adhesions on serum stimulation (Gilmore and Burridge, 1996). Given the likely interaction of PEPP2

and PI(4,5)P2 *in vivo*, PEPP2 may therefore be involved in regulating actin polymerization through controlling the availability of PI(4,5)P2 for actin binding proteins.

The polymerization of actin and microtubules are coordinated by Rho family GTPases (see section 1.7.2). The ruffled leading lamellipodium of migrating cells reflects the underlying polarized organization of the cytoskeleton, which is characterized by actin polymerization at the leading edge and the balanced microtubule-dependent retrograde flow of lamellum actin meshwork, the dendritic actin network at the lamellipodia (Rodriguez *et al.*, 2003). The structural linkage between microtubules and actin also orients the plus end of microtubules towards the leading edge along moving actin bundles (Gundersen and Bretscher, 2003). Therefore, PEPP2 may be involved in coupling the reorganization of microtubules with actin polymerization in directing cell migration due to its interaction with microtubule-bound MID2.

In the future, clarification of the detailed function of PEPP2 could be helped by determining the effects on actin polymerization in PEPP2 knocked-down or PEPP2 null cell lines. The potential role PEPP2 plays in the coupling of microtubules and actin dynamics could be analyzed by dual-wavelength fluorescent speckle microscopy (FSM) using spectrally distinct fluorophore labeling of microtubules and actin.

Both phospholipids and the cytoskeleton (as well as cholesterol and integral membrane proteins) affect the viscosity of membranes (viscosity being the reciprocal of membrane fluidity) (Vereb *et al.*, 2003). A change in membrane viscosity can in turn affect essential cellular processes, such as the efficiency of ligand-binding, intercellular interactions and cell migration. In this regard, recent studies have revealed a linkage between membrane microviscosity and actin dynamics in migrating endothelial cells (Vasanji *et al.*, 2004). Given the membrane-association of PEPP2 and its possible role

in regulating actin polymerization, the potential influence of PEPP2 on membrane microviscosity was investigated using FRAP. The rate of fluorescence recovery within a small bleached area on the plasma membrane is representative of the rate of lateral membrane diffusion and is inversely proportional to membrane microviscosity (Ghosh *et al.*, 2002). Furthermore, the diffusion rate in a lipid bilayer is expected to be independent of the size of the bleached area (Vereb *et al.*, 2003). However, monitoring of fluorescence recovery was undermined due to the motility of the live cells, which made restriction of the laser scanning in the bleached spot on the plasma membrane difficult. This caused the considerable variation between each scanning of the fluorescence intensity on the same spots (see the data table of Appendices 1-5). This may be minimized by increasing sample sizes in further analyses. Nevertheless, a notable increase in the lateral movement of the plasma membrane was observed in cells overexpressing GFP-PEPP2 (i.e. the membrane microviscosity decreased), whereas the opposite situation was found for cells overexpressing the C-terminally truncated MID2 that would be expected to recruit wild-type PEPP2 into its cytoplasmic aggregates. Unexpectedly, the membrane viscosity of the OS derived fibroblast cells remained apparently normal when compared with that of fibroblast cells derived from an unaffected individual. Unfortunately, it is not known whether the control fibroblasts were derived from a similarly aged and sex matched person, and thus conclusions must be drawn with caution at this time. Membrane lateral diffusion kinetics can also vary dramatically among different cell types, such that comparison between the transfected cells and the fibroblasts are strictly not comparable. Furthermore, the heterogeneity of the cellular localization of endogenous wild type MID2 in the OS fibroblasts, reflected by both normal microtubule-association and cytoplasmic co-clumping with endogenous

MID1R495X seen with overexpressed wild type MID2 (see section 3.2.2), may also minimize the influence of MID2 on membrane viscosity in these cells.

The relationship between membrane microviscosity and cell motility is biphasic. Increased cell motility has been seen with increased microviscosity to a threshold, beyond which resulted in significantly decreased motility (Ghosh *et al.*, 2002). The potential influence the PEPP2/MID2 complex may have on the membrane viscosity was also consistent with the finding that an increased endothelial cell activation and mesenchymal invasion (increased cell motility) was observed with treatment of endocardial cushion explants with antisense oligos to *cMID2* (Runyan, unpublished).

How PEPP2 and MID2 affect plasma membrane dynamics still remains unclear. An increased plasma membrane viscosity and more productive actin filament formation has been observed at the cell front of migrating endothelial cells (Vasanji *et al.*, 2004) and a reduction in cell motility and increase in membrane tension has been associated with depolymerization of microtubules (due to the possible interruption in focal complex turnover) (Horwitz and Parsons, 1999). Given this, the possibility of the involvement of PEPP2/MID2 in regulating actin dynamics and microtubule-dependent trafficking (such as focal complex turnover) seems a plausible explanation.

Given that endocytosis can be subsequently affected by the changes in membrane viscosity (due to affected receptor clustering and membrane invagination), the potential influence that the PEPP2 and MID2 interaction may have on this actin- and microtubule-dependent process was investigated. Extra-cellular materials are internalized through three major endocytic pathways: fluid-phase endocytosis, receptor-mediated endocytosis (also known as clathrin-mediated endocytosis) and phagocytosis. Two widely used endocytic markers HRP and EGF-Texas red for fluid-phase endocytosis and clathrin-mediated endocytosis, respectively, were used to monitor the



possible influence of PEPP2 and MID1/MID2 on these two endocytic pathways in cultured cells.

Increased HRP uptake was observed with increasing cellular levels of PEPP2 and MID2. The facilitated HRP uptake was unlikely to be a direct consequence of the PEPP2-induced increase in membrane fluidity alone, as an increase of HRP uptake was not seen in control cells over-expressing PEPP2 only. Other mechanisms, such as the interaction between PEPP2 and phosphoinositides, the possible modification of actin dynamics by PEPP2 during membrane invagination or the coordinated vesicle transportation on actin and microtubules could however explain this.

An involvement of PI(4,5)P<sub>2</sub> in receptor-mediated endocytosis has in fact been suggested from the studies addressing the proper formation of clathrin-coated pits (recruits AP-2 and AP-180 for the proper formation of coated pits), vesicle fission (recruits dynamin, which triggers the GTP-dependent mechanochemical conformation change of the membrane) and vesicle fusion (which is required to define the site of vesicle docking) (Martin, 2001). Similarly, a role of PI(4,5)P<sub>2</sub> has also been implicated in fluid-phase endocytosis and phagocytosis, although evidence for this is less definitive (Simonsen *et al.*, 2001). Membrane-associated PEPP2 may also be involved in the transient loading of vesicles onto microtubules through its interaction with MID2. The possible involvement of PEPP2 in these mentioned processes may account for the increase of HRP uptake alone or in combination with each other.

Interestingly, overexpression of PEPP2 and MID2 did not appear to affect EGF internalization, whereas impaired EGF internalization was observed in cells overexpressing MID2 $\Delta$ CTD. In this case, it is possible that inhibited EGF internalization is secondary to the increased plasma membrane microviscosity induced by overexpressed MID2 $\Delta$ CTD, since an increase over a certain threshold has previously

been noted to completely stop endocytosis (Callaghan *et al.*, 1990). However, this effect on clathrin-mediated endocytosis may also be due to removal of PEPP2 from the plasma membrane since wild type PEPP2 is recruited into the cytoplasmic aggregates in cells overexpressing MID2 $\Delta$ CTD (see section 4.2.5). The same mechanisms may also be applied to explain a similar inhibition of EGF internalization in cells overexpressing MID1 $\Delta$ CTD, i.e. via the clumping of wild type PEPP2 due to the recruitment of wild type MID2 in higher order complexes by overexpressed MID1 $\Delta$ CTD.

It has been known for some time that microtubule-dependent trafficking from early to late endosomes/lysosomes and late vesicle recycling are shared by all different endocytic pathways. Recent studies have shown that the initial uptake as well as steady-phase uptake of cell surface transferrin receptors is also microtubule dependent, indicating the involvement of microtubules in even earlier stages of the endocytotic pathway (Hamm-Alvarez *et al.*, 1998). This may not necessarily involve microtubule-dependent vesicle transport but rather imply a role for microtubules in receptor clustering or sequestration, such as seen with the clustering of NMDR receptor and gamma-aminobutyric acid type A receptors (GABA(A)Rs) (Matsuda and Hirai, 1999; Coyle and Nikolov, 2003). Therefore, it is feasible that PEPP2/MID2 could also affect early receptor clustering and membrane invagination on the plasma membrane as well as the later microtubule-dependent vesicle transport.

The hypothesis that MID1/MID2 and PEPP2 is involved in membrane-trafficking is indirectly supported by the finding that TRIM9, which is a member of the CI subfamily of RBCC proteins that includes MID2 and MID1 as its closest homologues (see chapter 1), plays a role in regulating synaptic vesicle exocytosis (Li *et al.*, 2001). TRIM9, also known as Spring, regulates vesicle trafficking through its interaction with both the cytoskeleton and SNAP-25. SNAP-25 interacts with VAMP on the synaptic vesicles

and syntaxin on the presynaptic plasma membrane to assemble the SNARE (Soluble N-ethylmaleimide-sensitive fusion protein association protein receptor) complexes for vesicle fusion (Bonifacino and Glick, 2004). Overexpression of Spring and SNAP-25 abolished the interaction of SNAP-25 with VAMP and syntaxin and prevented the assembly of SNARE complexes, resulting in the reduced exocytosis (Li *et al.*, 2001).

More recently, another member of the CI subfamily, Haprin (Trim36), was also shown to have a role in controlling the \*acrosomal exocytosis—its overexpression inhibiting the acrosome reaction (Kitamura *et al.*, 2003). Like MID1 and MID2, both TRIM9 and Haprin were found to associate with microtubules (Short *et al.*, unpublished). Further understanding of its role is likely to come from identifying specific interactors.

There are an increasing number of RBCC proteins that have been implicated in regulating vesicle transport, such as ADP-ribosylation factor domain protein 1 (ARD1) and brain-expressed RING finger protein (BERP), suggesting the possibility of a general molecular basis for these RBCC proteins in regulating the vesicle trafficking events.

Recently, a potential ubiquitin E3-ligase activity has been ascribed to MID1 (Troockenbacher *et al.*, 2002) and is also expected to be possessed by MID2. Ubiquitination is a post-translational modification in which the addition of a single ubiquitin, or polyubiquitin chains, to target proteins, directs their membrane trafficking or degradation (see section 1.5.5). Alpha4, a regulatory subunit of PP2-type phosphatases and a key target of the TOR signaling pathway, possibly directs ubiquitination and degradation of the PP2A catalytic subunit by mediating its interaction with MID1 (Troockenbacher *et al.*, 2002).

---

\* Acrosome reaction is the sperm exocytotic event that involves the multiple fusion steps between the plasma membrane and the Golgi-derived acrosome, which contains enzymes to digest the zona pellucida coating around the egg.

It is well accepted that membrane trafficking and the function of proteins involved in trafficking are fine-tuned by phosphorylation and ubiquitylation (Riezman, 2002). PP2A has been found to be associated with microtubule motors and modifies their function by phosphorylation/dephosphorylation (Smith, 2002) and inhibition of its activity by okadaic acid in hepatocytes has been noted to reduce vesicle recycling and microtubule-dependent endocytosis (Runnegar *et al.*, 1997). Therefore, the recycling of the EGF-receptor may also be affected as a consequence of the interrupted PP2A turnover in cells overexpressing MID2 $\Delta$ CTD or MID1 $\Delta$ CTD, such that decreased EGFR on the plasma membrane would result thus terminating further EGF internalization. Besides the direct involvement of PEPP2 in regulating membrane trafficking through its interaction with phosphoinositides, as discussed earlier, the interaction between PEPP2 and MID2 also raises the possibility that PEPP2 directs the MID2-dependent ubiquitylation of unknown membrane targets. Considering this, MID1/MID2 could alternatively or in addition be involved in membrane trafficking at the level of regulating phosphorylation of trafficking proteins through PP2A or by directly ubiquitylating trafficking proteins.

In conclusion, MID2 is likely to be involved in microtubule-dependent membrane trafficking through its interaction with PEPP2, which associates with membrane lipids and/or membrane-bound proteins. A potential role in regulating this process can also be attributed to MID1, considering that the heterodimerization of MID1 and MID2 appears to regulate the MID2/PEPP2 interaction. During early development, cell migration, signal transduction and EMT are important for proper embryonic development, with the latter especially critical for craniofacial and urogenital morphogenesis as well as atrioventricular septation. Since these developmental events all rely on inter-/intra-cellular trafficking (see chapter 1), the potential role for MID2 in regulating endothelial

activation and mesenchymal invasion (in the endocardial cushion explants) may be due to its role in regulating membrane trafficking. A similar role for MID1 would adequately explain the spectrum of defects seen in OS patients.

## Chapter Six: Dissecting MID1/MID2 protein complexes

### 6.1 Introduction

RBCC proteins have been implicated in a variety of processes by association of mutations with different disease states, including oncogenesis, development and a few human developmental disorders (Reymond *et al.*, 2001). Although MID1 and MID2 localize to microtubules, the majority of RBCC proteins localize to unknown subcellular compartments.

The order of the RING-finger, B-box and Coiled-Coil domains from the N- to the C-terminal of the protein is conserved throughout evolution, suggesting that the correct orientation and relative spacing of these domains is functionally significant. Each of the individual motifs comprising the RBCC domain has been implicated in protein-protein interactions either directly or indirectly (Borden, 1998). The RING domain of RBCC and non-RBCC proteins, can act as an interface for a variety of protein interactions, although commonly for mediating the interaction and the subsequent promotion of E2-dependent ubiquitin conjugation (reviewed by Jackson *et al.*, 2000). The B-box motifs may also be directly involved in mediating protein-protein interaction (i.e. providing the interface for interaction between Alpha4 and MID1 or MID2) (Short *et al.*, 2002), although in some instances it also appears to be crucial for the orientation of the leucine rich Coiled-Coil that mediates oligomerization and other molecular interactions (Borden, 1998; Burkhard *et al.*, 2001; Torok and Etkin, 2001).

A variety of unrelated domains are found associated with the RBCC tripartite motif. Two of the more commonly found C-terminal domains are the B30.2-like and NHL domains. These domains are putatively involved in ligand binding (Torok and Etkin, 2001). The B30.2 domain consists of two distinct subdomains which are likely to be

members of the Ig superfamily (Seto *et al.*, 1999). Although a specific biological function has not been assigned to the B30.2 domain, it is the only domain that is found in transmembrane proteins, intracellular proteins and secreted proteins, thus indicating that it serves as a generally used interface for protein interaction (Henry *et al.*, 1998).

Due to the multiple interfaces for protein-protein interaction, RBCC proteins normally exist in higher order protein complexes, which are critical for their cellular functions. For example, the homo-oligomerization of KAP-1, the corepressor of the TIF family, is necessary for its interaction with the KRAB domain of various transcription repressors (Peng *et al.*, 2000). Similarly, the oligomerization of PML is required for its subsequent interaction with p53 and Ubch9 (Jensen *et al.*, 2001). This has also been found for MID1 and MID2, the homo-dimerization of which is also a prerequisite for their microtubule binding (Short *et al.*, 2002).

In addition to the homo-dimerization, MID1 and MID2 also hetero-dimerize, which is rarely found among RBCC proteins, even among members of the CI subfamily (see chapter 3.3). The homo-/hetero-dimerization of MID1 and MID2 may be used as a regulatory mechanism to direct interactions with common or specific protein partners, thus giving rise to different cellular functions and different protein compositions for the putative MID1/MID2 protein complexes. This hypothesis was supported by the identification of a number of MID1/MID2 interactors (common and specific) both in the previous studies and in the work presented in this thesis (see section 1.6.4 and chapter 4).

In this chapter, gel filtration has been used initially to determine the existence of MID1/MID2 complexes. Proteomic tools were then employed to begin to identify the components in these complexes. Since most of the OS-associated mutations in MID1 are C-terminal truncating mutations, the protein components lost in MID1 $\Delta$ CTD

complexes have been extensively investigated. Further characterization of these components will assist in understanding the cellular function of MID1/MID2 and the pathogenesis of OS.

## 6.2 Results

### 6.2.1 *Immuno-precipitation of the MID1 protein complexes*

#### 6.2.1.1 1-D electrophoresis of MID1 complexes purified by immunoprecipitation

An anti-GFP monoclonal antibody was used for immunoprecipitation to purify the MID1 protein complexes from cell lysates collected from 293T cells transiently expressing GFP-MID1 or GFP as a control. The GFP-MID1 protein complexes were separated on a 10% SDS polyacrylamide gel and stained with coomassie blue (Figure 6.1). The protein band representing overexpressed GFP-MID1 was clearly seen. As expected, several protein bands appeared to associate with GFP-MID1 complexes, when compared with the proteins non-specifically associated with GFP alone. Among them, a protein of the matched molecular weight of Alpha4 (38.5kDa) was observed associated with GFP-MID1, although this was not verified by Western blot analysis. However, none of these bands were further selected for protein peptide fingerprinting due to their poor resolution and/or low amounts observed.

#### 6.2.1.2 2-D electrophoresis of MID1 complexes purified by immunoprecipitation

To obtain increased resolution, the MID1 protein complexes purified from the cell lysates by immunoprecipitation were subjected to two-dimensional protein separation. Cell lysates from 293T cells transiently overexpressing GFP, GFP-MID1 or GFP-MID1 $\Delta$ CTD constructs were precipitated with an anti-GFP antibody. The resultant immunoprecipitant was solubilized in 2-D sample buffer and separated using isoelectric



focusing (IEF) and subsequently separated on a 10% SDS poly-acrylamide gel according to their different molecular weights. Upon comparison of the protein profiles on the gels after silver staining, several protein spots specifically associated with GFP-MID1 were observed (Figure 6.2B). Some of these proteins were not seen in the complexes pulled down with GFP-MID1 $\Delta$ CTD (Figure 6.2C). These results indicate that MID1 indeed forms protein complexes with specific interactors. Unfortunately, immunoprecipitation did not yield sufficient sample for protein identification. Therefore, an alternative approach was sought in order to scale up the sample preparation of these protein complexes to permit identification of the components specifically associated with the MID1 complexes.

## ***6.2.2 MID1 and MID2 exist in high molecular weight complexes***

### **6.2.2.1 Determination of protein complexes using FPLC**

Gel filtration is commonly used for determining the molecular weight of proteins. Due to its broad range of size differentiation (1—5000kDa) and high resolution, Superose 6 matrix was chosen for the separation of MID1/MID2 complexes. Four markers of different molecular weight: blue dextran 2000 (2000kDa); thyroglobulin (660kDa); ferritin (440kDa); and BSA (68kDa) were used to calibrate the Superose 6 HR 10/30 column. Approximately 40 ug of each standard was mixed in 200 ul 1 X PBS plus 0.1% NP-40 and injected onto the Superose 6 column. The elution profile of these standards is presented in Figure 6.3. The elution volume for blue dextran 2000 represented the column void volume ( $V_0$ ), which was about 30% (7 ml) of the total volume (24 ml). The elution volumes of these protein standards were measured and their corresponding elution volume parameter ( $K_{av}$ ) values were plotted against the logarithm of their

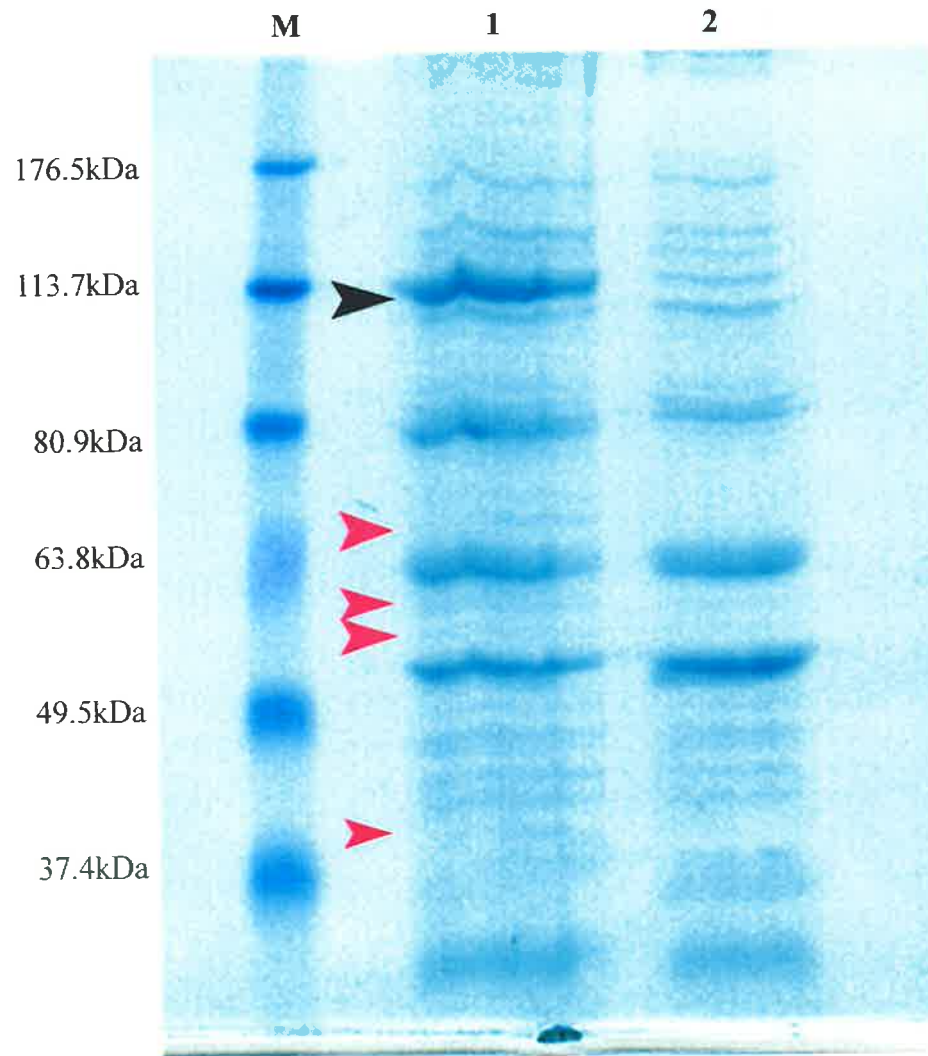


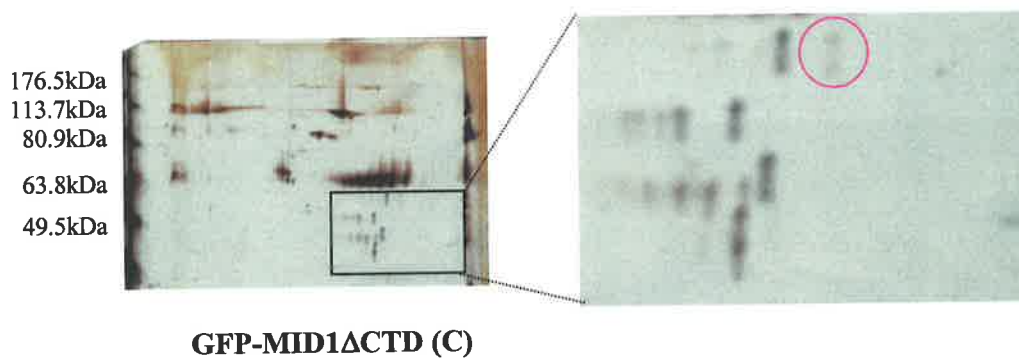
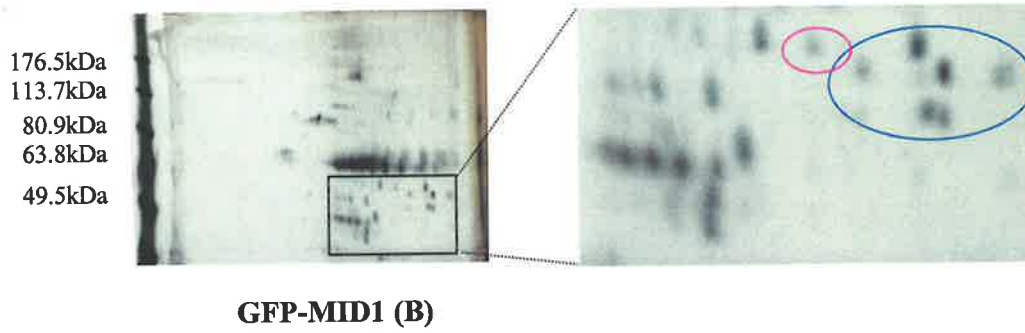
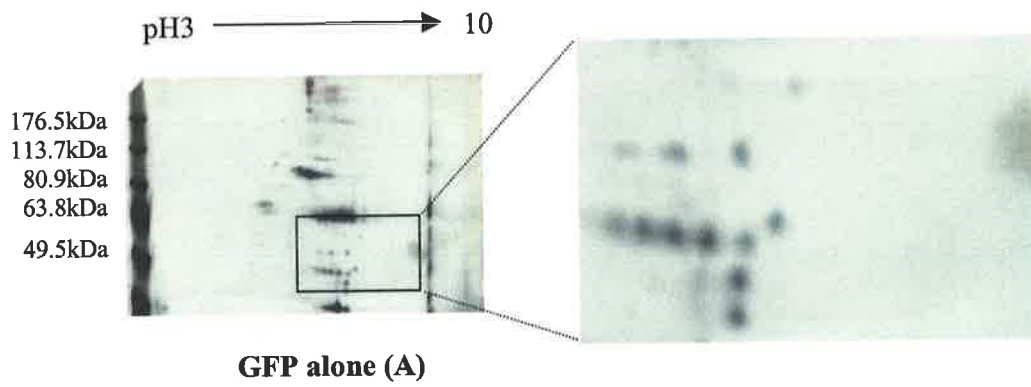
**Figure 6.1 Protein complexes containing GFP-MID1 purified by immunoprecipitation with anti-GFP antibody.**

HEK-293T cells were transfected with constructs expressing GFP-MID1 or GFP only. The proteins associated with GFP-MID1 or GFP were pulled down by immunoprecipitation with an anti-GFP antibody. Protein marker (lane M), protein complexes containing GFP-MID1 (lane 1) and protein complexes containing control GFP (lane 2) were separated out on a 10% SDS-polyacrylamide gel. The overexpressed GFP-MID1 (about 110kDa) is indicated by the black arrowhead and potential protein bands associated with MID1 are indicated with pink arrowheads. A protein of the similar molecular weight (~38.5kDa) to Alpha4 was associated with MID1.

**Figure 6.2 Analysis of the GFP-MID1 and GFP-MID1 $\Delta$ CTD protein complexes by 2-D electrophoresis.**

Cell lysate was prepared from HEK-293T cells ( $\sim 10^7$ ) transiently expressing GFP (A), GFP-MID1 (B) and GFP-MID1 $\Delta$ CTD (C). Protein complexes containing the fusion protein or GFP alone were purified by immunoprecipitation with an anti-GFP monoclonal antibody. The purified protein complexes were resuspended in 2-D sample buffer and separated by 2-D electrophoresis. Proteins on 2-D gels were visualized by silver staining.

By comparing the protein profiles on these 2-D gels, a few proteins appeared to be associated with the GFP-MID1 complexes (circled in both red and blue), but not with GFP alone. Some of these MID1 specific proteins (circled in blue) were not present in GFP-MID1 $\Delta$ CTD complexes. The association of the red circled proteins with MID1 remained with MID1 $\Delta$ CTD, indicating N-terminal MID1 mediated protein-protein interaction.



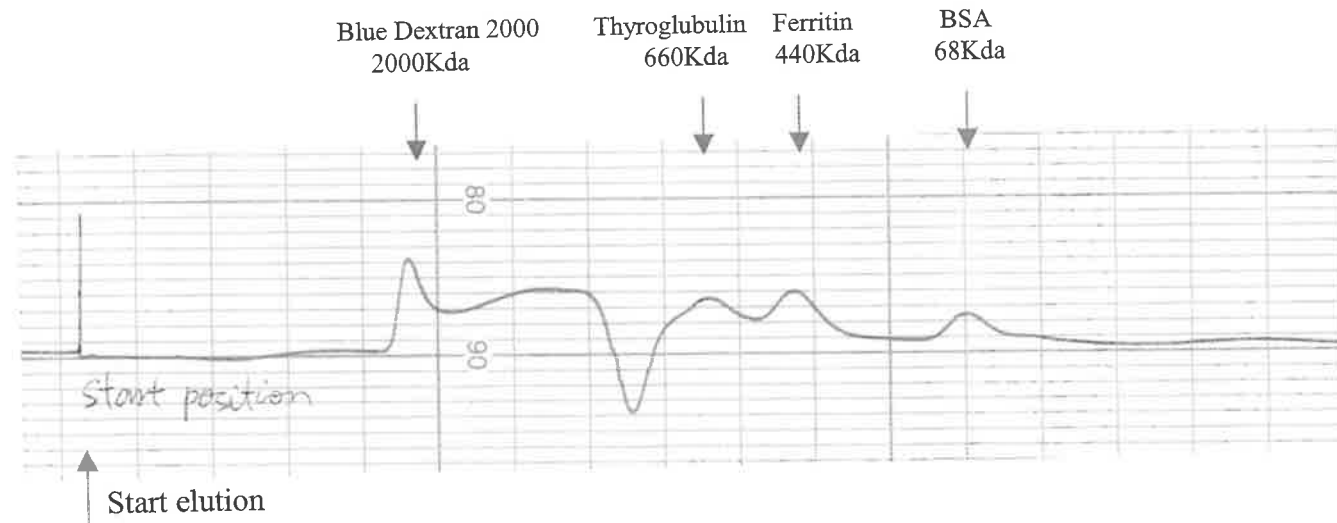


**Figure 6.3 The elution profile of calibration standards.**

Calibration of the Superose 6 HR 10/30 FPLC column with standards of different molecular weights was performed using a Pharmacia FPLC system and was monitored using a UV spectrophotometer at  $OD_{280}$ . The sample injection volume was 200  $\mu$ l. The elution started as indicated on the chart at a flow rate of 0.4 ml/min and chart speed of 0.25 cm/min. According to the elution profile,  $V_e$  (Blue Dextran 2000) = 7 ml;  $V_e$  (Thyroglubulin) = 13.5 ml;  $V_e$  (Ferritin) = 15.4 ml;  $V_e$  (BSA) = 19 ml.

molecular weight. This calibration curve was subsequently used to determine the molecular weight of the MID1 and MID2 protein complexes (Figure 6.4).

#### **6.2.2.2 MID1/MID2 protein complexes determined by FPLC**

MID protein complexes were separated from cell lysates of HEK-293T cells transiently expressing GFP fusions of MID1, MID2 or truncated MID1 (>70% transfected, determined by counting GFP positive cells) using FPLC. Eluted fractions from the gel filtration with the Superose 6 column were collected and the presence of overexpressed MID1, MID2 or MID1 $\Delta$ CTD in these fractions detected by Western blotting using an anti-GFP antibody (Figure 6.5).

After calculating the  $K_{av}$  values of the peak elution of the overexpressed MID protein complexes, the molecular weights of the complexes were determined according to the calibration curve (Figure 6.6). Although no obvious peak elution was observed for MID2 it did display an overlapping elution profile with GFP-MID1, with both existing in large protein complexes of  $\sim$ 1.5MDa (size determined with the peak elution of GFP-MID1). The size of the protein complexes formed by MID1 $\Delta$ CTD is smaller ( $\sim$ 1MDa), which is likely due to the loss of protein interactions with the MID1 C-terminal domain.

### **6.2.3 Decoding the MID protein complexes**

The identification of large protein complexes formed by MID1 and MID2 highlighted the importance of identifying the different protein components in these complexes for elucidating the cellular function of MID1 and MID2.

#### **6.2.3.1 The presence of Dynein heavy chain in MID1 complexes**

Large samples were prepared from the peak elution (Figure 6.5, fractions 12, 13 and 14) for the MID1 complexes from 293T cells transiently overexpressing GFP-MID1. The same fractions from 293T cells transiently overexpressing GFP-MID1 $\Delta$ CTD were used as a control. After dialyzing and sample concentration, about 1mg of total protein was run on a 10% SDS polyacrylamide gel. However, poor resolution that was likely related to overloading the gel prevented the observation of protein components specifically associated with GFP-MID1 (Figure 6.7). Surprisingly, despite the seemingly increased sample amount of the GFP-MID1 $\Delta$ CTD complexes, a protein band of greater molecular weight was observed associated that was not seen with GFP-MID1.

This protein band was subsequently subjected to “in-gel” tryptic digestion. The extracted peptides were introduced onto a Q-TOF<sup>2</sup> mass spectrometer by reversed phase HPLC using a 1  $\times$  30 mm column. The eluted peaks were analysed and the monoisotopic (no <sup>13</sup>C) forms of the component ions and their charge states were measured. These were converted into a virtual singly charged state corresponding to the mass of the peptide plus one proton as recorded in Table 6.1. The deduced masses of the singly charged ions were used to search for matching human proteins in the NCBI non-redundant protein database (version NCBIInr.01.22.2003) and Genpept (version 11.30.2002 ) using MS-Fit ( <http://prospector.ucsf.edu/ucsfhtml4.0/msfit.htm> ). A match

Calibration standards (kDa)	LgMW (Y)	Kav (X)
Blue Dextran (2000)	6.30	0.00
Thyroglobulin (660)	5.82	0.38
Ferritin (440)	5.64	0.49
BSA (68)	4.83	0.70

$$K_{av} = (V_e - V_o) / (V_t - V_o)$$

$V_e$  = elution volume for the protein

$V_o$  (column void volume) = elution volume for Blue Dextran

$V_t$  = total bed volume

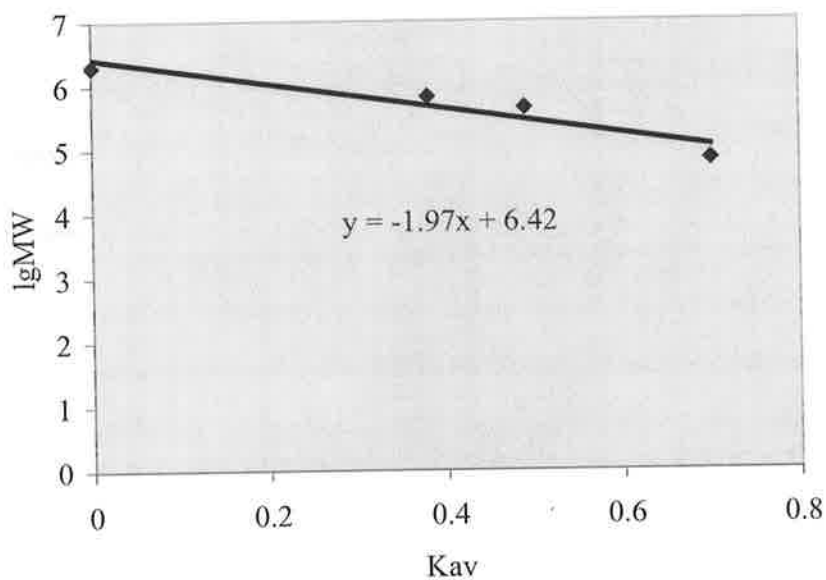


**Figure 6.4** The calibration curve for the Superose 6 column.

The  $K_{av}$  value of each standard was calculated using the above formula. The calibration curve was drawn by plotting the  $K_{av}$  values of several standards against the logarithm of their molecular weight ( $K_{av} : \lg Mr$ ).



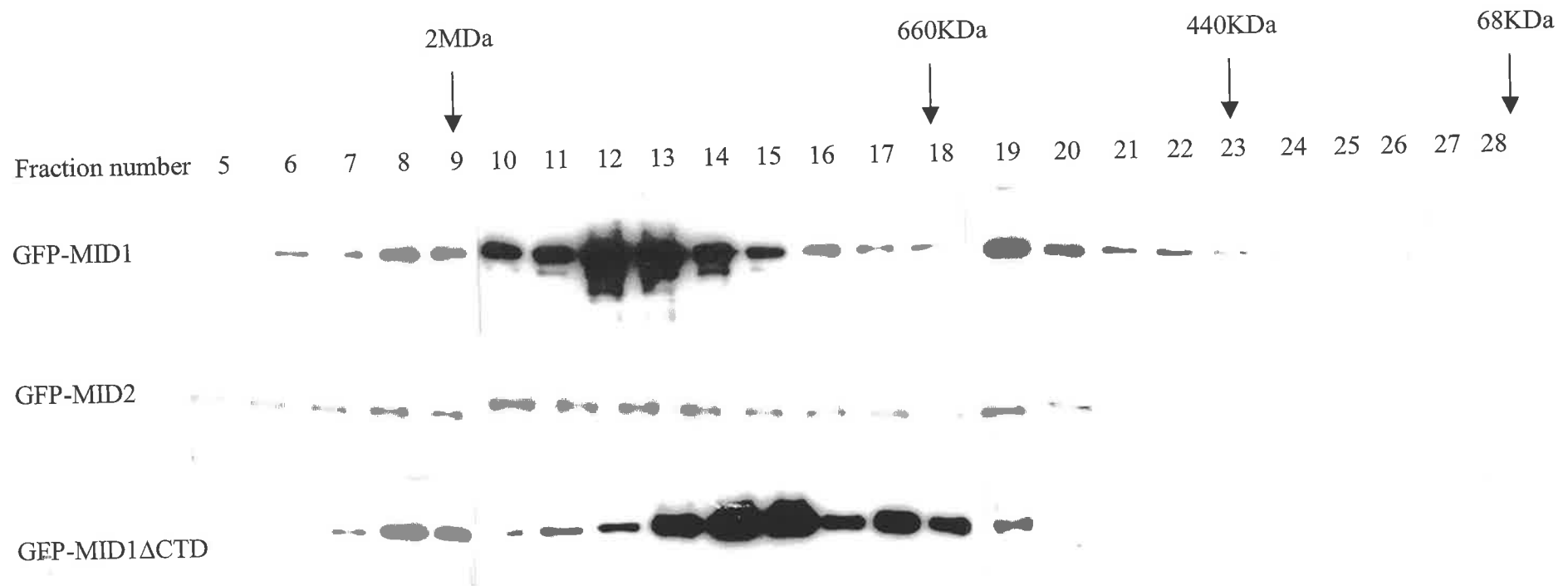


**Figure 6.5 MID1 and MID2 exist in macromolecular protein complexes.**

FPLC fractions of cell lysate from 293T cells overexpressing GFP-MID1, GFP-MID2 or GFP-MID1 $\Delta$ CTD were collected. The presence of the GFP fusion protein in these fractions <sup>was</sup> were detected by western blotting with an anti-GFP antibody. MID1 and MID2 form high order protein complexes (fractions 8-16, peak  $V_e$  = 9ml). GFP-MID1 $\Delta$ CTD was present in smaller protein complexes (fractions 12-18, peak  $V_e$  = 10.5ml).

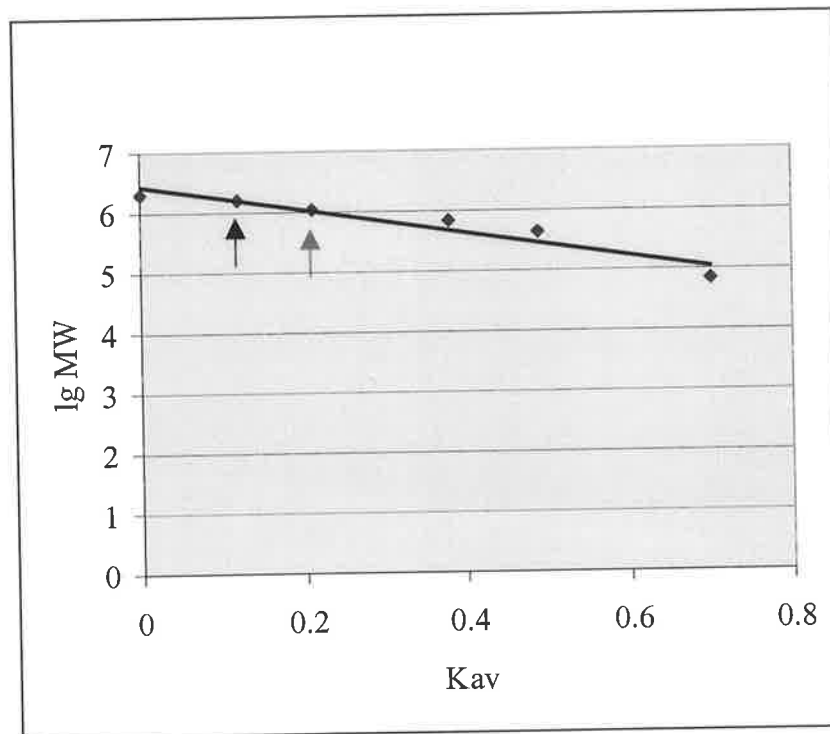


**Figure 6.6 Molecular weight determination for MID1 protein complexes.**

The molecular weights of MID1 and MID1 $\Delta$ CTD complexes were determined using the calibration curve ( $Y = -1.97X + 6.42$ ). The Kav values for MID1 and MID1 $\Delta$ CTD complexes are 0.12 and 0.21 respectively, as indicated by arrows on the chart. Their deduced molecular weights are ~1.5MDa and ~1MDa, respectively.

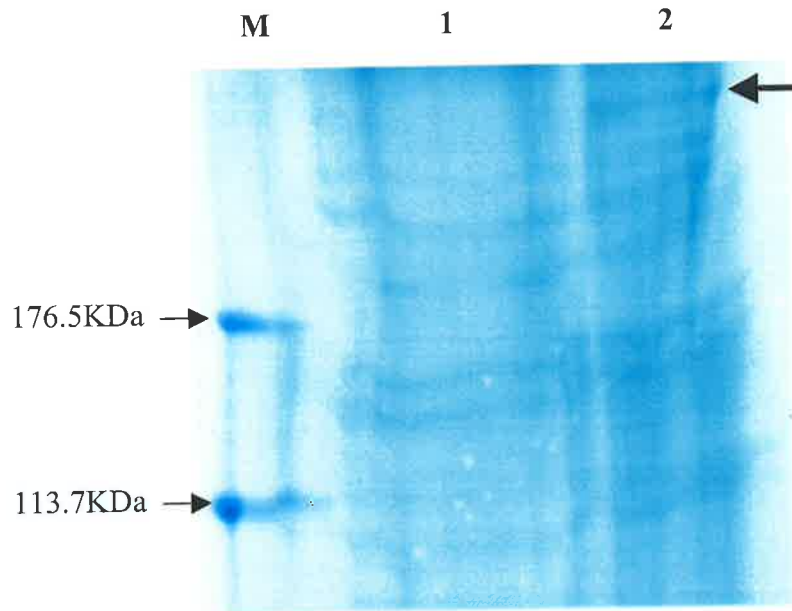


**Figure 6.7 Protein components in MID1 complexes.**

Cell lysate was collected from 293T cells transiently overexpressing GFP-MID1 or GFP-MID1 $\Delta$ CTD. Fractions containing the peak elution of GFP-MID1 (lane 1) and the corresponding fractions containing GFP-MID1 $\Delta$ CTD (lane 2) were separated (about 1mg total protein of each sample) along with protein markers (lane M) on a 10% SDS polyacrylamide gel. The gel was stained with coomassie blue.

Poor resolution of the sample separation was due to the large amount of sample loaded. However, despite more sample having been loaded in lane 2, a protein band of high molecular weight (as indicated with the arrow) was observed in GFP-MID1 $\Delta$ CTD, but not, or much less, in GFP-MID1 complexes. This protein was subsequently excised and subjected to in-gel trypsin digestion and peptide finger printing.

**Table 6.1 Masses and charge states of the resultant peptides of unidentified protein in the MID1 $\Delta$ CTD complexes.**

The mass/charge ( $m/z$ ) of peptides were measured by mass spectrometry and were converted into a virtual single charged state ( $Z=1$ ) corresponding to the mass of the peptide plus one proton ( $[M+H]^+$ ). The deduced masses of the peptides were then sorted into an ascending order and used to search for matching human proteins in the NCBI non-redundant protein database and the Genpept database.

<b>m/z</b>	<b>z</b>	<b>[M+H]<sup>+</sup></b>	<b>search list</b>
671.402	2	1341.796	714.417
843.465	3	2528.379	900.530
962.507	2	1924.006	1008.551
1150.651	2	2300.294	1172.640
818.965	2	1636.922	1264.700
1023.557	2	2046.106	1341.796
1048.547	3	3143.625	1558.886
1113.585	3	3338.739	1559.934
1347.664	2	2694.320	1628.950
779.947	2	1558.886	1635.892
780.471	2	1559.934	1636.922
804.450	3	2411.334	1873.032
900.530	1	900.530	1874.034
937.521	2	1874.034	1904.076
980.533	2	1960.058	1924.006
1048.230	3	3142.674	1960.058
1062.131	2	2123.254	2028.018
1112.566	5	5558.798	2046.106
1130.568	4	4519.248	2123.254
1299.713	2	2598.418	2181.158
1329.666	3	3986.982	2265.202
1390.200	4	5557.776	2299.270
1853.892	3	5559.660	2300.294
971.515	3	2912.529	2411.334
1091.083	2	2181.158	2476.376
1014.513	2	2028.018	2486.254
1150.139	2	2299.270	2528.370
1172.640	1	1172.640	2528.379
1264.700	1	1264.700	2598.418
714.417	1	714.417	2694.320
818.450	2	1635.892	2912.529
937.020	2	1873.032	3142.674
1081.210	3	3241.614	3143.625
1238.692	2	2476.376	3241.614
952.542	2	1904.076	3338.739
1008.551	1	1008.551	3986.982
1133.105	2	2265.202	4519.248
1243.631	2	2486.254	4816.584
1204.902	4	4816.584	5557.776
814.979	2	1628.950	5558.798
1264.689	2	2528.370	5559.660

of moderate quality was obtained against the Genpept database. With a \*MOWSE score =  $5.293e+004$ , 8 peptides matched HOMO SAPIENS (AB002323) KIAA0325, which appears to encode a Dynein heavy chain fragment (Table 6.2).

### 6.2.3.2 Identification of eukaryotic translation elongation factor 1 beta in MID1 complexes

Given the poor resolution of one dimensional SDS-PAGE for the amount of sample loaded, samples collected from fractions 12, 13 and 14 were pooled and separated on two dimensional gels. Several attempts were undertaken to optimise the resolution of the two-dimensional gels. Two protein dots, around 110kDa (could be the overexpressed GFP-MID1 itself) and 100kDa, that appeared to be associated with GFP-MID1 were processed (Figure 6.8). Unfortunately, the in-gel digestion and the subsequent HPLC separation of these proteins did not yield enough peptide for mass spectrometry.

Since the protein samples collected after gel filtration have a relatively simpler protein composition when compared with crude cell lysates, a larger sample (1.5 mg) was loaded in another attempt to increase yield. A group of abundant proteins (circled in red), between 50kDa—110kDa/PI 5—7, which separated well in the above mentioned attempt, gave poor resolution this time (Figure 6.9). However, a few proteins of lower abundance, which were not seen on the 2-D gel using the initial sample load, were

---

\* MOWSE (Molecular Weight Search) scoring system (Pappin *et al.*, 1993): The peptide fragment masses determined by mass spectrometry and the molecular weight of the intact protein (if known) are used to search against the theoretical molecular weight of protein fragments in the database. Proteins in the database were initially grouped into 10kDa intervals between 100kDa and 10kDa, all proteins over 100kDa fell into another group. Each matching molecular weight is scored for its distribution frequency value (the number of times a particular fragment molecular weight occurred in a protein of any given size is divided by the total number of peptides in each 10kDa interval, and then normalized to the largest cell frequency to give a value between 0 and 1). Each of the fragment distribution frequency values are multiplied in a protein contains multiple matches, and then inverted to give a final MOWSE score.

observed in the GFP-MID1 complexes. Two slightly more abundant proteins (~49kDa and ~30kDa) among them were subjected to mass-spectrometry protein finger printing (Table 6.3). After searching the NCBI non-redundant protein database using MS-FIT, no relevant matches were found with the 49KDa protein (data not shown) while the ~30KDa protein matched with “eukaryotic translation elongation factor 1 beta” (Table 6.3 and Table 6.4).

In summary, two recognisable proteins, dynein heavy chain and Eukaryotic Elongation Factor 1 Beta, were identified as potential components of the MID1 complexes. Further investigation into the fidelity of the association between these factors under physiological conditions and the functional significance of their potential interaction is therefore warranted.

**Table 6.2 MS-Fit search results of unidentified protein in GFP-MID1ΔCTD complexes.**

The MS-Fit search selected 39 entries. Results are displayed for the top 5 matches with the top match highlighted.

	MOWSE Score	#/41(%) Masses Matched	% Cov	% TIC	Mean Err ppm	Data Tol ppm	MS-Digest Index #	Protein MW (Da)/pI	Accession #	Species	Protein Name
<u>1</u>	5.293e+004	8 (19)	7.0	19.5	7.44	33.4	"345180"	238447/6.2	"2224591"	HOMO SAPIENS	(AB002323) KIAA0325 (Dynein heavy chain)
<u>2</u>	58.9	4 (9)	4.0	9.8	14.7	17.0	"103345"	284284/5.2	"179106"	HOMO SAPIENS	(J05243) nonerythroid alpha-spectrin
<u>3</u>	58.8	4 (9)	4.0	9.8	14.7	17.0	"1017730"	285068/5.2	"1805280"	HOMO SAPIENS	(U83867) alpha II spectrin
<u>4</u>	58.1	6 (14)	4.0	14.6	7.38	43.0	"572024"	269656/5.8	"6739602"	HOMO SAPIENS	(AF178534) talin
<u>5</u>	58.1	6 (14)	4.0	14.6	7.38	43.0	"571305"	269720/5.7	"6682361"	HOMO SAPIENS	(AF177198) talin



**Figure 6.8 2-D separation of MID1 complexes.**

MID1 protein complexes were purified from the cell lysates of HEK-293T cells transiently overexpressing GFP-MID1 using FPLC (fraction 12-14). The corresponding FPLC fractions (12-14) were also collected from cells transiently overexpressing GFP-MID1 $\Delta$ CTD. Proteins in these fractions were pooled and separated on 2-D gels. Proteins specifically associated with GFP-MID1 (~110 kDa, circled in orange and ~100 kDa, circled in black) were excised and subjected to peptide finger printing. The other protein (circled in pink) with the same molecular weight as the 100 kDa protein but slightly different PI was likely to be a different charge state of the same protein. The overexpressed GFP-MID1 (~110kDa, PI 6.3) and GFP-MID1 $\Delta$ CTD (~86kDa, PI 6.0) were not definitive on the 2-D gels, although a smear (may be due to the poor focusing of the overexpressed protein, indicated by the arrow) around 110kDa was observed on the GFP-MID1 gel. Western blotting has not been done to confirm their profile on the 2-D gel.

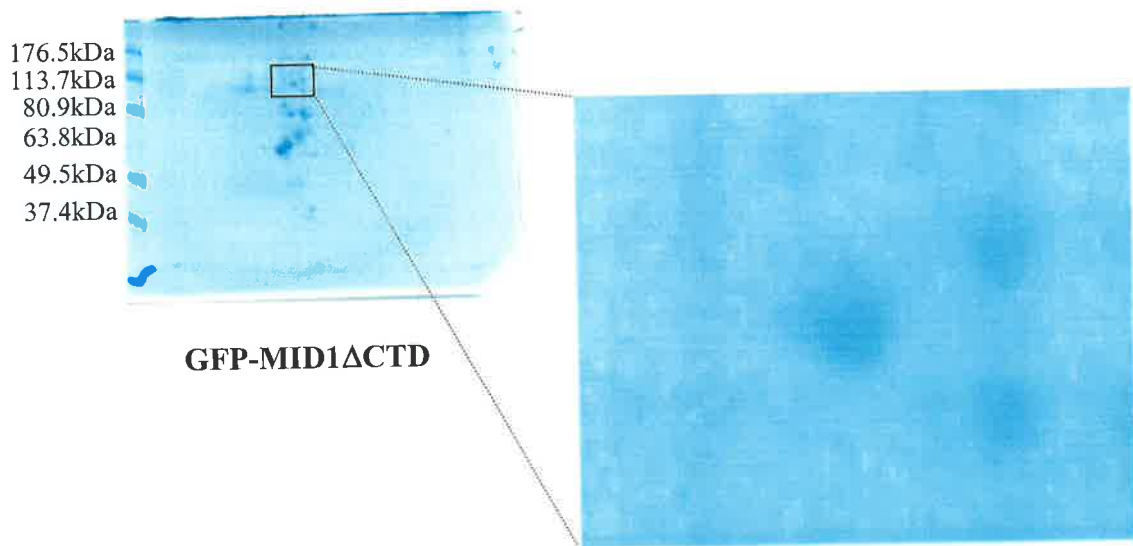
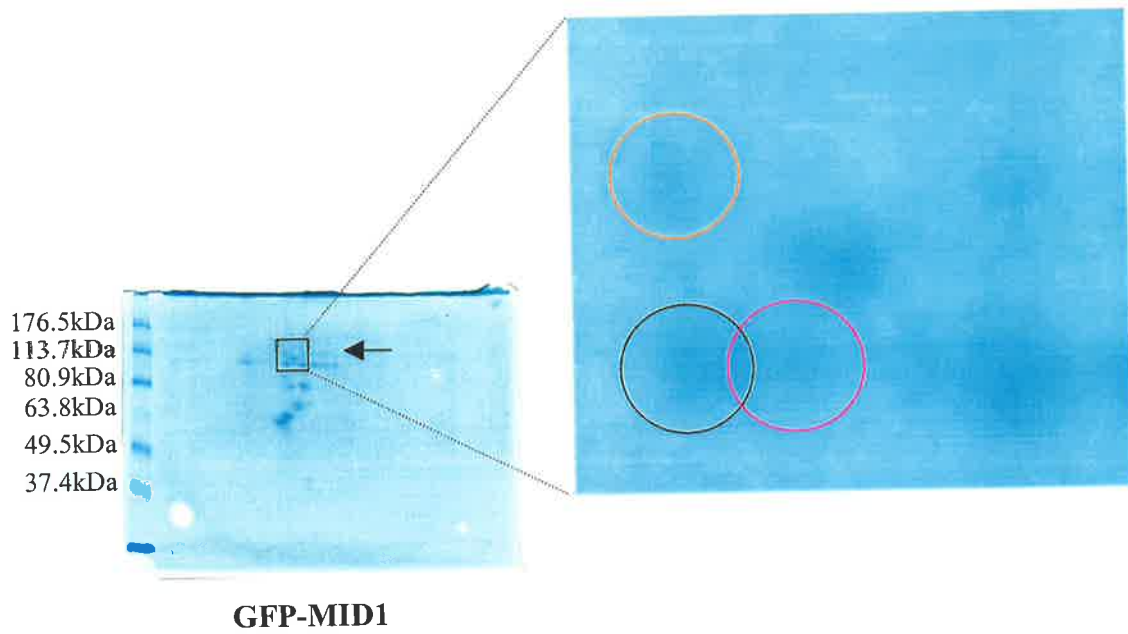
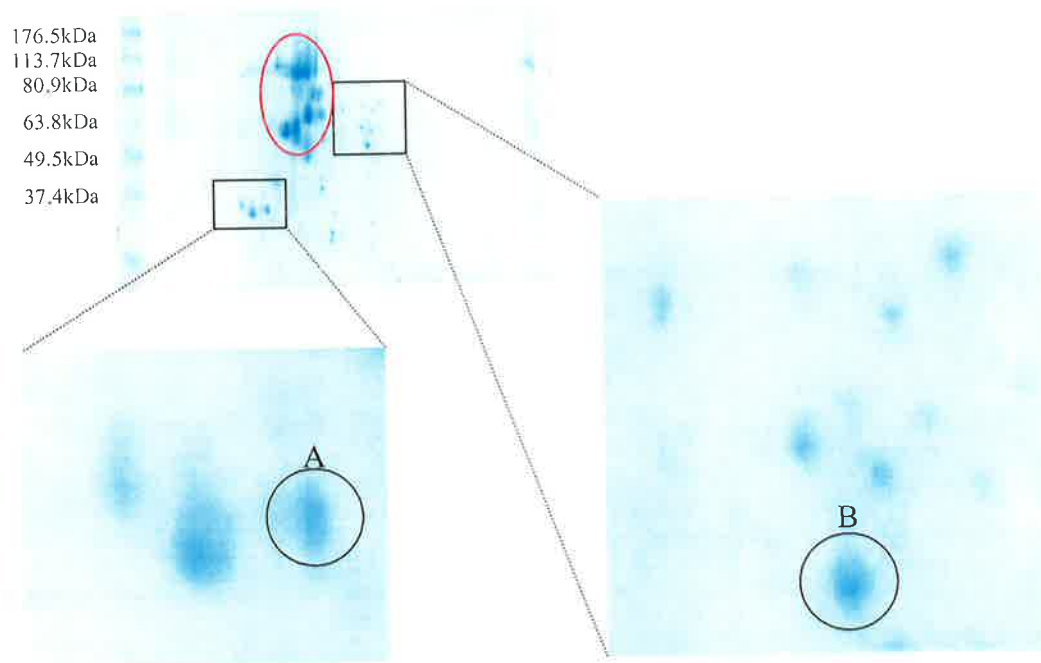


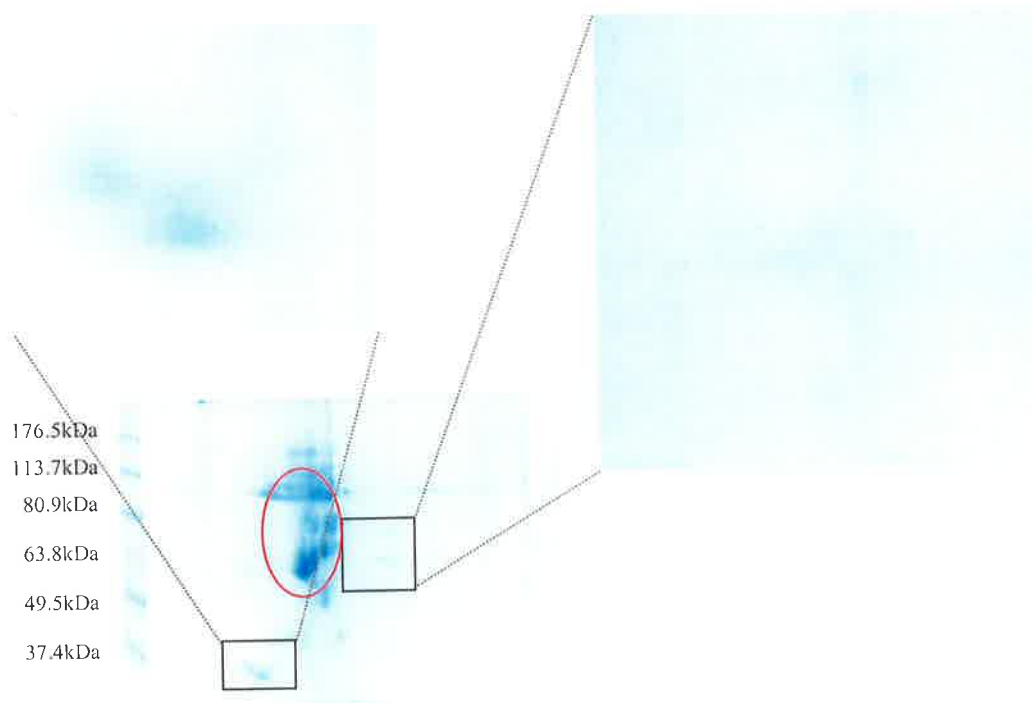
**Figure 6.9 2-D separation of MID1 complexes following FPLC purification.**

MID1 protein complexes were purified from the cell lysate of HEK-293T cells transiently overexpressing GFP-MID1 using FPLC (fraction 12-14). The corresponding FPLC fractions (12-14) were also collected from cells transiently overexpressing GFP-MID1 $\Delta$ CTD.

Proteins in these fractions were pooled and larger amount of samples (1.5 mg) were separated on 2-D gels. A few less abundant proteins (indicated in the enlarged picture), which were not detected in the first attempt, were found associated with GFP-MID1. Two slightly more abundant proteins, about 30kDa and 49kDa (A and B, as circled on the enlarged picture), were excised and subjected to peptide finger printing. Abundant proteins (circled in red) which were well separated on the 2-D gels in the first attempt (see Figure 6.8), were poorly resolved in this attempt due to sample overloading. The overexpressed GFP-MID1 (~110kDa, PI 6.3) and GFP-MID1 $\Delta$ CTD (~86kDa, PI 6.0) are not definitive on the gels due to the poor separation of proteins within this molecular weight and PI range.



**GFP-MID1 complexes**



**GFP-MID1 $\Delta$ CTD complexes**

M/Z	Z	[M+H] <sup>+</sup>	search list
671.381	1	671.381	599.355
726.484	1	726.484	636.328
747.364	2	1493.7201	671.381
768.551	1	768.551	713.414
782.798	1	782.798	726.484
860.459	1	860.459	733.422
945.583	1	945.583	768.551
574.252	2	1147.4961	782.798
599.355	1	599.355	860.459
636.328	1	636.328	882.599
674.331	2	1347.6541	945.583
733.422	1	733.422	945.608
802.42	2	1603.8321	1019.516
945.608	1	945.608	1147.4961
1019.516	1	1019.516	1347.6541
1032.021	2	2063.0341	1493.7201
1040.01	2	2079.0121	1603.833
1040.471	2	2079.9341	1656.7981
1394.231	3	4180.6772	2063.0341
1420.855	3	4260.5492	2079.0121
713.414	1	713.414	2079.9341
828.903	2	1656.7981	3020.3963
882.599	1	882.599	4180.6772
802.421	2	1603.8341	4260.5492
599.355	1	599.355	
755.855	4	3020.3963	

**Table 6.3 Masses and charge states of peptides from the unidentified ~30kDa protein.**

The mass/charge (m/z) of peptides were measured by mass spectrometry and were converted into a virtual single charged state corresponding to the mass of the peptide plus one proton ( $[M+H]^+$ ). The deduced mass of the peptides were sorted in ascending order and used to search for matching human proteins in the NCBI non-redundant protein database.

**Table 6.4 MS-FIT search results for the unidentified ~30KDa protein.**

MS-Fit search selected 5 entries. Results were displayed for the top 5 matches with the top match highlighted.

	MOWSE Score	#/24(%) Masses Matched	% Cov	% TIC	Mean Err ppm	Data Tol ppm	MS-Digest Index #	Protein MW (Da)/pI	Accession #	Species	Protein Name
<u>1</u>	8.968e+04	9 (37)	33.0	37.5	0.853	46.6	"574630"	24764/4.5	"4503477"	UNREADABLE	gi 4503477 ref NP_001950.1  eukaryotic translation elongation factor 1 beta 2; eukaryotic translation elongation factor 1 beta 1 [Homo sapiens]
<u>2</u>	16.8	4 (16)	9.0	16.7	9.56	36.3	"851833"	31980/7.7	"10440510"	H. SAPIENS	FLJ00101 protein
<u>3</u>	11.1	4 (16)	7.0	16.7	12.2	58.1	"638169"	37229/5.1	"29611340"	H. SAPIENS	AngRem104
<u>4</u>	9.11	4 (16)	7.0	16.7	14.5	57.3	"824762"	39429/5.5	"6330157"	H. SAPIENS	KIAA1160 protein
<u>5</u>	8.12	4 (16)	21.0	16.7	24.3	72.9	"1258854"	25570/9.2	"15929382"	H. SAPIENS	Unknown (protein for IMAGE:3829029)

### 6.3 Discussion

Protein-protein interactions can be grouped into different categories that include: homo- versus hetero-oligomeric complexes, non-obligate versus obligate complexes and transient versus permanent complexes, depending on the different aspects or properties of the interaction (Nooren and Thornton, 2003). Non-obligate, transient interactions between MID1/MID2 and their interactors can make it difficult to purify such components. Nevertheless, this chapter outlined a number of different approaches used to identify the protein interactors of MID1 with the successful approaches now possible to extend to the identification of MID2 complex components.

Ideally, precipitation of endogenous MID1 in complexes could be best, however, the available antiserum is not of sufficient purity and specificity for this approach. Consequently, immuno-precipitation was initially employed to pull down MID1 complexes from cell lysates from cells overexpressing GFP-MID1. Several protein bands specifically associated with GFP-MID1 were observed by SDS-PAGE, however, it is possible that more protein interactors exist than actually observed following separation of the immunoprecipitates, as weak interactions might not be retained under the conditions of immuno-precipitation. Furthermore, native MID1 and MID2, which would not be pulled down by an anti-GFP antibody unless that they dimerized with the overexpressed GFP-MID1, can also compete with the overexpressed GFP-MID1 for binding the limited endogenous interactors, thus reducing the complexity of the precipitated GFP-MID1 complexes.

Gel filtration was then used to purify the MID1 protein complexes due to the milder conditions for protein solubilization and ease of scale-up for better protein yields. Gel filtration suggested that MID1 existed in relatively large protein complexes (~1.5MDa). This result contradicts the ~400kDa MID1 complexes reported previously using a

similar approach but utilizing MYC-tagged MID1 fusion protein in COS7 cells (Cainarca *et al.*, 1999). The much larger GFP-MID1 complexes seen in this study may be due to the influence of the GFP vs MYC- tag on the oligomerization of MID1/MID2 and/or their interaction with other protein factors. In this regard, however, it may be pertinent to note that the GFP-fusion protein gives a more consistent microtubule distribution as seen by immunofluorescence than does <sup>the</sup> MYC-tagged form which can be more speckled in some cells. However, it is also possible that MID1/MID2 utilize different protein interactors in different tissues and cell types: COS7 cells are monkey kidney fibroblasts whereas 293T cells are human fetal kidney epithelia.

In contrast to full-length MID1, the elution peak of overexpressed GFP-MID1 $\Delta$ CTD complexes was  $\sim 0.5$  MDa smaller than the GFP-MID1 complexes, possibly due to the loss of B30.2 domain-specific interactors, or partly due to the loss of the B30.2 domain itself in the MID1 multimer

The peak elute fractions containing GFP-MID1 were collected and concentrated to reduce the sample volume. As the co-concentration of salt and detergent in these samples could affect the protein performance in electrophoresis, the protein samples were dialysed after concentration (see section 2.3.30). The resultant samples were dried and solubilized in different sample buffer to optimize their separation in 1-D and 2-D protein electrophoresis. A high concentration (2%) of ampholytes in the 2-D sample buffer was found to increase the sample solubilization without increasing the salt included in sample buffer and this condition was used in all 2-D electrophoreses.

The relatively large protein (which was shown to be dynein heavy chain) associated with the GFP-MID1 $\Delta$ CTD complexes in the 1-D gel, was not observed again in the separation of the same protein samples on the 2-D gel. The same was also found for other large proteins present in both the MID1 and MID1 $\Delta$ CTD complexes on the 1-D



gels. Good separations on 2-D gels were only observed for proteins of molecular weights less than ~150kDa. This may be due to the difficulties for larger proteins to enter into the SDS polyacrylamide gel from the IEF focusing strips. Despite varying several conditions (sample preparation, protein solubilization and the amount of sample loaded), the conditions of two-dimensional protein electrophoresis still require further optimization. Narrow pH range IPG strips may be useful for maintaining the resolution when larger amounts of sample must be loaded.

Despite the limited protein yields and separation obtained in this study, two protein factors were successfully identified in MID1 complexes. Whether these protein factors are *bona fide* interactors under physiological conditions and furthermore what their actual role might be in the overall function of the complexes are yet to be answered. Given that dynein, a minus-end directed microtubule-based motor, plays a central role in vesicle trafficking and the proteolysis pathway (i.e. to direct damaged protein to the proteasome), the association between MID1 $\Delta$ CTD and dynein may direct this overexpressed truncated protein to the proteasome for degradation. Although the presence of dynein was not observed in MID1 protein complexes separated on the 1-D gel, a yeast two-hybrid screen for potential MID1 interactors (accomplished by Dr. Blair Hopwood and Kieran Short in the lab) did uncover an interaction between dynein and native MID1. It is likely that the dynein may also be involved in the normal cellular function of MID1 instead of only representing the general pathway for protein degradation of the mutant MID1, in line with a predicted role for MID1 in regulating trafficking. The dynein-dependent trafficking from early endosomes to late endosomes/lysosomes and late recycling would also fit with the influence of PEPP2 and MID1/MID2 on endocytosis.

The second potential component identified in MID1 complexes was a translation factor, eukaryotic translation elongation factor 1 beta. This association is not surprising given that polyribosomes are associated with the cytoskeleton in eukaryotic cells and are transported along microtubules and actin filaments (Hamill *et al.*, 1994). mRNAs and components of the protein synthetic machinery have all been found also associated with microtubules whilst the microtubule motor, kinesin, has been found incorporated into mRNA/protein complexes as well (Hesketh, 1994; Ohashi *et al.*, 2002). It is believed that the microtubule-associated polyribosomes are enriched in certain mRNAs, indicating localized translation of specific proteins. It has also been well known that the elongation factor-1alpha (although sharing no sequence homology with elongation factor 1 beta) is also a microtubule-associated protein, which stabilizes microtubules in a calcium-dependent manner (Moore *et al.*, 1998). These facts reflect a general mechanism for a coordinated function for microtubules and polyribosomes.

Since PP2Ac can dephosphorylate the eukaryotic initiation factor 4E binding protein 1 (4E-BP1) and lead eventually to the inhibition of mTOR-induced mRNA translation, while Alpha4-PP2Ac complex can not (Janssens and Goris, 2001), the interaction between MID1/MID2 and Alpha4-PP2Ac may reflect their role in microtubule-dependent regulation of translation. Therefore, a role for MID1 in coordinating the microtubule-dependent regulation of protein synthesis can be envisaged if its interaction with the eukaryotic translation elongation factor 1 beta is proven to be physiologically relevant. Further studies are needed to clarify this.

## Chapter Seven: Final summary

The work in this thesis was aimed at understanding the cellular function of the X-linked Opitz syndrome gene, *MID1*, and its homologue, *MID2*. Opitz syndrome (OS) is an intriguing genetic disorder characterized by defects in ventral midline structures (Cox *et al.*, 2000). The disorder is genetically heterogeneous with both X-linked and autosomal loci confirmed by linkage analysis and cytogenetic anomalies. Higher penetration of craniofacial anomalies, laryngotracheo-oesophageal (LTE) defects, structural heart defects, genital anomalies and developmental delay has been found in X-linked cases, compared with that of the major autosomal form (De Falco *et al.*, 2003).

*MID1* was independently identified by a few groups as the gene responsible for X-linked OS using a positional cloning approach (Quaderi *et al.*, 1997, Perry *et al.*, 1998 and Van den Veyver *et al.*, 1998). Since then different *MID1* mutations have been identified in both isolated and familial cases with OS (Gaudenz *et al.*, 1998; Cox *et al.*, 2000; De Falco *et al.*, 2003; Winter *et al.*, 2003). The *MID1* gene is expressed widely throughout embryogenesis in chick, mouse, and humans albeit at varying levels depending on the tissue and cell type (Dal Zotto *et al.*, 1998; Richman *et al.*, 2002). Notably, the highest levels of expression are found in the craniofacial complex and in the region of the external genitalia. In the face, expression is strongest in the ectoderm and in rapidly proliferating mesenchyme that underlies epithelia preparing for contact and fusion (Richman *et al.*, 2002), failure of which may cause clefting.

*MID1* and *MID2* display 83% amino acid similarity and are both RBCC (RING-finger, B-box and Coiled-coil) proteins. RBCC proteins are characterized by their ability to act as a scaffold for formation of large protein complexes. *MID1* and *MID2* are grouped into the CI subfamily of RBCC proteins with four other members: SPRING, TNL,

TRIFIC and HAPRIN, based on their Fibronectin type III motifs and B30.2 (RFP-like) domains identified at the C-terminus (Cox lab's unpublished data). All RBCC proteins exist in an oligomeric state through their Coiled-coil domains (Reymond *et al.*, 2001). Hetero-dimerization of MID1/MID2 has been shown both *in vivo* and *in vitro* (Short *et al.*, 2002), however, cross-talk with other members of the CI subfamily has not been observed, indicating the specificity of MID1/MID2 dimerization.

In order to address the function of each domain, different constructs were generated to express domain-specific deletions of both MID1 and MID2 ( $\Delta$ RF,  $\Delta$ BB,  $\Delta$ CC,  $\Delta$ FNIII and  $\Delta$ CTD). In contrast to wild type MID1 and MID2 which display a similar microtubule-associated distribution, most domain-specific deletions of MID1 and MID2 had distinct subcellular localizations. Cytoplasmic clumps identifying unknown compartments or structures were found with  $\Delta$ RF,  $\Delta$ BB,  $\Delta$ FNIII and  $\Delta$ CTD constructs of both MID1 and MID2, while a cytoplasmic pattern has been found with MID1/MID2  $\Delta$ CC. A similar altered cellular localization of MID1 was observed when OS causative MID1 mutations were overexpressed in COS1 cells (Cox *et al.*, 2000). This suggested that the microtubular localization may be critical for the proper cellular function of MID1 and MID2 and that many domains may be involved (directly or indirectly) in facilitating this localization.

Since its cloning, the cellular function of MID1 has been intensively investigated. Significant milestones have included: the identification of several MID1 protein interactors such as Alpha4 and Mig12 and the assignment of a E3 ubiquitin ligase activity to MID1, a function associated with the RING-finger motif. However, the physiological role(s) played by MID1 still remains unknown.

There is emerging evidence to suggest that MID1 and MID2 are functionally similar: their homo- or hetero-dimerization is a prerequisite for their microtubule-association;

both MID1 and MID2 interact with Alpha4; and both have potential E3 ubiquitin ligase activity. Furthermore, investigations in this study support a role for MID2 in the pathogenesis of OS. A MID2 variant resulting in an Alanine358 to Aspartic acid (A358D) exchange, has been found in three unrelated OS patients with only one of these carrying a MID1 mutation. A role for both MID1 and MID2 in regulating the activation of endothelia of the endocardial cushions and their subsequent invasion following conversion into mesenchymal cells has been found as part of a collaboration with Prof. Runyan (Arizona). Defects in this process result in anomalies of cardiac septation, consistent with those commonly found in OS patients. Although these findings strongly support a role for MID2 in the pathogenesis of OS, very little research has been carried out with regards to the functions of MID2. For this reason, the work presented in this thesis was aimed primarily at investigating the cellular function of MID2 and how it might be involved in the presentation of OS.

In chapter three, direct evidence for the involvement of MID2 in OS pathogenesis came from the finding that the overexpressed wild type MID2 clumped in some cells with the endogenous MID1R495X in OS fibroblasts, a truncating mutation similar to the generated MID1 $\Delta$ CTD. However, apparently normal microtubule-associated MID2 was also observed in other fibroblast cells from the same patient. The non-uniform distribution of wild type MID2 in OS cells may indicate a non-obligate interaction between MID1 and MID2, with the relative amount of MID1:MID2 perhaps critical for their cellular distribution. In support of this, MID2 was recruited only into the cytoplasmic aggregates when co-expressed with MID1 $\Delta$ CTD. Consequently, it was reasoned that functional studies on MID2 may also give clues to understanding the cellular role of MID1.

Using a yeast two-hybrid screen for MID2 interactors and subsequently verified using immunofluorescence and co-immunoprecipitation, both Alpha4 and PEPP2, a newly identified PH domain-containing protein, were found to interact with MID2 (chapter 4). The work in this thesis describes the considerable effort undertaken to characterize the MID2/PEPP2 interaction. Given the similarity between MID1 and MID2, it was surprising that MID1 failed to interact with PEPP2 in any of the systems utilized. However, in the presence of excess MID1, the interaction between MID2 and PEPP2 was attenuated. It has been proposed that MID1 might regulate the PEPP2/MID2 interaction by competing for the same binding site on MID2 since the Coiled-Coil domain is necessary for both MID2/PEPP2 interaction and MID2/MID1 heterodimerization. However, this may simply reflect a requirement that MID2 forms homodimers (through the Coiled-Coil) and this increases the affinity of the RING-finger domain for PEPP2. In this scenario, heterodimers with MID1 would not lead to increased affinity for PEPP2. In either situation, a regulatory mechanism exists. Therefore, by adjusting the relative levels of MID1 and/or MID2, the MID1/MID2 oligomers may interact with different protein factors and exert different biological functions. In this regard, it is envisaged that the interaction between PEPP2 and MID2 and the cellular processes in which they are involved may be affected in tissues/cells harbouring *MID1* mutations. Therefore, disruption of the cellular function of both MID2 and PEPP2 may contribute to the pathogenesis of Opitz syndrome where the disorder is associated with mutations in MID1.

The specific function of PEPP2 is still unknown. A pleckstrin homology (PH) domain, which consists of 100-120 amino acids, is present in PEPP2, and suggests that the protein binds phosphoinositides. Phosphatidylinositols are intrinsic components of membrane lipids on the cytoplasmic surface of the membrane. The different

combination of phosphorylation on the inositol rings gives rise to different phosphoinositides and their synthesis is temporally and spatially controlled by kinases and phosphatases. Their controlled synthesis helps to limit their protein effectors to particular locations on the membrane.

PH domains from different proteins have different affinities and specificities for the different phosphoinositides. The PH domain of PEPP2 reportedly binds  $\text{PI}(4,5)\text{P}_2$ , which is abundant on the plasma and Golgi membranes, but also bind other phosphoinositides with medium specificity. Verification of the lipid-binding activity of PEPP2 was also performed during the final stage of this thesis preparation using the PH domain of PEPP2 in a commercial *in vitro* protein-lipid overlay assay. This assay showed that the PEPP2 PH domain could also bind  $\text{PI}(4)\text{P}$ , a precursor of  $\text{PI}(4,5)\text{P}_2$  that displays a similar cellular distribution as  $\text{PI}(4,5)\text{P}_2$  (Hsuan *et al.*, 1998).  $\text{PI}(4,5)\text{P}_2$  is recognized as an important membrane signaling molecule that regulates vesicle trafficking, membrane movement and cytoskeleton assembly. Which phosphoinositide(s) is the actual ligand *in vivo* requires further work.

Of particular interest is the fact that PEPP2 also possesses two WW domains, a domain mediating interaction with a proline-rich motif that is commonly found in SH3 binding membrane-associated proteins (Sudol *et al.*, 1995). It is therefore worth considering that the interaction between PEPP2 and other protein partners at the plasma membrane may be as important as the protein-lipid interaction in specifying the physiological function of PEPP2 on membranes. In this regard, members of this lab have found that the mouse PDZx, a 324 amino acid-protein with unknown function that contains a single PDZ domain (a domain commonly found in membrane localized proteins), interacted with PEPP2 in an initial yeast two-hybrid screen for potential PEPP2 interactors.

Interestingly, when it was overexpressed alone in COS1 and MDCK cells, PEPP2 was microtubule and/or plasma-membrane associated. The microtubule-bound PEPP2 co-localized with wild-type MID2 but was specifically retained in the Golgi apparatus (close to the microtubule organizing center) when it was co-expressed with an artificially created MID2 (MID2 $\Delta$ BB) in which the B-boxes were deleted. These data imply a potential membrane-microtubule connection through PEPP2/MID2 due to their membrane and microtubule interactions.

The possible cellular processes in which PEPP2/MID2 may be involved have begun to be addressed in Chapter 5. Of interest, the plasma membrane associated PEPP2 concentrated at the actin polymerisation site in migrating cells, which is consistent with the conserved role of PI(4,5)P<sub>2</sub> in regulating actin rearrangement. It has been known for some time that PI(4,5)P<sub>2</sub> clusters at the actin nucleation site on the plasma membrane and that this is required for spatially restricted actin polymerization (Tall *et al.*, 2000). PI(4,5)P<sub>2</sub> regulates a number of different proteins that affect actin dynamics, such as Gelsolin, Profilin and the WASP protein family, the <sup>last of</sup> ~~latter~~ which regulates actin polymerization through the Arp2/3 complexes (reviewed by Hsuan *et al.*, 1998; Isall and Weiner, 2001).

Cell migration begins with a protrusion of the plasma membrane at the leading edge, which is driven by directed polymerization of actin and extension of microtubules, followed by the formation of adhesive complexes at the front and release of adhesion at the rear of the cell. During this process the plasma membrane undergoes dramatic morphological changes, accompanied by a change of membrane viscosity that is decreased at the leading edge and is increased at the rear plasma membrane. To test whether membrane-associated PEPP2 also affects membrane viscosity, FRAP was used to monitor the lateral diffusion of membrane which is inversely proportional to



membrane microviscosity (Ghosh *et al.*, 2002). In these assays, membrane microviscosity was found to be decreased in cells overexpressing GFP-PEPP2, while microviscosity was increased in cells overexpressing MID2 $\Delta$ CTD, which acts in a dominant fashion to pull wild-type PEPP2 from the membrane into cytoplasmic aggregates. How PEPP2 and MID2 affect the plasma membrane dynamics is, however, still unclear. One possibility is that PEPP2 might affect the membrane dynamics through its involvement in actin polymerization. Alternatively, through its interaction with MID2, PEPP2 could be involved in microtubule-dependent turnover of focal complexes, interruption of which results in reduced cell mobility and increased membrane tension (Horwitz and Parsons, 1999). The same mechanism may cause the increased membrane viscosity that has been observed in cells overexpressing MID2 $\Delta$ CTD.

Consistent with the observation of the influence on plasma membrane viscosity, the process of endocytosis was also affected by PEPP2 and MID2. Extracellular materials are internalised through receptor-mediated or non-receptor-mediated endocytosis, the latter including fluid-phase endocytosis, caveolae-mediated endocytosis and macropinocytosis. By using HRP as a marker, it was found that fluid-phase endocytosis, was promoted in HEK-293T cells co-expressing PEPP2 and MID2. This increased HRP uptake is not likely to be a direct consequence of just increased plasma membrane lateral diffusion seen previously with excess cellular PEPP2 since a similar effect on HRP uptake was not observed in HEK-293T cells expressing PEPP2 only. It is therefore proposed that microtubule-dependent vesicle transportation (vesicle recycling, trafficking from early to late endosomes/lysosomes), in which microtubule-associated MID2/PEPP2 complexes could be involved, may also contribute to the increase in HRP uptake.

In other experiments using EGF-Texas-Red as a fluorescent marker, it was found that receptor-mediated endocytosis remained unaffected in cells overexpressing either PEPP2 or MID2, while this process was impaired in cells overexpressing MID2 $\Delta$ CTD. As previously mentioned, wild type PEPP2 aggregates with MID2 $\Delta$ CTD. Therefore, the effect of MID2 $\Delta$ CTD on receptor-mediated endocytosis may reflect a depletion of endogenous PEPP2 from the plasma membrane. However, the possible role of PEPP2 in regulating endocytosis could be complicated since PI(4,5)P<sub>2</sub> is involved in almost all steps of receptor-mediated endocytosis including vesicle formation, membrane fission, vesicle transportation on the cytoskeleton and vesicle fusion. Overexpression of MID2 $\Delta$ CTD might disrupt the normal PEPP2 function, which results in an impaired endocytosis.

Like some other characterized RBCC proteins, both MID1 and MID2 are found in high order protein complexes of ~1.5MDa. The composition of such complexes may however vary in different cells or in the same cells at different stages, and this may explain the broad elution profiles of MID-containing complexes by gel filtration. A full understanding of the cellular function of MID1 and MID2 therefore depends on the decoding of these protein components. For this purpose, the MID1 protein complexes were purified by gel filtration and the components subjected to two-dimensional protein separation, followed by peptide finger printing using mass spectrometry. Using database searches with the individual peptide profiles, dynein heavy chain and elongation factor 1-beta were identified as possible components of the MID1 complexes (chapter 6): the former involved directly in microtubule-dependent trafficking, and the latter with a possible role in ribosome trafficking and microtubule-dependent regulation of gene translation (Hamill *et al.*, 1994; Hatakeyama and Nakayama, 2003). Further characterization of these proteins and the identification of additional components of

these complexes will provide valuable insight into the cellular function and developmental role of both MID1 and MID2 and ultimately how these various factors affect the presentation of malformations characteristic of Opitz Syndrome.



## Future Directions

Craniofacial anomalies reflect a global health issue with both genetic and environmental factors recognized as contributing to the etiology of isolated defects and the variability within syndromal forms. The MID1 gene (defects in which cause Opitz syndrome) represents one of only a handful of genes directly linked to common craniofacial anomalies such as cleft lip and palate. Therefore, elucidating the cellular events in which this factor participates will undoubtedly reveal the molecular pathway(s) important in these early developmental processes. Much of the effort in this thesis has therefore centred on understanding the cellular biology of MID1 and its highly related protein, MID2, with a view to investigating the pathogenesis of Opitz syndrome.

Recent investigations on the cellular function of MID1 have focused on the following areas: identifying protein factors that are functional partners of MID1; protein family analysis; and developmental studies. For the former approach, the yeast two-hybrid system was successfully used by a few different groups, as well as in this study, for identifying MID1 interactors. Notably, the initial data in this study showed that proteomic tools were also useful in identifying interactors in protein complexes, given they permitted identification of those protein factors that may not necessarily interact with MID1 directly but that are important for the integrity of the functional MID1 protein complexes.

So far, a number of different proteins involving protein phosphorylation (Alpha4), ubiquitylation (UbcH7) and trafficking (dynein) have been identified as interactors of MID1. The connections between these different pathways have been addressed in detail in chapter one (section 1.5.5) but raise a number of major questions for future investigations. For example: 1). How does MID1 coordinate different pathways? and 2).

If MID1 is indeed a ubiquitin E3-ligase, how does this enzyme activity affect trafficking and/or protein phosphorylation via Alpha4/PP2A pathway. These questions would be answered by confirming the MID1 regulated turnover of PP2A in an *in vitro* ubiquitylation assay and monitoring the phosphorylation status of potential targets for PP2A on microtubules, such as dynein, in OS derived cells and/or MID1 mutant overexpressing cells, given that the overall hypophosphorylation of microtubule-associated proteins has previously been observed in OS cells (Trockenbacher et al., 2001).

Sequence similarity searches of MID1 identified a closely related homologue, MID2, and a number of other RBCC proteins with the same overall domain organization. Consistent with the high level of sequence identity, MID1 and MID2 heterodimerize and this heterodimerization was found to be functionally significant in this study by showing that the cellular distribution of wild type MID1/MID2 could be perturbed by their heterodimerization with the truncated forms of MID1/MID2.

Through identifying PEPP2, a membrane associated PI-binding protein, as a specific MID2 interactor, a potential role for MID1/MID2 in regulating membrane trafficking was suggested for the first time. It should be noted, however, that most of the results with MID2 in this thesis (i.e. the influence of MID2 on membrane viscosity and endocytosis analysis) were obtained using overexpression of wild type or mutant MID1/MID2 in cultured cells. These approaches were necessary since both MID1 and MID2 are expressed at very low level in most cell types. However, the lack of phenotype of OS derived cells (expressing mutant MID1 at endogenous level) in the above assays, as well as lack of gross phenotype of *Mid1* knockout mice, has posed a major obstacle in understanding the pathogenesis of OS. Possibilities to overcome these issues include statistical analysis of the membrane viscosity in a large number of cells

and quantitative immunofluorescence assay for the EGF uptake in OS cells to increase the sensitivities of these assays. In addition, investigation of the cellular function of MID1 in the context of altered cellular levels of MID2 using gene knockdown in cultured cells and/or *in vivo* in a mouse knockout may also give some answers to these questions.

Interestingly, a common role in regulating membrane trafficking is now emerging based on the studies in this thesis and data on two of the other related RBCC proteins (Spring and Haprin), which show a similar each shows a similar microtubule-associated cellular distribution (Li *et al.*, 2001; Kitamura *et al.*, 2003). For example, the interaction between Spring and SNAP-25 affects the assembly of SNARE complex formation which is critical for membrane fusion and subsequently affects exocytosis. Similar mechanisms may also operate for the other related RBCC proteins, including MID1/MID2. Investigation on the possible influence of MID1/MID2 on membrane fusion, as well as the microtubule-dependent trafficking events such as movement of late endocytic vesicles and exocytic vesicle budding using isolated organelles in cell free systems, is going to give further insight into the molecular basis of the MID1/MID2 regulated cellular processes.

Signaling from key growth factors such as FGFs, BMPs and SHH is critical for early development. Despite the different molecular mechanisms of such factors, the fundamental processes governing early development of the ventral midline, which include events such as cell migration and EMT, are known to be dependent on regulated membrane activity. In this regard, the etiology of the midline malformations can be explained by defects in membrane trafficking, in line with that observed with overexpression of MID1/MID2 mutants. Verification of this hypothesis could be carried out using growth factor stimulation in OS cells and the subsequent monitoring of

cellular changes. Additional support could be gained by determining the expression of these signaling proteins and MID1/MID2 using *in situ* hybridization in MID1/MID2 knockout/knockdown mice (or vice versa) at early developmental stages, on which current research in the lab is focused.



## Bibliography

- Andersen, S. S., and Wittmann, T. (2002). Toward reconstitution of in vivo microtubule dynamics in vitro. *Bioessays* 24, 305-307.
- Anderson, R. G., and Jacobson, K. (2002). A role for lipid shells in targeting proteins to caveolae, rafts, and other lipid domains. *Science* 296, 1821-1825.
- Apodaca, G. (2001). Endocytic traffic in polarized epithelial cells: role of the actin and microtubule cytoskeleton. *Traffic* 2, 149-159.
- Bence, N. F., Sampat, R. M., and Kopito, R. R. (2001). Impairment of the ubiquitin-proteasome system by protein aggregation. *Science* 292, 1552-1555.
- Berti, C., Fontanella, B., Ferrentino, R., and Meroni, G. (2004). Mig12, a novel Opitz syndrome gene product partner, is expressed in the embryonic ventral midline and co-operates with Mid1 to bundle and stabilize microtubules. *BMC Cell Biol* 5, 9.
- Bonifacino, J.S., and Glick, B.S. (2004). The mechanisms of vesicle budding and fusion. *Cell* 116, 153-166.
- Borden, K. L. (1998). RING fingers and B-boxes: zinc-binding protein-protein interaction domains. *Biochem Cell Biol* 76, 351-358.
- Borden, K. L. (2000). RING domains: master builders of molecular scaffolds? *J Mol Biol* 295, 1103-1112.
- Brown, J. R., Stafford, P., and Langford, G. M. (2004). Short-range axonal/dendritic transport by myosin V: A model for vesicle delivery to the synapse. *J Neurobiol* 58, 175-188.
- Bucci, C., Parton, R.G., Mather, I.H., Stunnenberg, H., Simons, K., Hoflack, B., and Zerial, M. (1992). The small GTPase rab5 functions as a regulatory factor in the early endocytic pathway. *Cell* 70, 715-728.
- Buchner, G., Montini, E., Andolfi, G., Quaderi, N., Cainarca, S., Messali, S., Bassi, M. T., Ballabio, A., Meroni, G., and Franco, B. (1999). MID2, a homologue of the Opitz syndrome gene MID1: similarities in subcellular localization and differences in expression during development. *Hum Mol Genet* 8, 1397-1407.
- Burkhard, P., Stetefeld, J., and Strelkov, S. V. (2001). Coiled coils: a highly versatile protein folding motif. *Trends Cell Biol* 11, 82-88.
- Burkhardt, J. K., Echeverri, C. J., Nilsson, T., and Vallee, R. B. (1997). Overexpression of the dynamitin (p50) subunit of the dynactin complex disrupts dynein-dependent maintenance of membrane organelle distribution. *J Cell Biol* 139, 469-484.
- Cainarca, S., Messali, S., Ballabio, A., and Meroni, G. (1999). Functional characterization of the Opitz syndrome gene product (midin): evidence for homodimerization and association with microtubules throughout the cell cycle. *Hum Mol Genet* 8, 1387-1396.
- Callaghan, T.M., Metzzeau, P., Gachelin, H., Redziniak, G., Milner, Y., Goldberg, M.E. (1990). Modulation of the binding and endocytosis of concanavalin A by guinea pig keratinocytes: reversible antagonistic effects of cholesterol and phospholipid-liposomes. *J Invest Dermatol* 94(1):58-64.
- Cao, T., Duprez, E., Borden, K. L., Freemont, P. S. and Etkin, L. D. (1998). Ret finger protein is a normal component of PML nuclear bodies and interacts directly with PML. *J Cell Sci* 111, 1319-1329
- Clague, M. J. (2002). Membrane transport: a coat for ubiquitin. *Curr Biol* 12, R529-531.
- Cockcroft, S., De Matteis, M.A. (2001). Inositol lipids as spatial regulators of membrane traffic. *J Membr Biol* 180(3):187-194.
- Conner, S. D., and Schmid, S. L. (2003). Regulated portals of entry into the cell. *Nature* 422, 37-44.
- Cox, T. C. (2004). Taking it to the max: the genetic and developmental mechanisms coordinating midfacial morphogenesis and dysmorphology. *Clin Genet* 65, 163-176.
- Cox, T. C., Allen, L. R., Cox, L. L., Hopwood, B., Goodwin, B., Haan, E., and Suthers, G. K. (2000). New mutations in MID1 provide support for loss of function as the cause of X-linked Opitz syndrome. *Hum Mol Genet* 9, 2553-2562.
- Coyle, J.E., and Nikolov, D.B. (2003). GABARAP: lessons for synaptogenesis. *Neuroscientist* 9(3), 205-216.
- Dal Zotto, L., Quaderi, N. A., Elliott, R., Lingerfelter, P. A., Carrel, L., Valsecchi, V., Montini, E., Yen, C. H., Chapman, V., Kalcheva, I., et al. (1998). The mouse Mid1 gene: implications for the pathogenesis of Opitz syndrome and the evolution of the mammalian pseudoautosomal region. *Hum Mol Genet* 7, 489-499.

## Bibliography

---

- De Falco, F., Cainarca, S., Andolfi, G., Ferrentino, R., Berti, C., Rodriguez Criado, G., Rittinger, O., Dennis, N., Odent, S., Rastogi, A., *et al.* (2003). X-linked Opitz syndrome: novel mutations in the MID1 gene and redefinition of the clinical spectrum. *Am J Med Genet* 120A, 222-228.
- De Luca, A., Pasini, A., Amati, F., Botta, A., Spalletta, G., Alimenti, S., Caccamo, F., Conti, E., Trakalo, J., Macciardi, F., *et al.* (2001). Association study of a promoter polymorphism of UFD1L gene with schizophrenia. *Am J Med Genet* 105, 529-533.
- De Zeeuw, C. I., Hoogenraad, C. C., Goedknecht, E., Hertzberg, E., Neubauer, A., Grosveld, F., and Galjart, N. (1997). CLIP-115, a novel brain-specific cytoplasmic linker protein, mediates the localization of dendritic lamellar bodies. *Neuron* 19, 1187-1199.
- Dowler, S., Currie, R. A., Campbell, D. G., Deak, M., Kular, G., Downes, C. P., and Alessi, D. R. (2000). Identification of pleckstrin-homology-domain-containing proteins with novel phosphoinositide-binding specificities. *Biochem J* 351, 19-31.
- Dupre, S., Volland, C., and Haguenaer-Tsapis, R. (2001). Membrane transport: ubiquitylation in endosomal sorting. *Current Biology* : Cb 11, R932-934.
- Edelmann, L., Pandita, R. K., Morrow, B. E. (1999). Low-copy repeats mediate the common 3-Mb deletion in patients with velo-cardia-facial syndrome. *Am J Med Genet* 64, 1076-1086.
- Farndon, P. A. and Donnai, D. (1983). Male to male transmission and G syndrome. *Clinical Genetics* 24, 446-448.
- Friant, S., Zanolari, B., and Riezman, H. (2000). Increased protein kinase or decreased PP2A activity bypasses sphingoid base requirement in endocytosis. *Embo J* 19, 2834-2844.
- Garg, V., Yamagishi, C., Hu, T., Kathiriya, I. S., Yamagishi, H., and Srivastava, D. (2001). Tbx1, a DiGeorge syndrome candidate gene, is regulated by sonic hedgehog during pharyngeal arch development. *Dev Biol* 235, 62-73.
- Gent, J., van Kerkhof, P., Roza, M., Bu, G., and Strous, G. J. (2002). Ligand-independent growth hormone receptor dimerization occurs in the endoplasmic reticulum and is required for ubiquitin system-dependent endocytosis. *Proc Natl Acad Sci U S A* 99, 9858-9863.
- Gillooly, D. J., Simonsen, A., and Stenmark, H. (2001). Cellular functions of phosphatidylinositol 3-phosphate and FYVE domain proteins. *Biochem J* 355, 249-258.
- Gilmore, A.P., Burrige, K. (1996). Molecular mechanisms for focal adhesion assembly through regulation of protein-protein interactions. *Structure* 15;4(6):647-651.
- Glover, T. W. (1995). CATCHing a break on 22. *Nat Genet* 10, 257-258.
- Graham, J. M., Jr., Wheeler, P., Tackels-Horne, D., Lin, A. E., Hall, B. D., May, M., Short, K. M., Schwartz, C. E., and Cox, T. C. (2003). A new X-linked syndrome with agenesis of the corpus callosum, mental retardation, coloboma, micrognathia, and a mutation in the Alpha 4 gene at Xq13. *Am J Med Genet* 123A, 37-44.
- Guatimosim, C., Hull, C., Von Gersdorff, H., and Prado, M. A. (2002). Okadaic acid disrupts synaptic vesicle trafficking in a ribbon-type synapse. *J Neurochem* 82, 1047-1057.
- Guion-Almeida, M. L., Richieri-Costa, A. CNS midline anomalies in the Opitz G/BBB syndrome: report on 12 Brazilian patients. (1992). *Am J Med Genet* 43, 918-928.
- Gundersen, G.G., Bretscher, A. (2003). Microtubule asymmetry. *Science Cell biology* 300(5628):2040-2041.
- Hamill, D., Davis, J., Drawbridge, J., and Suprenant, K. A. (1994). Polyribosome targeting to microtubules: enrichment of specific mRNAs in a reconstituted microtubule preparation from sea urchin embryos. *J Cell Biol* 127, 973-984.
- Hamm-Alvarez, S. F., and Sheetz, M. P. (1998). Microtubule-dependent vesicle transport: modulation of channel and transporter activity in liver and kidney. *Physiol Rev* 78, 1109-1129.
- Harris, D. M., Myrick, T. L., and Rundle, S. J. (1999). The Arabidopsis homolog of yeast TAP42 and mammalian alpha4 binds to the catalytic subunit of protein phosphatase 2A and is induced by chilling. *Plant Physiol* 121, 609-617.
- Hatakeyama, S., and Nakayama, K. I. (2003). Ubiquitylation as a quality control system for intracellular proteins. *J Biochem (Tokyo)* 134, 1-8.
- Heald, R., and Nogales, E. (2002). Microtubule dynamics. *J Cell Sci* 115, 3-4.
- Henry, J., Mather, I. H., McDermott, M. F., Pontarotti, P., Ribouchon, M. T., and Offer, C. (1998). B30.2-like domain proteins: update and new insights into a rapidly expanding family of proteins. *Mol Biol Evol* 15, 1696-1705.
- Hesketh, J. (1994). Translation and the cytoskeleton: a mechanism for targeted protein synthesis. *Mol Biol Rep* 19, 233-243.
- Horwitz, A. R., and Parsons, J. T. (1999). Cell migration--movin' on. *Science* 286, 1102-1103.
- Hsuan, J. J., Minogue, S., and dos Santos, M. (1998). Phosphoinositide 4- and 5-kinases and the cellular roles of phosphatidylinositol 4,5-bisphosphate. *Adv Cancer Res* 74, 167-216.

- Infante, C., Ramos-Morales, F., Fedriani, C., Bornens, M., and Rios, R. M. (1999). GMAP-210, A cis-Golgi network-associated protein, is a minus end microtubule-binding protein. *J Cell Biol* 145, 83-98.
- Insall, R. H., and Weiner, O. D. (2001). PIP3, PIP2, and cell movement--similar messages, different meanings? *Dev Cell* 1, 743-747.
- Inui, S., Sanjo, H., Maeda, K., Yamamoto, H., Miyamoto, E., and Sakaguchi, N. (1998). Ig receptor binding protein 1 (alpha4) is associated with a rapamycin-sensitive signal transduction in lymphocytes through direct binding to the catalytic subunit of protein phosphatase 2A. *Blood* 92, 539-546.
- Itoh, K., Itoh, Y., Frank, M. B. (1991). Protein heterogeneity in the human Ro/SSA ribonucleoproteins: The 52- and 60-Kd Ro/SSA autoantigens are encoded by separated genes. *J Clin Invest* 87, 177-186.
- Itoh, T., and Takenawa, T. (2002). Phosphoinositide-binding domains: Functional units for temporal and spatial regulation of intracellular signalling. *Cell Signal* 14, 733-743.
- Jackson, P. K., Eldridge, A. G., Freed, E., Furstenthal, L., Hsu, J. Y., Kaiser, B. K., and Reimann, J. D. (2000). The lore of the RINGs: substrate recognition and catalysis by ubiquitin ligases. *Trends Cell Biol* 10, 429-439.
- Janssens, V., and Goris, J. (2001). Protein phosphatase 2A: a highly regulated family of serine/threonine phosphatases implicated in cell growth and signalling. *Biochem J* 353, 417-439.
- Jensen, K., Shiels, C., and Freemont, P. S. (2001). PML protein isoforms and the RBCC/TRIM motif. *Oncogene* 20, 7223-7233.
- Jerome, L. A., and Papaioannou, V. E. (2001). DiGeorge syndrome phenotype in mice mutant for the T-box gene, *Tbx1*. *Nat Genet* 27, 286-291.
- Karcher, R. L., Deacon, S. W., and Gelfand, V. I. (2002). Motor-cargo interactions: the key to transport specificity. *Trends Cell Biol* 12, 21-27.
- Katzmann, D. J., Babst, M., and Emr, S. D. (2001). Ubiquitin-dependent sorting into the multivesicular body pathway requires the function of a conserved endosomal protein sorting complex, ESCRT-I. *Cell* 106, 145-155.
- Keyes, W. M., Logan, C., Parker, E., and Sanders, E. J. (2003). Expression and function of bone morphogenetic proteins in the development of the embryonic endocardial cushions. *Anat Embryol (Berl)* 207, 135-147.
- Kimber, W. L., Hsieh, P., Hirotsune, S., Yuva-Paylor, L., Sutherland, H. F., Chen, A., Ruiz-Lozano, P., Hoogstraten-Miller, S. L., Chien, K. R., Paylor, R., *et al.* (1999). Deletion of 150 kb in the minimal DiGeorge/velocardiofacial syndrome critical region in mouse. *Hum Mol Genet* 8, 2229-2237.
- Kitamura, K., Tanaka, H., and Nishimune, Y. (2003). Haprin, a novel haploid germ cell-specific RING finger protein involved in the acrosome reaction. *J Biol Chem* 278, 44417-44423.
- Klapisz, E., Sorokina, I., Lemeer, S., Pijnenburg, M., Verkleij, A. J., and van Bergen en Henegouwen, P. M. (2002). A ubiquitin-interacting motif (UIM) is essential for Eps15 and Eps15R ubiquitination. *J Biol Chem* 277, 30746-30753.
- Klopfenstein, D. R., Kappeler, F., and Hauri, H. P. (1998). A novel direct interaction of endoplasmic reticulum with microtubules. *Embo J* 17, 6168-6177.
- Kurczynski, T. W., Micale, M. A., Assad, S., Gaba, C. G., French, B. F. (1998). Opitz G/BBB syndrome in male child with an unbalanced del(3) t(3:14)(q29;q11.2), -14 karyotype. *Am J Hum Genet Suppl* 63 (4), 610.
- Le Bot, N., Antony, C., White, J., Karsenti, E., and Vernos, I. (1998). Role of *xklp3*, a subunit of the *Xenopus* kinesin II heterotrimeric complex, in membrane transport between the endoplasmic reticulum and the Golgi apparatus. *J Cell Biol* 143, 1559-1573.
- Lee, J. S., and Gotlieb, A. I. (2002). Microtubule-actin interactions may regulate endothelial integrity and repair. *Cardiovasc Pathol* 11, 135-140.
- Leichtman, L. G., Werner, A., Bass, W. T., Smith, D., Brothman, A. R. (1991). Apparent Opitz BBBG syndrome with a partial duplication of 5p. *Am J Med Genet* 40, 173-176.
- Lemmon, M. A. (2003). Phosphoinositide recognition domains. *Traffic* 4, 201-213.
- Lemmon, M. A., Ferguson, K. M., and Abrams, C. S. (2002). Pleckstrin homology domains and the cytoskeleton. *FEBS Lett* 513, 71-76.
- Li, Y., Chin, L. S., Weigel, C., and Li, L. (2001). Spring, a novel RING finger protein that regulates synaptic vesicle exocytosis. *J Biol Chem* 276, 40824-40833.
- Lindsay, E. A., Botta, A., Jurecic, V., Carattini-Rivera, S., Cheah, Y. C., Rosenblatt, H. M., Bradley, A., and Baldini, A. (1999). Congenital heart disease in mice deficient for the DiGeorge syndrome region. *Nature* 401, 379-383.

## Bibliography

---

- Lippincott-Schwartz, J., and Zaal, K.J.M. (2000). Cell cycle maintenance and biogenesis of the golgi complex. *Histochem Cell Biol* 114, 93-103.
- Liu, J., Prickett, T. D., Elliott, E., Meroni, G., and Brautigan, D. L. (2001). Phosphorylation and microtubule association of the Opitz syndrome protein mid-1 is regulated by protein phosphatase 2A via binding to the regulatory subunit alpha 4. *Proc Natl Acad Sci U S A* 98, 6650-6655.
- Longva, K. E., Blystad, F. D., Stang, E., Larsen, A. M., Johannessen, L. E., and Madshus, I. H. (2002). Ubiquitination and proteasomal activity is required for transport of the EGF receptor to inner membranes of multivesicular bodies. *J Cell Biol* 156, 843-854.
- Marsh, M., Schmid, S., Kern, H., Harms, E., Male, P., Mellman, I., and Helenius, A. (1987). *J Cell Biol* 104, 875-886.
- Martin, T. F. (2001). PI(4,5)P(2) regulation of surface membrane traffic. *Curr Opin Cell Biol* 13, 493-499.
- Matsuda, S., and Hirai, H. (1999). The clustering of NMDA receptor NR1 subunit is regulated by the interaction between the c-terminal exon cassettes and the cytoskeleton. *Neurosci Res* 34, 157-163.
- May, M., Huston, S., Wilory, R. S., Schwartz, C. (1997). Linkage analysis in a family with the Opitz G/BBB syndrome refines the location of the gene in Xp22 to a 4 cm region. *Am J Med Genet* 68, 224-248
- Mayer, U., and Jurgens, G. (2002). Microtubule cytoskeleton: a track record. *Curr Opin Plant Biol* 5, 494-501.
- McDonald-McGinn, D. M., Driscoll, D. A., Bason, L., Christensen, K., Lynch, D., Sullivan, K., Canning, D., Zevod, W., Quinn, N., Rome, J., *et al.* (1995). Autosomal domain "Opitz" G/BBB syndrome due to a 22q11.2 deletion. *Am J Med Genet* 59, 103-113
- McDonald-McGinn, D. M., Tonnesen, M. K., Laufer-Cahana, A., Finucane, B., Driscoll, D. A., Emanuel, B. S., and Zackai, E. H. (2001). Phenotype of the 22q11.2 deletion in individuals identified through an affected relative: cast a wide FISHing net! *Genet Med* 3, 23-29.
- MacDonald, M. R., Bradley, S. G., Olney, A. H. (1993). Brain magnetic resonance imaging findings in the Opitz G/BBB syndrome: Extension of the spectrum of midline brain anomalies. *Am J Med Genet* 46, 706-711
- Matsuda, S., Hirai, H. (1999). The clustering of NMDA receptor NR1 subunit is regulated by the interaction between the C-terminal exon cassettes and the cytoskeleton. *Neurosci Res* 34(3):157-63.
- Merscher, S., Funke, B., Epstein, J. A., Heyer, J., Puech, A., Lu, M. M., Xavier, R. J., Demay, M. B., Russell, R. G., Factor, S., *et al.* (2001). TBX1 is responsible for cardiovascular defects in velo-cardio-facial/DiGeorge syndrome. *Cell* 104, 619-629.
- Millard, T.H., Sharp, S.J., Machesky, L.M. (2004). Signalling to actin assembly via the WASP (Wiskott-Aldrich syndrome protein)-family proteins and the Arp2/3 complex. *Biochem J* 380(Pt 1):1-17.
- Nabi, I.R. (1999). The polarization of the motile cell. *J Cell Sci* 112 ( Pt 12):1803-1811.
- Nakagawa, T., Setou, M., Seog, D., Ogasawara, K., Dohmae, N., Takio, K., and Hirokawa, N. (2000). A novel motor, KIF13A, transports mannose-6-phosphate receptor to plasma membrane through direct interaction with AP-1 complex. *Cell* 103, 569-581.
- Nooren, I. M., and Thornton, J. M. (2003). Diversity of protein-protein interactions. *Embo J* 22, 3486-3492.
- Ohashi, S., Koike, K., Omori, A., Ichinose, S., Ohara, S., Kobayashi, S., Sato, T. A., and Anzai, K. (2002). Identification of mRNA/protein (mRNP) complexes containing Puralpha, mStaufen, fragile X protein, and myosin Va and their association with rough endoplasmic reticulum equipped with a kinesin motor. *J Biol Chem* 277, 37804-37810. Epub 32002 Jul 37829.
- Oldham, C. E., Mohny, R. P., Miller, S. L., Hanes, R. N., and O'Bryan, J. P. (2002). The ubiquitin-interacting motifs target the endocytic adaptor protein epsin for ubiquitination. *Curr Biol* 12, 1112-1116.
- Opitz, J. M., Smith, D. W., Summit, R. L. (1965). Hypertelorism and hypospadias. A newly recognized hereditary malformation syndrome. *J Pediatr* 67, 968
- Opitz, J. M., Frías, J. L., Gutenberger, J. E., Pellet, J. R. (1969a). The G syndrome with multiple congenital anomalies. *BD:OAS* V(2), 95-101
- Opitz, J. M., Summit, R. L., Smith, D. W. (1969b). The BBB syndrome: familiar telecanthus with associated congenital anomalies. *BD:OAS* V(2), 86-94
- Opitz, J. M. (1987). Editorial comment: G syndrome (hypertelorism with esophageal abnormality and hypospadias, or hypospadias-dysphagia, "or Opitz-Frias" or "Opitz-G" syndrome) perspective in 1987 and bibliography. *Am J Med Genet* 28, 275-285

- Orzech, E., Livshits, L., Leyt, J., Okhrimenko, H., Reich, V., Cohen, S., Weiss, A., Melamed-Book, N., Lebendiker, M., Altschuler, Y., and Aroeti, B. (2001). Interactions between adaptor protein-1 of the clathrin coat and microtubules via type 1a microtubule-associated proteins. *J Biol Chem* 276, 31340-31348.
- Paulozzi, L. J. (1999). International trends in rates of hypospadias and cryptorchidism. *Environ Health Perspect* 107, 297-302.
- Paulozzi, L. J., Erickson, J. D., and Jackson, R. J. (1997). Hypospadias trends in two US surveillance systems. *Pediatrics* 100, 831-834.
- Peng, H., Feldman, I., Rauscher, F. J., 3rd, Berti, C., Messali, S., Ballabio, A., Reymond, A., Meroni, G., Short, K. M., Hopwood, B., *et al.* (2002). Hetero-oligomerization among the TIF family of RBCC/TRIM domain-containing nuclear cofactors: a potential mechanism for regulating the switch between coactivation and corepression. *J Mol Biol* 320, 629-644.
- Pereira, A.J., Dalby, B., Stewart, R.J., Doxsey, S.J., Goldstein, L.S. (1997). Mitochondrial association of a plus end-directed microtubule motor expressed during mitosis in *Drosophila*. *J Cell Biol* 10;136(5):1081-1090.
- Perez, F., Pernet-Gallay, K., Nizak, C., Goodson, H. V., Kreis, T. E., and Goud, B. (2002). CLIPR-59, a new trans-Golgi/TGN cytoplasmic linker protein belonging to the CLIP-170 family. *J Cell Biol* 156, 631-642.
- Perry, J., Short, K. M., Romer, J. T., Swift, S., Cox, T. C., Ashworth, A., Seto, M. H., Liu, H. L., Zajchowski, D. A., Whitlow, M., *et al.* (1999). FXY2/MID2, a gene related to the X-linked Opitz syndrome gene FXY/MID1, maps to Xq22 and encodes a FNIII domain-containing protein that associates with microtubules. *Genomics* 62, 385-394.
- Pinson, L., Auge, J., Audollent, S., Mattei, G., Etchevers, H., Gigarel, N., Razavi, F., Lacombe, D., Odent, S., Le Merrer, M., *et al.* (2004). Embryonic expression of the human MID1 gene and its mutations in Opitz syndrome. *J Med Genet* 41, 381-386.
- Pizzuti, A., Novelli, G., Ratti, A., Amati, F., Mari, A., Calabrese, G., Nicolis, S., Silani, V., Marino, B., Scarlato, G., *et al.* (1997). UFD1L, a developmentally expressed ubiquitination gene, is deleted in CATCH 22 syndrome. *Hum Mol Genet* 6, 259-265.
- Popova, J. S., Greene, A. K., Wang, J., and Rasenick, M. M. (2002). Phosphatidylinositol 4,5-bisphosphate modifies tubulin participation in phospholipase Cbeta1 signaling. *J Neurosci* 22, 1668-1678.
- Puech, A., Saint-Jore, B., Merscher, S., Russell, R. G., Cherif, D., Sirotkin, H., Xu, H., Factor, S., Kucherlapati, R., and Skoultschi, A. I. (2000). Normal cardiovascular development in mice deficient for 16 genes in 550 kb of the velocardiofacial/DiGeorge syndrome region. *Proc Natl Acad Sci U S A* 97, 10090-10095.
- Quaderi, N. A., Schweiger, S., Gaudenz, K., Franco, B., Rugarli, E. I., Berger, W., Feldman, G. J., Volta, M., Andolfi, G., Gilgenkrantz, S., *et al.* (1997). Opitz G/BBB syndrome, a defect of midline development, is due to mutations in a new RING finger gene on Xp22. *Nat Genet* 17, 285-291.
- Raiborg, C., and Stenmark, H. (2002). Hrs and endocytic sorting of ubiquitinated membrane proteins. *Cell Struct Funct* 27, 403-408.
- Rameh, L. E., Tolias, K. F., Duckworth, B. C., and Cantley, L. C. (1997). A new pathway for synthesis of phosphatidylinositol-4,5-bisphosphate. *Nature* 390, 192-196.
- Reymond, A., Meroni, G., Fantozzi, A., Merla, G., Cairo, S., Luzzi, L., Riganelli, D., Zanaria, E., Messali, S., Cainarca, S., *et al.* (2001). The tripartite motif family identifies cell compartments. *Embo J* 20, 2140-2151.
- Richman, J. M., Fu, K. K., Cox, L. L., Sibbons, J. P., and Cox, T. C. (2002). Isolation and characterisation of the chick orthologue of the Opitz syndrome gene, *Mid1*, supports a conserved role in vertebrate development. *Int J Dev Biol* 46, 441-448.
- Riezman, H. (2002). Cell biology: the ubiquitin connection. *Nature* 416, 381-383.
- Robin, N. H., Feldman, G. L., Aronson, A. L., Mitchell, H. F., Weksberg, R., Leonard, C. O., Berton, B. K., Josephson, K. D., Laxová, R., Aleck, K. A., *et al.* (1995). Opitz syndrome is genetically heterogeneous, with one locus on Xp22, and a second locus on 22q11.2. *Nature Genetics* 11, 459-461.
- Robin, N. H., Opitz, J. M., and Muenke, M. (1996). Opitz G/BBB syndrome: clinical comparisons of families linked to Xp22 and 22q, and a review of the literature. *Am J Med Genet* 62, 305-317.
- Rodriguez, O. C., Schaefer, A. W., Mandato, C. A., Forscher, P., Bement, W. M., and Waterman-Storer, C. M. (2003). Conserved microtubule-actin interactions in cell movement and morphogenesis. *Nat Cell Biol* 5, 599-609.

## Bibliography

---

- Runnegar, M., Wei, X., Berndt, N., and Hamm-Alvarez, S. F. (1997). Transferrin receptor recycling in rat hepatocytes is regulated by protein phosphatase 2A, possibly through effects on microtubule-dependent transport. *Hepatology* 26, 176-185.
- Russo, C., Gao, Y., Mancini, P., Vanni, C., Porotto, M., Falasca, M., Torrissi, M. R., Zheng, Y., and Eva, A. (2001). Modulation of oncogenic DBL activity by phosphoinositol phosphate binding to pleckstrin homology domain. *J Biol Chem* 276, 19524-19531.
- Scambler, P. J. (2000). The 22q11 deletion syndromes. *Hum Mol Genet* 9, 2421-2426.
- Scanlan, M. J., Chen, Y. T., Williamson, B., Gure, A. O., Stockert, E., Gordan, J. D., Tureci, O., Sahin, U., Pfreundschuh, M., and Old, L. J. (1998). Characterization of human colon cancer antigens recognized by autologous antibodies. *Int J Cancer* 76, 652-658.
- Schafer, D. A. (2003). Actin puts on the squeeze. *Nat Cell Biol* 5, 693-694.
- Schlessinger, J. (2002). Ligand-induced, receptor-mediated dimerization and activation of EGF receptor. *Cell* 110, 669-672.
- Schroer, T. A. (2000). Motors, clutches and brakes for membrane traffic: a commemorative review in honor of Thomas Kreis. *Traffic* 1, 3-10.
- Schweiger, S., Foerster, J., Lehmann, T., Suckow, V., Muller, Y. A., Walter, G., Davies, T., Porter, H., van Bokhoven, H., Lunt, P. W., *et al.* (1999). The Opitz syndrome gene product, MID1, associates with microtubules. *Proc Natl Acad Sci U S A* 96, 2794-2799.
- Schweiger, S., and Schneider, R. (2003a). The MID1/PP2A complex: a key to the pathogenesis of Opitz BBB/G syndrome. *Bioessays* 25, 356-366.
- Schweiger, S., and Schneider, R. (2003b). The MID1/PP2A complex: a key to the pathogenesis of Opitz BBB/G syndrome. *Bioessays* 25, 356-366.
- Schweizer, A., Ericsson, M., Bachi, T., Griffiths, G., and Hauri, H. P. (1993). Characterization of a novel 63 kDa membrane protein. Implications for the organization of the ER-to-Golgi pathway. *J Cell Sci* 104 (Pt 3), 671-683.
- Seto, M. H., Liu, H. L., Zajchowski, D. A., Whitlow, M., Henry, J., Mather, I. H., McDermott, M. F., Pontarotti, P., Ribouchon, M. T., and Offer, C. (1999). Protein fold analysis of the B30.2-like domain. *Proteins* 35, 235-249.
- Shih, S. C., Katzmann, D. J., Schnell, J. D., Sutanto, M., Emr, S. D., and Hicke, L. (2002). Epsins and Vps27p/Hrs contain ubiquitin-binding domains that function in receptor endocytosis. *Nat Cell Biol* 4, 389-393.
- Short, K. M., Hopwood, B., Yi, Z., and Cox, T. C. (2002). MID1 and MID2 homo- and heterodimerise to tether the rapamycin-sensitive PP2A regulatory subunit, alpha 4, to microtubules: implications for the clinical variability of X-linked Opitz GBBB syndrome and other developmental disorders. *BMC Cell Biol* 3, 1.
- Simonsen, A., Wurmser, A. E., Emr, S. D., and Stenmark, H. (2001). The role of phosphoinositides in membrane transport. *Curr Opin Cell Biol* 13, 485-492.
- Smith, A. J., Pfeiffer, J. R., Zhang, J., Martinez, A. M., Griffiths, G. M., and Wilson, B. S. (2003). Microtubule-dependent transport of secretory vesicles in RBL-2H3 cells. *Traffic* 4, 302-312.
- Smith, E. F. (2002). Regulation of flagellar dynein by the axonemal central apparatus. *Cell Motil Cytoskeleton* 52, 33-42.
- So, J., Suckow, V., Kijas, Z., Kalscheurer, V., Moser, B., Winter, J., Baars, M., Firth, H., Lunt, P., Hamel, B., Meinecke, P. *et al.* (2004). Unexpected mild phenotypes in a series of patients with opitz GBBB syndrome with MID1 mutations. in press
- Sorkin, A., and von Zastrow, M. (2002). Signal transduction and endocytosis: close encounters of many kinds. *Nature* 3, 600-614.
- Stoll, C., Geraudel, A., Berland, H., Roth, M. P., and Dott, B. (1985). Male-to-male transmission of the hypertelorism-hypospadias (BBB) syndrome. *Am J Med Genet* 20, 221-225.
- Takeda, S., Yamazaki, H., Seog, D. H., Kanai, Y., Terada, S., and Hirokawa, N. (2000). Kinesin superfamily protein 3 (KIF3) motor transports fodrin-associating vesicles important for neurite building. *J Cell Biol* 148, 1255-1265.
- Tall, E.G., Spector, I., Pentylala, S.N., Bitter, I., Rebecchi, M.J. (2000). Dynamics of phosphatidylinositol 4,5-bisphosphate in actin-rich structures. *Curr Biol* 10(12):743-746.
- Thiemann, M., Schrader, M., Volkl, A., Baumgart, E., and Fahimi, H. D. (2000). Interaction of peroxisomes with microtubules. In vitro studies using a novel peroxisome-microtubule binding assay. *Eur J Biochem* 267, 6264-6275.
- Thomas, C. C., Deak, M., Alessi, D. R., and van Aalten, D. M. (2002). High-resolution structure of the pleckstrin homology domain of protein kinase b/akt bound to phosphatidylinositol (3,4,5)-trisphosphate. *Curr Biol* 12, 1256-1262.

- Thyberg, J., and Moskalewski, S. (1999). Role of microtubules in the organisation of the golgi complex. *Exp cell biol* 246, 263-279.
- Torok, M., and Etkin, L. D. (2001). Two B or not two B? Overview of the rapidly expanding B-box family of proteins. *Differentiation* 67, 63-71.
- Trockenbacher, A., Suckow, V., Foerster, J., Winter, J., Krauss, S., Ropers, H. H., Schneider, R., and Schweiger, S. (2001). MID1, mutated in Opitz syndrome, encodes an ubiquitin ligase that targets phosphatase 2A for degradation. *Nat Genet* 29, 287-294.
- Tronchere, H., Laporte, J., Pendaries, C., Chaussade, C., Liaubet, L., Pirola, L., Mandel, J. L., and Payrastra, B. (2004). Production of phosphatidylinositol 5-phosphate by the phosphoinositide 3-phosphatase myotubularin in mammalian cells. *J Biol Chem* 279, 7304-7312.
- Truong, K., and Ikura, M. (2002). Identification and characterization of subfamily-specific signatures in a large protein superfamily by a hidden Markov model approach. *BMC Bioinformatics* 3, 1.
- Tyers, M., Rachubinski, R. A., Stewart, M. I., Varrichio, A. M., Shorr, R. G., Haslam, R. J., and Harley, C. B. (1988). Molecular cloning and expression of the major protein kinase C substrate of platelets. *Nature* 333, 470-473.
- Urioste, M., Arroyo, I., Villa, A., Lorda-Shánchez, I., Barrio, R., López-Cuesta, M., Rueda, J. (1995). Distal deletion of chromosome 13 in a child with the "Opitz" GBBB syndrome. *Am J Med Genet* 59, 114-122
- Van den Veyver, I. B., Cormier, T. A., Jurecic, V., Baldini, A., and Zoghbi, H. Y. (1998). Characterization and physical mapping in human and mouse of a novel RING finger gene in Xp22. *Genomics* 51, 251-261.
- Varlamov, O., Kalinina, E., Che, F. Y., and Fricker, L. D. (2001). Protein phosphatase 2A binds to the cytoplasmic tail of carboxypeptidase D and regulates post-trans-Golgi network trafficking. *J Cell Sci* 114, 311-322.
- Vasanji, A., Ghosh, P.K., Graham, L.M., Eppell, S.J., Fox, P.L. (2004). Polarization of plasma membrane microviscosity during endothelial cell migration. *Dev Cell*. 6(1):29-41.
- Vereb, G., Szollosi, J., Matko, J., Nagy, P., Farkas, T., Vigh, L., Waldmann, T.A., Damjanovich, S. (2003). Dynamic, yet structured: the cell membrane three decades after Singer-Nicolson model. *PNAS* 100 (14), 8053-8058.
- Verloes, A., Merrer, M. L., Briard, M. L. (1989). BBG syndrome or Opitz syndrome: new family. *Am J Med Genet* 34, 313-316
- Verloes, A., Albert, D., Sylvie, O., et al. (1995). Opitz syndrome: Chromosomal evidence of an X-linked form. *Am J Hum Genet* 95, 123-128
- Vernet, C., Boretto, J., Mattei, M. G., Takahashi, M., Jack, L. J., Mather, I. H., Rouquier, S., and Pontarotti, P. (1993). Evolutionary study of multigenic families mapping close to the human MHC class I region. *J Mol Evol* 37, 600-612.
- Vincent, J-P. (2003). Membranes, trafficking, and signaling during animal development. *Cell* 112, 745-749.
- Vitelli, F., Taddei, I., Morishima, M., Meyers, E. N., Lindsay, E. A., and Baldini, A. (2002). A genetic link between Tbx1 and fibroblast growth factor signaling. *Development* 129, 4605-4611.
- Wadey, R., McKie, J., Papapetrou, C., Sutherland, H., Lohman, F., Osinga, J., Frohn, I., Hofstra, R., Meijers, C., Amati, F., et al. (1999). Mutations of UFD1L are not responsible for the majority of cases of DiGeorge Syndrome/velocardiofacial syndrome without deletions within chromosome 22q11. *Am J Hum Genet* 65, 247-249.
- Walenta, J. H., Didier, A. J., Liu, X., and Kramer, H. (2001). The Golgi-associated hook3 protein is a member of a novel family of microtubule-binding proteins. *J Cell Biol* 152, 923-934.
- Winter, J., Lehmann, T., Suckow, V., Kijas, Z., Kulozik, A., Kalscheuer, V., Hamel, B., Devriendt, K., Opitz, J., Lenzner, S., et al. (2003). Duplication of the MID1 first exon in a patient with Opitz G/BBB syndrome. *Hum Genet* 112, 249-254.
- Yamagishi, C., Hierck, B. P., Gittenberger-De Groot, A. C., Yamagishi, H., and Srivastava, D. (2003). Functional attenuation of UFD1L, a 22q11.2 deletion syndrome candidate gene, leads to cardiac outflow septation defects in chicken embryos. *Pediatr Res* 53, 546-553. Epub 2003 Feb 2020.



Time after photo-bleaching (sec)	Fluorescence recovery (%)						
	Sample 1	Sample 2	Sample 3	Sample 4	Sample 5	Sample 6	Average
1	0.10	0.04	0.07	0	0.02	0	0.05
2	0.09	0.08	0.10	0.01	0.05	0.04	0.08
3	0.14	0.10	0.13	0.10	0.14	0.09	0.12
4	0.24	0.08	0.20	0.06	0.07	0.06	0.12
5	0.10	0.14	0.24	0.10	0.06	0.05	0.11
6	0.14	0.15	0.18	0.21	0.04	0.18	0.15
7	0.15	0.15	0.31	0.23	0.08	0.16	0.18
8	0.30	0.13	0.22	0.23	0.06	0.16	0.18
9	0.17	0.11	0.23	0.19	0.13	0.18	0.17
10	0.17	0.08	0.13	0.22	0.11	0.19	0.15

**Appendix 1. Percentage of fluorescence recovery after photo-bleaching on the plasma membrane of six different COS1 cells, monitored every second within the first 10 seconds. Average recovery of these six samples are calculated.**



Time after photo-bleaching (sec)	Fluorescence recovery (%)				
	Sample 1	Sample 2	Sample 3	Sample 4	Average
1	0.12	0.11	0.11	0.13	0.12
2	0.04	0.06	0.03	0.08	0.05
3	0.18	0.13	0.13	0.17	0.15
4	0.22	0.28	0.25	0.26	0.25
5	0.11	0.29	0.21	0.20	0.20
6	0.25	0.29	0.24	0.30	0.27
7	0.19	0.25	0.20	0.24	0.22
8	0.16	0.28	0.22	0.23	0.22
9	0.16	0.44	0.23	0.25	0.23
10	0.34	0.25	0.26	0.34	0.30

**Appendix 2. Percentage of fluorescence recovery after photo-bleaching on the plasma membrane of four different COS1 cells overexpressing GFP-PEPP2, monitored every second within the first 10 seconds. Average recovery of these four samples are calculated.**

Time after photo-bleaching (sec)	Fluorescence recovery (%)							Average
	Sample 1	Sample 2	Sample 3	Sample 4	Sample 5	Sample 6	Sample 7	
1	0.00	0.00	0.08	0.01	0.06	0.00	0.07	0.03
2	0.07	0.01	0.13	0.00	0.13	0.03	0.03	0.05
3	0.02	0.03	0.13	0.03	0.10	0.12	0.04	0.07
4	0.04	0.00	0.12	0.06	0.12	0.12	0.04	0.07
5	0.13	0.00	0.09	0.08	0.13	0.12	0.09	0.09
6	0.08	0.02	0.14	0.10	0.22	0.06	0.19	0.11
7	0.11	0.02	0.15	0.08	0.13	0.25	0.07	0.11
8	0.12	0.07	0.14	0.09	0.18	0.11	0.07	0.11
9	0.19	0.04	0.15	0.09	0.22	0.06	0.04	0.11
10	0.20	0.08	0.13	0.13	0.16	0.11	0.04	0.11

**Appendix 3. Percentage of fluorescence recovery after photo-bleaching on the plasma membrane of seven different COS1 cells overexpressing GFP-MID2 $\Delta$ CTD, monitored every second within the first 10 seconds. Average recovery of these seven samples are calculated.**

Time after photo-bleaching (sec)	Fluorescence recovery (%)								Average
	Sample 1	Sample 2	Sample 3	Sample 4	Sample 5	Sample 6	Sample 7	Sample 8	
1	0.08	0.00	0.04	0.09	0.06	0.00	0.13	0.00	0.05
2	0.04	0.09	0.06	0.03	0.07	0.07	0.21	0.04	0.08
3	0.12	0.12	0.21	0.14	0.25	0.14	0.15	0.00	0.14
4	0.10	0.13	0.31	0.27	0.10	0.24	0.28	0.00	0.18
5	0.29	0.12	0.22	0.22	0.12	0.08	0.25	0.00	0.16
6	0.08	0.21	0.30	0.42	0.17	0.12	0.22	0.07	0.20
7	0.30	0.16	0.33	0.43	0.22	0.18	0.29	0.01	0.23
8	0.29	0.13	0.27	0.52	0.42	0.23	0.20	0.05	0.26
9	0.13	0.25	0.28	0.40	0.17	0.05	0.21	0.02	0.21
10	0.17	0.16	0.22	0.41	0.19	0.09	0.29	0.11	0.20

**Appendix 4. Percentage of fluorescence recovery after photo-bleaching on the plasma membrane in OS derived fibroblast cells, monitored every second within the first 10 seconds. Average recovery of these eight samples are calculated.**

Time after photo-bleaching (sec)	Fluorescence recovery (%)										Average
	Sample 1	Sample 2	Sample 3	Sample 4	Sample 5	Sample 6	Sample 7	Sample 8	Sample 9	Sample 10	
1	0.21	0.03	0.07	0.12	0.10	0.12	0.05	0.09	0.06	0.07	0.09
2	0.24	0.05	0.20	0.17	0.04	0.04	0.05	0.17	0.13	0.10	0.12
3	0.12	0.15	0.10	0.19	0.15	0.30	0.00	0.12	0.12	0.12	0.14
4	0.17	0.00	0.25	0.31	0.14	0.29	0.05	0.11	0.03	0.12	0.15
5	0.10	0.10	0.32	0.25	0.13	0.19	0.09	0.14	0.18	0.15	0.16
6	0.16	0.09	0.23	0.35	0.06	0.23	0.06	0.10	0.08	0.16	0.15
7	0.11	0.22	0.14	0.36	0.18	0.31	0.12	0.12	0.11	0.17	0.19
8	0.12	0.31	0.28	0.45	0.07	0.16	0.18	0.11	0.10	0.17	0.20
9	0.20	0.38	0.36	0.29	0.02	0.26	0.06	0.16	0.12	0.21	0.21
10	0.12	0.30	0.06	0.33	0.02	0.25	0.15	0.19	0.24	0.16	0.20

**Appendix 5. Percentage of fluorescence recovery after photo-bleaching on the plasma membrane in control fibroblast cells, monitored every second within the first 10 seconds. Average recovery of these ten samples are calculated.**

Research article

## MIDI and MID2 homo- and heterodimerise to tether the rapamycin-sensitive PP2A regulatory subunit, Alpha 4, to microtubules: implications for the clinical variability of X-linked Opitz GBBB syndrome and other developmental disorders

Kieran M Short<sup>1</sup>, Blair Hopwood<sup>1</sup>, Zou Yi<sup>1</sup> and Timothy C Cox\*<sup>1,2</sup>

Address: <sup>1</sup>Department of Molecular Biosciences & ARC Special Research Centre for the Molecular Genetics of Development, University of Adelaide, Adelaide, South Australia, Australia 5005 and <sup>2</sup>South Australian Clinical Genetics Service, Women's & Children's Hospital, North Adelaide, South Australia, Australia 5006

E-mail: Kieran M Short - kieran.short@adelaide.edu.au; Blair Hopwood - blair.hopwood@adelaide.edu.au; Zou Yi - julie.zou@adelaide.edu.au; Timothy C Cox\* - timothy.cox@adelaide.edu.au

\*Corresponding author

Published: 4 January 2002

Received: 5 November 2001

Accepted: 4 January 2002

BMC Cell Biology 2002, 3:1

This article is available from: <http://www.biomedcentral.com/1471-2121/3/1>

© 2002 Short et al; licensee BioMed Central Ltd. Verbatim copying and redistribution of this article are permitted in any medium for any non-commercial purpose, provided this notice is preserved along with the article's original URL. For commercial use, contact [info@biomedcentral.com](mailto:info@biomedcentral.com)

### Abstract

**Background:** Patients with Opitz GBBB syndrome present with a variable array of developmental defects including craniofacial, cardiac, and genital anomalies. Mutations in the X-linked *MIDI* gene, which encodes a microtubule-binding protein, have been found in ~50% of Opitz GBBB syndrome patients consistent with the genetically heterogeneous nature of the disorder. A protein highly related to *MIDI*, called *MID2*, has also been described that similarly associates with microtubules.

**Results:** To identify protein partners of *MIDI* and *MID2* we undertook two separate yeast two-hybrid screens. Using this system we identified Alpha 4, a regulatory subunit of PP2-type phosphatases and a key component of the rapamycin-sensitive signaling pathway, as a strong interactor of both proteins. Analysis of domain-specific deletions has shown that the B-boxes of both *MIDI* and *MID2* mediate the interaction with Alpha 4, the first demonstration in an RBCC protein of a specific role for the B-box region. In addition, we show that the *MIDI/2* coiled-coil motifs mediate both homo- and hetero-dimerisation, and that dimerisation is a prerequisite for association of the *MID*-Alpha 4 complex with microtubules.

**Conclusions:** Our findings not only implicate Alpha 4 in the pathogenesis of Opitz GBBB syndrome but also support our earlier hypothesis that *MID2* is a modifier of the X-linked phenotype. Of further note is the observation that Alpha 4 maps to Xq13 within the region showing linkage to FG (Opitz-Kaveggia) syndrome. Overlap in the clinical features of FG and Opitz GBBB syndromes warrants investigation of Alpha 4 as a candidate for causing FG syndrome.

### Background

Opitz GBBB syndrome (OS; Opitz syndrome) is a genetically and phenotypically complex disorder defined by characteristic facial anomalies (hypertelorism and varia-

bly labiopalatine and laryngotracheo-esophageal (LTE) clefting), structural heart defects, as well as anal and genital anomalies [1,2]. Recently, we and others identified the *MIDI* gene (also called *FXY*) as the underlying cause of

the X-linked form of the disease [3–5]. Defects in *MID1* have been found in ~50% of OS cases consistent with evidence from genetic linkage and cytogenetic studies that at least one autosomal form of the disorder, at chromosome position 22q11.2, also exists [6–8]. The deletion of the same interval produces the 22q11 deletion syndrome, which encompasses a group of disorders (eg. DiGeorge and velocardiofacial syndromes) showing some phenotypic overlap with OS [6,9]. Collectively, 22q11 anomalies represent one of the most common genetic causes of malformations (estimated 1 in 5000 live births) [10]. Although progress has recently been made towards elucidating the genes contributing to the 22q11 deletion phenotype [11–14], a specific autosomal OS gene has not yet been identified.

The *MID1* gene encodes the defining member of a new subclass of the RBCC (RING, B-box, Coiled-Coil) family of proteins. This subclass is characterised by the combination of both a fibronectin type III motif and a B30.2-like (or SPRY) domain positioned C-terminal to the RBCC domain [15,16]. As in other members of the RBCC protein family, *MID1* forms multiprotein complexes of between 250 and 450 kDa [17]. The *MID1* protein, presumably as part of these complexes, has been shown to associate with cytoplasmic microtubules along their length and throughout the cell cycle using immunofluorescence detection of endogenous *MID1*, transient expression of GFP-*MID1* fusion proteins, and cellular fractionation [5,18]. Most mutations in *MID1* that cause OS are truncating mutations with many, but not all, directly affecting the C-terminal half of the protein [5]. Interestingly, all examined *MID1* mutations disrupt the normal microtubule-associated distribution and this has been demonstrated to occur *in vivo* with endogenous mutant protein and in transient transfection studies using GFP fusion proteins [5,17,18].

An intriguing aspect of OS is the marked intrafamilial variability seen even among related males with the same X-linked mutation. This observation may be explained by the fact that other proteins, such as the highly related *MID2* protein that is expressed in some of the same tissues and also associates with the microtubule network [15,19], could at least partially compensate for the loss of *MID1* [5]. Such a mechanism has also been proposed for other microtubule-associated proteins, such as tau [20]. Alternatively, variations in the level or action of other factors in the same molecular pathway (for example, a factor encoded by the 22q11.2 locus and/or another component of the *MID1* macromolecular complex) could contribute to this variability. Both explanations are consistent with the conclusion that OS is caused by loss of function of *MID1* [5].

In this paper we report the identification of Alpha 4 as an interacting partner of both the Opitz syndrome protein,

*MID1*, and the highly related *MID2* protein. Alpha 4 is a unique and highly conserved regulatory subunit of PP2-type phosphatases, such as PP2A [21–24], and an integral component of the rapamycin-sensitive signaling pathway [25]. Our finding that both *MID1* and *MID2*, either as homo- or hetero-dimers, are able to tether a key regulator of intracellular signaling to microtubules has significant implications for our understanding of the pathophysiological basis of OS and provides additional support for the hypothesis that *MID2* could act as a modifier of the OS phenotype. Furthermore, as the *Alpha 4* gene maps to Xq13 [26], our results identify it as a candidate for other X-linked disorders such as FG (Opitz-Kaveggia) syndrome that overlaps clinically with Opitz GBBB syndrome.

## Results

### Yeast two-hybrid screens identify Alpha 4 as an interacting partner of both *MID1* and *MID2*

In order to begin to determine the identity of potential interacting factors and the processes with which *MID1* is involved, we performed a yeast two-hybrid assay utilising the full length *MID1* protein (which shares 94.9% identity, 99.9% similarity with mouse *Mid1*) as bait in a screen of a mouse 10.5 dpc (days post-coitum) whole embryo cDNA library. At 10.5 dpc, expression of *Mid1* is seen essentially throughout the embryo although strongest levels of expression are evident in highly proliferating tissues such as the developing craniofacial region [27]. The use of the mouse 10.5 dpc whole embryo library was therefore chosen to maximise the likelihood of detecting functionally relevant interactors.

Approximately  $1 \times 10^6$  cDNAs were initially screened using *MID1* as bait. Potential interacting clones were selected based on the activation of the three endogenous reporter genes (*His*, *lacZ*, and *Leu*). Recovery and sequencing of the positives from the library screen demonstrated nine cDNA clones with insert sizes ranging from 1.0 kb to 1.3 kb but representing the same gene. Five additional, singly represented putative interacting clones were also identified but do not constitute part of this report. Database searches identified the nine similar clones as encoding Alpha 4, a rapamycin-sensitive regulatory subunit of protein phosphatases 2A (PP2A) and other PP2-type phosphatases. By comparison with the published murine *Alpha 4* sequence, all clones were judged as being essentially full-length. Notably, the nine in-frame cDNAs represented a minimum of seven independent clones as 5' fusion to the GAL4 activation domain occurred at either nucleotide +4, +7, +10 or +13 and most clones containing different length polyadenylated tails. To confirm that this interaction was not an artefact of the independent GAL4 activation domain and DNA binding domain fusion events, the full-length cDNAs were interchanged such that Alpha 4 was fused to the GAL4-DBD and *MID1* to GAL4-



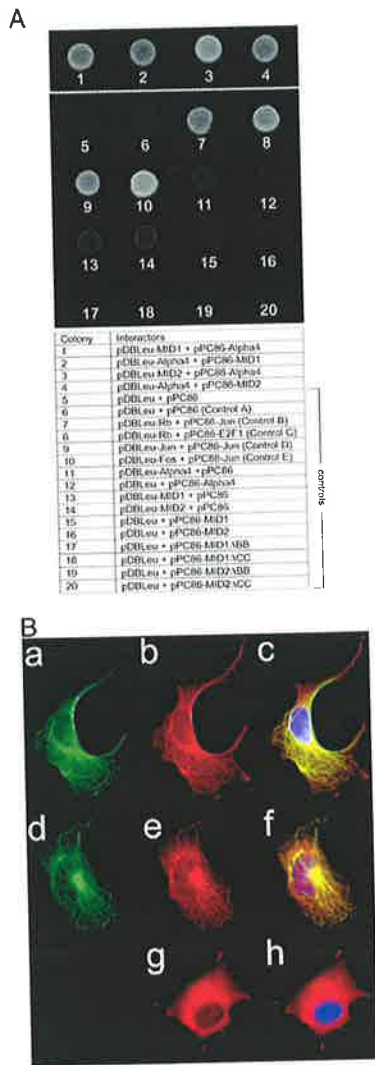


**Figure 1**  
 Alpha 4 interacts with MID1 and MID2. (A) Yeast two-hybrid analysis of the interaction between MID1 and Alpha 4 as well as MID2 and Alpha 4. Yeast agar plate (leu<sup>-</sup> trp<sup>-</sup> his<sup>-</sup>, 75 mM 3-AT) showing growth for MID1/Alpha 4 and MID2/Alpha 4 interactions as well as positive control two-hybrid combinations and no growth for negative controls. (B) Detection of full-length myc tagged-Alpha 4 when co-expressed with GFP-MID1 and GFP-MID2 fusion proteins in transiently transfected Cos1 cells. (a) GFP-MIDI1 fluorescence (green), (b) anti-myc antibody detecting myc-Alpha 4 localisation (red), (c) overlay of (a), (b) showing co-localisation of the myc-Alpha 4 fusion protein and GFP-MIDI1, with DAPI stain for DNA (blue). (d) GFP-MID2 fluorescence (green), (e) myc-Alpha 4 localisation (using same detection as b) (red), (f) overlay of (d), (e) with DAPI (blue) showing co-localisation of the myc-Alpha 4 fusion protein and GFP-MID2. (g) Detection of transiently expressed myc-Alpha 4 fusion protein in Cos1 cells, (h) overlay of (g) and DAPI stain showing cytoplasmic distribution of myc-Alpha 4 fusion protein.

AD. Co-transformation of these two constructs into MaV203 gave similar levels of growth on 3AT (Fig 1A), ie. a level of activation comparable to the strongest interacting proteins, Fos and Jun (Fig 1A, Control E - colony 10).

Given that MID1 and MID2 share 77% overall amino acid identity (92% similarity), we wished to investigate whether MID2 was capable of binding to the same proteins, such as Alpha 4, or whether this interaction was specific for MID1. This was investigated using two approaches: a direct yeast two-hybrid test of the ability of MID2 to bind Alpha 4, and a full two-hybrid screen of the 10.5 dpc whole mouse embryo cDNA library this time using MID2 as bait. The direct test demonstrated that MID2 did indeed interact with Alpha 4. Comparison of the growth of the MID2/Alpha 4 transformed yeast on plates (SC -Leu, -Trp, -His) containing 75 mM 3AT indicated the interaction between MID2 and Alpha 4 was as strong, or stronger, than that observed for MID1 (Fig 1A). A similar result was obtained when assessing the conversion of Xgal (data not shown). In the full yeast two-hybrid screen, some potentially novel interactors were identified for MID2. However, the majority of the putative interacting clones, and again the only sequences represented more than once in the isolates, represented Alpha 4.

**MID1 and MID2 tether Alpha 4 to the microtubles**

To investigate whether Alpha 4 also associated with MID1 and MID2 in a homologous (mammalian) system, we co-transfected both GFP-MID1 (or MID2) with myc epitope-tagged Alpha 4. Transfection of the myc-tagged Alpha 4 expression construct alone resulted in a diffuse distribution of the myc-Alpha 4 fusion protein throughout the cytoplasm in most cells (Fig 1B; g, h). However, in some cells, a faint filamentous distribution that resembled the appearance of microtubules could be seen along with the cytoplasmic protein (data not shown). In contrast, in all cells co-transfected with GFP-MID1 and myc-tagged Alpha 4, there was negligible diffuse cytoplasmic staining. Instead, essentially all the myc-tagged Alpha 4 protein displayed a filamentous meshwork of staining that completely co-localised with MID1 along the length of the microtubules (Fig 1B; a-c). This result also suggested that MID1 was a limiting factor in the tethering of Alpha 4 to the microtubule network, a conclusion supported by western analysis that shows low levels of MID1 in these cells (data not shown). Co-expression of GFP-MID2 and myc-tagged Alpha 4 similarly resulted in co-localisation along the microtubules (Fig 1B; d-f).

**Alpha 4 does not co-localise with MID1 or MID2 proteins harboring in-frame B-box deletions**

Both endogenous mutant MID1 protein in OS patient cells [18] and various transiently expressed mutant MID1-GFP fusion proteins form cytoplasmic clumps

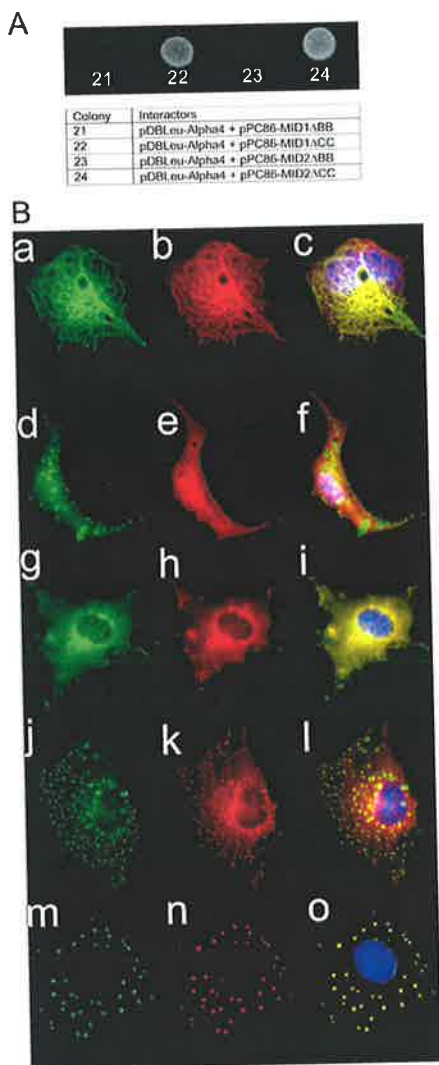


**Figure 2**  
MID1/Alpha 4 and MID2/Alpha 4 interactions are maintained in all MID domain-specific deletions except for those involving the B-boxes. (A) Yeast two hybrid analysis shows that the MID B-boxes are required for interaction with Alpha 4. The interaction of Alpha 4 with MID1 $\Delta$ BB (21), or MID2 $\Delta$ BB (23), is compared to its interaction with MID1 $\Delta$ CC (22), or MID2 $\Delta$ CC (24). (B) Subcellular localisation of myc tagged-Alpha 4 when co-expressed in Cos-1 cells with MID1 domain-specific deletions as GFP fusion proteins. Fluorescence detection of GFP-MID1 $\Delta$ RF (a), GFP-MID1 $\Delta$ BB (d), GFP-MID1 $\Delta$ CC (g), GFP-MID1 $\Delta$ FNIII (j), and GFP-MID1 $\Delta$ CTD (m). Anti-myc antibody detection of myc-Alpha 4 in the same cells as expressing the various MID1 domain-specific deletions (b,e,h,k,n). Overlay of the GFP and anti-myc images of the same cells merged with DAPI stain of nuclei (c,f,i,l,o). All merged images, with the exception of (f) show co-localisation of myc-Alpha 4 with the various MID1 domain deletions. In (f), myc-Alpha 4 fails to co-localise with GFP-MID1 $\Delta$ BB in small cytoplasmic aggregates.

[5,15,17,18]. We chose to exploit this previous observation by co-transfecting GFP-tagged MID1 $\Delta$ CTD (or MID2 $\Delta$ CTD) with a construct expressing a myc-tagged Alpha 4 protein in order to investigate whether Alpha 4 still remained bound to MID1 within such aggregates. The results clearly showed a distribution of myc-Alpha 4 that was indistinguishable from the clumped MID1 $\Delta$ CTD and MID2 $\Delta$ CTD truncated proteins, indicating that Alpha 4 indeed aggregates with the truncated MID1 and MID2 proteins (Fig 2B; m-o).

To further define the motif in MID1 (and MID2) responsible for the interaction with Alpha 4, we generated in-frame deletions of all other motifs (Table 1) and fused the resulting clones to GFP. We initially transfected each construct alone to examine the effect of each deletion on the intracellular localisation of the proteins. The results showed that each motif, or at least their conserved spacing or arrangement, was essential for the distribution of MID1 (and MID2) along the length of the microtubules. The distribution of the individual domain deleted MID proteins when transfected alone was indistinguishable from their distributions when transfected along with myc-Alpha 4 (see below). Consequently, the GFP fluorescence images in Fig 2B can also be considered a representation of each distribution pattern in the absence of co-transfected myc-Alpha 4. Like the  $\Delta$ CTD constructs, deletion of either the B-boxes or the FNIII domain also resulted in cytoplasmic clumps or speckles although these usually appeared smaller and greater in number and the speckles still appeared to co-localise with microtubules (data not shown). Both  $\Delta$ RING proteins, in contrast, showed variability in their distribution with most transfected cells still showing association along the length of the microtubules. However, the microtubule association of these  $\Delta$ RING proteins often did not extend to the cell periphery. Notably, deletion of the coiled-coil motif in each protein resulted a diffuse cytoplasmic distribution, suggesting that these proteins had lost their ability to associate with microtubules (see Fig 2B; g-i).

We then individually co-transfected each MID1 (and MID2) deletion construct with myc-Alpha 4 in an attempt to define the domain responsible for the interaction with Alpha 4. Co-transfection of either the  $\Delta$ RING or  $\Delta$ FNIII proteins with myc-Alpha 4 (Fig 2B; a-c and j-l, respectively) resulted in co-localisation of Alpha 4 with the abnormally distributed MID1 and MID2 proteins, as seen with the  $\Delta$ CTD proteins. Co-expression of either  $\Delta$ CC construct with Alpha 4 resulted in both proteins exhibiting a diffuse cytoplasmic distribution although the pattern of each was still suggestive of the two proteins being able to interact (Fig 2B; g-i). Strikingly, when either of the  $\Delta$ BB constructs was co-expressed with Alpha 4, the mutant MID1 and MID2 proteins still formed cytoplasmic clumps but, in



**Table 1: The MID1 and MID2 deletion constructs used in pEGFP-C2 for cellular co-localisation analysis, co-immunoprecipitation and in pPC86/pDBLeu for interaction analysis with Alpha 4.**  
**Terms: RF denotes a C3HC4 RING finger; BB denotes C2H2 B-Boxes; CC denotes a Coiled-coil motif; FNIII denotes a Fibronectin Type III domain and CTD denotes a C-terminal domain (encompassing a SPRY domain).**

Construct	Amino Acids deleted
Mid1 $\Delta$ RF	1-69
Mid1 $\Delta$ BB	71-213
Mid1 $\Delta$ ACC	214-349
Mid1 $\Delta$ FNIII	370-473
Mid1 $\Delta$ CTD	483-667
Mid2 $\Delta$ RF	1-69
Mid2 $\Delta$ BB	71-213
Mid2 $\Delta$ ACC	214-349
Mid2 $\Delta$ FNIII	370-473
Mid2 $\Delta$ CTD	483-686
BB(Mid1)	1-70 and 214-667
CC(Mid1)	1-213 and 350-667
BCC(Mid1)	1-70 and 350-667

both cases, Alpha 4 remained diffuse in the cytoplasm (Fig 2B; d-f). These results imply that the B-boxes (and/or the linker residues between the B-boxes and RING motifs) are primarily responsible for the interaction with Alpha 4.

To confirm these results, we cloned the MID1 and MID2 domain-deletion constructs in-frame into pPC86 and co-transformed into MaV203 with pDBLeu-Alpha 4. As expected from the immunofluorescence data, activation of all two-hybrid reporter genes, at a level similar to that seen with the full-length MID proteins, was observed with the  $\Delta$ RING,  $\Delta$ FNIII and  $\Delta$ CTD proteins (results not shown), confirming that neither of these domains mediated binding to Alpha 4. Notably, both  $\Delta$ CC proteins also interacted with Alpha 4 (Fig 2A) suggesting that the two proteins were indeed still interacting in the cytoplasm in the immunofluorescence experiments despite not being associated with microtubules. However, the strength of the interaction between the  $\Delta$ CC proteins and Alpha 4 appeared to be reduced compared to the full-length,  $\Delta$ RING,  $\Delta$ FNIII and  $\Delta$ CTD (data not shown). In contrast, but again confirming the immunofluorescence result, the  $\Delta$ BB constructs did not activate reporter gene expression indicating the interaction between Alpha 4 and either MID protein was abolished by removal of this motif (Fig 2A).

#### **The coiled-coil domains of MID1 & MID2 are required for homodimerisation and microtubule binding but not Alpha 4 interaction**

Immunoprecipitation experiments have previously shown that MID1 can form homodimers/homomultimers [17]. To investigate whether homodimerisation was a prerequisite for binding Alpha 4 and/or association with the microtubules, we first tested whether MID1 can interact with itself in the context of the yeast two-hybrid system. The results clearly indicated that the MID1-MID1 interaction is strong (Fig 3A). Domain-deletion constructs (in pDBLeu and pPC86 vectors) were then introduced into the yeast two-hybrid system. Unlike the proteins harboring a deletion of either the RING, B-boxes or FNIII motifs, the MID1 protein lacking the coiled-coil motif had significantly reduced capacity to bind the wild-type MID1 protein, inferring that the coiled-coil domain is critical for efficient homodimerisation (result not shown). Assessment of MID1 using the MultiCoil algorithm [28] supports the conclusion of dimer formation (not trimer) and that the first of the two coiled-coils in this domain is largely responsible for this property. Interestingly, the MID1 protein in which the CTD motif was removed also demonstrated a reduced ability to bind the wild-type MID1 in this system, although this effect was not as marked as that seen for the  $\Delta$ CC proteins. Notably, the yeast two-hybrid and immunofluorescence experiments demonstrate that Alpha 4 can still interact with the MID1 and MID2  $\Delta$ CC proteins. This observation indicates that Alpha 4 must be able to interact with MID monomers although its tethering to the microtubule network is dependent on MID dimerisation, that is; the MID proteins only associate with microtubules as dimers.

#### **MID1 & MID2 can form heterodimers on microtubules**

Given their high level of identity, we investigated whether MID1 and MID2 can also form heterodimers using the yeast two-hybrid system, immunofluorescence of transiently transfected Cos1 cells and co-immunoprecipitation. Co-transformation of the yeast MaV203 strain with both pDBLeu-MID1 and pPC86-MID2 (or in the reverse vector combination) resulted in high level activation of all reporter genes indicating a strong interaction that was comparable to the strength of the MID1-MID1 homo-interaction (Fig 3A). These findings are contradictory to initial reports from a study by Cainarca et al [17] but have been confirmed in experiments involving transient transfection of GFP-MID1 and myc-MID2 fusion constructs (Fig 3B) as well as by co-immunoprecipitation (Fig 3C). Introduction of individual domain-deletions of MID1 together with full-length or domain-deletion MID2, and vice versa, into Cos1 cells and the yeast strain MaV203 using the relevant constructs showed, as expected, that the coiled-coil motif was largely responsible for mediating this heterodimerisation (data not shown).

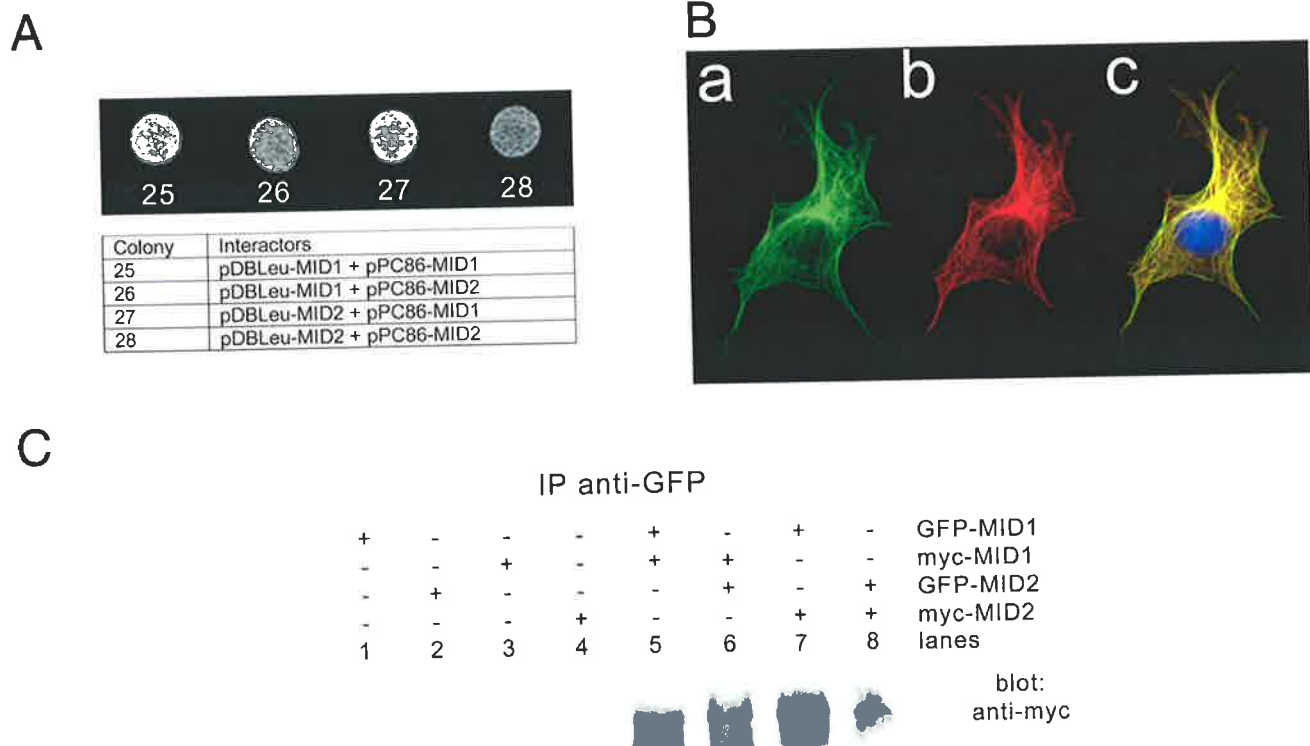


**Figure 3**

MID1 and MID2 can homo- and heterodimerise with one another. (A) Yeast two-hybrid assay for MID1 and MID2 multimerisation. Yeast agar plate (*leu<sup>-</sup> trp<sup>-</sup> his<sup>-</sup>*, 75 mM 3-AT) showing growth for MID1/MID1 (25), MID1/MID2 (26 and 27) and MID2/MID2 (28). (B) MID1 and MID2 co-localise to the microtubules. Co-expression of GFP-MID1 (a) and myc-MID2 (b) in transiently transfected Cos1 cells showing co-localisation to the microtubular cytoskeleton in an overlay (c) with a DAPI stained nucleus (blue). (C) Co-immunoprecipitation of MID1 and MID2 homo- and heterodimers. Shown are extracts from Cos1 cells, transfected with GFP-MID1 (lane 1), GFP-MID2 (lane 2), myc-MID1 (lane 3), myc-MID2 (lane 4), GFP-MID1 and myc-MID1 (lane 5), GFP-MID2 and myc-MID1 (lane 6), GFP-MID1 and myc-MID2 (lane 7) and GFP-MID2 and myc-MID2 (lane 8). Samples were immunoprecipitated with anti-GFP antibody/protein-A sepharose beads, separated on a 8% SDS polyacrylamide gel, transferred to a nitrocellulose membrane and blotted with anti-c-myc antibody to detect co-precipitate protein.

**The B-boxes of MID1 & MID2 are sufficient to bind Alpha 4**

To verify that the Alpha 4 interaction and the association of the complex with microtubules were indeed dependent on the B-boxes and coiled-coil, respectively, and not just an artefact of altering the relative spacing of remaining domains, we fused the MID1 B-boxes and coiled-coil motif, or the coiled-coil motif alone, in-frame to GFP and co-transfected with the myc-Alpha 4 construct. Of interest was the observation that the MID1 coiled-coil domain alone fused to GFP (GFP-M1CC) resulted in cytoplasmic clumping (Fig 4B; a), supporting the notion that the coiled-coil domain is required for MID1 dimerisation. Consistent with this is that the phenomenon of cytoplasmic clumping seen in most OS patients has only been observed in those cases where the expressed mutant MID1 protein harbours a mutation outside the coiled coil motif [5]. Notably, however, in cells co-transfected with the

GFP-M1CC and myc-Alpha 4 constructs, Alpha 4 did not co-localise with these M1CC clumps (Fig 4B; a-c). Like the M1CC protein, the construct expressing the fusion between GFP and the MID1 B-boxes plus coiled-coil domains (GFP-M1BBCC) resulted in clumps within the cytoplasm. Importantly, and in contrast to the co-transfection of M1CC, Alpha 4 was found to co-localise with the GFP-M1BBCC fusion protein (see Fig 4B; d-f). We did not undertake the generation of a GFP-M1BB (B-boxes alone) construct as it was predicted that the resultant GFP fusion protein would show a diffuse cytoplasmic distribution largely indistinguishable from Alpha 4. Instead, the MID1 B-boxes were cloned into pDBLeu and tested directly for their ability to interact with Alpha 4 in the two-hybrid system. The result (Fig 4A) clearly supports the conclusion that the B-boxes are sufficient to bind Alpha 4.

A



Colony	Interactors
29	pDBLeu + pPC86-M1BB
30	pDBLeu-Alpha4 + pPC86-MID1
31	pDBLeu-Alpha4 + pPC86-M1BB

B

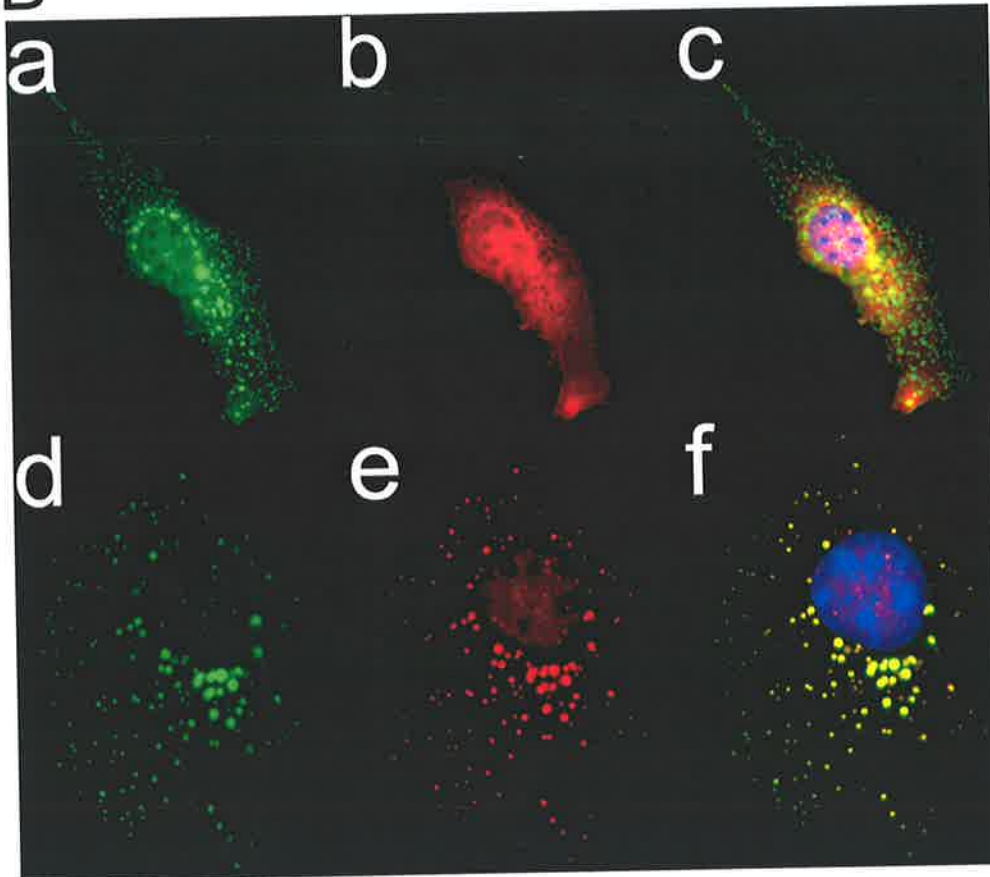


**Figure 4**

The B-boxes of MIDI are sufficient to bind Alpha 4. (A) Yeast two-hybrid analysis shows that the MIDI B-boxes (pPC86-M1BB) alone can interact with Alpha 4 (pDBLeu-Alpha 4) (31). The wild-type MIDI-Alpha 4 interaction (30) and a control with the pPC86-M1BB and no interaction partner (29) were included for comparison. (B) Immunofluorescence assay highlights the importance of the B-boxes for Alpha 4 binding. Subcellular distribution of the GFP-fused MIDI coiled coil domain, GFP-M1CC (a) and myc-Alpha 4 (b) in the same cell shows that the two proteins do not co-localise, as seen in the merged image (c). However, the MIDI fragment, GFP-M1BCC (d) and the myc-Alpha 4 (e) do co-localise in cytoplasmic speckles as seen in the merged image (f). Both merged images, (c) and (f), also show DAPI stain (blue), which indicates the position of the nucleus.



**MID1 is phosphorylated on serine and threonine residues**

As Alpha 4 is a regulator of PP2-type serine/threonine phosphatases, we investigated whether MID1 and MID2 might themselves be phosphorylated and hence possible targets of Alpha 4/phosphatase action. Due to the low levels of endogenous MID1 and MID2 in all tested cultured cell lines, we performed western analysis of immunoprecipitated MID-GFP proteins using extracts of Cos1 cells that had been transiently transfected with the various expression constructs. Immunoprecipitation with anti-GFP antibodies followed by western analysis using anti-phosphoserine and anti-phosphothreonine antibodies showed that MID1- and MID2-GFP fusion proteins were phosphorylated on both serine and threonine residues (Fig 5A). Similar analysis using anti-phosphotyrosine antibodies failed to demonstrate phosphorylation of tyrosine residues on either protein (result not shown).

In an attempt to define the location of the sites in MID1 that were phosphorylated, we performed similar immunoprecipitation and western analysis but this time using extracts of Cos1 cells that had been transfected with the individual domain-specific deletion constructs (Fig 5B). That the overall phosphorylation of the MID1 fusion protein was not significantly affected by deletion of any individual domain may suggest that MID1 is phosphorylated at multiple threonine residues along the protein. However, using the anti-phosphoserine antibody, no serine phosphorylation of the  $\Delta$ BB protein was detected suggesting that most serine phosphorylation in MID1 occurs at or near the B-boxes.

**Identification of potential sites of phosphorylation in MID1 and MID2**

Computer prediction of potential target residues for phosphorylation by serine/threonine kinases not surprisingly identified numerous consensus sites throughout both human MID1 and MID2. Given the conservation of the rapamycin-sensitive pathway from yeast to mammals and the fact that Alpha 4 binds to both MID1 and MID2 which are only 77% identical, we reasoned that any functionally relevant phosphorylation site should be conserved across species and in both MID1 and MID2 proteins. Examination of available orthologous MID1 and MID2 sequences (from seven and three species, respectively) showed that sixteen of these sites (6 threonines and 10 serines) were fully conserved between all MID proteins (Fig 5C). Interestingly, two of these sites (Ser92 and Ser96), which represent consensus phosphorylation sites for GSK3 and MAPK/CKI/CKII respectively, are the only two conserved serine residues in the amino-terminal half of the protein and, as both are located in the region deleted in the  $\Delta$ BB constructs of MID1 and MID2, are likely to be the primary sites of serine phosphorylation in these proteins.

**Discussion**

We have previously shown that the X-linked form of Opitz GBBB syndrome (OS) results from loss of function mutations in *MID1*, a gene that encodes a member of a new class of microtubule-associated proteins [5]. A highly related factor, termed MID2, has also been identified which shares 77% amino acid identity (92% similarity) with MID1 and is expressed in many of the same embryological tissues, albeit at a lower level in most [15,19]. Both MID1 and MID2 are members of the RBCC family of proteins, a group of proteins with diverse intracellular localisations and presumably varied functions. Despite these differences, an ability to function as part of large multi-protein complexes is common to RBCC proteins [29]. Consistent with this is the observation that the 67 kDa MID1 is mostly found in complexes of between 250 kDa and 450 kDa [17]. However, no function has been definitively ascribed to any of the motifs in the MID proteins or indeed either protein as a whole. In this study, we have undertaken yeast two-hybrid screens to identify interacting partners that were likely to constitute part of these MID-complexes as well as performed precise deletion analysis of the MID proteins to begin to elucidate the role of individual motifs.

The only apparent similarity between all the *MID1* mutations identified in patients with OS is that the resultant mutant protein is no longer able to completely decorate the microtubules. This observation implies that the function of one or more proteins within the MID1 complex is absolutely required along the length of the microtubules. Identification of such *bona fide* interactors might therefore be expected to shed light on the possible role of the OS protein and thus provide a better understanding of the molecular pathogenesis of the disorder. To this end, we performed yeast two-hybrid screens using MID1 and MID2 as bait and a 10.5 dpc mouse embryo cDNA library as prey. Significantly, we identified the phosphoprotein, Alpha 4 (also known as IGBP1) as an interactor of both MID proteins. This interaction between the MID proteins and Alpha 4 was confirmed by both vector swapping in the two-hybrid system as well as by co-localisation of differentially tagged proteins to the microtubule network. The specificity of this interaction is also supported by the fact that mouse Mid1 (but not mouse Mid2 presumably because of its lower abundance) was recently identified in the reverse two-hybrid screen of a 9 dpc murine embryonic cDNA library where the mouse Alpha 4 was used as the bait [30]. To characterise this interaction further, we chose to exploit the observation that C-terminal mutations of MID1 form cytoplasmic clumps both *in vivo* [18] and in transformed cell lines over-expressing GFP-mutant MID1 fusion proteins [5,15,17,18] by co-transfecting constructs expressing the  $\Delta$ CTD proteins (and the other domain-specific deletions of MID1 and MID2) as GFP fusions with

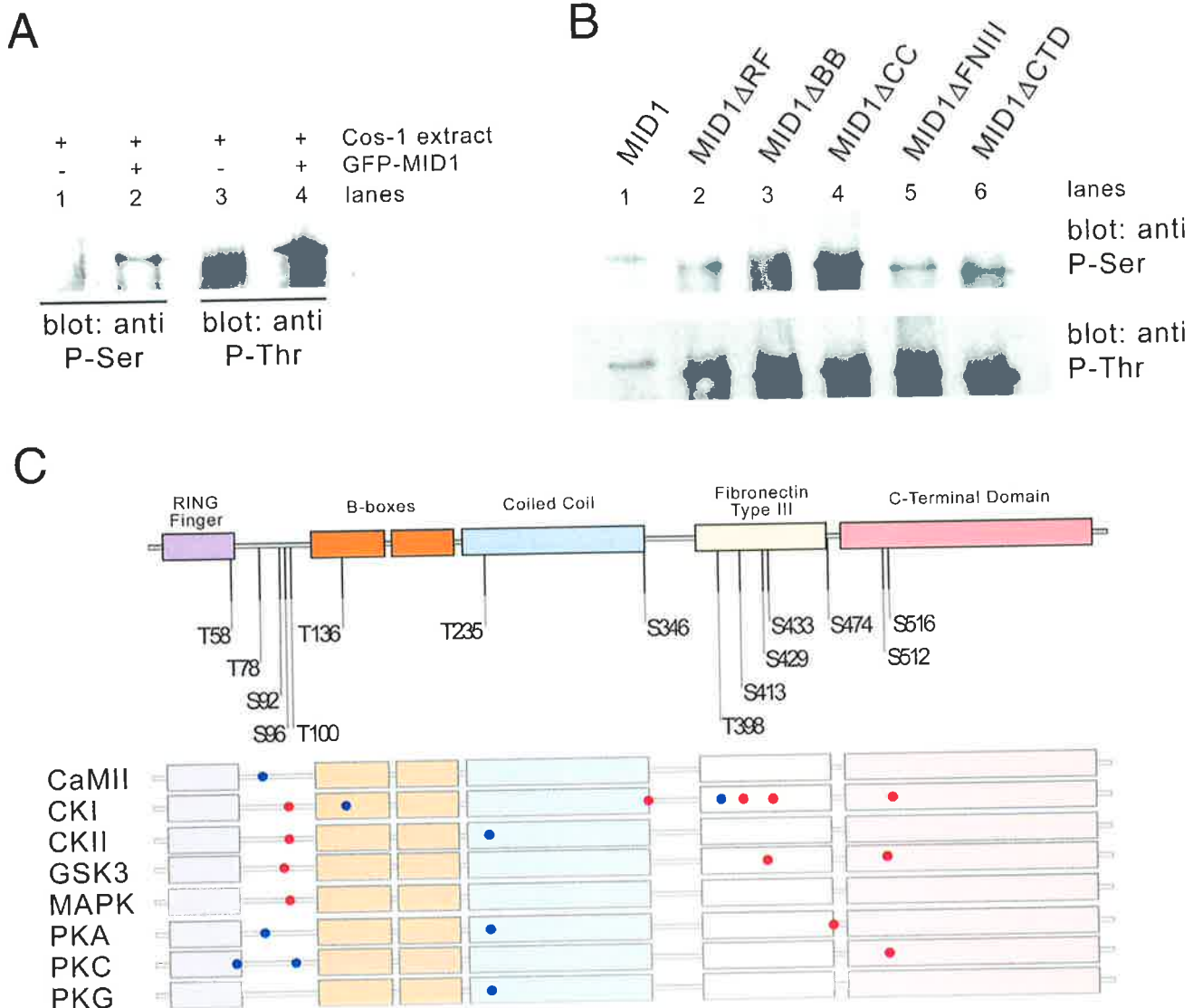


**Figure 5** MID1 contains phosphorylated serine and threonine residues. (A) Extracts from untransfected Cos1 cells (lanes 1 & 3) or Cos1 cells transfected with GFP-MID1 (lanes 2 & 4) were immunoprecipitated with anti-GFP antibody/protein-A sepharose beads and analysed by western blot analysis using either an anti-phosphoserine antibody (lanes 1 & 2) or anti-phosphothreonine antibody (lanes 3 & 4). Protein bands in lanes 2 and 4 indicated that GFP-MID1 contains both phosphoserine and phosphothreonine residues. (B) Domain-specific deletions of MID1 were used in an attempt to crudely map locations of the phosphorylated serine and threonine residues. Shown are extracts from Cos1 cells transfected with full length GFP-MID1 (lane 1), GFP-MID1 $\Delta$ RF (lane 2), GFP-MID1 $\Delta$ BB (lane 3), GFP-MID1 $\Delta$ CC (lane 4), GFP-MID1 $\Delta$ FNIII (lane 5), and GFP-MID1 $\Delta$ CTD (lane 6). The samples were immunoprecipitated with anti-GFP antibody/protein-A sepharose beads, separated on 8% SDS polyacrylamide gels, transferred to nitrocellulose membranes and blotted with anti-phosphoserine antibody (top panel) or anti-phosphothreonine antibody (bottom panel). (C) Computer assisted detection of potential serine/threonine phosphorylation sites in MID1. Potential serine/threonine kinase consensus phosphorylation sites in MID1 were identified using NetPhos 2.0 software [38]. Examination of a multiple alignment of available MID1 and MID2 sequences was carried out to identify fully conserved putative phosphorylation sites. A diagrammatic representation of this analysis shows 16 conserved sites depicted as dots (red for serine and blue for threonine) along the length of a representative MID1 protein (numbered residue positions are also depicted at the top of diagram). The actual kinases that recognise the residues are listed on the left of the figure; CaMII (R-X-X-S/T-X), CKI (Sp/Tp-X<sub>2-3</sub>-S/T-X), CKII (X-S/T-X-X-D/E), GSK3 (X-S/T-X-X-X-Sp), MAPK (P-X-S/T-P), PKA (R-X<sub>1-2</sub>-S/T-X), PKC (X-S/T-X-R/K), PKG ((R/K)<sub>2-3</sub>-X-S/T-X).

the myc-tagged Alpha 4 construct. These experiments were complemented by yeast two-hybrid analysis of the same combinations of constructs.

Through a series of in-frame deletions of both MID1 and MID2 employed in both immunofluorescence and yeast two-hybrid assays, we have demonstrated functions for three domains of these RBCC proteins. We have shown a direct role for an RBCC B-box region in protein-protein interactions, that being the binding of Alpha 4, a regulatory subunit of the PP2-type phosphatases including the principal cellular phosphatase, protein phosphatase 2A (PP2A; [21-24]). In addition to the identified role for the B-boxes, we have shown that the coiled-coil domain not only mediates the homodimerisation of these proteins but also their ability to heterodimerise. Finally, our data, together with previous observations by others [18], support a role for the C-terminal domain in microtubule binding and to a lesser extent in dimerisation. Collectively, the immunofluorescence and yeast two-hybrid data indicate that MID dimerisation is a prerequisite for association of each MID-Alpha 4 complex with microtubules.

The interaction of MID1 and MID2 with Alpha 4 raised the possibility that these RBCC proteins, like Xnf7, are phosphoproteins. Indeed, western blot analysis of the transiently expressed MID-GFP fusion proteins using anti-phosphoserine and anti-phosphothreonine antibodies has confirmed these suspicions. Analysis of the domain-specific deletion proteins using these same antibodies showed that most serine phosphorylation of MID1 seems to occur at, or immediately adjacent to, the B-boxes, whereas threonine phosphorylation was likely to occur at residues in more than one domain. As a preliminary step towards identifying those residues that are phosphorylated, computer-based searches identified numerous potential sites for phosphorylation by serine/threonine kinases. However, only sixteen of these (see Fig 5C) are completely conserved across all MID species isolated to date. Of note are the potential phosphorylation sites at serine 96 (S96; [30]) and serine 92 (S92) that are located immediately amino-terminal to the B-boxes of MID1 and MID2 and are deleted in the  $\Delta$ BB constructs. S92 is a consensus site for GSK3 that would be dependent on prior phosphorylation of S96. S96 falls within a consensus phosphorylation sequence for the MAP-kinase (MAPK), ERK2 (P-N-S/T-P; [31]), as well as casein kinases I and II. Therefore, either of these kinases could conceivably play a priming role for GSK3 phosphorylation of S92. Similar phosphorylation mechanisms have been observed for other proteins including some microtubule-associated proteins, eg. tau and MAP2, where it has been implicated in the regulation of specific functions of those proteins [32,33]. Notably, in the case of both eIF2Bepsilon (at serine residues 535 &

539) and tau (at serine residues 208 & 212), DYRK, a MAPK-related kinase, plays such a priming role for GSK3 [34]. However, DYRK is unlikely to be involved in phosphorylation of MID1 S96 because of a single amino acid difference in its surrounding sequence required for recognition of this site for phosphorylation. In fact, Liu et al [30] have provided evidence to support the involvement of a MAPK, although the target of this activity was not shown. Irrespective of the identity of the kinase(s) responsible, it is conceivable that phosphorylation at these or other sites in MID1 and MID2 could play an important role in the overall function of the MID proteins, for example: regulation of the Alpha 4-MID interaction and hence regulation of PP2-type phosphatase activity. However, our preliminary analysis of a MID1 Ser92/Ser96 double mutant has suggested that MID dimerisation and the MID-Alpha 4 interaction are not dependent on phosphorylation at these residues (unpublished observations).

Regardless of the role of MID phosphorylation, the implication of both MID1 and MID2 in the Alpha 4-mediated regulation of phosphatase activity may provide valuable clues as to the pathophysiological consequences of MID1 mutations that underlie Opitz syndrome. It can be envisaged that, in tethering Alpha 4 to the microtubules, MID1 (and MID2) could be affecting the activity of the PP2-type phosphatases and thereby, in-turn, modulating the rapamycin-sensitive signaling pathway. This could conceivably occur by one of a number of mechanisms. Firstly, the MID proteins may control the availability of Alpha 4 to the phosphatases either by its 1) sequestration or 2) turnover, facilitated by the possible role of the MID RING finger motif in ubiquitination. Secondly, the Alpha 4-MID interaction may direct PP2A (and PP2-related) phosphatase activity to specific targets on the microtubules, which may include MID1 and MID2 themselves. The fact that both endogenous MID1 and transiently expressed GFP-MID1 and GFP-MID2 decorate microtubules throughout the cell cycle ([17]; unpublished observations) suggests that binding of MID1 and MID2 to the microtubule network may not itself be regulated by targeted Alpha 4-dependent PP2A activity. However, it remains possible that dynamic regulation of MID1 microtubule binding may escape detection by immunofluorescence as endogenous levels of MID1 and Alpha 4 in examined cell lines are both low (unpublished observations). The fact that we have not been able to demonstrate PP2A(C) co-localisation with the MID-Alpha 4 complexes on the microtubules, despite a known microtubule-associated pool of PP2A [35], would perhaps support the former of these mechanisms. However, we cannot exclude the possibility that recognition of PP2A(C) by this antibody is blocked by the interaction of Alpha 4 and MID1/2. If this is indeed the case, then it could be envisaged that PP2A(C) is also a target of MID RING-mediated degradation through its in-

dependent interaction with Alpha 4. An alternate hypothesis is that MID function is indeed controlled by Alpha 4-PP2-type phosphatases but through the regulated binding of additional factors that might be components of the MID1 macromolecular complexes. The characterisation of additional interacting partners will therefore be important to assess this possibility.

Numerous studies in mice have demonstrated that Alpha 4, like its yeast homologue Tap42, plays an essential regulatory role within the cell through its regulated binding to the catalytic (C) subunit of PP2-type serine/threonine protein phosphatases [21–24]. The interaction of Alpha 4 with PP2A(C) has been most extensively studied and shown to be dependent on phosphorylation of Alpha 4 by the mTOR (target of rapamycin) kinase. Although PP2A has a wide range of biological functions, Alpha 4 regulates a distinct subset of events in a rapamycin-sensitive manner, including progression through the cell cycle and the regulation of protein biosynthesis (for a review see [36]). The implication that disruption to some aspects of this rapamycin-sensitive pathway might be associated with the pathogenesis of the developmental disorder, Opitz syndrome, raises two intriguing possibilities. Firstly, it can be envisaged that mutations in other components of the pathway may give rise to similar clinical phenotypes. It is therefore perhaps worthy to note that the Alpha 4 gene maps to Xq13 [26] in the vicinity of the critical interval for FG syndrome, a malformation disorder with some clinical overlap with that of Opitz GBBB syndrome. We are currently investigating whether molecular defects in Alpha 4 indeed underlie FG syndrome or other developmental disorders mapping to the proximal long arm of the X chromosome. Secondly, it is also feasible that genetic polymorphisms that reflect a variation in the level of expression or activity of one or more components of the rapamycin-sensitive pathway might also contribute to the clinical variability of OS. In this regard, the indication from our immunofluorescence studies that the microtubular localisation of Alpha 4 is likely to be limited by the level of the MID1 and MID2 proteins within a particular cell type provides indirect support for our earlier hypothesis that MID2 may be able to compensate, at least partially, for the loss of MID1 in Opitz syndrome [5].

## Conclusions

The finding that Alpha 4, a rapamycin-sensitive regulatory subunit of PP2-type phosphatases, interacts strongly with the RBCC proteins, MID1 and MID2, implicates this signaling pathway in the pathogenesis of the X-linked form of Opitz GBBB syndrome and provides a possible explanation for the intrafamilial variability in clinical presentation of the disorder. Other components of the rapamycin-sensitive pathway should be considered as candidates for similar malformation disorders.

## Materials & Methods

### Miscellaneous enzymes and chemicals

All restriction endonucleases were purchased from New England Biolabs (Genesearch Pty Ltd, Arundel, Queensland), Klenow fragment from GeneWorks Pty Ltd (Thebarton, South Australia), and both T4 ligase and T4 DNA polymerase from Roche Diagnostics Australia (Castle Hill, New South Wales). 4',6-diamidino-2-phenylindole dihydrochloride (DAPI) and 3-Amino Triazole (3AT) were obtained from Sigma-Aldrich (Castle Hill, New South Wales).

### The yeast two-hybrid screen

The ProQuest™ yeast two-hybrid system (Invitrogen, Mulgrave, NSW) was employed to screen for potential interacting partners of MID1. In order to generate the "bait" construct, the full-length human MID1 cDNA was subcloned from pBSMID1 [5] using SalI and NcoI into the similarly restricted pDBLeu vector. Subsequent digestion with SalI, end-filling with Klenow fragment and religation generated the full-length MID1 cDNA in-frame with the GAL4 DNA binding domain (Gal4DBD). The construct, pDBLeu-MID1, was verified by sequencing.

The selection of an appropriate cDNA library was deemed critical to maximise the chance of detecting *bona fide* interacting factors. The expression of the murine *Mid1* gene during embryological development is consistent with the clinical presentation of OS [27]. Given the very high level of primary sequence identity between all vertebrate MID1 proteins (unpublished data), a murine 10.5 dpc whole embryo cDNA library (Invitrogen) directionally cloned in the GAL4 activation domain (GAL4-AD) plasmid, pPC86, was selected for use as the "prey" in the two-hybrid screen.

The pDBLeu-MID1 construct was transformed into MaV203 strain (Genotype: *MATα*, *leu2-3, 112*, *trp1-901*, *his3Δ200*, *ade2-101*, *gal4Δ*, *gal80Δ*, *SPAL10::URA3*, *GAL1::lacZ*, *HIS3<sup>UAS</sup> GAL1::HIS3@LYS2*, *can1<sup>R</sup>*, *cyh2<sup>R</sup>*) along with the parental pPC86 plasmid as per the manufacturers instructions (Invitrogen). The HIS3 reporter was used to determine the level of self-activation of the MID1-GAL4DBD fusion based on the level of 3-amino triazole resistance (3AT<sup>R</sup>) of the fusion protein. A concentration of 50 mM 3AT was found to be an adequate level for the assay, although subsequent analyses were performed on 75 mM 3AT plates to further reduce background transactivation of the reporter genes. To screen for potential interacting proteins, the pDBLeu-MID1 fusion construct was co-transformed with the 10.5 dpc mouse embryo cDNA-pPC86 library according to standard protocols (ProQuest™ Yeast Two-Hybrid Manual, Invitrogen) and plated on a synthetic complete medium (SC-Leu-Trp-His) containing either 50 mM or 75 mM 3AT.



The full-length MID2 (FXY2) cDNA was cloned from pEGFP-FXY2. ORF [15] into pDBLeu using the same strategy as used for MID1. As *Mid2* is generally expressed in many of the same tissues during embryological development as *Mid1* albeit at considerably lower levels [19], the resultant clone, pDBLeu-MID2, was consequently used as "bait" in a similar screen of the 10.5 dpc embryo cDNA library as well as directly against the identified MID1 interacting clones.

For confirmation of putative interacting clones, constructs and library clone isolates (in both parental vectors and swapped vectors) were re-transformed into the MaV203 yeast strain using the LiAc method [37]. Transformed yeast cultures were incubated for 24 hours at 30°C in selective media. Cultures (10 µl – 0.1 OD<sub>600</sub>) were then spotted onto selective plates and incubated at 30°C for 48 hours. Replica cleaning of plates was performed as required.

#### **Generation of GFP- and myc-full-length cDNA fusion constructs for immunofluorescence**

The generation of full-length MID1-GFP and MID2-GFP fusions in pEGFP have previously been reported [15,5]. A vector for the production of myc-tagged fusion proteins was generated by modification of the pEGFP-N2 vector (Clontech, Palo Alto, CA). Briefly, the GFP coding region was excised from pEGFP-N2 with NotI and BamHI, the 5' overhangs filled using T4 DNA polymerase and the vector religated to give pCMV-N2. Six copies of the myc epitope containing a start codon was amplified from pGEM-6mycT (gift from M. Whitelaw, University of Adelaide), and cloned into the HindIII site of pCMV-N2. To facilitate in-frame insertion of cDNAs directly from the pPC86 library vector, the plasmid was linearised with EcoRI, end-filled and re-ligated to create pCMV-6myc-ΔE. In order to clone Alpha 4 into pCMV-6myc-ΔE, pPC86-Alpha 4 was digested with Sall/AatII and the full-length cDNA insert ligated into Sall/SmaI restricted pCMV-6Myc-ΔE vector. The reading frame of the construct was confirmed by automated sequencing.

#### **Generation of MID1 and MID2 domain-specific deletion constructs for immunofluorescence and yeast two-hybrid analyses**

The FNIII domain-specific deletions in both MID1 and MID2 were generated by precise deletion of the domains by a two-step PCR strategy. The other domain-specific deletion constructs were generated using QuickChange™ site-directed mutagenesis (Stratagene, La Jolla, CA) to introduce unique restriction sites, as required, at the start and end of each domain within MID1 and MID2. Exceptions to this were the RING and B-box deletions of MID1 where a native XbaI site located at nucleotides +207–212 was used as the 3' and 5' excision point in the respective

constructs, and the CTD deletions in both MID1 and MID2 where a native BamHI site located at nucleotides +1464–1469 was used as the 5' excision point for these constructs. Restriction sites were chosen so that, where possible, the encoded amino acid sequence remained unaltered or only resulted in conservative substitutions. Furthermore, the sites were positioned such that excision of individual domains did not alter the reading frame of the encoded protein (Table 1). In any one construct, a maximum of two restriction sites were introduced. Details of the strategies and primers (for both PCR and site-directed mutagenesis) used in the generation of these deletion constructs will be forwarded upon request to the corresponding author. Each introduced restriction site was confirmed by digestion and sequencing and then independently tested for its effect on the microtubule binding capacity of the respective proteins. In each case, this was determined by direct visualisation of fluorescence of the created GFP fusion protein. No introduced change had any appreciable effect on the microtubular distribution of the proteins.

To further test the function of some of the regions of the MID1 protein, selected separate motifs were generated using the appropriate existing, and/or inserted, restriction sites and ligated in-frame and C-terminal to either EGFP (in pEGFP) or Gal4DBD (in pDBLeu). The following constructs were generated: the MID1 B-box fusion (pDBLeu-M1BB) containing residues 71–213, the MID1 coiled-coil fusion (pEGFP-M1CC) containing residues 214–349, and the MID1 B-boxes plus coiled-coil fusion (pEGFP-M1BBCC) containing residues 71–349.

#### **Transfection and immunofluorescence analysis of GFP-MID1 constructs**

Preparations of the various GFP- and myc-tagged expression constructs were made using the Qiagen Midi kit (Qiagen, Clifton Hill, Victoria). Two picomoles (approximately 1 microgram) of each construct were transfected into cultured cell lines (Cos1, HeLa, NIH3T3) using FuGene transfection reagent (Roche Diagnostics Australia). Transfected cells were grown on coverslips in DMEM plus 10% FBS and fixed 24 hours post-transfection as previously described [5].

In test transfections, where only a single GFP expression construct was introduced into cells, control microtubule staining was performed post-fixation using an anti-α tubulin antibody plus an anti-mouse Texas Red-conjugated secondary antibody (Jackson Laboratories, Bar Harbor, Maine). In cells transfected with myc-tagged expression constructs (either alone or in combination with a GFP-tagged expression construct), anti-α tubulin staining was not performed. Instead the Texas Red-conjugated secondary antibody was used in combination with an anti-myc



monoclonal antibody (9E10) to detect the expression of the myc-tagged protein. In all cases, nuclei were stained using the DNA-specific stain, DAPI. GFP and Texas Red fluorescence were visualised under appropriate wavelength light on an Olympus AX70 microscope. Images were captured using a Photometrics CE200A Camera Electronics Unit and processed using Photoshop 6.01 software (Adobe Systems Incorporated, San Jose, California).

#### Immunoprecipitation and western analysis

Preparations of the various GFP- and myc-tagged expression constructs were made using a DNA plasmid Midi kit (Qiagen). Six picomoles (approximately 3 micrograms) of each construct were transfected into approximately  $10^7$  Cos1 cells using FuGene transfection reagent (Roche Diagnostics Australia). After 24 hours incubation, cells were scraped from the culture dish and lysed on ice for 30 minutes in 1 ml lysis buffer (50 mM Tris-HCl pH 7.4, 300 mM NaCl, 5 mM EDTA, 1.0 % Triton X-100). Cell lysates were cleared by centrifugation at 4°C (15 minutes,  $16 \times g$ ), and protein extract recovered as supernatant. After pre-clearing 200  $\mu$ l of protein extract with 10  $\mu$ l of 50% protein-A sepharose bead slurry, extracts were incubated with 1  $\mu$ g of antibody for 2 hours at 4°C and then for another 2 hours with 20  $\mu$ l of fresh 50% protein-A sepharose bead slurry. The beads were washed four times with wash buffer (50 mM Tris-HCl pH 7.4, 300 mM NaCl, 5 mM EDTA, 0.1% Triton X-100) and protein eluted from the beads by boiling in  $2 \times$  SDS load buffer. Proteins were separated by 8% SDS PAGE and blotted onto Hybond-C membranes (Amersham Pharmacia) using a semi-dry transfer apparatus (BioRad). Membranes were blocked, incubated with the appropriate primary antibody, washed, incubated with the appropriate HRP-conjugated secondary antibody and washed again according to established method described in Current Protocols in Cell Biology. Detection was carried out using an enhanced chemiluminescence reagents (ECL) kit (Amersham Pharmacia) as per the manufacturer's instructions. Antibodies used in immunoprecipitation and western blot analysis included; rabbit polyclonal anti-GFP antibody (gift from Pam Silver, Dana-Farber Cancer Institute, Boston), mouse anti-myc monoclonal antibody (gift from Stephen Dalton, University of Adelaide), rabbit polyclonal anti-phosphoserine and anti-phosphothreonine antibodies (Zymed) and HRP conjugated anti-rabbit and anti-mouse secondary antibodies (Amersham Pharmacia).

#### Computer-assisted detection of serine/threonine phosphorylation sites

Analysis of putative consensus serine/threonine phosphorylation sites in MID1 was performed using NetPhos version 2.0 [<http://www.cbs.dtu.dk/services/NetPhos/>] software [38]. Examination of a multiple sequence alignment of all available MID1 and MID2 sequences was per-

formed in order to determine if any putative phosphorylation site was fully conserved. For this analysis, orthologous MID1 sequences were assessed from a variety of species, including human, mouse, rat, chick, tammar wallaby, zebrafish (partial sequence only) and fugu, and MID2 orthologous sequences from human, mouse and rat (partial sequence only).

#### Note Added In Proof

During the review of this manuscript, a paper by Trockenbacher *et al* [Trockenbacher A, Suckow V, Foerster J, Winter J, Krauß S, Roper H-H, Schneider R. and Schweiger S: MID1, mutated in Opitz syndrome, encodes an ubiquitin ligase that targets phosphatase 2A for degradation. *Nature Genetics* 2001, 29:287-294] independently reported the interaction of Alpha 4 and MID1. These investigators also showed that MID1, possibly through Alpha 4, regulates the turnover of the microtubule-associated fraction of PP2AC and hence may represent a possible pathological mechanism for the Opitz syndrome phenotype.

#### Acknowledgements

We would like to thank Professor David Brautigan for kindly sharing data prior to publication. This work was supported by project grant #157958 and in part by an R. Douglas Wright Award (#997706) (to T.C.C.) from the National Health and Medical Research Council of Australia.

#### References

1. Opitz JM: **G syndrome (hypertelorism with esophageal abnormality and hypospadias, or hypospadias-dysphagia, or "Opitz-Frias" or "Opitz-G" syndrome) – perspective in 1987 and bibliography.** *American Journal of Medical Genetics* 1987, 28:275-285
2. Robin NH, Opitz JM, Muenke M: **Opitz G/BBB syndrome: clinical comparisons of families linked to Xp22 and 22q, and a review of the literature.** *American Journal of Medical Genetics* 1996, 62:305-317
3. Quaderi NA, Schweiger S, Gaudenz K, Franco B, Rugarli EI, Berger W, Feldman GJ, Volta M, Andolfi G, Gilgenkrantz S, Marion RW, Hennekam RC, Opitz JM, Muenke M, Ropers HH, Ballabio A: **Opitz G/BBB syndrome, a defect of midline development, is due to mutations in a new RING finger gene on Xp22.** *Nature Genetics* 1997, 17:285-291
4. Gaudenz K, Roessler E, Quaderi N, Franco B, Feldman G, Gasser DL, Wittwer B, Horst J, Montini E, Opitz JM, Ballabio A, Muenke M: **Opitz G/BBB syndrome in Xp22: mutations in the MID1 gene cluster in the carboxy-terminal domain.** *American Journal of Human Genetics* 1998, 63:703-710
5. Cox TC, Allen LR, Cox LL, Hopwood B, Goodwin B, Haan E, Suthers GK: **New mutations in MID1 provide support for loss of function as the cause of X-linked Opitz syndrome.** *Human Molecular Genetics* 2000, 9:2553-2562
6. Robin NH, Feldman GJ, Aronson AL, Mitchell HF, Weksberg R, Leonard CO, Burton BK, Josephson KD, Laxova R, Aleck KA: **Opitz syndrome is genetically heterogeneous, with one locus on Xp22, and a second locus on 22q11.2.** *Nature Genetics* 1995, 11:459-461
7. McDonald-McGinn DM, Driscoll DA, Bason L, Christensen K, Lynch D, Sullivan K, Canning D, Zavod W, Quinn N, Rome J: **Autosomal dominant "Opitz" GBBB syndrome due to a 22q11.2 deletion.** *American Journal of Medical Genetics* 1995, 59:103-113
8. Fryburg JS, Lin KY, Golden WL: **Chromosome 22q11.2 deletion in a boy with Opitz (G/BBB) syndrome.** *American Journal of Medical Genetics* 1996, 62:274-275
9. McDonald-McGinn DM, Tonnesen MK, Laufer Cahana A, Finucane B, Driscoll DA, Emanuel BS, Zackai EH: **Phenotype of the 22q11.2 deletion in individuals identified through an affected relative: cast a wide FISHing net!** *Genet Med* 2001, 3:23-29

10. Glover TW: **CATCHING a break on 22.** *Nature Genetics* 1995, **10**:257-258
11. Guris DL, Fantes J, Tara D, Druker BJ, Imamoto A: **Mice lacking the homologue of the human 22q11.2 gene CRKL phenocopy neurocristopathies of DiGeorge syndrome.** *Nature Genetics* 2001, **27**:293-298
12. Jerome LA, Papaioannou VE: **DiGeorge syndrome phenotype in mice mutant for the T-box gene, Tbx1.** *Nature Genetics* 2001, **27**:286-291
13. Lindsay EA, Vitelli F, Su H, Morishima M, Huynh T, Pramparo T, Jurecic V, Ogunrinu G, Sutherland HF, Scambler PJ, Bradley A, Baldini A: **Tbx1 haploinsufficiency in the DiGeorge syndrome region causes aortic arch defects in mice.** *Nature* 2001, **410**:97-101
14. Merscher S, Funke B, Epstein JA, Heyer J, Puech A, Lu MM, Xavier RJ, Demay MB, Russell RG, Factor S, Tokooya K, Jore BS, Lopez M, Pandita RK, Lia M, Carrion D, Xu H, Schorle H, Kobler JB, Scambler P, Wynshaw-Boris A, Skoultschi AI, Morrow BE, Kucherlapati R: **TBX1 is responsible for cardiovascular defects in velo-cardio-facial/DiGeorge syndrome.** *Cell* 2001, **104**:619-629
15. Perry J, Short KM, Romer JT, Swift S, Cox TC, Ashworth A: **FXV2/MID2, a gene related to the X-linked Opitz syndrome gene FXY/MID1, maps to Xq22 and encodes a FNIII domain-containing protein that associates with microtubules.** *Genomics* 1999, **62**:385-394
16. Short KM, Hopwood B, Cox TC: **Further subdivision of the RBCC family of proteins defined by the presence of a Fibronectin type III motif.** *in preparation*
17. Cainarca S, Messali S, Ballabio A, Meroni G: **Functional characterization of the Opitz syndrome gene product (midin): evidence for homodimerization and association with microtubules throughout the cell cycle.** *Human Molecular Genetics* 1999, **8**:1387-1396
18. Schweiger S, Foerster J, Lehmann T, Suckow V, Muller YA, Walter G, Davies T, Porter H, van Bokhoven H, Lunt PW, Traub P, Ropers HH: **The Opitz syndrome gene product, MID1, associates with microtubules.** *Proceedings of the National Academy of Sciences of the United States of America* 1999, **96**:2794-2799
19. Buchner G, Montini E, Andolfi G, Quaderi N, Cainarca S, Messali S, Bassi MT, Ballabio A, Meroni G, Franco B: **MID2, a homologue of the Opitz syndrome gene MID1: similarities in subcellular localization and differences in expression during development.** *Human Molecular Genetics* 1999, **8**:1397-1407
20. Takei Y, Teng J, Harada A, Hirokawa N: **Defects in axonal elongation and neuronal migration in mice with disrupted tau and map1b genes.** *Journal of Cell Biology* 2000, **150**:989-1000
21. Chen J, Peterson RT, Schreiber SL: **Alpha 4 associates with protein phosphatases 2A, 4, and 6.** *Biochemical and Biophysical Research Communications* 1998, **247**:827-832
22. Inui S, Sanjo H, Maeda K, Yamamoto H, Miyamoto E, Sakaguchi N: **Ig receptor binding protein 1 (alpha4) is associated with a rapamycin-sensitive signal transduction in lymphocytes through direct binding to the catalytic subunit of protein phosphatase 2A.** *Blood* 1998, **92**:539-546
23. Murata K, Wu J, Brautigam DL: **B cell receptor-associated protein alpha4 displays rapamycin-sensitive binding directly to the catalytic subunit of protein phosphatase 2A.** *Proceedings of the National Academy of Sciences of the United States of America* 1997, **94**:10624-10629
24. Nanahoshi M, Tsujishita Y, Tokunaga C, Inui S, Sakaguchi N, Hara K, Yonezawa K: **Alpha4 protein as a common regulator of type 2A-related serine/threonine protein phosphatases.** *FEBS Letters* 1999, **446**:108-112
25. Schmelzle T, Hall MN: **TOR, a central controller of cell growth.** *Cell* 2000, **103**:253-262
26. Onda M, Inui S, Maeda K, Suzuki M, Takahashi E, Sakaguchi N: **Expression and chromosomal localization of the human alpha 4/IGBP1 gene, the structure of which is closely related to the yeast TAP42 protein of the rapamycin-sensitive signal transduction pathway.** *Genomics* 1997, **46**:373-378
27. Dal Zotto L, Quaderi NA, Elliott R, Lingerfelter PA, Carrel L, Valsecchi V, Montini E, Yen CH, Chapman V, Kalcheva I, Arrigo G, Zuffardi O, Thomas S, Willard HF, Ballabio A, Disteche CM, Rugarli EI: **The mouse Mid1 gene: implications for the pathogenesis of Opitz syndrome and the evolution of the mammalian pseudoautosomal region.** *Human Molecular Genetics* 1998, **7**:489-499
28. Wolf E, Kim PS, Berger B: **a program for predicting two- and three-stranded coiled coils.** *Protein Science* 1997, **6**:1179-1189
29. Borden KL: **RING fingers and B-boxes: zinc-binding protein-protein interaction domains.** *Biochemistry and Cell Biology* 1998, **76**:351-358
30. Liu J, Prickett TD, Elliott E, Meroni G, Brautigam DL: **Phosphorylation and microtubule association of the Opitz syndrome protein mid-1 is regulated by protein phosphatase 2A via binding to the regulatory subunit alpha 4.** *Proceedings of the National Academy of Sciences of the United States of America* 2001, **98**:6650-6655
31. Himpel S, Tegge W, Frank R, Leder S, Joost HG, Becker W: **Specificity determinants of substrate recognition by the protein kinase DYRK1A.** *Journal of Biological Chemistry* 2000, **275**:2431-2438
32. Chu B, Soncin F, Price BD, Stevenson MA, Calderwood SK: **Sequential phosphorylation by mitogen-activated protein kinase and glycogen synthase kinase 3 represses transcriptional activation by heat shock factor-1.** *Journal of Biological Chemistry* 1996, **271**:30847-30857
33. Sanchez C, Perez M, Avila J: **GSK3beta-mediated phosphorylation of the microtubule-associated protein 2C (MAP2C) prevents microtubule bundling.** *European Journal of Cell Biology* 2000, **79**:252-260
34. Woods YL, Cohen P, Becker W, Jakes R, Goedert M, Wang X, Proud CG: **The kinase DYRK phosphorylates protein-synthesis initiation factor eIF2Bepsilon at Ser539 and the microtubule-associated protein tau at Thr212: potential role for DYRK as a glycogen synthase kinase 3-priming kinase.** *Biochemical Journal* 2001, **355**:609-615
35. Sontag E, Nunbhakdi Craig V, Bloom GS, Mumby MC: **A novel pool of protein phosphatase 2A is associated with microtubules and is regulated during the cell cycle.** *Journal of Cell Biology* 1995, **128**:1131-1144
36. Goldberg Y: **Protein phosphatase 2A: who shall regulate the regulator?** *Biochemical Pharmacology* 1999, **57**:321-328
37. Dunn B, Wobbe RC: **Introduction of DNA into yeast cells.** *In: Current Protocols in Molecular Biology* Edited by Ausubel FM, Brent R, Kingston RE, Moore DD, Seidman JG, Smith JA, Struhl K, vol. 13.7.1. New York: John Wiley & Sons, Inc.; 1993
38. Blom N, Gammeltoft S, Brunak S: **Sequence and structure-based prediction of eukaryotic protein phosphorylation sites.** *Journal of Molecular Biology* 1999, **294**:1351-1362

Publish with **BioMed Central** and every scientist can read your work free of charge

"BioMedcentral will be the most significant development for disseminating the results of biomedical research in our lifetime."

Paul Nurse, Director-General, Imperial Cancer Research Fund

Publish with **BMC** and your research papers will be:

- available free of charge to the entire biomedical community
- peer reviewed and published immediately upon acceptance
- cited in PubMed and archived on PubMed Central
- yours - you keep the copyright



Submit your manuscript here:  
<http://www.biomedcentral.com/manuscript/>

[editorial@biomedcentral.com](mailto:editorial@biomedcentral.com)